PhD-FSTM-2023-120
The Faculty of Science, Technology and Medicine

DISSERTATION

Defence held on 14/11/2023 in Esch-Sur-Alzette, Luxembourg

to obtain the degree of

DOCTEUR DE L'UNIVERSITÉ DU LUXEMBOURG

EN BIOLOGIE

by

Pelin KAYA
Born on 21st August 1991 in Osmangazi, Türkiye

CHARACTERIZATION OF NOVEL INHIBITORS OF THE TRAFFICKING CHAPERONE PDE6D

Dissertation defence committee

Prof. Dr. Daniel Abankwa, dissertation supervisor
Professor, Université du Luxembourg

Prof. Dr. Jens Christian Schwamborn, chairman
Professor, Université du Luxembourg

Prof. Dr. Shehab Ismail
Professor, KU LEUVEN

Dr. Silvia Bolognin
Assistant Professor, University of Maastricht

Dr. Oliver Rocks
Research group leader, Charité – University of Medicine Berlin

UNIVERSITY OF LUXEMBOURG
Department of Life Sciences and Medicine

Luxembourg National Research Fund

A dissertation by Pelin KAYA submitted to the University of Luxembourg in partial fulfillment of the requirements for the degree of

DOCTOR of PHILOSOPHY

This doctoral thesis is supported by the Luxembourg National Research Fund (FNR) (AFR Call PhD 2019-13589879)

Thesis supervisory committee:

Prof. Dr. Daniel Abankwa, Université du Luxembourg

Prof. Dr. Shehab Ismail, KU LEUVEN

Dr. Silvia Bolognin, University of Maastricht

AFFIDAVIT

I hereby confirm that the PhD thesis entitled “CHARACTERIZATION OF NOVEL INHIBITORS OF THE TRAFFICKING CHAPERONE PDE6D” has been written independently and without any other sources than cited.

Luxembourg, Pelin KAYA

ACKNOWLEDGEMENTS

I would like to express my sincere gratitude and appreciation to my thesis supervisor, **Professor Dr. Daniel Abankwa** for his invaluable guidance, unwavering support, and exceptional mentorship throughout the course of my research. Thank you for everything you taught me during all these years and your support through it all.

I am grateful to my CET committee members **Dr. Silvia Bolognin** and **Professor Dr. Shehab Ismail Mohamed** for the time and expertise they dedicated to reviewing and evaluating my work. Your constructive criticism and insights have significantly improved the quality of this thesis.

I would like to extend my appreciation to all my fellow colleagues especially **Dr. Elizabeth Schaffner-Reckinger** and **Dr. Rohan Chippalkatti** who shared their knowledge, experiences, and support. Your insights and discussions have enriched my research. **Lis**, I am grateful for your guidance and support as a mentor figure in my life. Your encouragement and assistance have been invaluable to me over the years, especially during those moments when I've faced various challenges. Your support has made me feel like I have a welcoming place to turn to, much like the comfort of family. I am really fortunate to have you in my life. I would like to extend my heartfelt thanks to my dear friend, **Rohan** for always being there with a listening ear, offering words of encouragement and sweet dalgona coffee. Thank you for being such a good and kind friend.

I express my sincere gratitude to **Dr. Karolina Pavic** and **Dr. Sara Bottone** for their kindness and motivation during my academic journey. I would like to thank **Christina Laurini** for her invaluable assistance and meticulous organization of the laboratory. Additionally, I would like to thank my fellow Ph.D. candidates **Candy Steffen** and **Bianca Parisi** for the fun moments we have shared.

I deeply appreciate previous members of cancer cell biology and drug development group. I had an opportunity to meet amazing people during these four years. I would like to thank **Dr. Ganesh babu Manoharan, Dr. Sunday Ojochegbe Okutachi, Dr. Farah Kouzi, Dr. Vladislav Stramiska, Dr. Farid A. Siddiqui, Nesrine Ben Fredj** and **Lynn Mangen** for being amazing colleagues and friends. I deeply appreciated our conversations regarding various aspects of life, scientific concepts, and a broad range of topics. In particular, I have gained valuable knowledge and insights from **Ganesh**. Your remarkable contributions to my

professional development have been truly enriching.
To my Luxembourgish sisters **Isabel** and **Kristine**. Thank you for making me feel at home and filling my evenings and weekends with very good food, tarot, coffee reading, raclette, love, hugs, laughter, and happiness. Dear **Sunny**, thank you for being the sunshine during my darkest times.

To my Boardgame family, **Laura**, **Jenny**, **Amanda**, **Alvile**, **Constance**, **Seli**, **Manuel , Puya,** and the **regulars of Bei de Minettsdapp**. Thank you for making me feel at home and filling my Friday evenings with laughter, and happiness.

To my girls, **Gizem**, **Deniz**, **Ekin**, **Esra**, **Nurcan**, **Gözde**, **Fatima**, **Kathleen**, **Isabel**, **Müge Aylin**, **Hande,** and **the MBG girls** thank you for everything. As I embark on this new chapter of my life, I want to take a moment to acknowledge and express my deepest gratitude to the extraordinary women who have stood by my side through every twist and turn, joy and sorrow. You are not just my friends; you are my sisters and my unwavering support system. Together, we have created a bond that is unbreakable, a sisterhood that is everlasting.

Now, I would like to thank the people who have always believed in me, my family back home. My dear mother, **Sırma Diyaroğlu Kaya**, thank you for your love, patience, and unwavering belief in me. From the moment I entered this world, your love has been a guiding light in my life. Today, as I reflect on the person I have become, I am overwhelmed with gratitude for the incredible mother you are. Here, I want to express my deepest love and appreciation for all that you have done for me. You are not just my mother; you are my hero, my role model, and my greatest blessing. I cherish every moment we've shared and look forward to creating many more cherished memories together. My dear father, **Ali Kaya**, thank you for being there and always wishing for my health and happiness. Our bond has developed over time, and I am truly fortunate to have you in my life.

My dear sister, **Selin**, I am really lucky to have a sister like you. In the face of adversity, you've been my pillars of strength. In moments of doubt, you've reminded me of my worth. In times of celebration, you've magnified my joy. Your presence in my life has made it immeasurably richer, brighter, and more meaningful. Dear brother, **İbrahim**, thank you for being there. It is important to prioritize your well-being and health rather than dedicating yourself to work. I also would like to thank my aunts **Aynur** and **Güler**. You have a special place in my heart. To my cousin **Dilara**, I am always thankful for your endless love and support. We shared a cherished childhood filled with fond memories.

To my late grandfather **Mahmut Diyaroğlu**, your favorite grandchild loves you a lot. Thank you for all the precious memories. Lastly, to my dearest **Uygar Argun**, my late brother and eldest cousin among us, as I write these sentences, my heart overflows with a mixture of love, sorrow, and gratitude for having had you as my brother. Your passing left an indelible void in my life, a space that can never truly be filled. Though you may no longer be here in person, your spirit lives on in with us. Your memory remains a guiding light in my life, reminding me to cherish every moment, to be kind, and to find strength in the face of hardships. I will always remember you. I am really sorry and thank you for everything.

This thesis would not have been possible without all of you. *Thank you all* for being a part of this important chapter in my life.

DEDICATIONS

This PhD thesis is dedicated to all the remarkable women in my life who have played a role in shaping the person I am today. Thank you for being the role models, mentors, and pillars of strength that have propelled me forward in this journey. I dedicate this work to you, with immense gratitude and admiration.

TABLE OF CONTENTS

LIST OF FIGURES

LIST OF TABLES

LIST OF ABBREVIATIONS

AKT	Protein Kinase B
APT	Acyl protein thioesterase
Arf	ADP ribosylation factor
Arl2/3	Arf-like protein 2/3
Arl13B	Arf-like protein 13B
ASPP2	Apoptosis-stimulating of p53 protein 2
Bcl-2	B-cell lymphoma 2
B-Raf	Rat-1 fibroblast kinase B homolog
BRET	Bioluminescence resonance energy transfer
CaM	Calmodulin
CAM	Chorioallantoic membrane
Cdc42	Cell division control protein 42 homolog
c-Fos	AP-1 transcription factor subunit
cGMP	Cyclic guanosine monophosphate
C-Raf	Rat-1 fibroblast kinase C homolog
DSS	Drug sensitivity score
E3-ligase	E3 ubiquitin ligase
ELK1	E twenty-six Like-1
ERK	Extracellular signal regulated kinase
F-Ator	FITC-labelled Atorvastatin
FITC	Fluorescein isothiocyanate
FRET	Fluorescence resonance energy transfer
F-Rheb	FITC-labelled PDE6D-binder RHEB
FTase	Farnesyl transferase
FTI	Farnesyl transferase inhibitor
G domain	GTPase domain
GAP	GTPase activating protein
GDF	GDI-like displacement factor
GDI	Guanosine nucleotide dissociation inhibitor
GDP	Guanosine 5’ diphosphate
GEF	Guanine nucleotide exchange factor
GFP	Green fluorescent protein
GGTase	Geranylgeranyltransferase

GNAT1	G Protein Subunit Alpha Transducin 1
GSF	GDI-like solubilizing factor
GTP	Guanosine 5’ triphosphate
GTPase	Guanosine triphosphatase
HDAC	Histone deacetylase
HSA	Highest single agent
H-Ras	Harvey rat sarcoma viral oncogene homolog
HVR	Hypervariable region
IC50	Half maximal inhibitory concentration
ICMT	Isoprenylcysteine carboxyl methyltransferase
K-Ras	Kirsten rat sarcoma viral oncogene homolog
MAPK	Mitogen-activated protein kinase
MEK	MAPK/ERK Kinase
mTOR	Mammalian target of Rapamycin
Myr	Myristoylation region
NPHP3	Nephrocystin 3
N-Ras	Neuroblastoma Ras viral oncogene homolog
NSCLC	Non-small cell lung cancer
OphA	Ophiobolin A
PA	Phosphatidic acid
PAT	Palmitoyl acyl transferase
PDAC	Pancreatic ductal adenocarcinoma
PDE5	Phosphodiesterase type 5
PDE6	Phosphodiesterase type 6
PDE6D	Phosphodiesterase subunit delta
PDE6Di	PDE6D inhibitor
PI3K	Phosphoinositide- 3-kinase
PKG2	Protein kinase cGMP-dependent 2
P-loop	Phosphate-binding loop
PP2A	Protein phosphatase 2
PROTAC	Proteolysis targeting chimera
PS	Phosphatidylserine
Rab	Ras analog in brain
Rac1	Ras-related C3 botulinum toxin substrate 1
RalGDS	Ral guanine nucleotide dissociation stimulator
Ran	Ras-related nuclear protein

Rap1	Ras-associated protein-1
Ras	Rat sarcoma protein
RCE1	Ras converting enzyme 1
RHEB	Ras homolog enriched in brain
Rho	Ras homologus
RhoA	Ras homologus A homolog
RLuc	Renilla Luciferase
RNA	Ribonucleic acid
RP2	Retinitis pigmentosa 2
RTK	Receptor tyrosine kinase
SII-P	Switch II-pocket
S6	Ribosomal protein S6
SHP2	Src homology 2 (SH2) domain-containing phosphatase 2
SmgGDS	Small GTP-binding protein GDP-dissociation stimulator
SOS1	Son of sevenless homologue 1
SPRED1	Sprouty-related, EVH1 domain-containing protein 1
SRC	SRC proto-oncogene receptor tyrosine kinase
STK19	Serine/threonine-protein kinase 19
UNC119	Uncoordinated119
VHL	Von Hippel–Lindau tumor suppressor
WHO	World Health Organization

LIST OF PUBLICATIONS AND MANUSCRIPTS

I. Review publication (shared first author)

Steffen CL, **Kaya P**, Schaffner-Reckinger E, Abankwa D. Eliminating oncogenic RAS: back to the future at the drawing board. Biochem Soc Trans. 2023 Feb 27;51(1):447-456. doi: 10.1042/BST20221343. PMID: 36688434; PMCID: PMC9987992.

II. Submitted research manuscript from thesis project (first author)

Pelin Kaya, Elisabeth Schaffner-Reckinger, Ganesh babu Manoharan, Vladimir Vukic, Alexandros Kiriazis, Mirko Ledda, Maria Burgos, Karolina Pavic, Anthoula Gaigneaux, Enrico Glaab, Daniel Kwaku Abankwa. An improved PDE6D inhibitor combines with Sildenafil to synergistically inhibit KRASmutant cancer cell growth. 2023. doi: https://doi.org/10.1101/2023.08.23.554263

III. Ready to submit research manuscript (co-author)

Rohan Chippalkatti, Bianca Parisi, **Pelin Kaya**, Elisabeth Schaffner-Reckinger, Sara Bottone, Lynn Mangen, Yashar Rouzbahani, Christian Eggeling, Daniel Kwaku Abankwa. Inhibition of ciliary K-Ras localization drives C2C12 cell differentiation.

ABSTRACT

The RAS protein has been considered undruggable for more than 30 years due to the absence of evident target sites. However, recent developments have paved the way for novel approaches in targeting Ras.

In the first part of my thesis, a concise review is provided of different strategies that focus on directly targeting four distinct druggable regions within Ras. Particular focus is given to the insights gained from the development of allele-specific covalent and non-covalent inhibitors against Ras. Furthermore, we address the utility of macromolecular binders to identify and validate targetable regions on Ras and we discuss the promising development of small molecule binders into degraders of Ras.

The second, main part of my thesis is dedicated to the characterization and evaluation of novel PDE6D inhibitors named Deltaflexins. The KRAS-trafficking chaperone protein PDE6D, which is also known as PDEδ (PDEdelta), was initially proposed as a surrogate therapeutic target for K-Ras. However, off-target effects, solubility issues and inefficient cell penetration have hampered the advancement of previously established PDE6D inhibitors to the clinical stage. In our study, we have developed Deltaflexins that display potent inhibitory effects against PDE6D at nanomolar concentrations and enhanced selectivity to PDE6D. Our findings indicate that increasing the affinity to the PDE6D hydrophobic pocket is linked to poorer solubility and also increased off-target binding to PDE6D-related UNC119. Therefore, we decided to take a combinatorial treatment approach to target K-Ras.

To this end, we combined Deltaflexin3 with the clinically approved drug Sildenafil. Deltaflexin3 was chosen among all investigated compounds as it displays the highest selectivity towards PDE6D and a high solubility. Sildenafil is known to promote phosphorylation of the K-Ras residue Ser181 thereby reducing the affinity between K-Ras and PDE6D. As a result, this combinatorial treatment efficiently suppressed K-Ras-dependent signaling and led to synergistic inhibitory effects on the cancer cell proliferation as well as tumor growth in chorioallantoic membrane assay.

Recently, we demonstrated that oncogenic K-Ras hinders cellular differentiation in our research project. Knowing that cell stemness is linked to primary cilia and that PDE6D can facilitate the trafficking of K-Ras to the primary cilium, another focus of our research was to study the novel molecular mechanisms of how PDE6D and K-Ras collaborate to impact cell differentiation, which may have significant implications for cancer evolution. Therefore, in the third part of my thesis, I will introduce K-Ras chimera that can be orthogonally trafficked into the primary cilium to validate ciliary functions of K-Ras and the impact of K-Ras localization on cell differentiation.

AIMS AND OBJECTIVES OF THE THESIS

Mutations in the *RAS* gene are observed in approximately 19% of cancer patients, with *KRAS* being the most frequently altered form and a key driver of cancer stemness (Prior *et al*, 2020). Efforts to develop treatments that specifically target K-Ras have been largely ineffective until the recent promising establishment of G12C inhibitors (Canon *et al*, 2019; Hallin *et al*, 2020; Hong *et al*, 2020; Janes *et al*, 2018). Using similar approaches, G12S and G12R covalent binders have been subsequently developed (Zhang *et al*, 2022a; Zhang *et al*, 2022b). However, most K-Ras mutants do not involve the G12C, G12S or G12R alteration and therefore cannot be effectively targeted by these covalent inhibitors. Additionally, resistance mechanisms against G12C inhibitors have been reported (Awad *et al*, 2021; Dunnett-Kane *et al*, 2021; Kwan *et al*, 2022).

Alternative strategies have been explored to overcome the challenge of targeting Ras proteins directly. Among these approaches, PDE6D has emerged as a potential surrogate target for K-Ras (Fansa & Wittinghofer, 2016; Yelland *et al*, 2022). Several potent inhibitors of PDE6D with strong binding affinity were developed. However, their effectiveness fell short of expectations (Canovas Nunes *et al*, 2022; Martin-Gago *et al*, 2017a; Papke *et al*, 2016; Siddiqui *et al*, 2020a; Zimmermann *et al*, 2013).

In this thesis, my research focuses on the development and analysis of novel PDE6D inhibitors that have an enhanced on-target activity and improved affinity in the low nanomolar range. Moreover, these inhibitors display an improved specificity towards K-Ras as compared to other Ras isoforms. Subsequently, my objective is to investigate possible therapeutic strategies for enhancing the disruption of K-Ras localization, thereby impeding oncogenic signaling pathways associated with cancer progression. Thus, our strategy involved a synergistic approach combining Deltaflexin3 with Sildenafil to effectively inhibit Ras-signaling and cancer cell proliferation as well as to examine the novel molecular mechanism of how PDE6D and K-Ras collaborate to impact on cell differentiation.

Therefore, **the specific objectives** of this study are:

1. In-depth evaluation of various approaches that focus on directly targeting four distinct druggable regions within Ras.
2. Comprehensive characterization and investigation of new PDE6D inhibitors and profiling of their activity against KRAS-mutant cancer cells.
3. Generation of chimeric K-Ras mutants that can be orthogonally trafficked into the primary cilium to study their impact on C2C12 cell differentiation.

1. SYNOPSIS

1.1. SYNOPSIS - INTRODUCTION

1.1.1. THE RAS PROTEIN FAMILY

Members of the Ras superfamily are small GTPases that act as "molecular switches" (Cherfils & Zeghouf, 2013) and play key roles in regulating many cellular events, including cell growth, differentiation, migration, and vesicle transport (Chiu *et al*, 2013; Citalan-Madrid *et al*, 2013; Crespo & Leon, 2000; Oliveira & Yasuda, 2014). The exact number of the Ras superfamily members can vary depending on the criteria used for classification. However, it is generally estimated that the Ras superfamily includes more than 150 members, which are divided into five major subfamilies based on their structural and functional characteristics: Ras, Rho, Rab, Arf, and Ran (**Figure 1**) (Bernal Astrain *et al*, 2022; Colicelli, 2004).

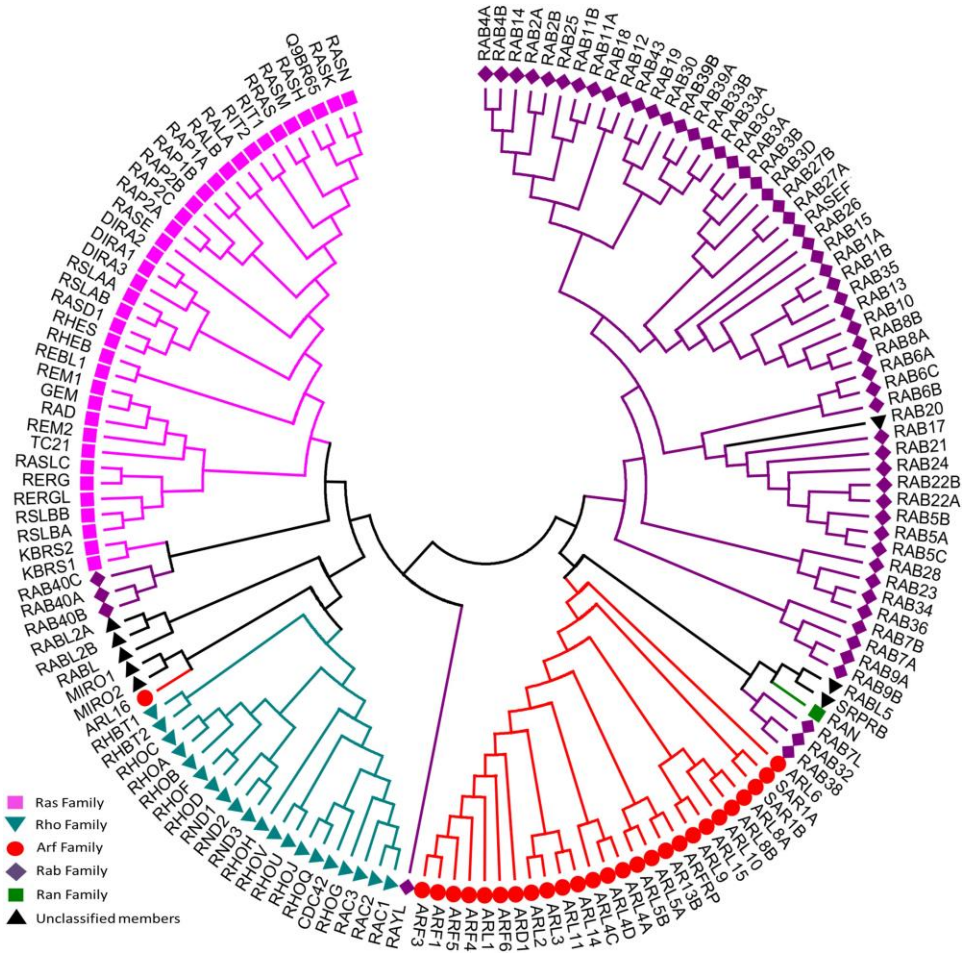

Figure 1: The RAS superfamily. A phylogenetic tree of 150 small GTPases from human was created using amino acid sequences obtained from the UniProt database. These sequences were aligned through multiple alignment techniques, and a distance matrix was derived to construct the tree. The neighbor-joining method was employed for this purpose (Qu *et al*, 2019).

The Ras subfamily is perhaps the most well-known member of the Ras superfamily and is involved in signal transduction pathways. The Ras subfamily consists of more than 30 members, including *KRAS, HRAS,* and *NRAS*, which are commonly associated with cancer. The Rho subfamily includes proteins that regulate actin cytoskeleton dynamics, cell adhesion, and cell migration. Members of the Rho subfamily are also involved in various cellular processes, including vesicle transport, gene expression, and cell cycle progression (David *et al*, 2012). The Rho subfamily includes approximately 20 members, including RhoA, Rac1, and Cdc42, which are involved in cytoskeleton dynamics (Citalan-Madrid *et al.*, 2013) and cell migration. The Rab subfamily includes proteins that regulate vesicle trafficking and membrane fusion events within cells (Banworth *et al*, 2022; Ebnet & Gerke, 2022). The Arf subfamily is involved in vesicle formation and membrane trafficking, and its members function in intracellular signaling and cytoskeleton organization. The Arf subfamily includes six members, including Arf1 and Arf6, which are involved in vesicle formation and membrane trafficking (Singh *et al*, 2019). Finally, the Ran protein regulates the nucleocytoplasmic transport of macromolecules, including proteins and RNAs, and is involved in spindle assembly during cell division. (Knyphausen *et al*, 2015).

1.1.2. RAS PROTEIN STRUCTURE

Ras proteins consist of a single polypeptide chain composed of 166-189 amino acids, with a molecular weight ranging from 21 kDa to 25 kDa depending on the type of Ras protein (Rojas et al, 2012). They have a globular shape with six major α-helices (α1-α6) and five β-strands (β1-β5). The Ras proteins belong to the group of phosphate-binding loop (P-loop) proteins and act as molecular switches (Han et al, 2017).

The three major ubiquitously expressed *RAS* genes – *HRAS*, *KRAS*, and *NRAS* – encode four distinct protein isoforms, since the *KRAS* gene produces two splice variants called K-Ras4A and K-Ras4B, which differ in the inclusion of exons 4A and 4B, respectively. The Ras protein consists of two main parts: the G-domain (aa 1-172), and the hypervariable region (aa 173-188/9). When compared to each other, all four Ras isoforms share identical residues in the first half of their G-domain (aa 1-86), which is called the effector lobe including switch 1 (aa 30-40) and switch 2 (aa 60-76) regions (Gorfe et al, 2008). The switch I region contains a binding site for GTP and GDP (**Figure 2**).

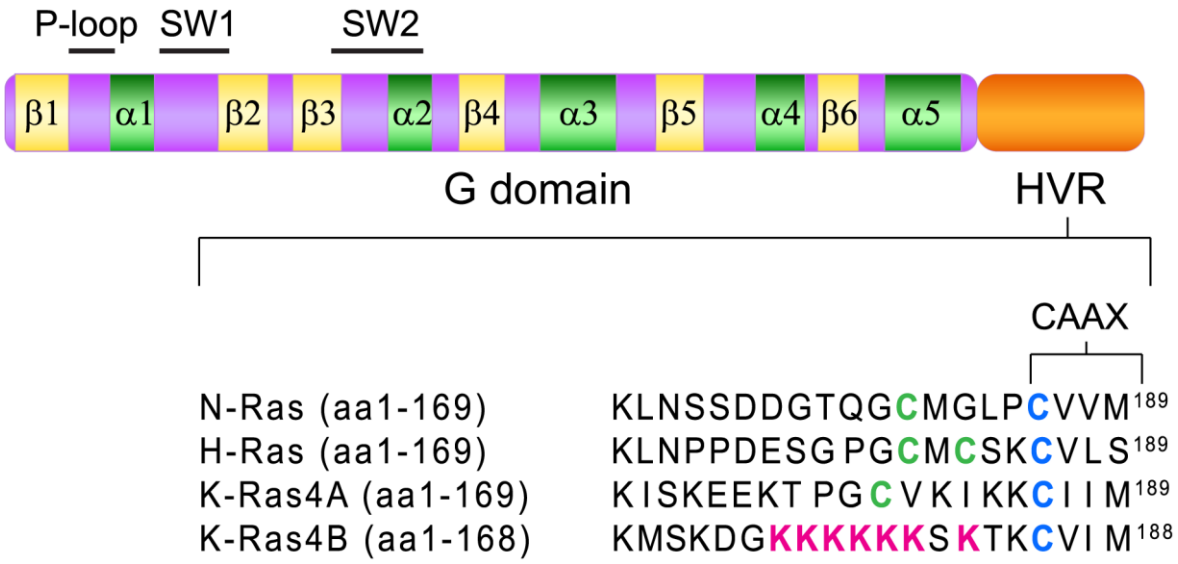

Figure 2: The hypervariable regions (HVRs) of Ras isoforms. The cysteine residue of the CAAX motifs that are prenylated are shown in blue. The palmitoylated cysteine residues are shown in green. The polybasic region of K-Ras4B with lysine residues is shown in pink (adapted from Khan et al, 2020).

Activation of Ras proteins triggers significant conformational changes within the effector lobe's switch I and II regions which enables its effector proteins to bind selectively to the activated form (Abdelkarim *et al*, 2019; Han *et al*, 2017). Upon the activation of guanine nucleotide exchange factors (GEFs), GTP is bound and triggers conformational changes in the switch I and switch II regions, which ultimately enable effector binding (Bandaru *et al*, 2019; Pechlivanis *et al*, 2007). For this switch mechanism to occur, key residues such as Tyr32 and Thr35 in the switch I region and Gly60 in the switch II region play a critical role by forming contacts with γ-phosphate (Shima *et al*, 2010).

The second half of G-domain constitutes the allosteric lobe (aa 87–172) which exhibits approximately 80% sequence similarity (**Figure 2**). However, the C-terminal end displays substantial variation among these isoforms with regards to its last 23-24 amino acids also known as the hypervariable region (Henis *et al*, 2009). The hypervariable region (HVR) is of significant research interest due to its crucial role in defining isoforms containing differential sequences responsible for membrane interaction (Simanshu *et al*, 2017).

1.1.3. RAS SIGNALLING FROM THE PLASMA MEMBRANE

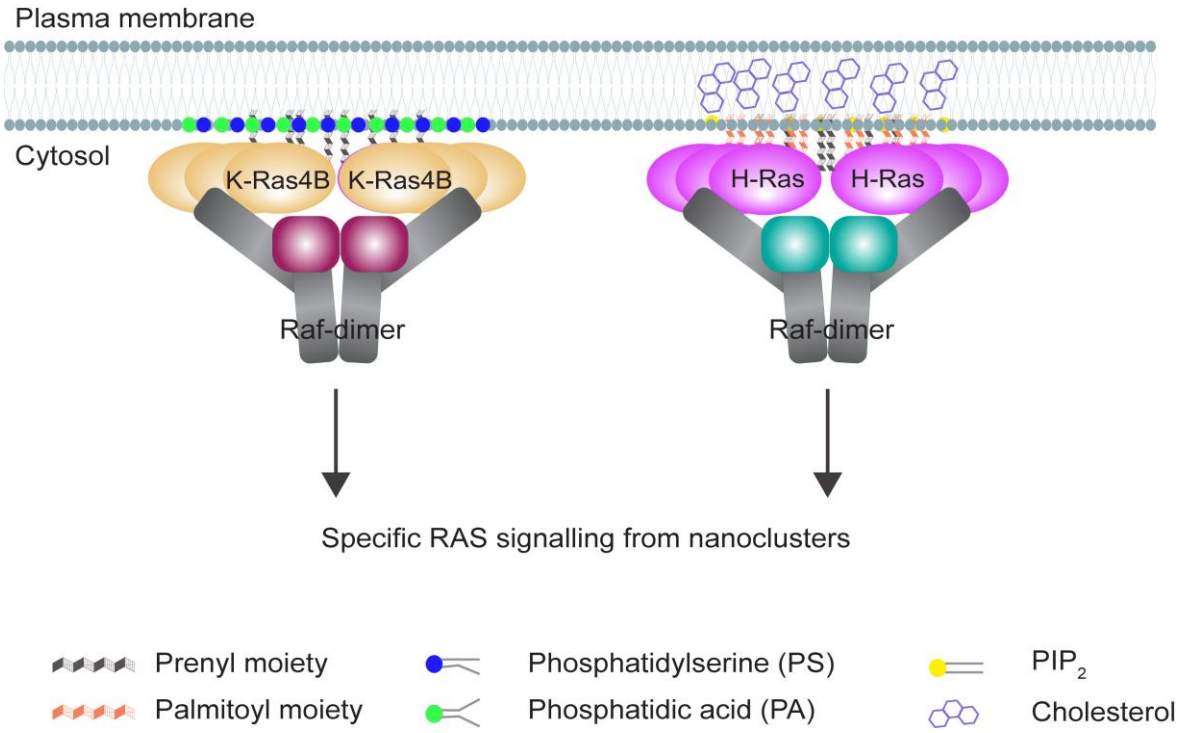

Figure 3: Ras nanocluster models. The Ras isoforms induce selective sorting with different lipid headgroups and acyl chains within nanoclusters (Adapted from Blaževitš et al, 2016; Zhou et al, 2017).

The Ras signaling cascade is initiated by activation of receptor tyrosine kinases (RTKs). When an RTK is activated, it recruits and activates a GEF such as Son of sevenless homologue 1 (SOS1), which in turn activates the Ras protein by promoting the exchange of GDP for GTP. The activated Ras protein then interacts with a variety of downstream effectors, including the Raf family of serine/threonine kinases. Raf kinases activate the downstream mitogen-activated protein kinase (MAPK) subcellular signaling pathway, which includes the activation of MEK1/2 and ERK1/2. In addition to the MAPK pathway, Ras can also activate other signaling pathways, such as the PI3K/Akt pathway, which regulates cell survival and metabolism (Vivanco & Sawyers, 2002), and the RalGDS pathway, which regulates cell proliferation and migration (Huang *et al*, 1998; Matsubara *et al*, 1999).

The Ras signaling pathway is inactivated by the activation of GAPs, which promote the hydrolysis of GTP to GDP, and the induction of inhibitors of the pathway, such as Sprouty and SPRED1 proteins (Courtois-Cox *et al*, 2006). Dysregulation of the Ras signaling pathway is a common feature of many human cancers and can occur through a variety of mechanisms, including mutations in Ras or its regulators, amplification of Ras pathway components, or overexpression of RTKs.

Proteo-lipid clusters known as nanoclusters form on the plasma membrane where Ras proteins are segregated laterally based on their intrinsic HVR differences into distinct dynamic groups with an average lifetime that varies between 0.1 s and 1 s depending on whether Ras proteins are in the inactive or active respectively (Prior *et al*, 2003). RAS nanoclusters have a specific lipid composition, which play a crucial role in facilitating the binding and activation of downstream proteins. For these RAS effectors to be effectively activated, they must synergistically bind to activated RAS molecules and specific lipids within the plasma membrane. For example, C-Raf is an effector of K-Ras4B that contains distinct domains for binding phosphatidylserine (PS, in its cysteine-rich domain) and phosphatidic acid (PA, in its C-terminus) (Zhou *et al.*, 2017). The activation and the kinase activity of C-Raf require the interaction with PS and PA lipids as well as binding of the GTP-bound active Ras (**Figure 3**) (Zhou *et al.*, 2017; Zhou *et al*, 2021). Furthermore, pre-assembling PIP2 molecules in H-Ras nanoclusters is also critical for their respective functionalities (Li & Buck, 2017). Disruption of these nanoclusters can have detrimental effects on multiple levels. Firstly, it affects the concentration of Ras molecules within the clusters, thereby reducing their efficiency in signal transduction (Van *et al*, 2021). Additionally, perturbation in nanocluster formation can alter the lipid composition between nano-domains, further compromising effector recruitment and subsequent signal transduction processes (Abankwa *et al*, 2008b).

1.1.4. CHAPERONE-MEDIATED RAS TRAFFICKING

Ras proteins are initially produced as soluble precursors on free polysomes. However, to become active and perform their biological functions, these proteins need to bind to cellular membranes or cytoplasmic protein granules (Tulpule *et al*, 2021). Therefore, they undergo a series of post-translational modifications specifically at their C-terminus which consists of one or several lipid modifications that are covalently attached (**Figure 4**) (Ahearn *et al*, 2012). The RAS protein sequence terminates with a CAAX motif, where C represents cysteine, A typically represents aliphatic amino acids, and X can be any type of amino acid(Wright & Philips, 2006). After farnesyltransferase attaches a C15 farnesyl isoprenoid lipid for catalysis to cysteine residue, the removal of -AAX sequence is facilitated by Ras Converting CAAX Endopeptidase 1 (Rce1). Then isoprenylcysteine carboxyl methyltransferase (ICMT) catalyzes the carboxy-methylation reaction on C-terminal prenylated cysteines (Ahearn *et al*, 2018). K-Ras and N-Ras can undergo prenylation by geranylgeranyltransferases (GGTases) alternatively. This enzymatic process involves the addition of a C20 geranylgeranyl isoprenoid. When a CAAX motif is terminated by either S or M, the protein is modified by FTase, while CAAX sequences ending in L are subject to

modification catalyzed by GGTase1(Seabra, 1998). K-Ras4A, N-Ras and H-Ras contain one or two cysteine residues, which undergo reversible acylation mediated by a protein palmitoyl acyltransferase (PAT) located in the Golgi (Resh, 2016). The subsequent rapid deacylation of these proteins is carried out by an enzyme known as an acyl protein thioesterase (APT1/2), resulting in their liberation for re-acylation and subsequent trafficking back to the plasma membrane (Rocks *et al*, 2005). K-Ras4B, lacking palmitoylatable cysteine residues but containing a stretch of six lysines known as the polybasic region, exhibits different subcellular trafficking compared to other isoforms such as through vesicular transport (Llavero *et al*, 2021; Zhou & Hancock, 2021).

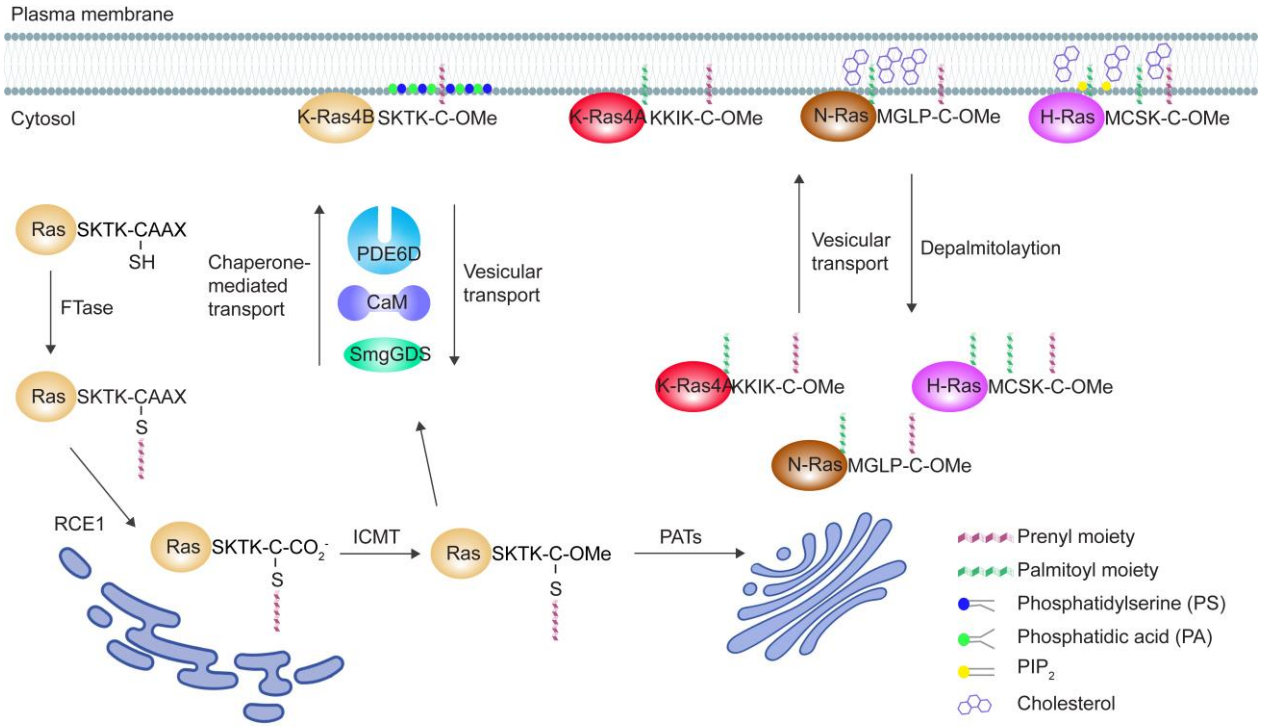

Figure 4: Post-translational modification of Ras proteins. Distinct RAS isoforms possess unique C-terminal hypervariable regions that undergo different lipid modifications. These different isoforms interact with specific lipids (Adapted from Ahearn *et al*, 2011).

Several chaperones are engaged in facilitating the trafficking of Ras proteins across cellular membranes (Cox *et al*, 2015). Some of the identified chaperones include cGMP-specific phospho-diesterase 6 delta subunit (PDE6D) (Nancy *et al*, 2002), small GDS (SmgGDS) (Berg *et al*, 2010), and calmodulin (CaM) (Ashery *et al*, 2006). CaM is a protein that plays a crucial role in various cellular activities, such as cell cycle regulation, muscular contraction, apoptosis, and cell proliferation (Tidow & Nissen, 2013). It has been reported that CaM binds to the G-domain of K-Ras4B in a nucleotide-dependent manner via the CaM-binding domain motif IN HVR (Abraham *et al*, 2009; Lopez-Alcalá *et al*, 2008). It plays a crucial role

in promoting the movement of K-Ras from the plasma membrane to the cytoplasm. This translocation process is reversible and requires calcium ions as initiators, specifically at regions within cells with lower calcium concentrations (Agamasu *et al*, 2019).

1.1.5. TRAFFICKING CHAPERONE PDE6D AND DETERMINANTS FOR PDE6D BINDING

The GDI-like solubilizing factor (GSF) PDE6D, also identified as phosphodiesterase subunit delta, is a protein which is involved in the regulation of intracellular trafficking of cyclic nucleotide phosphodiesterase 6 (PDE6), a key enzyme in the visual transduction pathway (Bender & Beavo, 2006; Nikolova *et al*, 2010). Moreover, it is involved in the regulation of intracellular trafficking of prenylated proteins to endomembrane or a specialized sensory organelles like primary cilium (Fansa *et al*, 2016; Ismail *et al*, 2012; Yelland *et al.*, 2022). The structure of PDE6D features an immunoglobulin-like β-sandwich fold, which interacts with the prenyl group of cargo (Dharmaiah *et al*, 2016; Stephen & Ismail, 2016).

The farnesyl moiety located at the C-terminus of K-Ras4B plays a role in facilitating the binding between K-Ras4B and PDE6D. The prenyl group of K-Ras4B fits into the PDE6D hydrophobic pocket characterized by an immunoglobulin-like β-sandwich fold. (Dharmaiah *et al.*, 2016; Schmick *et al*, 2014). Notably, K-Ras can interact with PDE6D regardless of whether it is in the active or inactive state (Chandra *et al*, 2011).

Structural analyses have uncovered two distinct modes of binding between K-Ras4B and PDE6D. In these modes, the farnesyl tail is alternatively inserted into the hydrophobic pocket. These structural findings imply that geranylgeranylated proteins could also interact with PDE6D (Yelland *et al.*, 2022). Furthermore, it is important to note that lack of carboxymethylation significantly reduces affinity of K-Ras4B towards PDE6D by more than 35-fold (Dharmaiah *et al.*, 2016).

The important aspect is that the interaction with PDE6D can be disrupted either by C-terminal palmitoylation or a second prenylation. According to the proposed model, for a prenylated protein to bind to PDE6D, it is suggested that the protein should feature small side-chain-containing amino acids at positions −1 and −2 relative to C-terminal Cys. It has been noted that the simultaneous occurrence of large amino acids such as Lys, Arg, and Glu at both positions may disrupt interactions with PDE6D cargo (Dharmaiah *et al.*, 2016). Another important finding is that mimicking Ras Ser181 phosphorylation through a Ser181Glu substitution significantly decreased the affinity by over 6-fold (Dharmaiah *et al.*, 2016). Moreover, binding experiments with INPP5E and RHEB S3I1 mutant shows that binding affinities of proteins could be reversed by changing the two residues that confer

high-affinity binding to PDE6D as an isoleucine at -1 position and serine at -3 position relative to C-terminal cysteine (Yelland *et al.*, 2022).

1.1.6. PDE6D- AND UNC119-MEDIATED CILIARY TRAFFICKING

It has been reported that GSFs are involved in the regulation of intracellular membrane trafficking (Stephen & Ismail, 2016) such as regulating the trafficking of small GTPases, including members of the Rab, Rho and Arf families (Singh *et al.*, 2019). Among GSFs, vertebrate genomes contain two Uncoordinated 119 (*UNC119*) genes, *UNC119A* and *UNC119B* that display 60 % sequence homology. Similar with PDE6D, they possess an immunoglobulin-like β-sandwich fold that interacts with lipid modified cargo (Wright *et al*, 2011). However, in contrast to PDE6D, UNC119 exhibits a distinct binding preference for N-terminally myristoylated cargo. These proteins play an important role in the trafficking of N-terminally myristoylated SRC, NPHP3, Cystin and G Protein Subunit Alpha Transducin 1 (GNAT1) (Garivet *et al*, 2019; Konitsiotis *et al*, 2017).

The process of sorting ciliary cargo by UNC119 and PDE6D requires the involvement of Arf-like proteins, namely the GDI-like displacement factors (GDFs) Arl2 and Arl3. Belonging to the Ras superfamily of small GTPases, these GDFs switch between GDP- and GTP-bound formations, regulated by GEFs and GAPs (Fansa & Wittinghofer, 2016). The structures of Arl2 and Arl3 are similar; however, their biochemical and biological functions differ significantly. Whereas Arl2 has a sub-micromolar affinity for PDE6D, that of Arl3 is within the nanomolar range (Fansa & Wittinghofer, 2016). Consequently, Arl2 is only able to release low affinity cargo from PDE6D, whereas Arl3 – when bound to GTP – is also able to specifically release high-affinity PDE6D cargo inside the primary cilium (Fansa & Wittinghofer, 2016). Following allosterically binding to PDE6D, these GDFs induce a conformational change within PDE6D with its cargo being squeezed out from the narrowing hydrophobic pocket (Ismail *et al*, 2011). On the other hand, Arl3 binding to UNC119 induces the opening of the UNC119 hydrophobic pocket and subsequent release of the cargo (Ismail *et al.*, 2012). Similar to PDE6D, low affinity peptides could be released from UNC119 by both activated Arl2 and Arl3, whereas high-affinity peptides could only be released by Arl3 (Jaiswal *et al*, 2016).

Finally, the N-terminal amphipathic α-helix of Arl3 has been identified as the determinant for the difference in Arl2- or Arl-3 mediated cargo release from PDE6D or UNC119. This helix has been shown to play a role in the ternary complex between Arl3-GSF-cargo and is strictly required, although not sufficient for cargo release (Fansa *et al.*, 2016; Fansa & Wittinghofer, 2016; Ismail *et al.*, 2012).

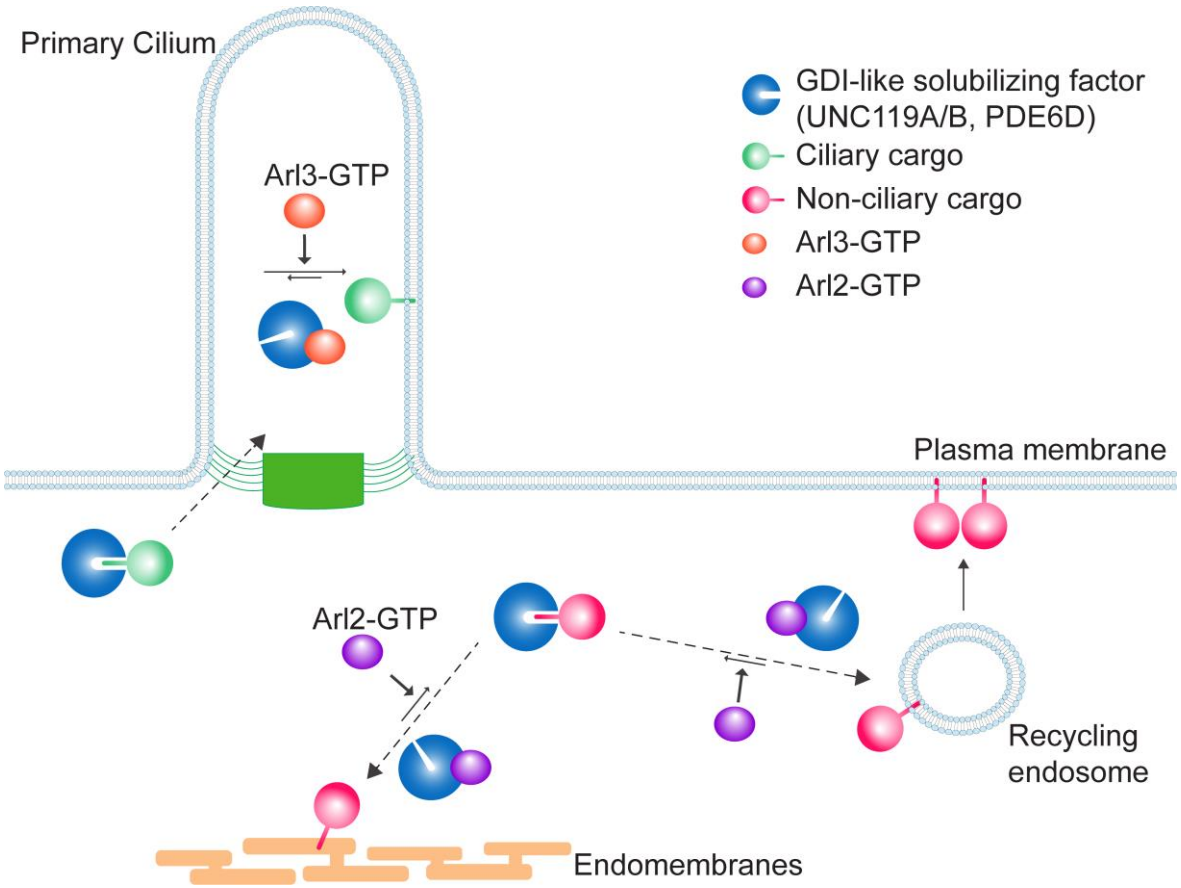

Figure 5: The cellular mechanism for organizing ciliary or non-ciliary cargo through GDI-like solubilizing factors (Adapted from Fansa et al., 2016)**.**

Activated Retinitis pigmentosa 2 (RP2) – a specific GAP for Arl3 – converts Arl3-GTP to inactive Arl3-GDP. By contrast, ADP-ribosylation factor-like 13B (Arl13B) protein acts as a guanine nucleotide exchange factor (GEF), converting inactive Arl3-GDP into active Arl3-GTP (Fansa & Wittinghofer, 2016). While RP2 is localized to ciliary base within primary cilia, Arl3 is localized mainly inside cilium (Hurd *et al*, 2011). Ciliary cargo is carried into the cilium and released by Arl3-GTP. On the other hand, non-ciliary cargo is released to cellular endomembranes and the plasma membrane via interaction of Arl2-GTP and GSFs (**Figure 5**) (Fansa & Wittinghofer, 2016; Wang *et al*, 1999).

1.1.7. Role of Ras in cancer and differentiation

Cancer is a complex and challenging public health issue that has significant impacts on millions of people worldwide. The incidence rate of cancer varies greatly across the globe, with some regions experiencing higher prevalence rates for certain types of cancer than others. According to the World Health Organization (WHO), the global burden of cancer has increased significantly in recent years, with an estimated 19.3 million new cases and 10 million deaths reported in 2020 alone (Sung *et al*, 2021) with lung, breast, colorectal,

prostate, and stomach cancers being among the most common cancer types. The projected future trajectory suggests that this trend will continue due to population growth and aging combined with changing environmental factors along with lifestyles (Ferlay *et al*, 2021).

Mutations in *RAS* genes can lead to the activation of Ras signaling pathways, resulting in uncontrolled cell growth, proliferation, and resistance to cell death signals. Mutant Ras and Ras signaling pathways are thus important targets in cancer therapy. However, developing effective therapies has been challenging, as Ras proteins are difficult to target with drugs (Hobbs *et al*, 2016; Parker & Mattos, 2018). The most common type of Ras mutations in cancer are point mutations within the *KRAS* gene, which are found in many types of cancer. The frequency of *KRAS* mutations in different cancers varies, with the highest rates observed in pancreatic, colorectal, and lung cancers. In pancreatic cancer, for example, *KRAS* mutations are found in up to 90% of cases. In colorectal cancer, *KRAS* mutations are found in approximately 40% of cases. In lung cancer, *KRAS* mutations are found in approximately 20% of non-small cell lung cancers (Prior *et al.*, 2020). Other *RAS* genes, including *HRAS* and *NRAS*, can also be mutated in cancer, but at lower frequencies than *KRAS*. *HRAS* mutations are found in some cases of bladder cancer, head and neck cancer, and squamous cell carcinoma of the skin (Chen *et al*, 2021b; Hobbs *et al.*, 2016) while *NRAS* mutations are mainly found in melanoma, leukemia, and colorectal cancer (Ahearn *et al*, 2021; Tanaka *et al*, 2021).

Embryonic stem cells have the capacity to self-renew and to differentiate into various cell types culminating in the formation of adult tissues. Inhibition of the Ras-MAPK signaling pathway has been shown to promote self-renewal of mouse embryonic stem cells (Burdon *et al*, 1999). In line, MAPK signaling was found to trigger lineage commitment of embryonic stem cells (Kunath *et al*, 2007) and was required for vertebrate neural specification (Stavridis *et al*, 2007). It is important to point out that the role of Ras in cell stemness/ differentiation is highly context dependent. Ras proteins have been described to have varying effects on differentiation depending on the cell type, the developmental stage, and the specific signaling pathways that are activated (Crespo & León, 2000). For example, in neuronal, adipocytic, and myeloid cells among others, Ras is known to promote differentiation (Crespo & Leon, 2000). On the other hand, activated K-Ras increased neural stem cell proliferation (Bender *et al*, 2015) and stimulated the expansion of an endodermal progenitor cell population and resistance to differentiation (Quinlan *et al*, 2008). In addition, oncogenic K-Ras promoted self-renewal and reduced neuronal differentiation propensity through induction of ERK signaling in human induced pluripotent stem cells (Kubara *et al*, 2018). In another study, oncogenic K-Ras induced cancer stem cell marker expression in

colorectal cancer through activation of the MAPK pathway and subsequent activation of the Wnt/β-catenin signaling pathway (Moon *et al*, 2014). Notably, oncogenic K-Ras has been demonstrated to be a key factor in maintain stemness and triggering tumor initiation through binding to calmodulin and suppressing non-canonical Wnt signaling in human pancreatic cancer (Wang *et al*, 2015a). In line, several cancer stem cell inhibitors have been found to interfere with K-Ras activity and K-Ras-Calmodulin interaction (Najumudeen *et al*, 2016). This stemness-related activity of oncogenic K-Ras could rely on its distribution to the primary cilium or the centrosome, both of which are cellular organelles that are involved in cell fate decisions (Chippalkatti & Abankwa, 2021).

1.1.8. THERAPEUTIC STRATEGIES FOR TARGETING ONCOGENIC RAS

Oncogenic Ras proteins are mutated forms of the normal Ras protein that promote uncontrolled cell growth and division, leading to cancer. Several strategies have been developed to direct inhibition or indirectly target Ras signaling and downstream pathways that are critical for cancer cell growth (Cox *et al*, 2014).

1.1.8.1. The exploration of novel binding sites and inhibition principles of RAS using direct binders (Manuscript I)

RAS has long been deemed difficult to target for drug development given its lack of apparent binding sites. To investigate the advancements in the development of direct targeted therapies for RAS inhibitors, we have analyzed both covalent and non-covalent inhibitors that have been designed to specifically target RAS (**Manuscript I, Figure 1B, p. 54**). Our analysis has been published as a comprehensive review article, which is referenced in **Manuscript I** of this thesis(Steffen *et al*, 2023). Additionally, our review explored how macromolecular binders contribute to the process of identifying and validating potential binding sites on the RAS (**Manuscript I, Figure 2, p. 56, and Table 1, p. 57**).

Upon GTP-binding, RAS have been observed to undergo conformational changes in two specific regions, known as switch I and switch II (Abankwa *et al*, 2008a). These structural alterations do not reveal any targetable binding sites on the RAS protein itself. Nevertheless, in 2013, the Shokat group made significant progress by uncovering an allosteric pocket known as switch II-pocket. Furthermore, the Gorfe group utilized computational methods in 2011 to identify four allosteric sites on RAS as P1, P2, P3 and P4 (**Manuscript I, Figure 1B, p. 54**).

In this review, we conducted an extensive analysis focusing on the identification of small molecule binders and potential avenues for future advancements in drug discovery. Employing a combination of computational and experimental methods, numerous small

molecules were discovered that exhibit binding affinity primarily towards P1 and P2 sites (**Manuscript I, Figure 1, p. 54 and Supplementary File 1**). Based on our analysis, the P2 pocket with its hydrophobic nature has emerged as a highly effective target site. It has been targeted by covalent inhibitors that specifically act on mutations such as G12C, G12S, and G12R to induce an OFF state. Furthermore, non-covalent inhibitors have also demonstrated efficacy against the G12D mutation (**Manuscript I, Figure 1A, p. 54**).

According to our analysis, the existing RAS-directed PROTACs (particularly XY-4-88, LC-2, KP-14) are all based on the G12C inhibitors (**Manuscript I, Supplementary File 1**). These degraders can selectively attract E3-ligases with varying expression levels, allowing for specific degradation of mutated variants of the RAS protein. By considering E3 ligase expression patterns within tissues and cells at different timescales, PROTACs could potentially offer more controlled drug action resulting in decreased toxicity and novel treatment approaches (Kannt & Dikic, 2021).

1.1.8.2. Inhibition of upstream proteins

An alternative approach to targeting RAS activity involves focusing on kinases or phosphatases that regulate its function. One such mediator is the tyrosine-protein phosphatase non-receptor type 11 (SHP2) which plays a role in stimulating the downstream of MAPK signal pathway (Dance *et al*, 2008). SHP099, a SHP2 inhibitor, showed low anti-proliferation effects on *KRAS* or *BRAF* mutant cell lines in vitro and it displayed promising results in vivo by reducing the size of *KRAS*-mutant tumors (Chen *et al*, 2016). Furthermore, combining MEK inhibition with SHP2 inhibition proved highly effective against engineered or xenograft models of *KRAS*-mutant pancreas, ovarian, and lung cancers. This combination strategy overcomes the rapid resistance observed with MEK inhibitors used as single therapies (Fedele *et al*, 2018; Lu *et al*, 2019).

In recent studies, the SHP2 inhibitor RMC-4630 has shown promising results in controlling disease progression in advanced NSCLC patients who have *KRAS* mutations. The use of this novel inhibitor resulted in a disease control rate of 67% (Ou *et al*, 2020). Another serine/threonine kinase STK19 plays a crucial role in N-Ras activation through phosphorylation of the N-Ras protein subsequently enhancing its binding to effectors. As a result, the inhibition of STK19 by ZT-12-037-01 effectively hinders oncogenic NRAS-mediated melanoma growth both in vitro and in vivo (Qian *et al*, 2020; Yin *et al*, 2019).

1.1.8.3. Inhibition of downstream signaling pathways

1.1.8.3.1. Inhibition of RAF kinases and MAPK cascade

To develop innovative drugs that specifically target Ras, researchers direct their attention toward the it's downstream effectors. Among these effectors, a crucial role is played by RAF kinases, which are integral components of the MAPK signaling pathway (Karoulia *et al*, 2017). Dabrafenib and vemurafenib, both inhibitors of B-Raf, have demonstrated significant efficacy in treating patients with melanoma harboring the *BRAF-V600E* mutation by disrupting aberrant MAPK signaling. Unfortunately, these same inhibitors produce a paradoxical activation in tumors carrying *KRAS* mutations and lacking *RAF* abnormalities; rather than inhibiting signaling pathways as intended, dabrafenib and vemurafenib activate the MAPK pathway (Hatzivassiliou *et al*, 2013; Hatzivassiliou *et al*, 2010; Poulikakos *et al*, 2010).

Given the lack of paradoxical activation and resistance to MEK inhibitors, there is growing interest in exploring combination therapies with MEK inhibitors. Furthermore, inhibiting the serine threonine phosphatase PP2A has been found to confer resistance to MEK inhibitors specifically in *KRAS*-mutant lung cancer cells (Kauko *et al*, 2018).

The strategy of inhibiting ERK shows promise as a therapeutic approach for the treatment of tumors with mutations in *RAS* (Germann *et al*, 2017). In mouse models carrying *KRAS* or *NRAS* mutations, SCH772984 - selectively target ERK - effectively induced regression of tumor growth (Morris *et al*, 2013). Similarly, AZD0364 demonstrated effectiveness in causing tumor regression through its ability to modulate signaling pathways dependent on ERK1/2 in xenografts sensitive to both *BRAF* and *KRAS* mutations (Flemington *et al*, 2021; Ward *et al*, 2019). Overall, inhibiting ERK signaling shows promise as a potential therapeutic approach for *RAS*-mutant cancers (Smalley & Smalley, 2018).

1.1.8.3.2. Inhibition of mTOR pathway

The activation of Ras triggers multiple signaling pathways in cells, including the PI3K/mTOR pathway. This particular pathway acts in conjunction with the MAPK cascade to regulate cell processes (Papke & Der, 2017). Consequently, researchers have explored the strategy of targeting both the MAPK and PI3K/mTOR pathways concurrently in preclinical trials. Specifically, when a combination of inhibitors that target PI3K and MEK is used, it exhibits synergistic effects by effectively inhibiting proliferation in *RAS*-mutant cells as well as causing regression of xenografted *RAS*-mutant tumors (Posch *et al*, 2013). An instance of the successful combination therapy involves NVP-BEZ235, which is a dual pan-PI3K and

mTOR inhibitor (Engelman *et al*, 2008). In vitro and in vivo studies have demonstrated that targeting the mTOR pathway, either through an mTOR inhibitor alone or in combination with other targeted inhibitors such as HDAC, Bcl-2, K-Ras, and MEK inhibitors can lead to inhibitory effects on *RAS*-driven tumors (Broutin *et al*, 2016; Chen *et al*, 2021a; Molina-Arcas *et al*, 2021).

Nevertheless, the efficacy of combining mTOR, PI3K and MEK inhibitors in clinical trials has been restricted by poorly tolerated toxicities or limited effectiveness (Bardia *et al*, 2020). The combination of GSK2126458, a pan-PI3K/mTOR inhibitor, with a MEK inhibitor displayed low efficiency in patients with solid tumors carrying *RAS/RAF/PI3K* mutations (Grilley-Olson *et al*, 2016). Another example, a phase II study assessing Everolimus (an mTOR inhibitor) in metastatic colorectal adenocarcinoma patients who had previously received chemotherapy revealed poor effectiveness (Ng *et al*, 2013).

1.1.8.4. Distrupting trafficking and correct localization of RAS proteins

Ras proteins undergo a translocation process that brings them to cellular membranes. Given the challenges associated with directly targeting Ras itself, researchers have proposed the disruption of Ras trafficking as an alternative targeting strategy (Abankwa & Gorfe, 2020). One initial approach involved the inhibition of farnesyltransferase, an enzyme responsible for modifying the CAAX motif of Ras by adding a farnesyl group. However, clinical trials exploring FTase inhibitors yielded disappointing results in cases of pancreatic cancer, which typically harbor mutations in *KRAS*. Further investigation revealed that in cells treated with FTIs, both K-Ras and N-Ras can acquire alternative prenylations via geranylgeranyltransferases (Lane & Beese, 2006; Lerner *et al*, 1997; Liu *et al*, 2010). Therefore, it is clear that focusing solely on the inhibition of FTase may not be sufficient to effectively target RAS-associated cancers. While co-inhibition of FTase and GGTase effectively halted tumorigenesis in laboratory mice models, the clinical application of such treatment was limited due to associated toxicity. Consequently, the advantages of targeting KRAS through combined inhibition of both FTase and GGTase were diminished (Kazi *et al*, 2019; Liu *et al.*, 2010).

Following post-translational modification, the cellular localization of RAS is regulated by chaperone proteins such as PDE6D and CaM (Canovas Nunes *et al.*, 2022; Hait & Lazo, 1986; Martin-Gago *et al.*, 2017a; Najumudeen *et al.*, 2016; Okutachi *et al*, 2021; Siddiqui *et al.*, 2020a).

Ophiobolin A is a potent inhibitor of CaM that suppresses spheroid formation in K-Ras mutated cancer cells (Najumudeen, 2016). Notably, OphA exhibits inhibitory activity against other molecular targets including phosphatidylethanolamine (Kong Au & Chow Leung,

1998). A recent study has described Calmirasone1 as a covalent inhibitor of CaM that is similar to OphA. Notably, Calmirasone1 exhibited a substantially higher binding affinity for CaM compared to OphA by up to four-fold. Furthermore, it displayed remarkable on-target effects and specifically blocked sphere formation driven by K-Ras while showcasing minimal non-specific cytotoxicity in cancer cell lines with *HRAS* mutations (Okutachi *et al.*, 2021).

Trafficking chaperone PDE6D facilitates K-Ras translocation to the plasma membrane. Therefore, it has been considered as a surrogate target for K-Ras. Pioneered by the Waldmann group, inhibitors that competitively bind to the prenyl-binding pocket of PDE6D were developed. However, the first two generations of these inhibitors, Deltarasin and Deltazinone1, exhibited off-target effects and inadequate metabolic stability in vivo, respectively (Papke *et al.*, 2016; Zimmermann *et al.*, 2013). Moreover, the compounds were prematurely released through an Arl2-GTP-dependent ejection mechanism. Only the Deltasonamides - their third-generation inhibitors - exhibited robustness against such ejection mediated by Arl2-GTP. This can be attributed to thorough optimization that led to sub-nanomolar affinity (Martin-Gago *et al*, 2017b). Nevertheless, the efficacy of these compounds was hindered by their insufficient cellular permeability (Klein *et al*, 2019). Notably, solely the initial compound Deltarasin exhibited in vivo anti-tumor activity among these compounds.

In more recent studies, a spiro-cyclic compound named 36l demonstrated promising efficacy against *KRAS* mutant primary cell lines when tested in vivo (Chen *et al*, 2022). In another study, the triazole 27 had nanomolar activity in a PDE6D binding assay and robustly inhibited MAPK-signaling (Chen *et al*, 2019). A Rac-inhibitor screening led to identification of DW0254 targeting the hydrophobic pocket of PDE6D with sub-micromolar activity. The compound suppressed Ras downstream signaling and showed anti-tumor activity in vivo. However, its effectiveness was reduced by inadequate solubility (Canovas Nunes *et al.*, 2022).

1.2. SYNOPSIS - RESULTS AND DISCUSSION

1.2.1. ELIMINATING ONCOGENIC RAS: BACK TO THE FUTURE AT THE DRAWING BOARD (MANUSCRIPT I)

The **1.1.8.1. chapter** of the synopsis-introduction extensively explores and discusses the analysis results related to **Manuscript I** under the topic "Therapeutic strategies for targeting oncogenic Ras". Additionally, it has been extensively studied and thoroughly discussed in **Manuscript I** within the Results section.

1.2.2. AN IMPROVED PDE6D INHIBITOR COMBINES WITH SILDENAFIL TO SYNERGISTICALLY INHIBIT KRAS MUTANT CANCER CELL GROWTH (MANUSCRIPT II)

1.2.2.1. Development of novel PDE6D inhibitors (II)

In a previous study, we successfully produced PDE6D inhibitors (PDE6i) using a hexamethylene-amide-backbone (Siddiqui *et al.*, 2020a). Building upon this backbone, we developed an in-silico library of hybrid compounds incorporating elements from established PDE6Di inhibitors. These known inhibitors also served as control compounds for our research (**Manuscript II, Figure 1A, p. 70**). A total of 313 compounds were generated in the first round and underwent computational docking with PDE6D. Compounds that exhibited favorable docking scores were selected for further analysis (**Manuscript II, Figure 1B 1C, p. 70; SI Data 1 and 2**). The results obtained from computational docking revealed that **4** and **15** revealed multiple van-der-Waals contacts to residues Met20, Arg61, Gln78, and Tyr149 (**Manuscript II, Figure 1D, E, p. 70**). Hydrogen bonds to these residues were only predicted for compound **15** with Arg61 and Gln78 (**Manuscript II, Figure 1E, p. 70**).

1.2.2.2. In vitro affinity and quantification of target engagement and K-Ras-selectivity (II)

To determine the affinities of our compounds for PDE6D, we utilized the FITC-labelled PDE6D-binder Atorvastatin (F-Ator) and FITC-labelled Rheb (F-Rheb) (**Manuscript II, SI Data 2**). The utilization of F-Ator as a probe resulted in the low nanomolar range affinities for reference compounds. Conversely, affinities fell within the sub-micromolar range using F-Rheb (**Manuscript II, SI Data 2**). However, both datasets exhibited a correlation and were used to assess the in vitro potencies of our 16 compounds. In following discussions, we will

primarily consider the values obtained with F-Ator (**Manuscript II, Figure S 1A, p. 151, SI Data 2**).

To investigate the disruption of the PDE6D/ K-Ras interaction and loss of plasma membrane organization of K-Ras we applied the BRET (Bioluminescence Resonance Energy Transfer) assays in HEK293-EBNA cells (**Manuscript II, Figure 2A, p. 73**). We implemented a BRET-assay with Rluc8-PDE6D and GFP2-K-RasG12V to examine on-target activity of our compounds (**Manuscript II, Figure 2A, p. 73; SI Data 2**).

In the context of cellular activity, the IC50-values were within the micromolar range. (**Manuscript II, SI Data 2**). However, for dose-response data analysis, we primarily utilized a more precise normalized area under the curve DSS3-score (Yadav *et al*, 2014). Notably, our DSS analysis showed a significant increase in potencies from the first to the second round of compounds (**Manuscript II, Figure 2A, p. 73**). Next, to assess K-Ras-membrane anchorage disruption and K-Ras-selectivity, we applied the BRET that emerges between a Rluc8- and GFP2-tagged RasG12V (**Manuscript II, Figure S 1B, p. 151**).

When the prenylated proteins such as dually palmitoylated H-Ras undergo palmitoylation, their ability to bind with PDE6D is diminished (Chandra et al., 2011; Dharmaiah et al., 2016). Therefore, loss of PDE6D function through siRNA-mediated knockdown, leads to selective decrease in the BRET-signal of K-RasG12V, but not of H-RasG12V (**Manuscript II, Figure S 1B-D, p. 151**). The data from BRET assays demonstrated enhanced potency amongst the second-round compounds (**Manuscript II, Figure 2A, p. 73; SI Data 2**). Among the tested compounds, compound **4** from the first round and compound **15** from the second round displayed the best overall K-RasG12V-selectivity (**Manuscript II, Figure 2B, p. 73**) compared to the most selective reference compound Deltazinone1 (**Manuscript II, Figure 2C-E, p. 73**).

1.2.2.3. Evaluation of the off-target activity (II)

Although several compounds effectively inhibited PDE6D, they did not demonstrate an exclusive K-Ras selectivity (**Manuscript II, Figure 2B, p. 73**). It could be attributed to off-target activities, a concern that has been previously observed with other PDE6Di. To assess broad off-target effects, we compared the anti-proliferative effect of these compounds on cells both with and without the target. Therefore, we specifically examined the anti-proliferative effects on MEF cells with a homozygous CRISPR-mediated PDE6D knockout (KO) in comparison to wild type (WT) (Dewees et al., 2022) (**Manuscript II, Figure S 1E, p. 151**). Consistent with the data on K-RasG12V-selectivity obtained through BRET analysis (**Manuscript II, Figure 2B, p. 73; Figure S 1F, p. 151**), first-round compounds demonstrated a higher PDE6D-selectivity compared to second-round compounds. Notably,

compound **4** exhibited again the highest overall selectivity (**Manuscript II, Figure 3A, p. 75**).

UNC119A serves as a trafficking chaperone for myristoylated proteins and structurally homologous to PDE6D (Fansa et al., 2016). This suggests that UNC119A could potentially be an off-target for PDE6D inhibitors. To examine the off-target activity directed towards UNC119A, we developed a BRET-assay to examine if the selected compounds interfered with the UNC119A/ Src interaction.

In BRET-titration experiments, the BRET ratio at the defined acceptor-to-donor ratio, known as BRETtop, serves as an indicator of complex stability (Manoharan et al., 2023). Squarunkin A, an UNC119A inhibitor, significantly decreased the BRETtop between UNC119A-Rluc8 and Src-GFP2 (**Manuscript II, Figure S 1G, p. 151**) (Garivet et al., 2019). Likewise, the N-myristoyl-transferase inhibitor IMP-1088 treatment reduced the BRETtop (Mousnier et al., 2018) (**Manuscript II, Figure S 1G, p. 151)** which confirms that our assay can detect the interference between UNC119A/ Src interaction. Interestingly, reference compounds Deltarasin and Deltasonamide1, but not Deltazinone1, significantly reduced the BRETtop which suggests off-target activity (**Manuscript II, Figure 3B, p. 75**). In contrast, none of our top first-round compounds showed off-target binding to UNC119A (**Manuscript II, Figure 3C, p. 75**), while the second-round compounds did, with 15 having the least effect (**Manuscript II, Figure 3D, p. 75**).

1.2.2.4. Top compounds inhibit RAS-signaling and cell proliferation (II)

Next, we proceeded with our selectivity evaluation by conducting experiments to assess the anti-proliferative activity of our selected compounds on *KRAS-, HRAS-* or *BRAF*-mutant cancer cells. Correlated with BRET-data (**Manuscript II, Figure 2A, p. 73**), the anti-proliferative activity of second round compounds were significantly increased, with cellular potencies increasing to the low- and sub-micromolar range (**Manuscript II, Figure 4A, p. 77; SI Data 2**), but this comes at the cost of selectivity (**Manuscript II, Figure 4B, p. 77**). In contrast to top compounds from second round, **4** exhibited the overall highest K-Ras selectivity (**Manuscript II, Figure 4B, p. 77; Figure S 1H, p. 151**) and lowest off-target activity (**Manuscript II, Figure 3, p. 75**) consistent with BRET assays. As a result, compound **4** surpassed the most selective reference compound, Deltazinone1, ~6-fold. Highest activity of **4** is observed in highest KRAS- and PDE6D-dependent MIA PaCa-2 cells (IC50 = 6 ± 1 µM; **Manuscript II, SI Data 2, Figure S 1H, p. 151**).

As supported by previous studies (Papke et al., 2016; Zimmermann et al., 2013), the reduction in pERK- (**Manuscript II, Figure 4C, p. 77**) and pS6-levels (**Manuscript II, Figure 4D, p. 77**) was not significant in MIA PaCa-2 cells upon treatment with our top compounds.

This reduction was superior to that observed with the best reference compound Deltazinone1.

1.2.2.5. Combinations of the Deltaflexin3 and Sildenafil synergize to inhibit K-Ras (II)

Sildenafil, which is an approved inhibitor of PDE5, stimulates the PKG2-dependent phosphorylation of Ser181 of K-Ras (Cho et al., 2016). It has been demonstrated that the phosphomimetic K-Ras-S181E mutation decreases the affinity to PDE6D ~6-fold (Dharmaiah et al., 2016). Therefore, the treatment with Sildenafil would also result in a decrease in the affinity. To enhance the anti-tumorigenic activity of Deltaflexin3, we combined it with Sildenafil. The findings from a comprehensive analysis of over 150 small GTPases indicate that Sildenafil could impact on PDE6D engagement of only 15 other known or predicted cargo proteins of PDE6D have serine or threonine residues in the upstream of the prenylated cysteine (**Manuscript II, SI Data 3**).

The data from BRET assay demonstrated that Sildenafil dose-dependently reduced the BRET-signal of PDE6D/ K-RasG12V-complex (IC50 ~17 µM) (**Manuscript II, Figure 5A, p. 80**). To evaluate the synergism, we combined Deltaflexin3 with Sildenafil at various concentrations (**Manuscript II, Figure 5A, B, p. 80**). The highest synergistic activity was observed at ~900 nM Deltaflexin3 and ~20 µM Sildenafil (**Manuscript II, Figure 5B, p. 80**). We evaluated the anti-proliferative effects of this combinatorial treatment in five KRAS-mutant and PDE6D-dependent cancer cell lines with different PDE6D- and PRKG2-dependency levels (**Manuscript II, Figure 5C, p. 80, Figure S 1H, p. 151**). The highest HSA synergism score was observed in MIA PaCa-2 cells (**Manuscript II, Figure 5C, D, p. 80**) at similar concentrations comparable to those used in the BRET assay (**Manuscript II, Figure 5B, D, p. 80**).

Based on 2D proliferation data indicating a potential synergistic effect of Deltaflexin3 and Sildenafil, our research was directed towards examining their impact on MIA PaCa-2 cells. To assess the impact of the combination treatment on downstream signaling of Ras. The concentrations of 20-30 µM Sildenafil and 10 µM Deltaflexin3 did not demonstrate a significant decrease in pERK- (**Manuscript II, Figure 6A, p. 81**) or pS6-levels (**Manuscript II, Figure 6B, p. 81**). Interestingly, the combinatorial treatment of 10 µM Deltaflexin3 and 20 µM Sildenafil leads to a significant decrease in both pERK and pS6 levels by ~ 28 % and ~ 35 %, respectively.

Subsequently, effect of Deltaflexin3 on the anti-tumor activity was assessed by utilizing chorioallantoic membrane (CAM) assay, that chorioallantoic membrane of fertilized chick eggs are utilized to form microtumors (Lokman et al., 2012; Siddiqui et al., 2021). In MDA-

MB-231 cells, 10 µM Deltaflexin3 alone significantly reduced microtumors (**Manuscript II, Figure S 1I, p. 151**), while a concentration as low as 2.5 µM of Deltaflexin3 demonstrated significant decrease in MIA PaCa-2 derived microtumors (**Manuscript II, Figure 6C, D, p. 81**). Consistent with 2D proliferation assay results, poorer response of MDA-MB-231 to Deltaflexin3 is observed (**Manuscript II, Figure 4A, p. 77**). Furthermore, combination of Deltaflexin3 and Sildenafil more potently reduced MIA PaCa-2 derived microtumor growth aligned with the increased synergistic effect observed in BRET-, signaling- and proliferation-assays, (**Manuscript II, Figure 6 C, D, p. 81**).

1.2.3. CILIARY K-RAS PROTECTS C2C12 PROGENITORS FROM DIFFERENTIATION (MANUSCRIPT III)

1.2.3.1. The targeting primary cilia with the high affinity chimeric K-Ras leads to a reduction in MAPK signaling (III)

The understanding of how KRAS influences cancer stemness and the potential approach to target this activity remains incomplete in scientific research. Our study aimed to analyze the distribution patterns of various KRAS variants within centriolar organelles, which are involved in regulating stemness, as well as investigating their impact on the differentiation process. Given that PDE6D is a major trafficking chaperone of ciliary cargo and that K-Ras has been observed in primary cilia, we focused on examining the molecular mechanism of PDE6D and K-Ras collaboration within centriolar organelles, known to play a role in regulating stemness, as well as investigating their impact on the differentiation. To investigate the potential for alternative transport to both the plasma membrane and PC/centrosomes, we examined myristoylated constructs to assess how different localization patterns of these variants affect MAPK signaling and cell differentiation. To enhance the ability of K-Ras4B to interact with UNC119A and UNC119B instead of PDE6D, novel chimeric expression constructs were developed. This involved substituting the cystine residue at the C-terminus with a serine residue in order to prevent carboxymethylation and prenylation. Additionally, an N-terminal myristoylation site composed of 16 amino acids was introduced to the N-terminus of K-Ras from both low affinity cargo Src and high affinity cargo NPHP3 proteins (**Manuscript III, Table 6**). Consequently, this modified version of K-Ras4B exhibited enhanced binding capabilities towards UNC119 proteins. According to the findings from BRET assays, it has been determined that myristoylated chimeric KRas4B constructs primarily interact with UNC119A rather than PDE6D (**Manuscript III, Figure6, p. 39**). Subsequently, I demonstrated that increasing the binding affinity of the chimeric construct towards both UNC119A (**Manuscript III, Figure7a, p. 40**) and UNC119B (**Manuscript III,**

Figure7b, p. 40) results in an increase in BRETtop values. This indicates a stronger interaction between the donor-acceptor pairs.

To investigate the effect of enforced primary cilium targeting with the high-affinity chimeric K-Ras mutant on Ras downstream signaling we have applied immunoblotting. The expression of GFP alone, which was employed as a negative control in this experiment, did not lead to phosphorylation of ERK (**Manuscript III, Figure7c, p. 40**). Conversely, when considering K-RasG12C as the reference condition (an oncogenic variant), it resulted in the highest signal for pERK (**Manuscript III, Figure7c, p. 40**). To further validate our findings and rule out any potential confounding factors, we also included another control condition where cells transfected with K-RasG12C were treated with an inhibitor specific to G12C called AMG 510 for a duration of 16 hours. This treatment led to a significant decrease in the pERK signal, thus confirming that the observed phosphorylation of ERK is indeed attributed to signaling mediated by K-Ras (**Manuscript III, Figure7c, p. 40**). According to our result, the co-expression of Unc119B with K-RasG12C resulted in a slight, but not statistically significant, increase in pERK levels. Interestingly, the presence of UNC119B did not affect MAPK signaling when co-expressed with Myr(SRC)-K-Ras-G12C. However, it significantly decreased ERK phosphorylation induced by high affinity Myr(NPHP3)-K-Ras-G12C (**Manuscript III, Figure7c, p. 40)**.

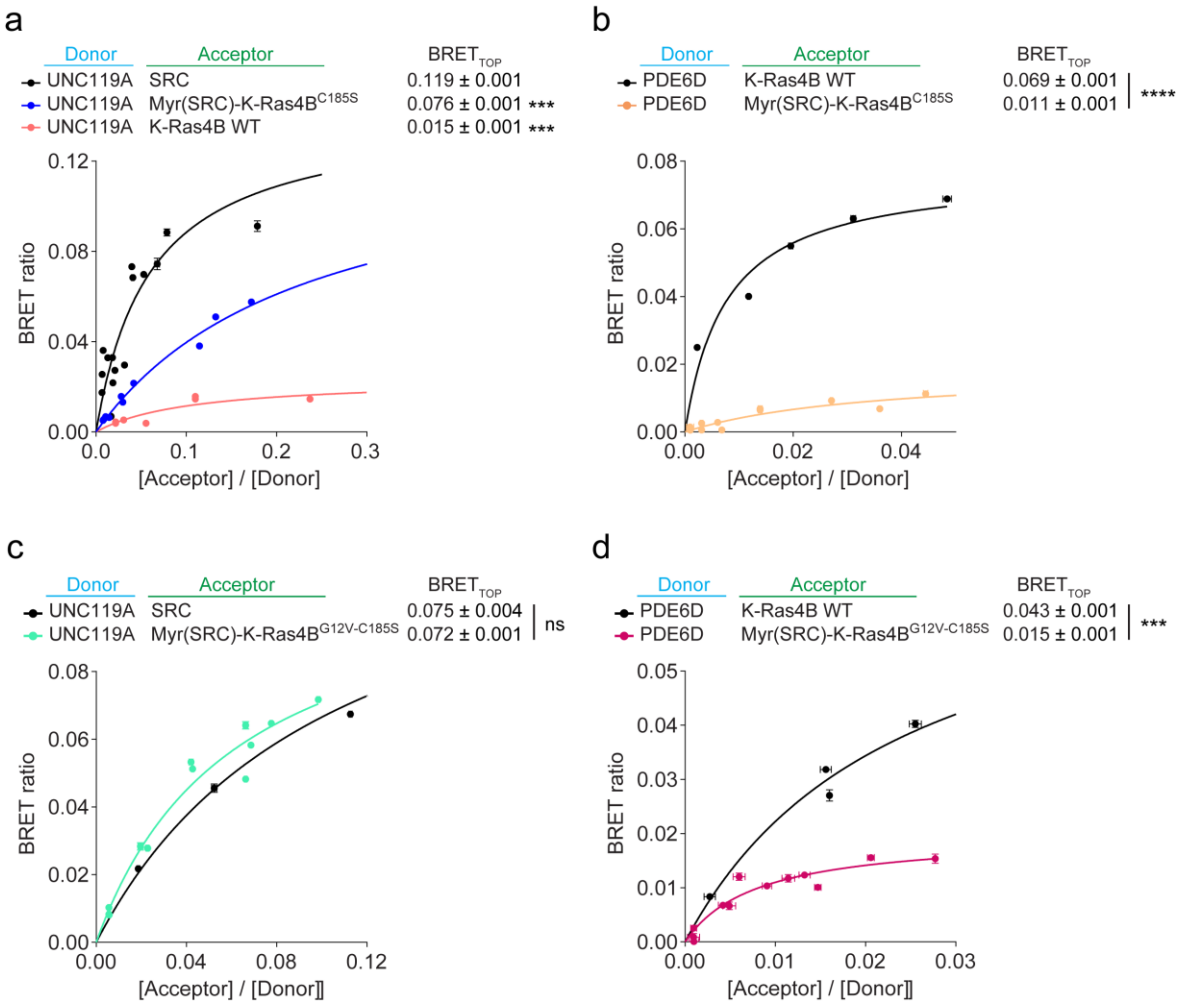

Figure 6: Myristoylated chimeric KRas4B constructs interact with UNC119A but not PDE6D in HEK293 EBNA cells. HEK293 EBNA cells were co-transfected with RLuc8-tagged PDE6D or UNC119A/B and GFP2-tagged KRas4B, SRC or chimeric constructs (donor: acceptor plasmid ratio from 1:0 to 1:40). Values represent the mean ± SEM of 2 independent biological repeats. Statistical significance levels are annotated in the plots as * = p < 0.05; ** = p < 0.01; *** = p < 0.001; **** = p < 0.0001.

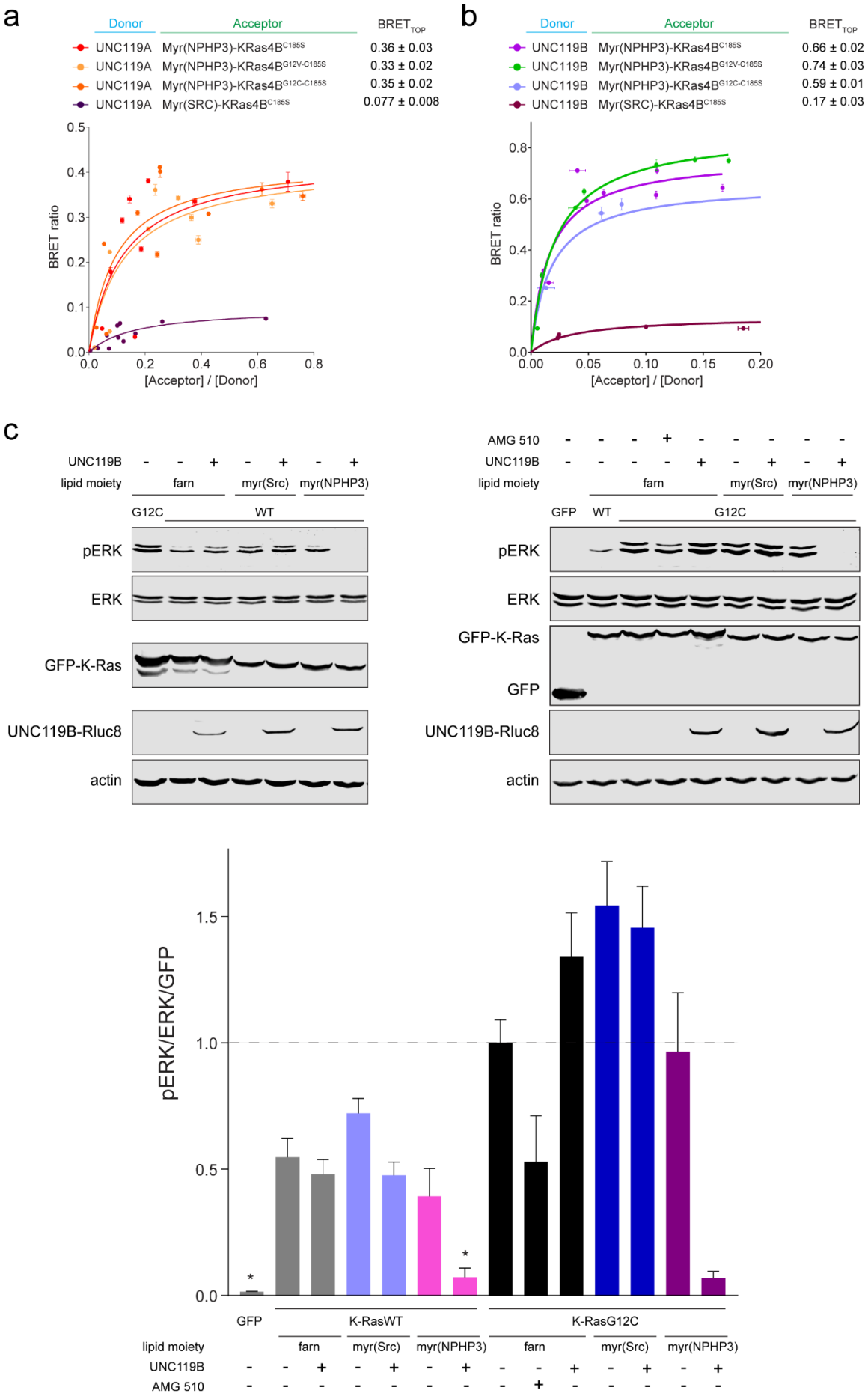
a
Donor
Acceptor
BRET$_{TOP}$
UNC119A Myr(NPHP3)-KRas4B^{C185S} 0.36 ± 0.03
UNC119A Myr(NPHP3)-KRas4B$^{G12V-C185S}$ 0.33 ± 0.02
UNC119A Myr(NPHP3)-KRas4B$^{G12C-C185S}$ 0.35 ± 0.02
UNC119A Myr(SRC)-KRas4B^{C185S} 0.077 ± 0.008
BRET ratio
[Acceptor] / [Donor]
b
Donor
Acceptor
BRET$_{TOP}$
UNC119B Myr(NPHP3)-KRas4B^{C185S} 0.66 ± 0.02
UNC119B Myr(NPHP3)-KRas4B$^{G12V-C185S}$ 0.74 ± 0.03
UNC119B Myr(NPHP3)-KRas4B$^{G12C-C185S}$ 0.59 ± 0.01
UNC119B Myr(SRC)-KRas4B^{C185S} 0.17 ± 0.03
BRET ratio
[Acceptor] / [Donor]
c
UNC119B
lipid moiety
farn
myr(Src)
myr(NPHP3)
G12C
WT
pERK
ERK
GFP-K-Ras
UNC119B-Rluc8
actin
AMG 510
GFP
pERK/ERK/GFP
K-RasWT
K-RasG12C

Figure 7: Coexpression of UNC119B with high-affinity Myr(NPHP3)K-Ras constructs disrupts Ras-dependent signaling. Enhancing the binding affinity of the chimeric construct to (a) UNC119A and (b) UNC119B leads to an elevation in BRETtop, which denotes stronger interaction between the donor-acceptor pairs. HEK293 EBNA cells were co-transfected with RLuc8-tagged UNC119A/B and GFP2-tagged chimeric constructs (donor: acceptor plasmid ratio from 1:0 to 1:40). Values represent the mean ± SEM of 2 independent biological repeats. (c) HEK293 ebna c18 cells were transiently transfected with GFP-tagged K-Ras constructs with or without co-transfection of an Rluc8-tagged UNC119B construct. Transfection of GFP alone was performed as a negative control. Blot analysis was performed for phospho-ERK (pERK) and total ERK, as well as for GFP and luciferase expression, respectively. Actin staining was carried out as a loading control. Treatment with 10 µM AMG 510 was performed for 16 h. Values represent the mean ± SEM of n = 3 independent biological repeats. Statistical significance levels were evaluated by comparison to the control condition (farnesylated K-RasG12C) and are annotated as * $p < 0.05$.

2. MATERIALS AND METHODS

2.1. MATERIALS

Table 1: List of cell lines

Cell line	Tissue / Tumor type	Mutation	Manuscript
Human cell line, HEK293-EBNA	Human embriyonic kidney	-	II, III
Human cell line, HEK293-EBNA c18	Human embriyonic kidney	-	III
Human cell line, SW620	Large intestine/ Carcinoma	KRAS-G12V	II
Human cell line, MIA PaCa-2	Pancreas/ Carcinoma	KRAS-G12C	II, III
Human cell line, cell line, PANC-1	Pancreas/ Carcinoma	KRAS-G12D	II
Human cell line, MDA-MB-231	Breast/ Carcinoma	KRAS-G13D	II
Human cell line, NCI-H358	Lung/ NSCLC Adeno	KRAS-G12C	II
Human cell line, SW480	Large intestine/ Carcinoma	KRAS-G12V	II
Human cell line, Hs 578T	Breast/ Carcinoma	HRAS-G12D	II
Human cell line, T24	Urinary tract/ Carcinoma	HRAS-G12V	II
Human cell line, IGR-39	Skin/ Melanoma	BRAF-V600E	II
Mouse cell line, WT MEF	Mouse embryonic fibroblasts	-	II
Mouse cell line, PDE6D KO MEF	Mouse embryonic fibroblasts	-	II

Table 2: List of antibodies

Antibodies	**Manuscript**
Phospho-p44/42 MAPK (Erk1/2) (Thr202/Tyr204) (E10) Mouse mAb	II, III
p44/42 MAPK (Erk1/2) Rabbit pAb	II, III
Phospho-S6 Ribosomal Protein (Ser235/236) (D57.2.2E) XP Rabbit mAb	II
S6 Ribosomal Protein (54D2) Mouse mAb	II
Mouse monoclonal anti-β-actin clone AC-15	II, III
Mouse monoclonal PDE6D (E-7)	II
RLuc8 or UNC119	III
Rabbit polyclonal anti-GAPDH	II
IRDye 680RD goat anti-rabbit IgG	II, III
IRDye 800CW donkey anti-mouse IgG	II, III

Table 3: List of compounds and peptides

Compound / Peptide	**Source**	**Manuscript**
Fluorescein-labelled Atorvastatin (F-Ator)	Piramal Pharma Solutions custom synthesis as in (Zimmermann *et al.*, 2013)	II
Fluorescein-labelled Rheb (F-Rheb)	Described in (Ismail *et al.*, 2011)	II
Benzethonium chloride	Sigma-Aldrich	II
AMG 510	MedChem Express	II, III
ARS-1620	MedChem Express	II
FTI-277 hydrochloride	VWR chemicals	II
Deltazinone1	Piramal Pharma Solutions custom synthesis as in (Papke *et al.*, 2016)	II
Deltarasin	Selleck Chemicals	II
Deltasonamide1	Piramal Pharma Solutions custom synthesis as in (Martin-Gago *et al.*, 2017a)	II
Mevastatin	Alfa Aesar by Thermo Fisher Scientific	II
Trametinib	MedChem Express	II

Vemurafenib (PLX4032, RG7204)	Selleck Chemicals	II
Squarunkin A	Axon Medchem	II
IMP-1088	Cayman Chemicals	II
Atorvastatin (calcium salt hydrate)	Cayman Chemicals	II
Sildenafil	MedChem Express	II
Tadalafil	MedChem Express	II
Deltaflexin-2	(Siddiqui *et al.*, 2020a)	II
1	Kaya et al., 2023	II
2		II
3		II
4 (Deltaflexin3)		II
5		II
6		II
7		II
8		II
9		II
10		II
11		II
12		II
13		II
14		II
15		II
16		II

Table 4: List of oligonucleotides and recombinant DNA

Oligonucleotides / Recombinant DNA	**Manuscript**
ON-TARGETplus SMARTpool siRNA Human PDE6D 5147 4 targets	II
ON-TARGETplus SMARTpool siRNA mouse PDE6d 4 targets	II
Hs_FNTA_6 CCGGGATGCTATTGAGTTAAA	II
Negative Control siRNA AATTCTCCGAACGTGTCACGT	II
C413-E36_CMV promoter, Addgene, #162927	II, III
C453-E04_CMV promoter, Addgene, #162973	II, III
pDest-305, Addgene, #161895	II, III
pDest-312, Addgene, #161897	II, III
C231-E13_Rluc8-stop, Addgene, FNL Combinatorial Cloning Platform, Kit # 1000000211	II, III
C511-E03_Rluc8-no stop, Addgene, FNL Combinatorial Cloning Platform, Kit # 1000000211	II, III
pDONR235-GFP2_stop	II, III
pDONR257-GFP2_no stop	II, III
Hs. KRa4B G12V, Addgene, #83132	II, III
Hs. HRas G12V, Addgene, #83184	II
Hs.PDE6D, Addgene, #159689	II, III
UNC119A (without stop codon), Genecust	II, III
UNC119B (without stop codon), Genecust	III
Src (without stop codon), Genecust	II, III
Myr(Src)-K-Ras4B-C185S	III
Myr(Src)-K-Ras4B-G12V-C185S	III
Myr(Src)-K-Ras4B-G12C-C185S	III
Myr(NPHP3)-K-Ras4B-C185S	III
Myr(NPHP3)-K-Ras4B-G12V-C185S	III
Myr(NPHP3)-K-Ras4B-G12C-C185S	III
pDest305-CMV-GFP2-K-Ras4B-G12V	II, III
pDest305-CMV-Rluc8-K-Ras4B-G12V	II
pDest305-CMV-GFP2-H-Ras-G12V	II

pDest305-CMV-RLuc8-H-Ras-G12V	II
pDest312-CMV-Rluc8-PDE6D	II, III
pDest312-CMV-UNC119A-Rluc8	II, III
pDest312-CMV-UNC119B-Rluc8	II, III
pDest312-CMV-SRC-GFP2	II, III
pDest305-CMV-GFP2-K-Ras4B	III
pDest305-CMV-GFP2-K-Ras4B-G12C	III
pDest312-CMV-Myr(SRC)-K-Ras4BC185S-GFP2	II, III
pDest312-CMV-Myr(NPHP3)-K-Ras4BC185S-GFP2	II, III
pDest312-CMV-Myr(NPHP3)-K-Ras4B-G12C-C185S-GFP2	II, III
pDest312-CMV-Myr(NPHP3)-K-Ras4B-G12V-C185S-GFP2	II, III
pDest305-CMV-GFP2-RHEB	II
pDest305-CMV-RLuc8-RHEB	II
pcDNA3.1(+)	II, III
pDest-His6-MBP-PDE6D	II

2.2. METHODS

Table 5: List of methods

Methods	Manuscript
In silico docking of compounds	II
Expression and purification of PDE6D	II
Fluorescence polarization (FP) assay	II
BRET assay	II, III
2D Cell proliferation assay	II
ATARiS Gene sensitivity score	II
Drug sensitivity score (DSS) analysis	II
Synergism analysis	II
Immunoblotting	II, III
Chorioallantoic membrane (CAM) assay	II

2.2.1. EXPRESSION CONSTRUCTS

Multi-site Gateway cloning technology was utilized to create expression constructs as described (**Table 6**) (Wall et al., 2014). Three entry clones with compatible LR recombination sites, encoding the CMV promoter, Rluc8 or GFP2 tag and a gene of interest, were received either from the Ras-Initiative (K-Ras4BG12V, H-RasG12V both from the RAS mutant clone collection, kit #1000000089 and PDE6D #R702-E30) or by custom synthesis from GeneCust (Src, UNC119A, UNC119B). The cDNAs encoding human c-Src kinase and human UNC119A/B inserted in the pDONR221 vector were obtained from GeneCust. Chimeric myristoylated K-Ras variants were ordered as gBlocks gene fragments from Integrated DNA Technologies. Then the gBlocks gene fragments were inserted to pDON221 vector using Gateway BP Clonase II enzyme mix (#11789020, Thermo Fisher Scientific) to create entry clone for gene of interest.

2.2.2. *BIOLUMINESCENCE RESONANCE ENERGY TRANSFER (BRET) ASSAY*

the concentration of donor plasmid UNC119A-Rluc8 (50 ng) was kept constant for the BRET donor saturation titration experiments. Then the concentration of acceptor plasmids Src-GFP2 or GFP2-tagged myristoylated chimeric constructs were increased from 0 to 1,000 ng. The pcDNA3.1 plasmid was used to complete the total DNA amount to 1050 ng. BRET assays were essentially performed as described before by us (Manoharan et al., 2023; Manoharan et al., 2022; Okutachi et al., 2021).

Table 6: Expression constructs generated by multi-site gateway cloning system.

Recombinant plasmid	Entry clone 1	Entry clone 2	Entry clone 3	Destination Plasmid
pDest305-CMV-RLuc8-PDE6D	C413-E36_CMV promoter	Hs.PDE6D	C511-E03_Rluc8-no stop	pDest-305
pDest312-CMV-UNC119A-RLuc8	C453-E04_CMV promoter	UNC119A (without stop codon)	C231-E13_Rluc8-stop	pDest-312
pDest312-CMV-UNC119B-RLuc8	C453-E04_CMV promoter	UNC119B (without stop codon)	C231-E13_Rluc8-stop	pDest-312
pDest312-CMV-SRC-GFP2	C453-E04_CMV promoter	SRC (without stop codon)	pDONR235-GFP2_stop	pDest-312
pDest305-CMV-GFP2-K-Ras4B	C413-E36_CMV promoter	Hs. KRa4B G12V	pDONR257-GFP2_no stop	pDest-305
pDest312-CMV-Myr(SRC)-K-Ras4BC185S-GFP2	C453-E04_CMV promoter	pDonor221_Myr(SRC)-K-Ras4BC185S	pDONR235-GFP2_stop	pDest-312
pDest312-CMV-Myr(NPHP3)-K-Ras4BC185S-GFP2	C453-E04_CMV promoter	pDonor221_Myr(NPHP3)-K-Ras4BC185S	pDONR235-GFP2_stop	pDest-312
pDest312-CMV-Myr(NPHP3)-K-Ras4B-G12C-C185S-GFP2	C453-E04_CMV promoter	pDonor221_Myr(NPHP3)-K-Ras4BC185S	pDONR235-GFP2_stop	pDest-312
pDest312-CMV-Myr(NPHP3)-K-Ras4B-G12V-C185S-GFP2	C453-E04_CMV promoter	pDonor221_Myr(NPHP3)-K-Ras4BC185S	pDONR235-GFP2_stop	pDest-312

3. RESULTS

3.1. Eliminating oncogenic RAS: back to the future at the drawing board (I)

Candy Laura Steffen[#], **Pelin Kaya[#],** Elisabeth Schaffner-Reckinger[#], Daniel Abankwa

Status: published

Personal contributions of Pelin Kaya

- Conducted literature search pertaining to small molecules that bind to Ras proteins, as well as molecular glues and PROTACs to generate **Figure 1C** and **Supplementary File 1**.
- Involved in discussions and drafting of corresponding data contribution.

Manuscript I: Introduction

In recent years, significant progress has been made in the development of drugs targeting Ras. Notably, the approval of the first direct KRAS inhibitor in 2021 represents a major milestone (Nakajima *et al*, 2022). Despite this clinical achievement with covalent KRAS-G12C inhibitors, acquired resistance to inhibitors often arise as is commonly observed with targeted therapies. Ras is considered "undruggable" due to its lack of obvious pockets amenable to pharmacological intervention, alternative strategies have emerged to tackle this oncoprotein (Molina-Arcas *et al.*, 2021). In this concise review, we present an overview of these approaches that directly target four distinct sites on RAS from different perspectives (Steffen *et al.*, 2023).

Our analysis aims at examining the significant discoveries made in the advancement of Ras inhibitors as targeted therapies. The focus will be on both covalent and non-covalent inhibitors that have been developed to specifically target distinct alleles of *RAS*. Furthermore, we investigated how macromolecular binders play a role in identifying and confirming potential binding sites on the Ras protein. Lastly, we offer insights into prospects within this domain of research about drug discovery based on small molecule binders. Recent progress in this field suggests two potential pathways for further advancements. Firstly, non-covalent inhibitors could be developed by expanding research on covalently binding compounds that have demonstrated effectiveness in targeting Ras as therapeutic agents (Feng *et al*, 2019; Hocker *et al*, 2013). Secondly, reversible small molecule binders present new opportunities for novel targeting strategies, such as the utilization of degraders against Ras. These degraders can selectively recruit E3-ligases that are differentially expressed to enable precise degradation of mutated forms of the Ras protein specific to tissues or developmental stages while minimizing any off-target toxic effects (Bond *et al*, 2020; Li *et al*, 2021; Zeng *et al*, 2020). In summary, it remains imperative to generate innovative concepts to eradicate Ras signaling in cancer and other disorders associated with the Ras pathway.

Biochemical Society Transactions (2023) **51** 447–456
https://doi.org/10.1042/BST20221343

PORTLAND PRESS

Review Article

Eliminating oncogenic RAS: back to the future at the drawing board

Candy Laura Steffen*, Pelin Kaya*, Elisabeth Schaffner-Reckinger* and Daniel Abankwa

Cancer Cell Biology and Drug Discovery Group, Department of Life Sciences and Medicine, University of Luxembourg, L-4362 Esch-sur-Alzette, Luxembourg

Correspondence: Daniel Abankwa (daniel.abankwa@uni.lu)

RAS drug development has made enormous strides in the past ten years, with the first direct KRAS inhibitor being approved in 2021. However, despite the clinical success of covalent KRAS-G12C inhibitors, we are immediately confronted with resistances as commonly found with targeted drugs. Previously believed to be undruggable due to its lack of obvious druggable pockets, a couple of new approaches to hit this much feared oncogene have now been carved out. We here concisely review these approaches to directly target four druggable sites of RAS from various angles. Our analysis focuses on the lessons learnt during the development of allele-specific covalent and non-covalent RAS inhibitors, the potential of macromolecular binders to facilitate the discovery and validation of targetable sites on RAS and finally an outlook on a future that may engage more small molecule binders to become drugs. We foresee that the latter could happen mainly in two ways: First, non-covalent small molecule inhibitors may be derived from the development of covalent binders. Second, reversible small molecule binders could be utilized for novel targeting modalities, such as degraders of RAS. Provided that degraders eliminate RAS by recruiting differentially expressed E3-ligases, this approach could enable unprecedented tissue- or developmental stage-specific destruction of RAS with potential advantages for on-target toxicity. We conclude that novel creative ideas continue to be important to exterminate RAS in cancer and other RAS pathway-driven diseases, such as RASopathies.

Introduction

The small GTPase RAS operates as a switchable recruitment site of downstream effectors to the membrane. Thus GTP-binding triggers multiple intracellular signalling pathways, notably the MAPK pathway, which drives proliferation and differentiation [1]. This central position to orchestrate hallmarks of life may explain why RAS is so frequently exploited in cancer, where the three RAS genes, *KRAS*, *NRAS* and *HRAS* combined are mutated in 19% of cancer patients [2]. Mutations typically occur in hotspot codons 12, 13 or 61, which essentially keep RAS GTP-bound and thus constitutively active.

In 2021 the first direct RAS inhibitor, sotorasib (AMG 510), was approved after a 40 year long quest to inhibit this major oncogene. Impressive initial clinical data with a median overall survival of 12.5 months in smoking-associated KRAS-G12C mutant NSCLC patients supported this effort [3]. A number of other G12C-specific inhibitors are currently being evaluated in patients, including adagrasib (MRTX849), which is the second G12C-inhibitor to enter clinical assessment [4,5]. However, the application of these inhibitors is limited to KRAS-G12C mutant tumours, such as found in 14% of NSCLC patients, and <5% in colorectal and pancreatic cancers. Moreover, emerging resistances have stunted overall patient response and the initially high expectations. Resistance mechanisms include additional oncogenic KRAS mutations in codons 12, 13 or 61 that are not susceptible to G12C-inhibitors [6,7].

*These authors contributed equally to this work.

Received: 30 November 2022
Revised: 11 January 2023
Accepted: 12 January 2023

Version of Record published: 23 January 2023

PORTLAND PRESS

Biochemical Society Transactions (2023) **51** 447–456
https://doi.org/10.1042/BST20221343

Nonetheless, the first direct RAS inhibitors are a tremendous first milestone that demarcate the extraordinary achievements in RAS drug development during the past decade. They impressively demonstrate what happens, if specifically the oncogenic version of a major cancer driver is drug-targeted. Yet they also clarify that even with exquisite (covalent) on-target specificity, side effects cannot be ruled out [8]. Most importantly, these inhibitors provide unequivocal proof of KRAS as a cancer drug target in humans.

The KRAS-G12C inhibitor development story is testimony to not take no for an answer, and pursue the targeting of cancer drivers, even if they were considered undruggable. This justifies and encourages novel drug development efforts against RAS. We will here review, which approaches are on the drawing boards of researchers and give an outlook on potential future developments.

The development of allele-specific and pan-RAS inhibitors for clinical applications

Crystal structures of RAS show that GTP-binding induces conformational changes in two regions of RAS, called switch I and switch II, without revealing targetable pockets on RAS [1]. However, seminal work from the Shokat group published in 2013 identified the cryptic allosteric switch II-pocket (SII-P), which manifests only upon binding of KRAS-G12C inhibitors [9]. Their first proof-of-concept inhibitor introduced the acrylamide warhead for covalent engagement of the nucleophilic cysteine on position 12, thus creating a paradigm that has until today been widely utilized (Figure 1). Since then, essentially every major pharma company has developed KRAS-G12C inhibitors and we refer to recent reviews for details on their pre-/clinical progress [5,10].

The common chemical theme of these compounds in addition to their identical warhead is the 4-piperazin-1-yl-pyrimidine scaffold core that was essentially introduced with ARS-1620 [11]. Intriguingly, with the development of the scaffold of adagrasib a significant non-covalent binding to wild-type KRAS and to a number of KRAS mutants that carry hotspot mutations on codons 12, 13 and 61 was achieved [12]. In line

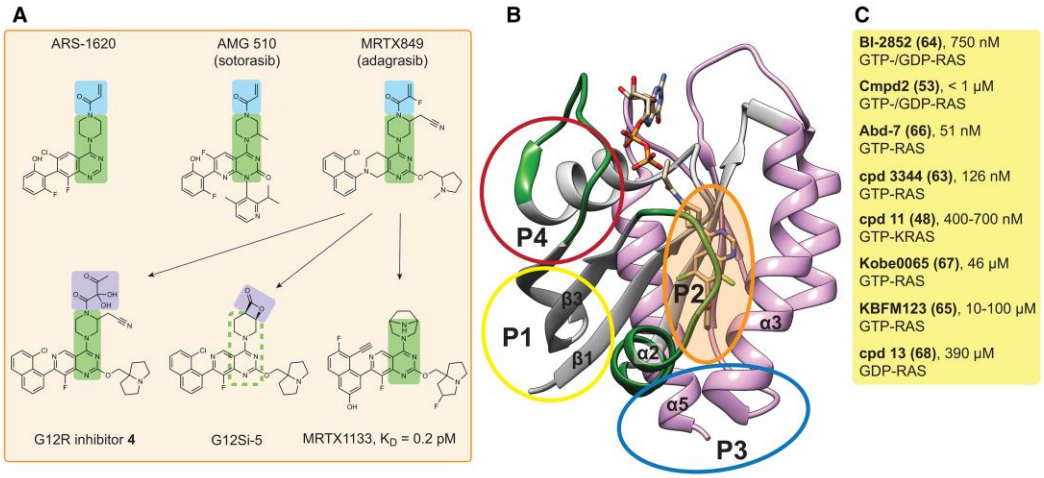

Figure 1. Overview of small molecule inhibitors targeting RAS.

(**A**) Selected SII-P small molecule inhibitors based on the 4-piperazin-1-yl-pyrimidine scaffold (green highlights). The common acrylamide warhead of KRAS-G12C inhibitors (top row) is highlighted in blue. Adagrasib served as a starting point for additional inhibitors (arrows), including covalent G12R- and G12S-inhibitors, with an α,β-diketoamide warhead or a strained β-lactone electrophile, respectively (purple). Note that the exact stereochemistry of displayed inhibitors has been largely omitted. (**B**) Crystal structure of GDP-KRAS-G12C in complex with ARS-1620 (PDB ID 5V9U). The RAS structure can be divided into the N-terminal effector lobe (grey), with the switch I and switch II regions labelled in green, and the allosteric lobe (pink). The allosteric binding sites P1–4 are indicated with circles. (**C**) Current experimental small molecule inhibitors (here those with an affinity <500 µM) target predominantly P1. The RAS affinity and selectivity is indicated for each compound (cpd). References are in brackets after the names [48,53,63–68]. The full list of small molecule inhibitors is contained in Supplementary File S1.

Biochemical Society Transactions (2023) **51** 447–456
https://doi.org/10.1042/BST20221343

with this, the adagrasib scaffold served as a starting point for the development of the first covalent inhibitors of KRAS-G12S and KRAS-G12R in the GDP-bound OFF-state [13,14]. These carry instead of the acrylamide warhead, a strained β-lactone electrophile in the case of the G12S-inhibitor, while an α,β-diketoamide warhead was used in the G12R-inhibitor (Figure 1A). All of these SII-P targeting compounds lock KRAS in an inactive conformation by distorting switch I and switch II, thus typically blocking access of RAS activating GEFs, such as SOS, and of RAS effectors, notably RAF [9,11–14]. In agreement with the reuse of the pharmacologically validated adagrasib scaffold, inhibitors are furthermore active in cells, to suppress MAPK signalling and selectively the growth of cancer cells carrying the targeted mutation.

One initially puzzling finding was that all of these covalent inhibitors rely on the GDP-bound, inactive KRAS. However, oncogenic KRAS mutants are generally approximated to be constitutively GTP-bound and ON. While it is commonly assumed that the GTPase activating protein (GAP) neurofibromin (NF1) turns RAS OFF, the heterotrimeric G protein-associated GAP RGS3 was identified as the enzyme that sufficiently inactivates all major oncogenic KRAS alleles [15]. Consequently, ablation of RGS3 severely decreased the antitumorigenic effect of adagrasib in a mouse xenograft model. This can be explained by the distinct catalytic mechanisms of NF1 and RGS3. NF1 provides a catalytic arginine (the Arg-finger) to speed-up GTP hydrolysis of RAS, a mechanism that is crucially inhibited by oncogenic hotspot mutants of RAS [16]. In contrast, RGS3 is from a different family of GAPs, which likely bind RAS also involving its switch regions, but employ asparagine as catalytic residue [17,18].

It is astonishing, but not the first time in RAS/ MAPK biology that such a fundamental biological mechanism was only discovered after the first RAS inhibitors entered the clinic. Both failure of farnesyl transferase inhibitors and paradoxical RAF activation were only fully recognized at the clinical stage [10]. The RGS3-catalyzed hydrolysis of RAS furthermore begs the question, in which biological context then is the NF1-associated GAP-activity required, given that all hotspot mutants of RAS evade it.

The OFF-state dependency of SII-P inhibitors is also liable to major resistance mechanisms, which increase the ON-state, such as mutational activation of EGFR or up-regulation of other receptor tyrosine kinases [5]. Additional resistance mechanisms after sotorasib treatment include mutations that disrupt binding of the inhibitors to the SII-P, most notably Y96D, which also blocks access of adagrasib [6,19]. *In vitro* studies furthermore forecast evasive mutations, which increase GTP-levels of KRAS, such as Y40A, N116H and A146V [20]. Xenograft data furthermore suggest that MAPK pathway reactivation occurs sooner or later in particular by the emergence of clones with other oncogenic KRAS alleles or overactivation of other RAS isoforms, including MRAS [7].

Some of these resistance issues can be overcome by inhibiting the ON-state of KRAS. The adagrasib-derived non-covalent inhibitor MRTX-EX185 demonstrates this potential even for a SII-P binder [12]. The non-covalent inhibitor MRTX1133 exploited this further and introduced sub-picomolar targeting of the most common KRAS mutation, KRAS-G12D, with potent inhibition of signalling and xenograft growth [21].

Another embodiment is seen in a completely different RAS inhibition approach that is being evaluated in clinical trials. A whole panel of allele-specific and pan-RAS inhibitors has been commercially developed, which tie together KRAS in the ON-state and the ubiquitous and abundant chaperone protein cyclophilin A [22]. These ‘molecular glue’ compounds lead to an inhibitory tri-complex formation that sterically blocks RAS interactions and thus downstream signalling. Molecular glues are small molecules, which link two proteins in a non-native complex to inhibit or modify at least one of the binding partners [23]. The interesting potential of this approach is demonstrated by the covalent KRAS-G12C inhibitor RM-018, which can overcome the Y96D-dependent resistance encountered with sotorasib and adagrasib [19]. In addition to KRAS-G12C, the tri-complex approach has been utilized to covalently target KRAS-G12D, KRAS-G13C and multiple RAS alleles non-covalently, as recently reviewed elsewhere [5].

The exploration of novel binding sites and inhibition principles of RAS using macromolecular binders

In the commercial tri-complex approach, binding to the part of RAS that engages effectors is obstructed. This first half of the RAS protein (residues 1–85) is therefore also referred to as effector lobe, while the second half of the G-domain (residues 86–166) is called the allosteric lobe. The effector lobe makes major contacts not only with effectors, but all other major regulators of RAS, such as GEFs and GAPs.

Biochemical Society Transactions (2023) **51** 447–456
https://doi.org/10.1042/BST20221343

Therefore, high affinity macromolecular binders raised against the effector lobe can potently inhibit RAS signalling. In addition to classical antibodies (~150 kDa) and Fab-fragments (~50 kDa), much smaller specific binders can be raised by directed evolution *in vitro*, such as designed ankyrin repeat proteins (DARPins; ~20 kDa), Affimers (~12 kDa), which are based on the artificial phytocystatin-derived scaffold called Adhiron, and monobodies (~10 kDa), which originate from an artificial fibronectin type III domain [24–26]. Such binders exhibit typically affinities in the nanomolar range and encode high binding specificities to a small contact area. The small contact site can be exploited for pharmacophore based computational or *in vitro* competitive screening for small molecule functional analogues.

Obvious targets on the effector lobe are the switch regions, for which both GTP-specific binders (antibodies iDab#6, RT11, inRas37, monobody 12VC1, DARPin K55) [27–30], as well as GDP-specific binders (monobody JAM20, DARPin K27) have been identified [27,31] (Figure 2). Accordingly, these reagents typically repress RAS/ effector-binding and RAS-activation, respectively, and several were shown to block RAS-mutant cancer cell growth *in vitro* and in murine tumour models.

The truly exciting potential of these artificial binders lies in their ability to discover novel binding sites on RAS, which is notoriously binding cavity free. In support of this potential, affimer K3 was found to bind at the same site of KRAS, where current covalent G12C-inhibitors are lodging. Similarly, another affimer K6 binds to a pocket in between the switch I and switch II regions, a site that is also targeted by inhibitors DCAI and BI-2852 (Figure 1 and Supplementary File S1) [32–34].

Several other macromolecular binders engage with RAS on the allosteric lobe, hence in a nucleotide-independent manner. Complexation creates significant sterical bulk around RAS, which plausibly impacts on higher complex formation, such as transient dimers and nanoclustering. Nanoclusters are proteolipid complexes containing transient di-/trimeric RAS assemblies, which act as membrane recruitment sites of RAF-effectors and are therefore necessary for MAPK signalling [35]. In addition, the conformational mobility of RAS at the membrane impacts on MAPK signalling [35–38]. Given that a bulky binder would most probably restrain such conformational motions it is plausible to assume that they also affect associated RAS activities.

The monobody NS1 binds to HRAS and KRAS, but not NRAS, at an epitope comprising helices α4 and α5 [39]. These make up the most common interface that is assumed to partake in RAS self-organization into nanoclusters on the plasma membrane [40]. This interface was also recognized by the affimer K69 [32]. In contrast, the DARPins K13 and K19 bind to helices α3 and α4, which have also been suggested as interface for transient RAS dimers at the membrane [40]. While such macromolecular binders are *per se* not pharmacologically tractable for an intracellular target such as RAS, they nevertheless provide crucial proof-of-concept data for the target site in cellular and *in vivo* models.

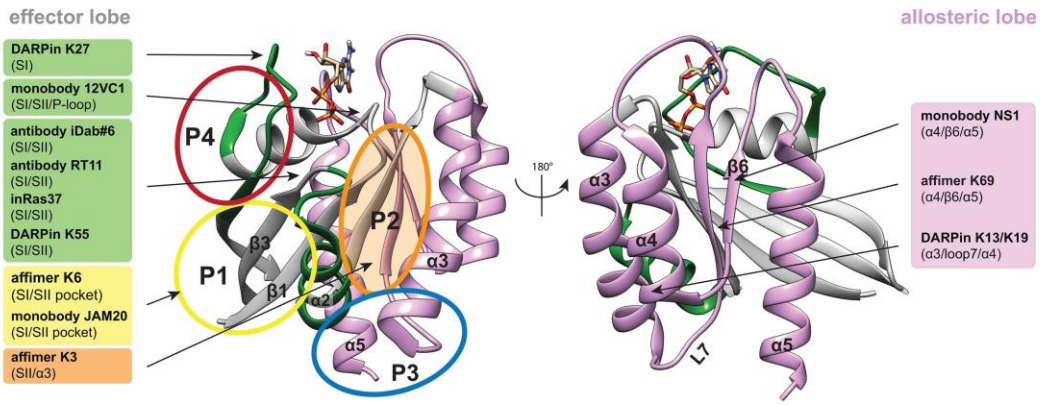

Figure 2. Overview of macromolecular RAS binders.

Crystal structure of GDP-KRAS (PDB ID 4OBE). Effector and allosteric lobes, as well as allosteric binding sites are indicated as in Figure 1. The names of macromolecular RAS binders are highlighted in the same colour as their binding sites, with more detailed binding site information given in brackets.

Biochemical Society Transactions (2023) **51** 447–456
https://doi.org/10.1042/BST20221343

Moreover, they can be further functionalized to enable new modes of action. By genetically fusing E3-ligase subunits such as von Hippel-Lindau (VHL) tumour suppressor to the monobodies NS1 and 12VC1 or the DARPin K19, RAS degrader constructs were generated [30,41,42]. In general degraders realized potent RAS signalling suppression and anti-proliferative activities, and in the case of the 12VC1 were also more potent than the competitively binding monobody alone [30]. Given that these degraders emulate the proteolysis targeting chimera (PROTAC) mode of action, which will be discussed in the next chapter, they may be useful to forecast the potential of analogous PROTACs [43].

On the pathway to develop smaller RAS binders, peptides are a natural intermediate. A number of peptides or peptidomimetics that target the GTP-KRAS effector lobe typically with nanomolar affinity and compete with effector binding and downstream signalling of RAS have been developed. These peptides have a median size of ∼14 residues, can be either linear or cyclic, and contain non-natural amino acids or other chemical modifications (i.e. peptidomimetics) (Table 1). Cyclic peptides are entropically advantageous and are more resistant against exopeptidases [44]. So far, none of these peptides have been harnessed for degrader development.

What is the future of RAS inhibition? From small molecule binders to PROTAC-degraders

RAS is a small mono-domain protein with a shallow surface that has been considered undruggable due to the lack of obvious binding pockets. The nucleotide binding site remains problematic as a target, due to the high cellular GTP concentration in combination with the picomolar affinity of the guanine nucleotides to RAS [5]. However, computational approaches led by the Gorfe group, have identified already in 2011, hence well before the discovery of first covalent inhibitors, altogether four low affinity (sub-/millimolar) allosteric sites on RAS named P1 to P4 that have all been experimentally validated [45–47]. P1 and P4 are situated in the effector lobe, P3 in the allosteric lobe and P2 in between both lobes (Figure 1B).

The hydrophobic pocket P1 is located between switch II and β-strands 1–3 and is partially closed in crystal structures of GDP-RAS [48]. It essentially corresponds to the switch I/switch II region that is targeted by several experimental ON- and OFF-state binders (Figure 1C and Supplementary File S1). P2 is at the interface

Table 1 Overview of RAS binding peptides

Name (PDB ID)	RAS specificity	K_D (nM)	Site on RAS	Properties	Ref.
Linear					
RBDv1, RBDv12	GTP-RAS	3.35 2.52	P4	14 aa, inhibits RAS signalling, reduces cancer cell growth	[69]
SAH-SOS1	GDP-/GTP-RAS	106–175	near P4	16 aa, blocks nucleotide exchange, reduces cancer cell growth	[70]
225-11 (5WPL)	GTP-RAS	3.3	P4	32 aa, blocks effector interaction	[71]
R11.1.6 (5UFQ)	RAS-G12D	4	switch II	61 aa, blocks effector interaction, inhibits RAS signalling	[72]
Cyclic					
Cyclorasin 9A5	GTP-RAS	440	near P4	11 aa, blocks effector interaction, inhibits RAS signalling	[73]
Cyclorasin B4-27	GTP-RAS	21	near P4	16 aa, blocks effector interaction (cellular BRET-assay)	[74]
KRpep-2d (5XCO)	KRAS-G12D	51	P2	19 aa, inhibits RAS signalling, reduces cancer cell growth	[75–77]
KS-58	KRAS-G12D	22	P2	11 aa, inhibits RAS signalling, reduces cancer cell growth *in vivo*	[78,79]
KD2 (6WGN)	GTP-KRAS-G12D	none	near P2	15 aa, blocks effector interaction	[80]

Peptide and peptidomimetic RAS binders and their properties. The PDB ID is given if the complex with RAS was determined.

Biochemical Society Transactions (2023) **51** 447–456
https://doi.org/10.1042/BST20221343

of helix α2 with helix α3. This cryptic hydrophobic pocket is currently the most successfully targeted site, as it harbours the covalent OFF-state inhibitors targeting G12C, G12S, G12R and non-covalent inhibitors targeting G12D (Figure 1A). The polar P3 site is located between helix α5 and loop 7 and is accessible in both GTP- and GDP-states of KRAS, but less in the other RAS isoforms [46]. However, currently few binders target this site, such as metal cyclens and KAL-21404358 [49,50]. P4 is also polar and situated behind switch I and possesses andrographolide derivatives as the most interesting ligands currently [51]. It thus appears that the number of targetable sites on RAS is limited.

By combining computational and experimental approaches several small molecules have been identified that bind primarily to P1 and P2 (Figure 1C and Supplementary File S1). These ligands cover a broad range of affinities from milli- to nanomolar, typically lack RAS isoform selectivity and can disrupt binding of RAS interaction partners, such as RAF, and suppress MAPK signalling or cell viability. Only for compound 11 was KRAS-selective on-target binding demonstrated *in vitro* [48]. Therefore, cellular effects of low affinity compounds have to be taken with caution, as at the early stages of compound discovery off-target effects will contribute to these readouts.

With the exception of the covalent and non-covalent SII-P binding inhibitors, none of the small molecule binders has advanced toward clinical development. This may suggest that before a non-covalent inhibitor (such as MRTX1133) can flourish, a covalent counterpart that is anchored at the desired site may be advantageous during compound development [9].

Given their size, small molecules are less likely to block protein–protein interfaces such as needed to inhibit RAS nanoclustering. However, membrane-bound RAS also undergoes potentially RAS isoform specific conformational changes that impact on its nanoclustering [36,37]. Interestingly, some very rare cancer-associated and RASopathy mutations seem to affect nanoclustering by perturbing conformational dynamics of RAS [38,52]. A similar conformational shift may therefore also be achievable by small molecules, which was indeed demonstrated by the Ikura group. They showed that Cmpd2 stabilizes a non-productive conformation of KRAS at the membrane, by binding in between the membrane and the P1 site [53]. Another intriguing concept originated from the serendipitous discovery of a RAS-dimer stabilizer BI-2852, which was developed as RAS switch I/switch II pocket binder [33,54]. This nanomolar ligand illustrates the potential to modulate RAS oligomerization, specifically by locking it in a non-productive dimer.

As compared with competitive inhibitors, PROTACs instruct protein degradation by recruiting the ubiquitin-proteasome system to the target protein [55]. They can therefore bind outside of an active or allosteric site of a protein and after degradation abrogate any scaffolding functions of the target. This is enabled by their hybrid structure, which contains one binder (the warhead) for the target protein that is tethered via a linker to a moiety that recruits an E3-ligase, most commonly VHL and cereblon. The latter was enabled by the finding that immunomodulatory thalidomide derivatives alone work as 'molecular glues' that stick cereblon to IKAROS-family transcription factors and thus instruct their degradation [55].

Both concepts, molecular glues and PROTACs are thus not only historically related but bear similar capabilities, as both types of inhibitors can be potentially reused after reversible binding to and degradation of the target protein. Of note, molecular glues may also act by incapacitating a protein in a non-functional complex, such as illustrated by the tri-complex approach described earlier. Given that PROTACs follow an apparent 'plug-and-play' design, where the E3-ligase recruiting moiety can be utilized in several molecules, this approach currently predominates [55]. However, significant optimization for linker length and pharmacological properties of the relatively large molecules still requires substantial developmental efforts [56].

Current RAS-targeting PROTACs (XY-4-88, LC-2, KP-14) all build on the covalent G12C-inhibitors and as such cannot benefit from PROTAC degrader recycling, as these inhibitors are consumed due to the covalent cysteine engagement (Supplementary File S1) [57–59]. An interesting advancement in this regard is the development of reversible covalent inhibitor YF135, which employs a cyanoacrylamide for cysteine linkage [60]. Side-by-side comparison with the RAS-binding warhead alone furthermore demonstrates a 30-fold higher activity of the PROTAC. It remains to be seen, how and whether any of the exploratory RAS-ligands (Figure 1C and Supplementary File S1) can be converted into PROTACs. Given the distinct spatio-temporal expression of some E3-ligases in tissues and inside of cells, PROTACs may provide a more controlled drug action, which could reduce toxicity and new treatment mechanisms [61,62].

RAS drug development is in full motion since 2007 (Figure 3) and it can be hoped that novel creative ideas will continue to provide new RAS drugs for cancer therapy or other RAS-associated diseases, such as RASopathies.

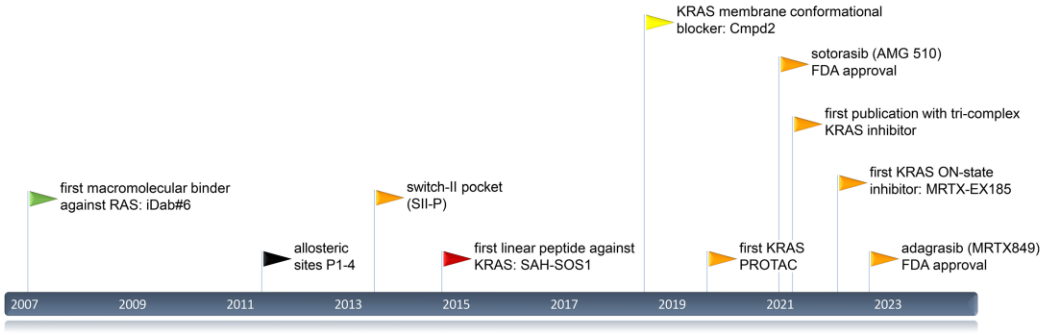

Figure 3. Timeline of notable RAS drug development events since 2007.

Arrowheads mark publications of binders and sites with colours corresponding to those used for binding sites in Figures 1 and 2.

Perspectives

- KRAS is the most frequently mutated oncogene and a major driver of cancer (stemness), which has finally become a clinically validated drug-target, thanks to KRAS-G12C targeting sotorasib and adagrasib. However, the performance of these compounds in the clinic warrants continuing efforts in RAS pathway drug development and further research to understand the essence of RAS in cancer.
- At least four targetable allosteric pockets and four surface areas on RAS have been identified and validated by the discovery of macromolecular-, peptidic- and small molecule-binders. These block upstream processes of RAS signalling, such as effector binding and nanoclustering.
- PROTAC degraders of RAS may offer new ways to inhibit RAS in a spatio-temporally (tissue type, differentiation stage, cell-cycle stage) more defined manner, with potential benefits for on-target toxicity. However, the viability of this approach awaits evaluation in the clinic.

Competing Interests

The authors declare that there are no competing interests associated with the manuscript.

Funding

This work was supported by grants from the Luxembourg National Research Fund (FNR): AFR individual grant 13589879 to P.K. and INTER/NWO/19/14061736 — HRAS-PPi to D.A.

Author Contributions

This review was jointly prepared by C.L.S., P.K., E.S.-R. and D.A.

Abbreviations

EGFR, Epidermal growth factor receptor; GEF, Guanine nucleotide exchange factor; MAPK, Mitogen-activated protein kinases; NSCLC, Non-small cell lung cancer; RGS3, Regulator of G-protein signalling 3; SOS, Son of sevenless guanine nucleotide exchange factor.

Biochemical Society Transactions (2023) **51** 447–456
https://doi.org/10.1042/BST20221343

References

1 Simanshu, D.K., Nissley, D.V. and McCormick, F. (2017) RAS proteins and their regulators in human disease. *Cell* **170**, 17–33 https://doi.org/10.1016/j.cell.2017.06.009

2 Prior, I.A., Hood, F.E. and Hartley, J.L. (2020) The frequency of Ras mutations in cancer. *Cancer Res.* **80**, 2969–2974 https://doi.org/10.1158/0008-5472.CAN-19-3682

3 Skoulidis, F., Li, B.T., Dy, G.K., Price, T.J., Falchook, G.S., Wolf, J. et al. (2021) Sotorasib for lung cancers with KRAS p.G12C mutation. *N. Engl. J. Med.* **384**, 2371–2381 https://doi.org/10.1056/NEJMoa2103695

4 Fell, J.B., Fischer, J.P., Baer, B.R., Blake, J.F., Bouhana, K., Briere, D.M. et al. (2020) Identification of the clinical development candidate MRTX849, a covalent KRAS(G12C) inhibitor for the treatment of cancer. *J. Med. Chem.* **63**, 6679–6693 https://doi.org/10.1021/acs.jmedchem.9b02052

5 Punekar, S.R., Velcheti, V., Neel, B.G. and Wong, K.K. (2022) The current state of the art and future trends in RAS-targeted cancer therapies. *Nat. Rev. Clin. Oncol.* **19**, 637–655 https://doi.org/10.1038/s41571-022-00671-9

6 Awad, M.M., Liu, S., Rybkin, I.I., Arbour, K.C., Dilly, J., Zhu, V.W. et al. (2021) Acquired resistance to KRAS(G12C) inhibition in cancer. *N. Engl. J. Med.* **384**, 2382–2393 https://doi.org/10.1056/NEJMoa2105281

7 Zhao, Y., Murciano-Goroff, Y.R., Xue, J.Y., Ang, A., Lucas, J., Mai, T.T. et al. (2021) Diverse alterations associated with resistance to KRAS(G12C) inhibition. *Nature* **599**, 679–683 https://doi.org/10.1038/s41586-021-04065-2

8 Kwan, A.K., Piazza, G.A., Keeton, A.B. and Leite, C.A. (2022) The path to the clinic: a comprehensive review on direct KRAS(G12C) inhibitors. *J. Exp. Clin. Cancer Res.* **41**, 27 https://doi.org/10.1186/s13046-021-02225-w

9 Ostrem, J.M., Peters, U., Sos, M.L., Wells, J.A. and Shokat, K.M. (2013) K-Ras(G12C) inhibitors allosterically control GTP affinity and effector interactions. *Nature* **503**, 548–551 https://doi.org/10.1038/nature12796

10 Moore, A.R., Rosenberg, S.C., McCormick, F. and Malek, S. (2020) RAS-targeted therapies: is the undruggable drugged? *Nat. Rev. Drug Discov.* **19**, 533–552 https://doi.org/10.1038/s41573-020-0068-6

11 Janes, M.R., Zhang, J., Li, L.S., Hansen, R., Peters, U., Guo, X. et al. (2018) Targeting KRAS mutant cancers with a covalent G12C-specific inhibitor. *Cell* **172**, 578–589.e517 https://doi.org/10.1016/j.cell.2018.01.006

12 Vasta, J.D., Peacock, D.M., Zheng, Q., Walker, J.A., Zhang, Z., Zimprich, C.A. et al. (2022) KRAS is vulnerable to reversible switch-II pocket engagement in cells. *Nat. Chem. Biol.* **18**, 596–604 https://doi.org/10.1038/s41589-022-00985-w

13 Zhang, Z., Guiley, K.Z. and Shokat, K.M. (2022) Chemical acylation of an acquired serine suppresses oncogenic signaling of K-Ras(G12S). *Nat. Chem. Biol.* **18**, 1177–1183 https://doi.org/10.1038/s41589-022-01065-9

14 Zhang, Z., Morstein, J., Ecker, A.K., Guiley, K.Z. and Shokat, K.M. (2022) Chemoselective covalent modification of K-Ras(G12R) with a small molecule electrophile. *J. Am. Chem. Soc.* **144**, 15916–15921 https://doi.org/10.1021/jacs.2c05377

15 Li, C., Vides, A., Kim, D., Xue, J.Y., Zhao, Y. and Lito, P. (2021) The G protein signaling regulator RGS3 enhances the GTPase activity of KRAS. *Science* **374**, 197–201 https://doi.org/10.1126/science.abf1730

16 Scheffzek, K., Ahmadian, M.R., Kabsch, W., Wiesmuller, L., Lautwein, A., Schmitz, F. et al. (1997) The Ras-RasGAP complex: structural basis for GTPase activation and its loss in oncogenic Ras mutants. *Science* **277**, 333–338 https://doi.org/10.1126/science.277.5324.333

17 Soundararajan, M., Willard, F.S., Kimple, A.J., Turnbull, A.P., Ball, L.J., Schoch, G.A. et al. (2008) Structural diversity in the RGS domain and its interaction with heterotrimeric G protein alpha-subunits. *Proc. Natl Acad. Sci. U.S.A.* **105**, 6457–6462 https://doi.org/10.1073/pnas.0801508105

18 Tesmer, J.J., Berman, D.M., Gilman, A.G. and Sprang, S.R. (1997) Structure of RGS4 bound to AlF4$^-$-activated Giα1: stabilization of the transition state for GTP hydrolysis. *Cell* **89**, 251–261 https://doi.org/10.1016/s0092-8674(00)80204-4

19 Tanaka, N., Lin, J.J., Li, C., Ryan, M.B., Zhang, J., Kiedrowski, L.A. et al. (2021) Clinical acquired resistance to KRAS(G12C) inhibition through a novel KRAS switch-II pocket mutation and polyclonal alterations converging on RAS-MAPK reactivation. *Cancer Discov.* **11**, 1913–1922 https://doi.org/10.1158/2159-8290.CD-21-0365

20 Lito, P., Solomon, M., Li, L.S., Hansen, R. and Rosen, N. (2016) Allele-specific inhibitors inactivate mutant KRAS G12C by a trapping mechanism. *Science* **351**, 604–608 https://doi.org/10.1126/science.aad6204

21 Hallin, J., Bowcut, V., Calinisan, A., Briere, D.M., Hargis, L., Engstrom, L.D. et al. (2022) Anti-tumor efficacy of a potent and selective non-covalent KRAS^{G12D} inhibitor. *Nat. Med.* **28**, 2171–2182 https://doi.org/10.1038/s41591-022-02007-7

22 Zhang, Z. and Shokat, K.M. (2019) Bifunctional small-molecule ligands of K-Ras induce its association with immunophilin proteins. *Angew. Chem. Int. Ed. Engl.* **58**, 16314–16319 https://doi.org/10.1002/anie.201910124

23 Geiger, T.M., Schäfer, S.C., Dreizler, J.K., Walz, M. and Hausch, F. (2022) Clues to molecular glues. *Curr. Res. Chem. Biol.* **2**, 14 https://doi.org/10.1016/j.crchbi.2021.100018

24 Koide, A., Bailey, C.W., Huang, X. and Koide, S. (1998) The fibronectin type III domain as a scaffold for novel binding proteins. *J. Mol. Biol.* **284**, 1141–1151 https://doi.org/10.1006/jmbi.1998.2238

25 Stumpp, M.T., Binz, H.K. and Amstutz, P. (2008) DARPins: a new generation of protein therapeutics. *Drug Discov. Today* **13**, 695–701 https://doi.org/10.1016/j.drudis.2008.04.013

26 Tiede, C., Tang, A.A., Deacon, S.E., Mandal, U., Nettleship, J.E., Owen, R.L. et al. (2014) Adhiron: a stable and versatile peptide display scaffold for molecular recognition applications. *Protein Eng. Des. Sel.* **27**, 145–155 https://doi.org/10.1093/protein/gzu007

27 Guillard, S., Kolasinska-Zwierz, P., Debreczeni, J., Breed, J., Zhang, J., Bery, N. et al. (2017) Structural and functional characterization of a DARPin which inhibits Ras nucleotide exchange. *Nat. Commun.* **8**, 16111 https://doi.org/10.1038/ncomms16111

28 Shin, S.M., Choi, D.K., Jung, K., Bae, J., Kim, J.S., Park, S.W. et al. (2017) Antibody targeting intracellular oncogenic Ras mutants exerts anti-tumour effects after systemic administration. *Nat. Commun.* **8**, 15090 https://doi.org/10.1038/ncomms15090

29 Tanaka, T., Williams, R.L. and Rabbitts, T.H. (2007) Tumour prevention by a single antibody domain targeting the interaction of signal transduction proteins with RAS. *EMBO J.* **26**, 3250–3259 https://doi.org/10.1038/sj.emboj.7601744

30 Teng, K.W., Tsai, S.T., Hattori, T., Fedele, C., Koide, A., Yang, C. et al. (2021) Selective and noncovalent targeting of RAS mutants for inhibition and degradation. *Nat. Commun.* **12**, 2656 https://doi.org/10.1038/s41467-021-22969-5

31 Wallon, L., Khan, I., Teng, K.W., Koide, A., Zuberi, M., Li, J. et al. (2022) Inhibition of RAS-driven signaling and tumorigenesis with a pan-RAS monobody targeting the switch I/II pocket. *Proc. Natl Acad. Sci. U.S.A.* **119**, e2204481119 https://doi.org/10.1073/pnas.2204481119

32 Haza, K.Z., Martin, H.L., Rao, A., Turner, A.L., Saunders, S.E., Petersen, B. et al. (2021) RAS-inhibiting biologics identify and probe druggable pockets including an SII-α3 allosteric site. *Nat. Commun.* **12**, 4045 https://doi.org/10.1038/s41467-021-24316-0
33 Kessler, D., Gmachl, M., Mantoulidis, A., Martin, L.J., Zoephel, A., Mayer, M. et al. (2019) Drugging an undruggable pocket on KRAS. *Proc. Natl Acad. Sci. U.S.A.* **116**, 15823–15829 https://doi.org/10.1073/pnas.1904529116
34 Maurer, T., Garrenton, L.S., Oh, A., Pitts, K., Anderson, D.J., Skelton, N.J. et al. (2012) Small-molecule ligands bind to a distinct pocket in Ras and inhibit SOS-mediated nucleotide exchange activity. *Proc. Natl Acad. Sci. U.S.A.* **109**, 5299–5304 https://doi.org/10.1073/pnas.1116510109
35 Abankwa, D. and Gorfe, A.A. (2020) Mechanisms of Ras membrane organization and signaling: Ras rocks again. *Biomolecules* **10**, 1522 https://doi.org/10.3390/biom10111522
36 Abankwa, D., Gorfe, A.A., Inder, K. and Hancock, J.F. (2010) Ras membrane orientation and nanodomain localization generate isoform diversity. *Proc. Natl Acad. Sci. U.S.A.* **107**, 1130–1135 https://doi.org/10.1073/pnas.0903907107
37 Abankwa, D., Hanzal-Bayer, M., Ariotti, N., Plowman, S.J., Gorfe, A.A., Parton, R.G. et al. (2008) A novel switch region regulates H-ras membrane orientation and signal output. *EMBO J.* **27**, 727–735 https://doi.org/10.1038/emboj.2008.10
38 Solman, M., Ligabue, A., Blazevits, O., Jaiswal, A., Zhou, Y., Liang, H. et al. (2015) Specific cancer-associated mutations in the switch III region of Ras increase tumorigenicity by nanocluster augmentation. *Elife* **4**, e08905 https://doi.org/10.7554/eLife.08905
39 Spencer-Smith, R., Koide, A., Zhou, Y., Eguchi, R.R., Sha, F., Gajwani, P. et al. (2017) Inhibition of RAS function through targeting an allosteric regulatory site. *Nat. Chem. Biol.* **13**, 62–68 https://doi.org/10.1038/nchembio.2231
40 Van, Q.N., Prakash, P., Shrestha, R., Balius, T.E., Turbyville, T.J. and Stephen, A.G. (2021) RAS nanoclusters: dynamic signaling platforms amenable to therapeutic intervention. *Biomolecules* **11**, 377 https://doi.org/10.3390/biom11030377
41 Bery, N., Miller, A. and Rabbitts, T. (2020) A potent KRAS macromolecule degrader specifically targeting tumours with mutant KRAS. *Nat. Commun.* **11**, 3233 https://doi.org/10.1038/s41467-020-17022-w
42 Roth, S., Macartney, T.J., Konopacka, A., Chan, K.H., Zhou, H., Queisser, M.A. et al. (2020) Targeting endogenous K-RAS for degradation through the affinity-directed protein missile system. *Cell Chem. Biol.* **27**, 1151–1163.e1156 https://doi.org/10.1016/j.chembiol.2020.06.012
43 Lim, S., Khoo, R., Juang, Y.C., Gopal, P., Zhang, H., Yeo, C. et al. (2021) Exquisitely specific anti-KRAS biodegraders inform on the cellular prevalence of nucleotide-loaded states. *ACS Cent. Sci.* **7**, 274–291 https://doi.org/10.1021/acscentsci.0c01337
44 Choi, J.S. and Joo, S.H. (2020) Recent trends in cyclic peptides as therapeutic agents and biochemical tools. *Biomol. Ther. (Seoul)* **28**, 18–24 https://doi.org/10.4062/biomolther.2019.082
45 Gorfe, A.A. and Cho, K.J. (2021) Approaches to inhibiting oncogenic K-Ras. *Small GTPases* **12**, 96–105 https://doi.org/10.1080/21541248.2019.1655883
46 Grant, B.J., Lukman, S., Hocker, H.J., Sayyah, J., Brown, J.H., McCammon, J.A. et al. (2011) Novel allosteric sites on Ras for lead generation. *PLoS ONE* **6**, e25711 https://doi.org/10.1371/journal.pone.0025711
47 Prakash, P., Hancock, J.F. and Gorfe, A.A. (2015) Binding hotspots on K-ras: consensus ligand binding sites and other reactive regions from probe-based molecular dynamics analysis. *Proteins* **83**, 898–909 https://doi.org/10.1002/prot.24786
48 McCarthy, M.J., Pagba, C.V., Prakash, P., Naji, A.K., van der Hoeven, D., Liang, H. et al. (2019) Discovery of high-affinity noncovalent allosteric KRAS inhibitors that disrupt effector binding. *ACS Omega* **4**, 2921–2930 https://doi.org/10.1021/acsomega.8b03308
49 Feng, H., Zhang, Y., Bos, P.H., Chambers, J.M., Dupont, M.M. and Stockwell, B.R. (2019) K-Ras(G12D) Has a potential allosteric small molecule binding site. *Biochemistry* **58**, 2542–2554 https://doi.org/10.1021/acs.biochem.8b01300
50 Rosnizeck, I.C., Graf, T., Spoerner, M., Trankle, J., Filchtinski, D., Herrmann, C. et al. (2010) Stabilizing a weak binding state for effectors in the human ras protein by cyclen complexes. *Angew. Chem. Int. Ed. Engl.* **49**, 3830–3833 https://doi.org/10.1002/anie.200907002
51 Hocker, H.J., Cho, K.J., Chen, C.Y., Rambahal, N., Sagineedu, S.R., Shaari, K. et al. (2013) Andrographolide derivatives inhibit guanine nucleotide exchange and abrogate oncogenic Ras function. *Proc. Natl Acad. Sci. U.S.A.* **110**, 10201–10206 https://doi.org/10.1073/pnas.1300016110
52 Mazhab-Jafari, M.T., Marshall, C.B., Smith, M.J., Gasmi-Seabrook, G.M., Stathopulos, P.B., Inagaki, F. et al. (2015) Oncogenic and RASopathy-associated K-RAS mutations relieve membrane-dependent occlusion of the effector-binding site. *Proc. Natl Acad. Sci. U.S.A.* **112**, 6625–6630 https://doi.org/10.1073/pnas.1419895112
53 Fang, Z., Marshall, C.B., Nishikawa, T., Gossert, A.D., Jansen, J.M., Jahnke, W. et al. (2018) Inhibition of K-RAS4B by a unique mechanism of action: stabilizing membrane-dependent occlusion of the effector-binding site. *Cell Chem. Biol.* **25**, 1327–1336.e1324 https://doi.org/10.1016/j.chembiol.2018.07.009
54 Tran, T.H., Alexander, P., Dharmaiah, S., Agamasu, C., Nissley, D.V., McCormick, F. et al. (2020) The small molecule BI-2852 induces a nonfunctional dimer of KRAS. *Proc. Natl Acad. Sci. U.S.A.* **117**, 3363–3364 https://doi.org/10.1073/pnas.1918164117
55 Bekes, M., Langley, D.R. and Crews, C.M. (2022) PROTAC targeted protein degraders: the past is prologue. *Nat. Rev. Drug Discov.* **21**, 181–200 https://doi.org/10.1038/s41573-021-00371-6
56 Paiva, S.L. and Crews, C.M. (2019) Targeted protein degradation: elements of PROTAC design. *Curr. Opin. Chem. Biol.* **50**, 111–119 https://doi.org/10.1016/j.cbpa.2019.02.022
57 Bond, M.J., Chu, L., Nalawansha, D.A., Li, K. and Crews, C.M. (2020) Targeted degradation of oncogenic KRAS(G12C) by VHL-Recruiting PROTACs. *ACS Cent. Sci.* **6**, 1367–1375 https://doi.org/10.1021/acscentsci.0c00411
58 Li, L., Wu, Y., Yang, Z., Xu, C., Zhao, H., Liu, J. et al. (2021) Discovery of KRas G12C-IN-3 and pomalidomide-based PROTACs as degraders of endogenous KRAS G12C with potent anticancer activity. *Bioorg. Chem.* **117**, 105447 https://doi.org/10.1016/j.bioorg.2021.105447
59 Zeng, M., Xiong, Y., Safaee, N., Nowak, R.P., Donovan, K.A., Yuan, C.J. et al. (2020) Exploring targeted degradation strategy for oncogenic KRAS (G12C). *Cell Chem. Biol.* **27**, 19–31.e16 https://doi.org/10.1016/j.chembiol.2019.12.006
60 Yang, F., Wen, Y., Wang, C., Zhou, Y., Zhou, Y., Zhang, Z.M. et al. (2022) Efficient targeted oncogenic KRAS(G12C) degradation via first reversible-covalent PROTAC. *Eur. J. Med. Chem.* **230**, 114088 https://doi.org/10.1016/j.ejmech.2021.114088
61 Kannt, A. and Dikic, I. (2021) Expanding the arsenal of E3 ubiquitin ligases for proximity-induced protein degradation. *Cell Chem. Biol.* **28**, 1014–1031 https://doi.org/10.1016/j.chembiol.2021.04.007
62 Schapira, M., Calabrese, M.F., Bullock, A.N. and Crews, C.M. (2019) Targeted protein degradation: expanding the toolbox. *Nat. Rev. Drug Discov.* **18**, 949–963 https://doi.org/10.1038/s41573-019-0047-y

Biochemical Society Transactions (2023) **51** 447–456
https://doi.org/10.1042/BST20221343

63 Bery, N., Cruz-Migoni, A., Bataille, C.J., Quevedo, C.E., Tulmin, H., Miller, A. et al. (2018) BRET-based RAS biosensors that show a novel small molecule is an inhibitor of RAS-effector protein-protein interactions. *Elife* **7**, e37122 https://doi.org/10.7554/eLife.37122
64 Kessler, D., Bergner, A., Bottcher, J., Fischer, G., Dobel, S., Hinkel, M. et al. (2020) Drugging all RAS isoforms with one pocket. *Future Med. Chem.* **12**, 1911–1923 https://doi.org/10.4155/fmc-2020-0221
65 Matsumoto, S., Hiraga, T., Hayashi, Y., Yoshikawa, Y., Tsuda, C., Araki, M. et al. (2018) Molecular basis for allosteric inhibition of GTP-bound H-Ras protein by a small-molecule compound carrying a naphthalene ring. *Biochemistry* **57**, 5350–5358 https://doi.org/10.1021/acs.biochem.8b00680
66 Quevedo, C.E., Cruz-Migoni, A., Bery, N., Miller, A., Tanaka, T., Petch, D. et al. (2018) Small molecule inhibitors of RAS-effector protein interactions derived using an intracellular antibody fragment. *Nat. Commun.* **9**, 3169 https://doi.org/10.1038/s41467-018-05707-2
67 Shima, F., Yoshikawa, Y., Ye, M., Araki, M., Matsumoto, S., Liao, J. et al. (2013) In silico discovery of small-molecule Ras inhibitors that display antitumor activity by blocking the Ras-effector interaction. *Proc. Natl Acad. Sci. U.S.A.* **110**, 8182–8187 https://doi.org/10.1073/pnas.1217730110
68 Sun, Q., Burke, J.P., Phan, J., Burns, M.C., Olejniczak, E.T., Waterson, A.G. et al. (2012) Discovery of small molecules that bind to K-Ras and inhibit Sos-mediated activation. *Angew. Chem. Int. Ed. Engl.* **51**, 6140–6143 https://doi.org/10.1002/anie.201201358
69 Wiechmann, S., Maisonneuve, P., Grebbin, B.M., Hoffmeister, M., Kaulich, M., Clevers, H. et al. (2020) Conformation-specific inhibitors of activated Ras GTPases reveal limited Ras dependency of patient-derived cancer organoids. *J. Biol. Chem.* **295**, 4526–4540 https://doi.org/10.1074/jbc.RA119.011025
70 Leshchiner, E.S., Parkhitko, A., Bird, G.H., Luccarelli, J., Bellairs, J.A., Escudero, S. et al. (2015) Direct inhibition of oncogenic KRAS by hydrocarbon-stapled SOS1 helices. *Proc. Natl Acad. Sci. U.S.A.* **112**, 1761–1766 https://doi.org/10.1073/pnas.1413185112
71 McGee, J.H., Shim, S.Y., Lee, S.J., Swanson, P.K., Jiang, S.Y., Durney, M.A. et al. (2018) Exceptionally high-affinity Ras binders that remodel its effector domain. *J. Biol. Chem.* **293**, 3265–3280 https://doi.org/10.1074/jbc.M117.816348
72 Kauke, M.J., Traxlmayr, M.W., Parker, J.A., Kiefer, J.D., Knihtila, R., McGee, J. et al. (2017) An engineered protein antagonist of K-Ras/B-Raf interaction. *Sci. Rep.* **7**, 5831 https://doi.org/10.1038/s41598-017-05889-7
73 Upadhyaya, P., Qian, Z., Selner, N.G., Clippinger, S.R., Wu, Z., Briesewitz, R. et al. (2015) Inhibition of Ras signaling by blocking Ras-effector interactions with cyclic peptides. *Angew. Chem. Int. Ed. Engl.* **54**, 7602–7606 https://doi.org/10.1002/anie.201502763
74 Buyanova, M., Cai, S., Cooper, J., Rhodes, C., Salim, H., Sahni, A. et al. (2021) Discovery of a bicyclic peptidyl pan-Ras inhibitor. *J. Med. Chem.* **64**, 13038–13053 https://doi.org/10.1021/acs.jmedchem.1c01130
75 Niida, A., Sasaki, S., Yonemori, K., Sameshima, T., Yaguchi, M., Asami, T. et al. (2017) Investigation of the structural requirements of K-Ras(G12D) selective inhibitory peptide KRpep-2d using alanine scans and cysteine bridging. *Bioorg. Med. Chem. Lett.* **27**, 2757–2761 https://doi.org/10.1016/j.bmcl.2017.04.063
76 Sakamoto, K., Kamada, Y., Sameshima, T., Yaguchi, M., Niida, A., Sasaki, S. et al. (2017) K-Ras(G12D)-selective inhibitory peptides generated by random peptide T7 phage display technology. *Biochem. Biophys. Res. Commun.* **484**, 605–611 https://doi.org/10.1016/j.bbrc.2017.01.147
77 Sogabe, S., Kamada, Y., Miwa, M., Niida, A., Sameshima, T., Kamaura, M. et al. (2017) Crystal structure of a human K-Ras G12D mutant in complex with GDP and the cyclic inhibitory peptide KRpep-2d. *ACS Med. Chem. Lett.* **8**, 732–736 https://doi.org/10.1021/acsmedchemlett.7b00128
78 Sakamoto, K., Lin, B., Nunomura, K., Izawa, T. and Nakagawa, S. (2022) The K-Ras(G12D)-inhibitory peptide KS-58 suppresses growth of murine CT26 colorectal cancer cell-derived tumors. *Sci. Rep.* **12**, 8121 https://doi.org/10.1038/s41598-022-12401-3
79 Sakamoto, K., Masutani, T. and Hirokawa, T. (2020) Generation of KS-58 as the first K-Ras(G12D)-inhibitory peptide presenting anti-cancer activity *in vivo*. *Sci. Rep.* **10**, 21671 https://doi.org/10.1038/s41598-020-78712-5
80 Zhang, Z., Gao, R., Hu, Q., Peacock, H., Peacock, D.M., Dai, S. et al. (2020) GTP-state-selective cyclic peptide ligands of K-Ras(G12D) block its interaction with Raf. *ACS Cent. Sci.* **6**, 1753–1761 https://doi.org/10.1021/acscentsci.0c00514

3.2. An improved PDE6D inhibitor combines with Sildenafil to synergistically inhibit KRAS mutant cancer cell growth (II)

Pelin Kaya[#], Elisabeth Schaffner-Reckinger, Ganesh babu Manoharan, Vladimir Vukic, Alexandros Kiriazis, Mirko Ledda, Maria Burgos, Karolina Pavic, Anthoula Gaigneaux, Enrico Glaab, Daniel Kwaku Abankwa

Status: under review /

preprint has posted on bioRxiv https://doi.org/10.1101/2023.08.23.554263

Personal contributions of Pelin Kaya

- Designed, performed, and analyzed the 2D cell proliferation assays, BRET assays and synergism data then generated and compiled listed figures submitted for this manuscript:
  - **Figure 2 (A-E)**
  - **Figure 3 (A-D)**
  - **Figure 4 (A-B)**
  - **Figure 5 (A-D)**
  - **Figure SI 1 (A, B, C, F, G, H)**
- Performed the DSS and synergism analysis. Created **Supplemantary Data 2 (SI Data 2)** by using the data from analyses.
- Conducted data analysis and literature search pertaining to generate **Supplemantary Data 3 (SI Data 3)**.
- Analyzed and generated the DRIVE project gene dependency profiling of the cell lines (**Figure SI 1H)**.
- Designed, generated, and validated the expression constructs for BRET assay by multi-site gateway cloning system.
- The personal contributions of all authors to the manuscript are listed in the Authors' contributions section at the end of the corresponding manuscript.

Manuscript II: Introduction

Dysregulated Ras signaling is implicated in the development and progression of many cancers, which presents a significant challenge for treatment due to limited therapeutic options. Trafficking chaperone PDE6D facilitates the localization of K-Ras to the plasma membrane. As such, it has been recognized as a viable surrogate target for K-Ras. Previously, our group has developed novel PDE6D inhibitors called Deltaflexin-1 and Deltaflexin-2. However, the first and second generation of Deltaflexins had a low in vitro potency (Siddiqui *et al.*, 2020a).

Efforts to enhance the effectiveness of inhibitors targeting the trafficking chaperone PDE6D in KRAS-mutant cancer cells did not meet the expected outcomes thus far. In response, we have successfully developed new generation of Deltaflexins that exhibit a significantly improved on-target profile and display low nanomolar affinity for the target enzyme. This improvement was validated through analysis using PDE6D-knockout MEFs and an assay designed to assess intracellular engagement of UNC119 homolog A protein (UNC119A), which is closely related to PDE6D. Our findings highlight that increasing the binding affinity for the hydrophobic pocket of PDE6D leads to both solubility issues and undesired off-target effects.

In order to enhance the selectivity of our highly soluble compound, Deltaflexin3, towards K-Ras protein, we conducted a study where we combined it with Sildenafil. This drug is mostly used in the treatment of erectile dysfunction and pulmonary arterial hypertension. It works by inhibiting the phosphodiesterase type 5 (PDE5) enzyme, which leads to increased levels of cGMP in the body (Booth, Roberts et al. 2014). Elevated cGMP levels have been shown to activate protein kinase G (PKG), which in turn can lead to the phosphorylation of Ras proteins. Given the role of Ras signaling in many cancers and other diseases, there has been interest in exploring the potential therapeutic benefits of using sildenafil to induce Ras phosphorylation (Cho, Casteel et al. 2016, Dent, Booth et al. 2019). Our aim was to promote the phosphorylation of Ser181 and subsequently reduce the affinity between K-Ras and its chaperone PDE6D. As a result, this combination effectively reduced Ras-signaling and demonstrated robust inhibitory effects on cancer cell proliferation as well as ex vivo tumor growth. These findings establish Deltaflexin3-Sildenafil as currently one of the most selective PDE6Di compounds available for targeting specifically K-Ras. Moreover, mechanistic insights from our work suggest that synergistic combinations can be explored further in order to achieve more focused inhibition on K-Ras.

An improved PDE6D inhibitor combines with Sildenafil to synergistically inhibit KRAS mutant cancer cell growth

Pelin Kaya [1], Elisabeth Schaffner-Reckinger [1], Ganesh babu Manoharan [1], Vladimir Vukic [2], Alexandros Kiriazis [3,#], Mirko Ledda [4], Maria Burgos [1], Karolina Pavic [1], Anthoula Gaigneaux [5], Enrico Glaab [4], Daniel Kwaku Abankwa [1,3 *]

[1] Cancer Cell Biology and Drug Discovery Group, Department of Life Sciences and Medicine, University of Luxembourg, 4362 Esch-sur-Alzette, Luxembourg

[2] University of Novi Sad, Faculty of Technology, 21000 Novi Sad, Serbia

[3] Turku Bioscience Centre, University of Turku and Åbo Akademi University, 20520 Turku, Finland

[4] Luxembourg Center for Systems Biomedicine, University of Luxembourg, 4365 Esch-sur-Alzette, Luxembourg

[5] Bioinformatics Core, Department of Life Sciences and Medicine, University of Luxembourg, 4362 Esch-sur-Alzette, Luxembourg

[#] current address: Orion Corporation, Orion Pharma, Espoo, Finland

[*] Corresponding author: daniel.abankwa@uni.lu

Running Title: PDE6D inhibitor synergism with Sildenafil

Abstract

The trafficking chaperone PDE6D (or PDEδ) was proposed as a surrogate target for K-Ras, leading to the development of a series of inhibitors that block its prenyl-binding pocket. These inhibitors suffered from low solubility and intracellular potency, preventing their clinical development.

Here we developed a highly soluble PDE6D inhibitor (PDE6Di), Deltaflexin3, which has the currently lowest off-target activity, as we demonstrate in dedicated assays. We further increased the K-Ras focus, by exploiting that PKG2-mediated phosphorylation of Ser181 lowers K-Ras binding to PDE6D. Thus, the combination of Deltaflexin3 with the approved PKG2-activator Sildenafil synergistically inhibits cell- and microtumor growth. However, the overall cancer survival of the high PDE6D/ low PKG2 target population is higher than of the group with the opposite signature. Our results therefore suggest re-examining the interplay between PDE6D and K-Ras in cancer, while recommending the development of PDE6Di that 'plug', rather than 'stuff' the hydrophobic pocket of PDE6D.

Significance

Combinations of a novel PDE6D inhibitor with Sildenafil synergistically focus the inhibition on K-Ras, however, survival data of the target population suggest an interplay of K-Ras and PDE6D that needs further exploration.

Keywords

KRAS; PDE6D; inhibitor; drug development; Ras trafficking; cancer

Introduction

The highly mutated oncogene KRAS is one of the best-established cancer targets. Only recently have two KRAS-G12C inhibitors, sotorasib and adagrasib, been approved for the treatment of lung cancer (Fell *et al*, 2020; Skoulidis *et al*, 2021). While other allele specific-, pan-Ras- and Ras-pathway inhibitors are under intense development (Punekar *et al*, 2022; Steffen *et al.*, 2023), there is still a need to target Ras more profoundly from various angles.

Inhibition of Ras membrane targeting remains a promising strategy for inhibitor development (Cox *et al.*, 2015; Pavic *et al*, 2022). The trafficking chaperone PDE6D (or PDEδ) has been proposed as a surrogate drug target in KRAS mutant cancers (Zimmermann *et al.*, 2013). PDE6D possesses a hydrophobic pocket, which can bind to one or even two prenyl-moieties, thus having a cargo spectrum that comprises farnesylated or geranylgeranylated Ras- and Rho-family proteins, as well as Rab proteins (Dharmaiah *et al.*, 2016; Yelland *et al.*, 2022). Only proteins that are not in addition palmitoylated in the

vicinity of the prenylated cysteine are accepted as cargo, making mono- and dual-palmitoylated N-Ras, K-Ras4A and H-Ras effectively worse cargo in cells than K-Ras4B (hereafter K-Ras) (Chandra *et al.*, 2011). Cargo affinity is critically modulated by the four residues upstream of the prenylated cysteine. Structure and sequence comparisons suggest that the two residues upstream of the prenylated cysteine cannot be large amino acids, like Lys, Arg or Glu (Dharmaiah *et al.*, 2016). This stretch of four residues also comprises Ser181 at the C-terminus of K-Ras, which can be phosphorylated by PKG2 (Cho *et al*, 2016). Binding data of PDE6D to K-Ras with a S181E mutation suggest a reduced interaction when K-Ras is phosphorylated on Ser181 (Dharmaiah *et al.*, 2016).
K-Ras has only micromolar affinity to PDE6D, while another cargo the inositol phosphatase INPP5E, has a low nanomolar affinity (Dharmaiah *et al.*, 2016; Fansa *et al.*, 2016). This has important consequences for their subcellular distribution. While K-Ras can be released in the perinuclear area by the allosteric release factor Arl2, which binds to PDE6D when GTP-bound (Ismail *et al.*, 2011; Schmick *et al.*, 2014), INPP5E is only dislodged by GTP-Arl3 inside the primary cilium (Fansa *et al.*, 2016).

The development of inhibitors that competitively bind to the prenyl-pocket of PDE6D was pioneered by the Waldmann group (Martin-Gago *et al.*, 2017a). However, their first two generations of PDE6D inhibitors (PDE6Di) Deltarasin and Deltazinone1 appeared to have off-target issues and poor metabolic stability, respectively (Papke *et al.*, 2016; Zimmermann *et al.*, 2013). In addition, both compounds were ejected by the GTP-Arl2-dependent mechanism, similar to the natural PDE6D cargo. Only their third-generation inhibitors, the Deltasonamides, could withstand GTP-Arl2-mediated ejection, as they were highly optimized for sub-nanomolar affinity. However, these compounds appeared to have low cell penetration (Martin-Gago *et al.*, 2017a). In an attempt to optimize the pharmacological properties, the chemotype was switched from benzimidazole to pyridazinones, such as Deltazinone (Papke *et al.*, 2016). This led to the development of low nanomolar inhibitors, such as candidate compound **99** that was pharmacokinetically evaluated in mice, without assessment of anti-tumorigenic activity (Murarka *et al*, 2017). Hence, from these pioneering compounds, anti-tumor activity in vivo was only demonstrated with the first-generation compound Deltarasin (Zimmermann *et al.*, 2013). All three compound generations were mostly evaluated in KRAS-mutant pancreatic cancer cell lines, yet both Deltarasin and Deltasonamide were also micromolar active in KRAS mutant and PDE6D-dependent colorectal cancer cell lines (Klein *et al.*, 2019).

Another class of more recent PDE6Di are proteolysis-targeting chimeras (PROTACs). Unlike classical competitive inhibitors they do not have to bind permanently i.e., they can

act sub-stoichiometrically (Paiva & Crews, 2019). Proof-of-concept PROTACs from two groups were developed based on previously established competitive PDE6Di, Deltasonamide and Deltazinone (Cheng *et al*, 2020; Winzker *et al*, 2020). These heterobifunctional compounds bind with their first functional moiety to the prenyl-pocket of PDE6D and with the second they recruit an E3 ubiquitin ligase complex to instruct proteasomal degradation of PDE6D. While the Deltasonamide-derived PROTAC effectively decreased PDE6D levels in pancreatic cancer cells (Winzker *et al.*, 2020), the Deltazinone-derived PROTAC was even efficacious in SW480 xenografts in mice (Cheng *et al.*, 2020).

Following the pioneering work of the Waldmann group, other PDE6D-pocket competitive inhibitors were investigated, although for several of them clear in vitro or cellular target engagement data are missing. However, the Sheng group developed compounds that bound to PDE6D in vitro with nanomolar affinity. Some suppressed MAPK-output, but again had only micromolar cellular activity (Chen *et al*, 2018; Jiang *et al*, 2017). Interestingly, in their most recent work their spiro-cyclic compound 36l (Kd = 127 nM) showed target engagement in cells, while also demonstrating in vivo efficacy in KRAS mutant primary cell lines (Chen *et al.*, 2022). In another study, the triazole **27** had nanomolar activity in a PDE6D binding assay and robustly inhibited MAPK-output at 10 µM and A549 cell growth at this concentration range (Chen *et al.*, 2019).

Another PDE6Di emerged from a Rac-inhibitor screen, which led to the oxadiazole DW0254 as a submicromolar active compound (Kd = 436 ± 6 nM) (Canovas Nunes *et al.*, 2022). This compound inhibited downstream signaling of Ras above 20 µM and in vivo activity was observed with pretreatment of transplanted T-cell cancer cells or application of a pump to the graft site, due to poor solubility.

We have previously published novel competitive PDE6Di called Deltaflexins, for which we determined low micromolar affinities in a dedicated surface plasmon resonance assay, that were matched by a similar level of activity in KRAS mutant HCT116 and MDA-MB-231 cancer cells (Siddiqui *et al.*, 2020a). Their chemical design features a hexamethylene-amide-backbone, which allowed simple derivatization and compound evolution. Importantly, Deltaflexins demonstrated the expected K-Ras- over H-Ras-selectivity in cells, an important on-target feature.

A number of questions remain unresolved regarding PDE6D as a surrogate target for K-Ras. Current PDE6Di are still at the hit stage and have various problems, such as poor solubility, metabolic instability and off-target issues (Murarka *et al.*, 2017; Papke *et al.*, 2016). This makes the interpretation of phenotypic data and validation of PDE6D as a drug

target in vivo difficult (Zimmermann *et al.*, 2013). Together with the broad cargo spectrum of PDE6D, which involves far more prenylated proteins than K-Ras, it is almost impossible to tell in which cancer type PDE6Di should be applied. Hence, clear genetic determinants that could indicate a susceptibility to PDE6D inhibition are lacking.

Here, we established an in silico library of compounds by cross-hybridizing moieties of existing PDE6Di with our previous hexamethylene-amide-backbone (Siddiqui *et al.*, 2020a). Aided by computational docking, we derived rationales for the synthesis of 16 novel PDE6Di, that we comprehensively characterized biochemically and in cells for potency and K-Ras- and PDE6D-on-target selectivity. We demonstrate that efficacy and more focused inhibition of K-Ras can be achieved by combining our most selective and highly soluble inhibitor Deltaflexin3 synergistically with the clinically approved Sildenafil.

Results

Computational docking aided design of novel PDE6D inhibitors

We previously demonstrated that PDE6Di can be efficiently generated by using a hexamethylene-amide-backbone (Siddiqui *et al.*, 2020a). Using this backbone as a base, we created an in silico library of hybrid compounds, which contained moieties of established PDE6Di, such as Deltarasin, Deltazinone1 and Deltasonamide1 that also served as references in this study (Figure 1A) (Martin-Gago *et al.*, 2017a; Papke *et al.*, 2016; Zimmermann *et al.*, 2013).

Altogether, 313 compounds were thus designed in the first round and computationally docked to PDE6D (PDB ID 4JV8), using Glide docking software (Friesner *et al*, 2006). Compounds selected based on the docking scores, MM-GBSA binding energy and visual inspection were prioritized and provided a rationale for the synthesis of a first round of eight compounds that were biochemically and cell-biologically characterized (Figure 1B; Data S1 and S2).

Subsequently, the best performing compound 4 was chosen as a starting point for derivatives that were again first evaluated by in silico docking using SeeSAR. In this second round, compounds were extended to attempt interactions with residues at the entry of the hydrophobic pocket of PDE6D. Based on these computational data a second round of eight candidate compounds was synthesized and characterized like the first-round compounds (Figure 1C; Data S1 and S2**)**.

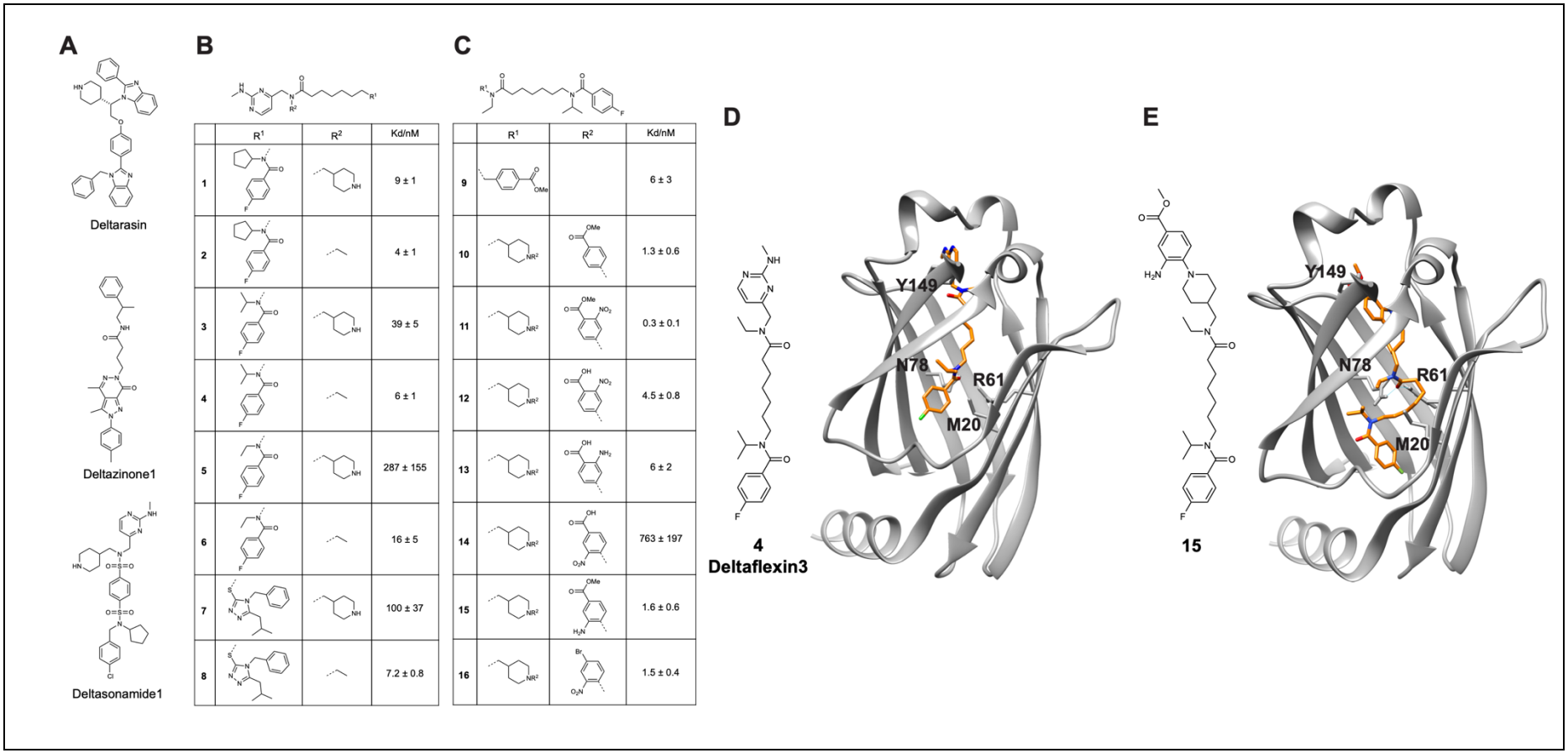

Figure 1. Investigated PDE6D inhibitors (PDE6Di) with affinities and computational docking.

(**A**) Structures of employed reference PDE6Di.

(**B,C**) Structures of developed first (B) and second (C) round PDE6Di with PDE6D dissociation constants measured using F-Ator in a fluorescence polarization assay; n ≥ 2.

(**D,E**) Computational docking of compounds **4** (later named Deltaflexin3; D) and **15** (E) to PDE6D in the open state (PDB ID 4JV8).

Computational docking data of two of our compounds 4 and 15 revealed multiple van-der-Waals contacts to residues Met20, Arg61, Gln78, and Tyr149 (Figure 1D,E). Hydrogen bonds to these residues were only predicted for **15** with Arg61 and Gln78 (Figure 1E). The Arg61 hydrogen bond is shared with the reference inhibitors Deltarasin and Deltazinone1 (Papke *et al.*, 2016; Zimmermann *et al.*, 2013).

In vitro affinity and intracellular BRET-assays quantify target engagement and K-Ras-selectivity

All 16 compounds that were prioritized for synthesis first underwent in vitro testing using a previously employed fluorescence polarization assay where the FITC-labelled PDE6D-binder Atorvastatin (F-Ator) was used as a probe (Zimmermann *et al.*, 2013) (Figure 1B,C; Data S2). In addition, we determined the affinities of compounds using the FITC-labelled farnesylated peptide derived from the C-terminus of the small GTPase Rheb (F-Rheb) (Ismail *et al.*, 2011) (Data S2). When using F-Ator as a probe, we recovered affinities in the low nanomolar range for reference compounds, Deltarasin (Kd = 39 ± 15 nM), Deltazinone1 (Kd = 3.8 ± 0.4 nM) and Deltasonamide1 (Kd = 0.11 ± 0.03 nM), similar to previously published values (Martin-Gago *et al.*, 2017a; Papke *et al.*, 2016; Zimmermann *et al.*, 2013). By contrast, affinities determined using F-Rheb were typically only in the sub-micromolar range (Data S2). However, both datasets overall correlated and served to rank the in vitro potencies of our 16 compounds and we will in the following refer to the values obtained with F-Ator, unless otherwise stated (Figure 2A, Figure S 1A).

Subsequently three cellular BRET (Bioluminescence Resonance Energy Transfer) assays were applied to profile the disruption of the PDE6D/ K-Ras interaction and loss of functional membrane organization of K-Ras as compared to H-Ras over a wider concentration range in HEK293-EBNA cells (Figure 2A). In analogy to our previous FRET-based target engagement assay (Siddiqui *et al.*, 2020a), we implemented a BRET-assay with Rluc8-PDE6D and GFP2-K-RasG12V to determine the intracellular potency of compounds to displace K-RasG12V from PDE6D (Figure 2A; Data S2).

While intracellular IC50-values were in the micromolar regime (Data S2), we generally employed the more robust normalized area under the curve DSS3-score for dose-response data (Yadav *et al.*, 2014). Overall, DSS3-scores from the PDE6D/ K-RasG12V-BRET correlated with in vitro affinities, and in both datasets, potencies increased markedly from the first to the second round of compounds (Figure 2A).

A second set of BRET-assays was likewise built in analogy to previous FRET-assays (Guzman *et al*, 2016; Siddiqui *et al*, 2020b). We assessed the BRET that emerges between a Rluc8-donor tagged RasG12V and a GFP2-acceptor tagged RasG12V, due to

nanoclustering (Parkkola *et al*, 2021). This type of assay can sensitively detect perturbations not only of Ras-nanoclustering, but also of any upstream process, such as correct membrane anchorage or lipid modifications (Najumudeen *et al*, 2013; Parkkola *et al.*, 2021) (Figure S 1B).

When palmitoylated, prenylated proteins such as dually palmitoylated H-Ras cannot bind to PDE6D, making them effectively worse intracellular cargo (Chandra *et al.*, 2011; Dharmaiah *et al.*, 2016). Hence, loss of PDE6D activity such as by siRNA-mediated knockdown, selectively decreases the BRET-signal of K-RasG12V, but not of H-RasG12V (Figure S 1B-D). Using these two BRET-assays, we assessed the intracellular K-RasG12V-membrane anchorage disruption and K-RasG12V-selectivity of compounds. This again revealed an increase in potency amongst the second-round compounds (Figure 2A). Compound 4 had the best overall K-RasG12V-selectivity and compound 15 the best selectivity of top second-round compounds (Figure 2B) and both compounds compared favorably in all three BRET-assays relative to the most selective reference compound Deltazinone1 (Figure 2C-E).

Assessing the off-target activity of top compounds

Despite clearly inhibiting PDE6D, several compounds did not display exclusive K-RasG12V-selectivity (Figure 2B). This may be due to off-target activities, a problem that was already noted for previous PDE6Di by others (Murarka *et al.*, 2017; Papke *et al.*, 2016).

Broad off-target effects are phenotypically determined by comparing the anti-proliferative effect of compounds on cells with and without the target. We therefore compared the cell growth inhibition of MEF cells with a homozygous CRISPR-mediated knockout (KO) of PDE6D to their wild type (WT) counterpart as a measure of PDE6D-selectivity (Dewees *et al*, 2022) (Figure S 1E). In line with the BRET-derived K-RasG12V-selectivity data (Figure 2B; Figure S 1F), first-round compounds exhibited a higher PDE6D-selectivity than second-round compounds, with 4 showing again the highest overall selectivity (Figure 3A).

UNC119A is a trafficking chaperone of myristoylated proteins and structurally homologous to PDE6D (Fansa *et al.*, 2016). Given this relatedness in structure and function, it is a plausible off-target for PDE6Di. We therefore established a BRET-assay to determine the UNC119A-directed off-

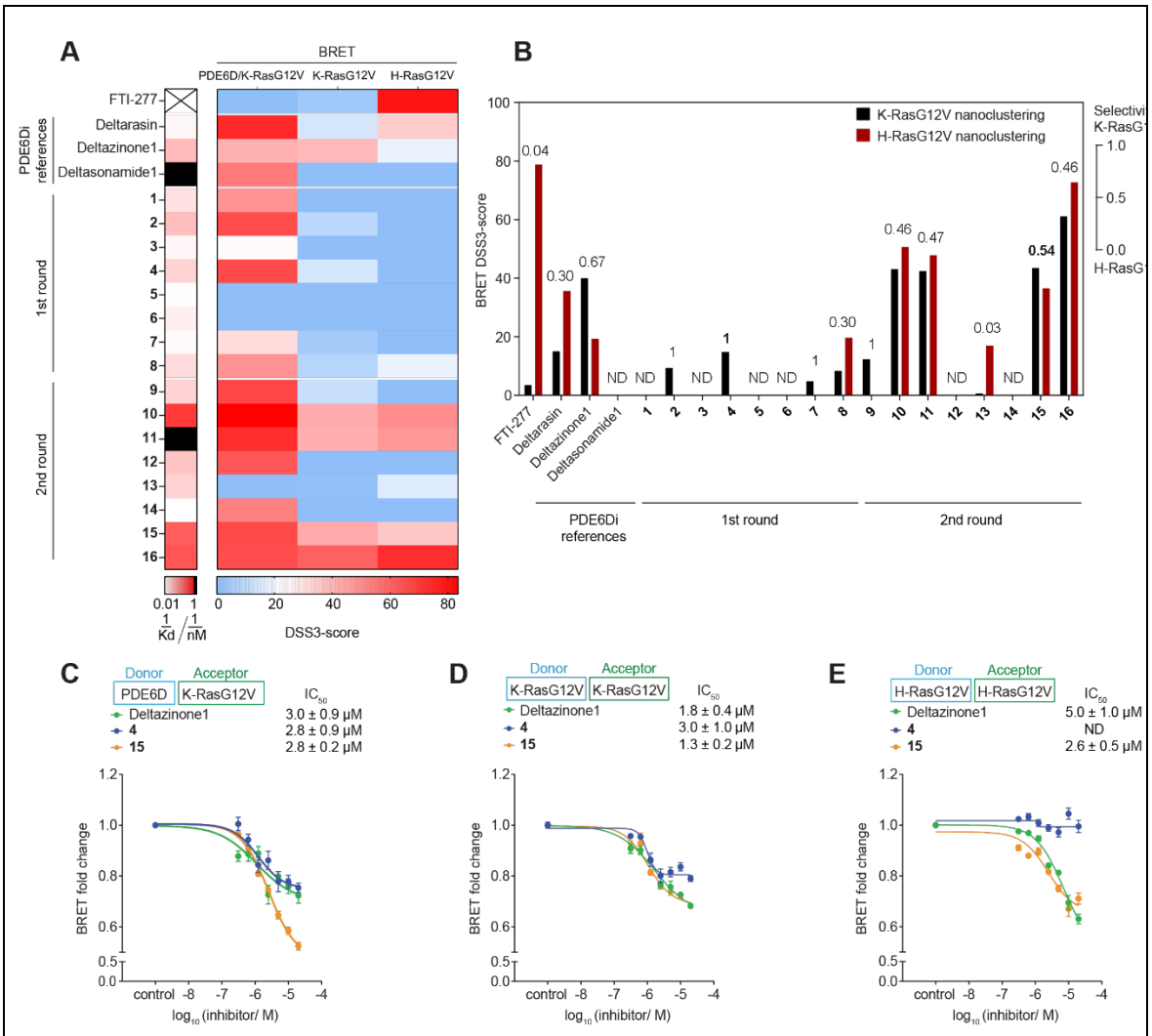

Figure 2. Quantification of on-target activity of PDE6Di in vitro and in cellular BRET-assays.

(A) Heatmaps of in vitro affinity of compounds determined using F-Ator (first column; n ≥ 2) and DSS3-scores from cellular BRET-experiments. The disruption of the PDE6D/ K-RasG12V complex (second column; n ≥ 2) and of K-RasG12V- and H-RasG12V-membrane anchorage (third and fourth columns, respectively; n ≥ 2) were measured by BRET over a wider concentration range and the area under the curve DSS3-score was determined.

(B) Quantification of K-RasG12V-selectivity (values above bars) was performed by determining the ratio of K-RasG12V and the sum of K-RasG12V- and H-RasG12V-BRET DSS3-scores from (A).

(C-E) Dose-dependent change of normalized BRET-signals after treatment with indicated compounds using BRET donor/ acceptor-pairs shown on top; n ≥ 4.

247

target activity, by quantifying if the top three compounds from each round disrupted the UNC119A/ Src-complex.

In BRET-titration experiments the characteristic BRET-ratio, BRETtop, that is reached within a defined acceptor-to-donor ratio is a measure for complex stability (Manoharan *et al*, 2023). A previously identified inhibitor of UNC119A, Squarunkin A, significantly reduced the BRETtop between UNC119A-Rluc8 and Src-GFP2 (Figure S 1G) (Garivet *et al.*, 2019). Similarly, treatment with the N-myristoyl-transferase inhibitor IMP-1088 reduced the BRETtop (Figure S 1G) (Mousnier *et al*, 2018), confirming that our assay can detect myristoyl-pocket dependent disruption of the UNC119A/ Src-interaction.

When testing the reference compounds, we found that surprisingly at 5 µM both Deltarasin and Deltasonamide1, but not Deltazinone1, significantly decreased the UNC119A/ Src-BRET, suggesting off-target binding of the compounds to UNC119A (Figure 3B). By contrast, none of our top first-round compounds decreased UNC119A/ Src-BRET (Figure 3C), while all our top second-round compounds did, with **15** having the least disruptive activity (Figure 3D).

Inhibition of Ras-signaling and cancer cell proliferation by the top compounds

Next, we continued our selectivity assessment by testing the anti-proliferative activity of the top three compounds from each round on *KRAS*-, *HRAS*- or *BRAF*-mutant cancer cells. In line with in vitro and BRET-data (Figure 2A), the anti-proliferative activity was significantly increased in compounds of the second optimization round, with cellular potencies increasing to the low- and sub-micromolar regime (Figure 4A; Data S2), but at the expense of selectivity (Figure 4B).

By contrast, 4 displayed the overall highest selectivity for *PDE6D*-dependent and *KRAS*-mutant, as compared to *HRAS*-mutant cancer cell lines (Figure 4B; Figure S 1H), consistent with its K-RasG12V-selectivity detected by BRET (Figure 2B) and its off-target activity being lowest amongst investigated compounds (Figure 3). It therefore surpassed the most selective reference compound, Deltazinone1, ~6-fold. The highest activity of 4 was seen in MIA PaCa-2 (*KRAS-G12C*-mutant) cells (IC50 = 6 ± 1 µM; Data S2), in line with the highest *KRAS*- and *PDE6D*-dependence of this cell line among the tested cell lines (Figure S 1H) (McDonald Iii *et al*, 2017).

For compounds that significantly disrupt K-RasG12V-membrane anchorage, it is expected that they also reduce Ras-signaling output. In line with previous data (Papke *et al.*, 2016; Zimmermann *et al.*, 2013), the reduction in phospho-ERK- (Figure 4C) and phospho-S6-

levels (Figure 4D) downstream of Ras was modest in MIA PaCa-2 cells upon treatment with our top compounds, but better than that seen with the overall best reference compound Deltazinone1.

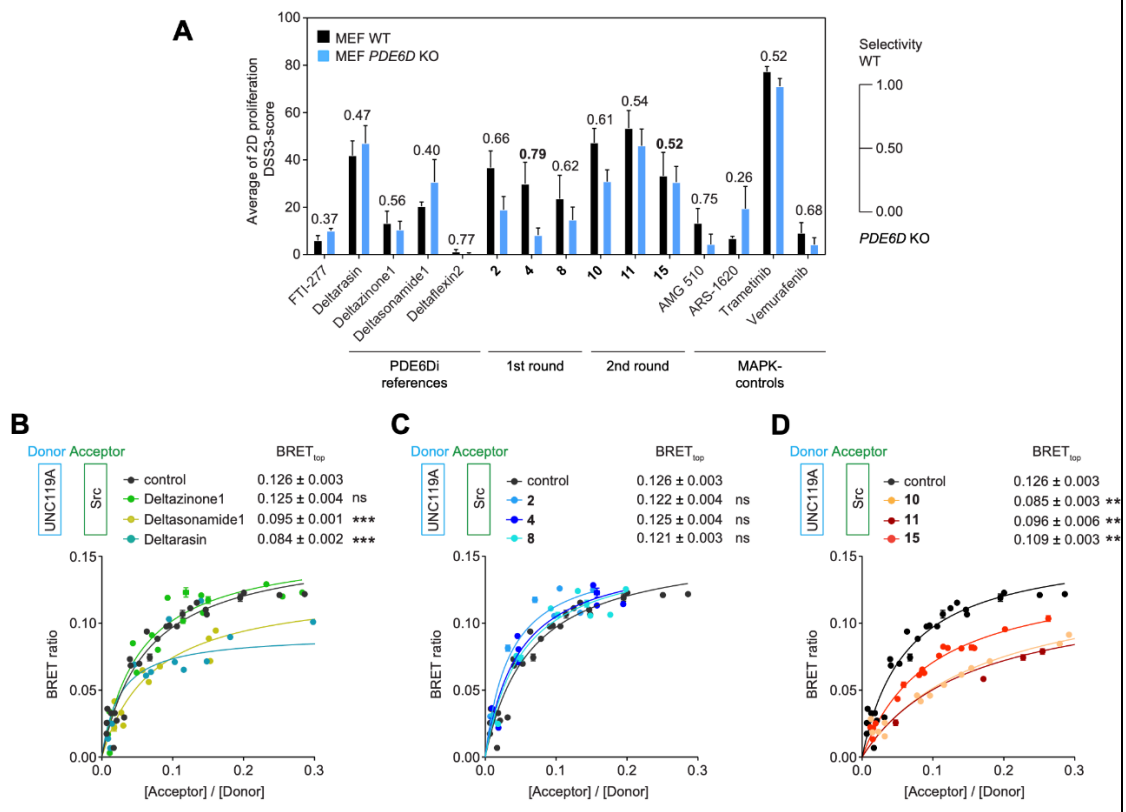

Figure 3. Analysis of PDE6Di off-target activities.

(A) DSS3-scores of indicated compounds from 2D proliferation assays acquired with WT or *PDE6D*-KO MEFs; n = 4. PDE6D-selectivity was determined as the ratio of the DSS3-scores from WT and the sum of WT and KO MEFs and is indicated above the bars.

(B-D) BRET-titration curves of UNC119A/ Src complex after treatment with indicated reference PDE6Di (B), top first round (C) or top second round (D) compounds at 5 µM; n ≥ 3. Statistical comparisons of BRETtop values to controls were done using two-tailed Student's t-test.

We subsequently focused our analysis on compound 4, hereafter named Deltaflexin3, given its overall best performance across all assays and its high water solubility (kinetic solubility, S = 5.68 mM in PBS, pH 7.4, 37 °C).

PDE6D inhibitor Deltaflexin3 and Sildenafil synergize to inhibit K-Ras activity

The approved drug Sildenafil, which is an inhibitor of cGMP-specific phosphodiesterase type 5 (PDE5), stimulates the PKG2-dependent phosphorylation of Ser181 on the C-terminus of K-Ras (Cho *et al.*, 2016). Given that the phospho-mimetic K-Ras-S181E mutation was shown to reduce the

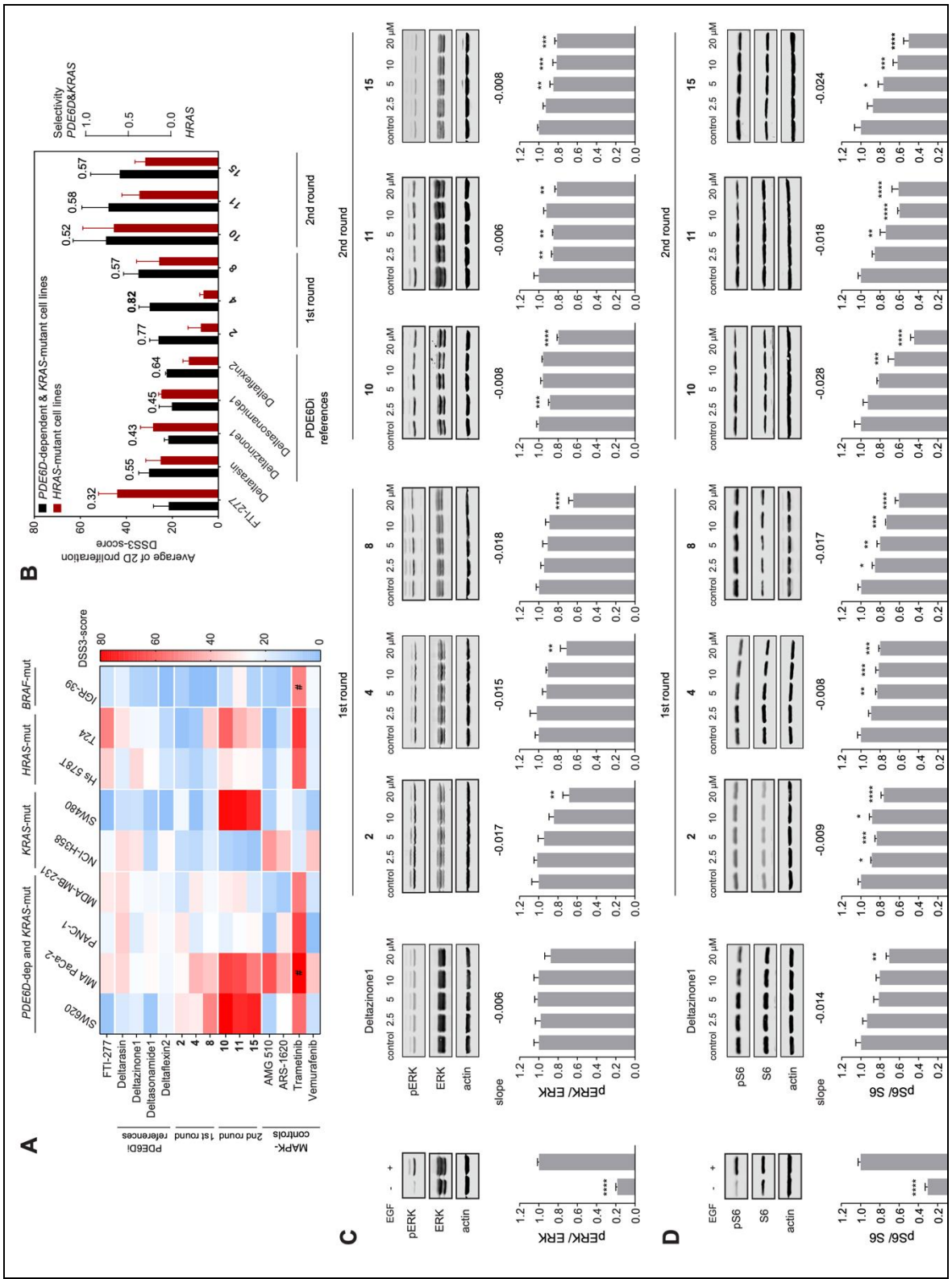

Figure 4: Inhibition of cell proliferation and Ras-signaling by PDE6Di.

(A) DSS3-scores of indicated compounds from 2D proliferation assays acquired with *PDE6D*-dependent and *KRAS*-mutant, *KRAS*-mutant, *HRAS*-mutant or *BRAF*-mutant cell lines; n ≥ 2; # n = 1.

(B) Quantification of *PDE6D*-dependent & *KRAS*-mutant-selectivity was

performed by determining the ratio of the average of DSS3-scores from *PDE6D*-dependent and *KRAS*-mutant cell lines and the sum of the former and the average DSS3-score of *HRAS*-mutant cell lines from (A); n ≥ 3, except for the condition T24/ compound 8, where n = 2.
(C,D) Quantified immunoblot data of phosphorylated and total ERK (C; n ≥ 4) or phosphorylated and total S6 (D; n ≥ 3) from *KRAS-G12C* mutated MIA PaCa-2 cells treated with indicated compounds for 4 h before EGF-stimulation; stimulation control data to the far left.

affinity to PDE6D ~6-fold (Dharmaiah *et al.*, 2016), we reasoned that Sildenafil treatment would likewise decrease the affinity.

We therefore sought to increase the anti-tumorigenic activity of Deltaflexin3 by combining it with Sildenafil, which would also focus the inhibitory activity on K-Ras. A more focused inhibition is supported by a survey of >150 small GTPases, which suggests that only 15 other established or predicted PDE6D cargo proteins possess serine or threonine residues in the four residue stretch upstream of the prenylated cysteine that could be affected by Sildenafil in a manner that could impact on PDE6D engagement (Data S3).

Using our PDE6D/ K-RasG12V-BRET assay, we found that indeed Sildenafil dose-dependently reduced the BRET-signal consistent with a disruption of the PDE6D/ K-RasG12V-complex (IC50 ~17 µM) (Figure 5A). We then combined Deltaflexin3 with Sildenafil at 10 µM, 20 µM and 30 µM i.e., concentrations that hardly affected the BRET-signal, to test for synergism of these two compounds (Figure 5A,B). This analysis revealed a high synergistic activity at ~20 µM Sildenafil and ~900 nM Deltaflexin3 (Figure 5B, right).

We therefore continued with a 2D proliferation analysis for synergism in five *KRAS*-mutant and -dependent cancer cell lines with diverse levels of PDE6D- and PKG2-dependencies (Figure 5C, Figure S 1H). Amongst the tested cell lines, MIA PaCa-2 showed the highest HSA synergism score and a clear shift of the inhibition curve to lower concentrations for combinations of the drugs (Figure 5C,D). Importantly, high synergism was observed at similar concentrations that were previously identified using the on-target BRET-assay (Figure 5B,D).

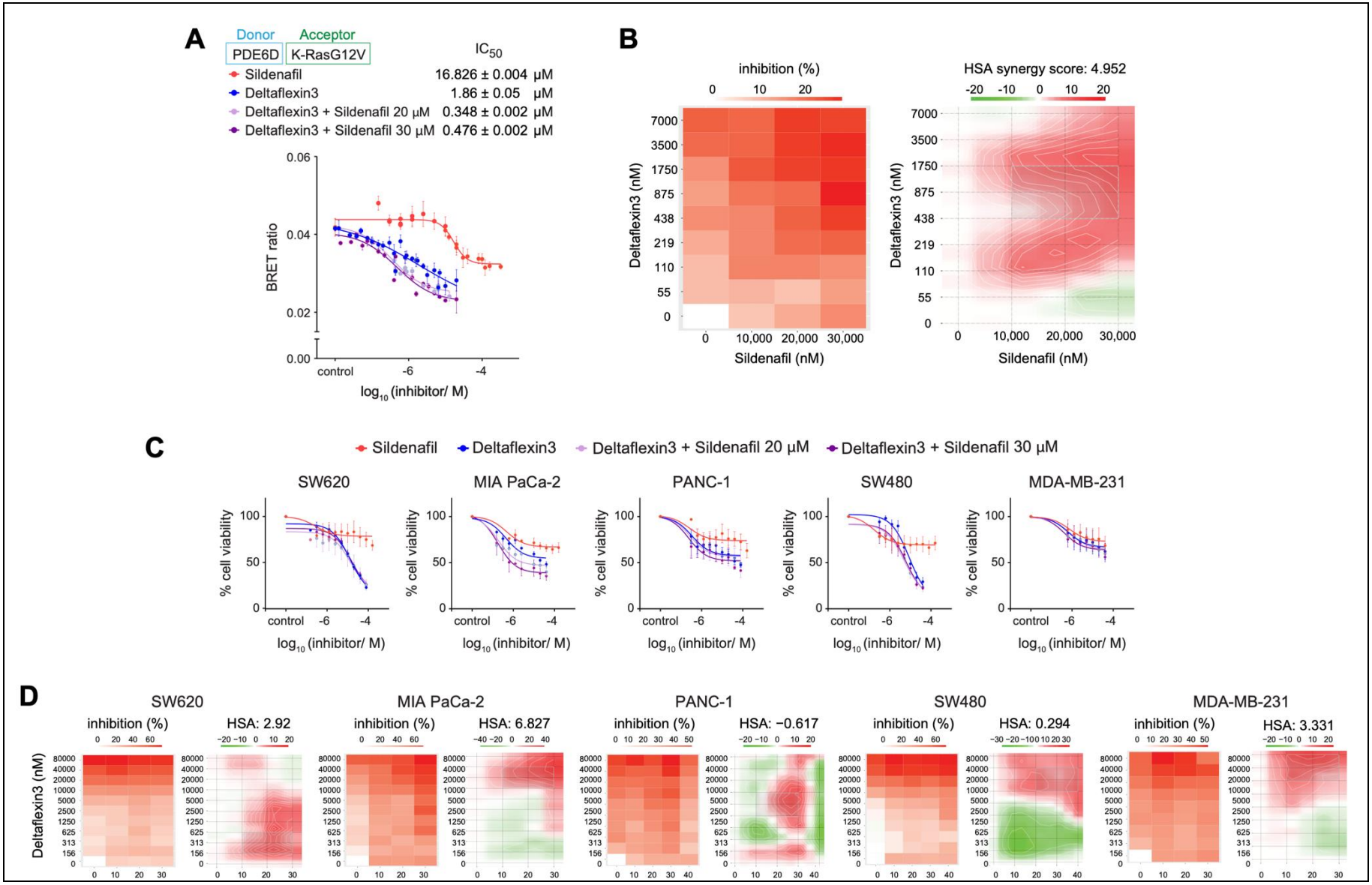
A
Donor
Acceptor
PDE6D
K-RasG12V
IC50
Sildenafil 16.826 ± 0.004 μM
Deltaflexin3 1.86 ± 0.05 μM
Deltaflexin3 + Sildenafil 20 μM 0.348 ± 0.002 μM
Deltaflexin3 + Sildenafil 30 μM 0.476 ± 0.002 μM
BRET ratio
log10 (inhibitor/ M)
B
inhibition (%)
HSA synergy score: 4.952
Deltaflexin3 (nM)
Sildenafil (nM)
C
Sildenafil
Deltaflexin3
Deltaflexin3 + Sildenafil 20 μM
Deltaflexin3 + Sildenafil 30 μM
SW620
MIA PaCa-2
PANC-1
SW480
MDA-MB-231
% cell viability
log10 (inhibitor/ M)
D
SW620
MIA PaCa-2
PANC-1
SW480
MDA-MB-231
inhibition (%)
HSA: 2.92
HSA: 6.827
HSA: −0.617
HSA: 0.294
HSA: 3.331
Deltaflexin3 (nM)

Figure 5. Analysis of Deltaflexin3 (4) and Sildenafil synergism.

(A) Dose-dependent disruption of PDE6D/ K-Ras complex after treatment with indicated compounds and combinations measured in cellular BRET-assays; n ≥ 3.

(B) Inhibition (drop in normalized BRET ratio, left) and HSA synergism (right) heatmaps of combinations in (A) and an additional combination with 10 µM Sildenafil; n ≥ 3. Positive HSA synergy scores indicate synergism, while negative scores signify antagonism.

(C) Compound-dose dependent change of cell proliferation after indicated treatments of *KRAS*-mutant cancer cell lines; n ≥ 2.

(D) Inhibition and HSA synergism heatmaps for combinatorial Deltaflexin3 and Sildenafil treatment as determined from 2D cell proliferation assays with indicated KRAS-mutant cancer cell lines; n ≥ 2.

Combinations of Deltaflexin3 and Sildenafil efficiently suppress Ras-signaling and microtumor growth

Supported by these proliferation data that suggested a synergism of Deltaflexin3 in combination with Sildenafil, we focused our investigations on MIA PaCa-2 cells.

We first reexamined, whether signaling downstream of Ras was more efficiently inhibited by the combination treatment. Neither Sildenafil at concentrations between 20-30 µM, nor Deltaflexin3 at 10 µM significantly reduced phospho-ERK- (Figure 6A) or phospho-S6-levels (Figure 6B). Intriguingly, however, the combination of 10 µM Deltaflexin3 and 20 µM Sildenafil significantly reduced phosphorylation levels of both ERK and S6 by ~ 28 % and ~ 35 %, respectively.

Next, we evaluated the anti-tumorigenic activity of Deltaflexin3 in the chorioallantoic membrane (CAM)-assay, where microtumors are raised on the chorioallantoic membrane of fertilized chick eggs (Lokman *et al*, 2012; Siddiqui *et al*, 2021). While 10 µM Deltaflexin3 alone significantly reduced MDA-MB-231 cell derived microtumors (Figure S 1I), already 2.5 µM Deltaflexin3 were sufficient to achieve a similar reduction in MIA PaCa-2-derived microtumors (Figure 6C,D). This is in agreement with the poorer response of MDA-MB-231 to Deltaflexin3 observed in 2D proliferation data (Figure 4A). Consistent with the synergistic increase in efficacy observed for the combination of Deltaflexin3 and Sildenafil in BRET-, signaling- and proliferation-assays, MIA PaCa-2-derived microtumor growth was more potently reduced by the combination than by each compound alone (Figure 6C,D).

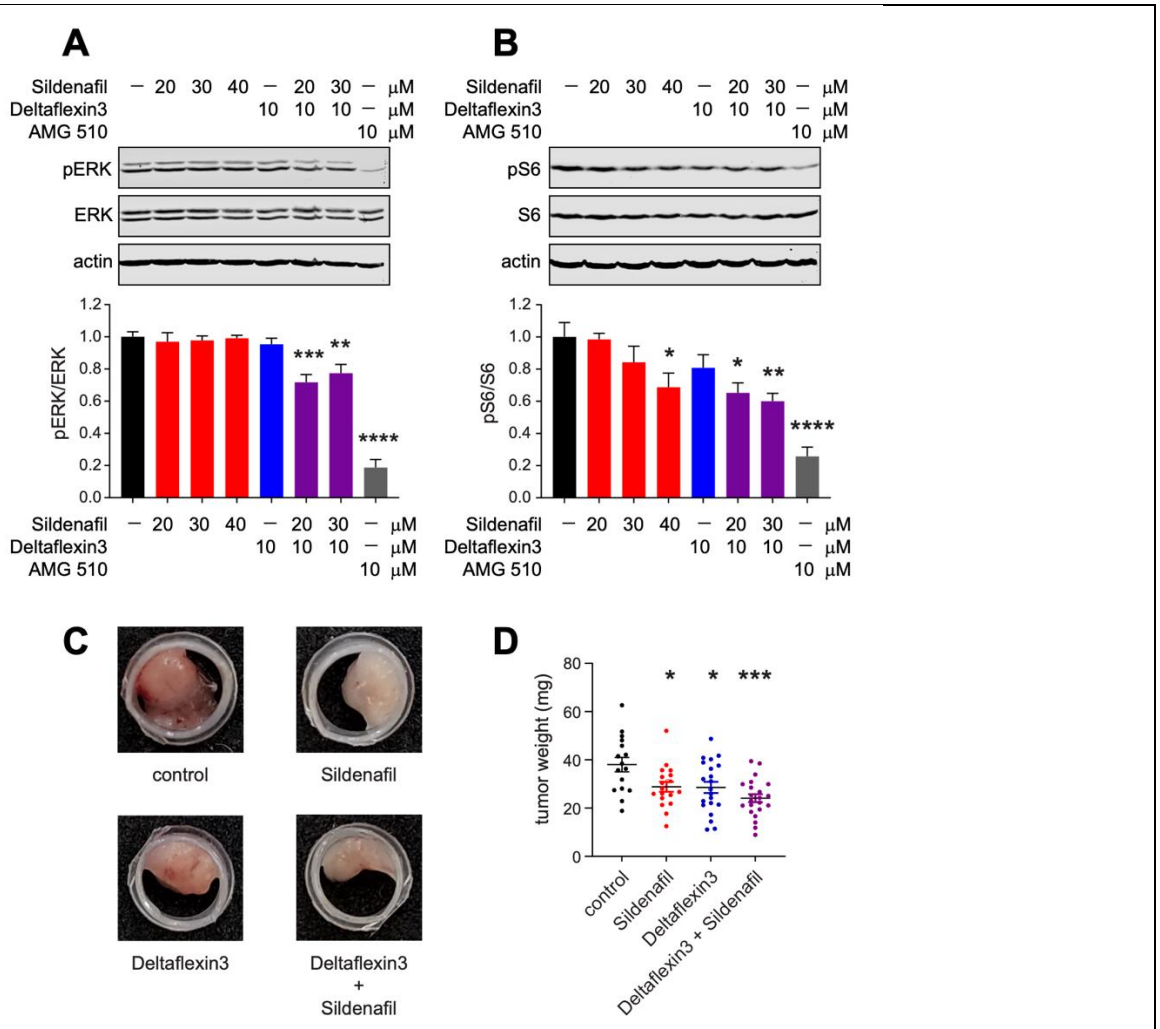

Figure 6. The Deltaflexin3/ Sildenafil combination more potently inhibits Ras-signaling and microtumor growth.

(**A,B**) Quantified immunoblot data of phosphorylated and total ERK (A; n ≥ 4) or phosphorylated and total S6 (B; n ≥ 4) from *KRAS-G12C*-mutated MIA PaCa-2 cells treated with indicated compounds for 4 h before EGF-stimulation.

(**C**) Representative images of microtumors formed by MIA PaCa-2 cells grown in the CAM assay and treated with inhibitors as indicated.

(**D**) Weights of the MIA PaCa-2-derived microtumors (≥ 16 per condition from n = 5) after treatment with 2.5 µM Deltaflexin3 or/ and 30 µM Sildenafil.

Discussion and Conclusions

We here developed Deltaflexin3, a nanomolar-active and highly soluble PDE6Di with superior on-target activity as compared to previous reference inhibitors Deltarasin, Deltazinone1 and Deltasonamide1. We show that combinations of Deltaflexin3 with the

approved drug Sildenafil synergistically inhibit intracellular binding of K-Ras to PDE6D, and Ras-signaling, proliferation and ex vivo tumor growth of MIA PaCa-2 cells.

Within our dedicated series of 16 compounds, computational docking enabled us to generate several low- and sub-nanomolar binders of PDE6D, which are thus equally potent as previous trailblazer compounds Deltazinone1 and Deltasonamide1. Surprisingly, we measured lower, only submicromolar affinities when employing F-Rheb instead of F-Ator as a probe in our fluorescence polarization-based assay. Interestingly, the submicromolar affinities are more in line with the micromolar activities observed in our BRET- and proliferation-assays (Data S2).
Previously, we also measured only low micromolar affinities for first generation Deltaflexins and Deltarasin using the F-Rheb probe and in an alternative surface plasmon resonance-based assay that detected the disruption of farnesylated K-Ras binding to PDE6D (Siddiqui *et al.*, 2020a). Hence it appears that F-Ator-derived affinities are systematically higher than F-Rheb-derived affinities. The reasons for this are unclear, but it is conceivable that two molecules of F-Ator insert into the hydrophobic pocket of PDE6D, which is large enough to accommodate also dually-geranylgeranylated cargo (Yelland *et al.*, 2022). If only one is displaced, the other F-Ator molecule might be able to stabilize the binding of compounds. However, when comparing the F-Rheb derived affinities from our previous compound Deltaflexin2 (Kd[F-Rheb] = 7.17 µM) and Deltaflexin3 (Kd[F-Rheb] = 0.63 µM), a more than 10-fold improvement in affinity becomes apparent.

Another important aspect of our characterization is the dedicated off-target analysis, which has not been done previously. From our BRET-based off-target analysis, it appears that compounds with a PDE6D-affinity below ~3 nM are more likely to engage UNC119A as an off-target (Figure 3B-D). It is plausible that also related UNC119B would be engaged in this way (Yelland *et al*, 2021). Depending on the expression levels of such lipid binding proteins, they may effectively act as sinks for PDE6Di.
In parallel to the UNC119A off-target engagement, water solubility and therefore suitability of compounds for in vivo applications go down. This may not be surprising, as raising compounds with a higher affinity to a highly hydrophobic pocket will render them likewise more hydrophobic. It is possible that this trend then also increases the likelihood of binding to other hydrophobic pockets, such as that of UNC119A.

Importantly, the highest K-RasG12V-selectivity is seen for Deltaflexin3 (Figure 2B**)**, consistent with its lowest off-target effect in both the BRET-based assay looking at UNC119A engagement and its assessment in *PDE6D*-KO MEFs (Figure 3). Overall, K-

RasG12V-BRET selectivity (Figure 2B) and PDE6D-selectivity derived from cell proliferation data of WT and KO-MEFs (Figure 3A) show a strong correlation for our compounds, supporting that our assessment selects for least off-target activity (Figure S 1F).

PDE6Di development could in the future adopt strategies illustrated in nature. When looking at known cargos of PDE6D, it becomes apparent that their affinity is not modulated within the hydrophobic pocket, but outside of it, at its entry site (Dharmaiah *et al.*, 2016; Fansa *et al.*, 2016; Yelland *et al.*, 2022). Contacts with entry site residues are typically not exploited with PDE6Di, albeit our second round of compounds were extended with this goal in mind. Notably for mono-prenylated cargo, it is known that the four residues upstream of the prenylated cysteine significantly modulate the cargo affinity to PDE6D (Dharmaiah *et al.*, 2016). While K-Ras has only a moderate micromolar PDE6D-affinity (Kd = 2.3 µM (Dharmaiah *et al.*, 2016)), the INPP5E-derived peptide has a high, nanomolar affinity (Kd = 3.7 ± 0.2 nM (Fansa *et al.*, 2016)), and this solely depends on two amino-acids in the four-residue stretch upstream of the farnesylated cysteine (Yelland *et al.*, 2022).
The potential of this kind of affinity modulation is essentially illustrated by our Sildenafil data (Figure 5A), as Ser181 of K-Ras is part of that four-residue stretch next to the farnesylated cysteine. Therefore, future PDE6Di may rather target that region of the protein, while using a minimal hydrophobic stretch to anchor inside the hydrophobic pocket. We propose that 'plugging', rather than 'stuffing' the hydrophobic pocket of PDE6D with novel inhibitors may present a way forward.

Inhibitors of Ras membrane anchorage are expected to shut down Ras-signaling output (Pavic *et al.*, 2022). For instance, farnesyl-transferase inhibitors that block the enzyme mediating Ras farnesylation are now applied with some success in *HRAS*-mutant head and neck cancers (Ho *et al*, 2021). While some PDE6Di were shown to dislodge K-Ras more or less from the plasma membrane within 60-90 min (Canovas Nunes *et al.*, 2022; Martin-Gago *et al.*, 2017a; Papke *et al.*, 2016; Zimmermann *et al.*, 2013), only in some cases was evidence for a moderate effect on Ras-signaling provided (Canovas Nunes *et al.*, 2022; Chen *et al.*, 2022; Papke *et al.*, 2016). Nevertheless, all of these PDE6Di demonstrated cell killing activity in *KRAS*-mutant pancreatic or colorectal cancer cells, however, these are assays that cannot detect off-target activities.
One explanation for these discrepancies, could be that only a fraction of K-Ras that is trafficked to the plasma membrane does actually depend on PDE6D. We therefore compared the knockdown of PDE6D or that of the alpha-subunit of farnesyl- and geranylgeranyl-transferases with Mevastatin treatment, which would completely block K-Ras membrane anchorage, using our BRET-assay that detects functional K-RasG12V

membrane organization (Figure S 1B). These data show that knockdown of the alpha subunit is 49 % as effective as Mevastatin treatment, while PDE6D-knockdown is only 26 % as efficient. This suggest that only between a quarter or a half of functional K-Ras membrane anchorage depends on PDE6D. It is plausible to assume that other trafficking chaperones compensate and salvage K-Ras membrane anchorage thus buffering the loss of PDE6D activity.

It may therefore not be astonishing that both reference PDE6Di Deltazinone1 and our own compounds have such a small effect on phospho-ERK- and phospho-S6-levels (Figure 4C,D). Only when combined with Sildenafil could a robust, synergistic ~28 %-reduction of phospho-ERK- and phospho-S6-levels be observed (Figure 6A,B). Indeed, this combination may in general be a way forward for PDE6Di application, as it focuses the inhibitory activity on K-Ras. Apart from K-Ras only 15 other small GTPases can potentially be modulated by both PDE6Di and Sildenafil (Data S3).

This synergistic combination also showed promise for the anti-tumorigenic activity of our most selective PDE6Di, Deltaflexin3 (Figure 6C,D). However, not all *KRAS*-mutant cancer cell lines respond clearly and synergistically to the Deltaflexin3/ Sildenafil combination (Figure 5C,D). MIA PaCa-2 may be particularly responsive, as they have a genetic dependence on both *KRAS* and *PDE6D*, while being not-dependent on *PRKG2* (the gene of PKG2) (Figure S 1H).

Consequently, this combination could find its application in the treatment of a subset of KRAS-mutant cancers that more often have a high *PDE6D* and a low *PRKG2* expression level, such as colorectal cancer (Figure S 1J). However, our analysis of the overall survival of patients with this expression signature across *KRAS*-mutant cancers in the PanCanAtlas dataset shows that they have a significantly better survival than those with the opposite signature (low *PDE6D*/ high *PRKG2*) (Figure S 1K). This may indicate a protective effect of the high *PDE6D*/ low *PRKG2* signature, that should not be drug targeted by a PDE6Di/ Sildenafil -combination.

This begs the question as to what specific role PDE6D has for K-Ras trafficking. Given that PDE6D is a major trafficking chaperone of ciliary cargo, and that K-Ras has indeed been observed inside the primary cilium (Yelland *et al.*, 2022), it is possible that PDE6D inhibition also affects trafficking of K-Ras to this destination. However, the significance of such an inhibition is unclear, given that no function of K-Ras in the cilium is known. Besides, cancer cells are typically not ciliated (Liu *et al*, 2018), and it would thus not be clear what effect PDE6D inhibition could have in this context.

Another complication of PDE6D as a drug target is its intrinsically broad cargo spectrum

(Dharmaiah *et al.*, 2016; Yelland *et al.*, 2022). Therefore, its inhibition will not only affect K-Ras and thus *KRAS*-mutant cancer cells, but a host of PDE6D cargos. Finally, the ontogenetic role of PDE6D may be worth considering. Loss of function mutations of PDE6D during development lead to the multisystemic ciliopathy Joubert-Syndrome (Thomas *et al*, 2014). The deletion of PDE6D in mice does not cause gross developmental abnormalities, as mice are fertile and viable (Zhang *et al*, 2007). Some progressive defects in photoreceptor physiology were however observed, as well as an overall reduced body weight. Even though such genetic data do not exactly translate into the effects observed with inhibitors that are typically applied to aged cancer patients, more insight into the PDE6D biology in conjunction with K-Ras seems warranted.

In conclusion, we provide a novel conceptual framework for the future development and application of PDE6Di to be redesigned as 'plugs' and to be used in combination with PKG2 activators, such as approved Sildenafil. However, we also recommend to better understand the involvement of PDE6D in cancer and the consequences of drug targeting it.
With our novel, potent PDE6D inhibitor Deltaflexin3, which has the highest K-Ras selectivity and lowest off-target activity so far described, we are now providing the currently best tool compound to investigate and further validate the significance of PDE6D (patho)biology.

Experimental Section

Materials and Equipment

All materials, reagents and equipment are listed in Table S1.

Table S1: Materials employed in the study

REAGENT or RESOURCE	SOURCE	IDENTIFIER
Antibodies		
Phospho-p44/42 MAPK (Erk1/2) (Thr202/Tyr204) (E10) Mouse mAb	Cell Signaling Technology	Cat#9106 RRID:AB_331768
p44/42 MAPK (Erk1/2) Rabbit pAb	Cell Signaling Technology	Cat#9102 RRID:AB_330744)
Phospho-S6 Ribosomal Protein (Ser235/236) (D57.2.2E) XP Rabbit mAb	Cell Signaling Technology	Cat#4858 RRID:AB_916156
S6 Ribosomal Protein (54D2) Mouse mAb	Cell Signaling Technology	Cat#2317 RRID:AB_2238583
Mouse monoclonal anti-β-actin clone AC-15	Sigma-Aldrich	Cat#A5441 RRID:AB_476744
Mouse monoclonal PDE6D (E-7)	Santa Cruz Biotechnology	Cat#sc-166854 RRID:AB_2161460
Rabbit polyclonal anti-GAPDH	Sigma-Aldrich	Cat#G9545, RRID:AB_796208
IRDye 680RD goat anti-rabbit IgG	LI-COR Biosciences	Cat#926-68071, RRID:AB_10956166
IRDye 800CW donkey anti-mouse IgG	LI-COR Biosciences	Cat#926-32212, RRID:AB_621847
Bacterial and virus strains		
E. coli DH10B	New England Biolabs	Cat#C3019I
E. coli BL21 Star (DE3)pLysS	Thermo Fisher Scientific	Cat#C602003
Biological samples		
N/A	N/A	N/A
Chemicals, peptides, and recombinant proteins		
Fluorescein-labelled Atorvastatin (F-Ator)	Piramal Pharma Solutions custom synthesis as in (Zimmermann *et al.*, 2013)	N/A
Fluorescein-labelled Rheb (F-Rheb)	Described in (Ismail *et al.*, 2011)	N/A
Benzethonium chloride	Sigma-Aldrich	Cat#53751-50G; CAS121-54-0
AMG 510	MedChem Express	Cat#HY-114277; CAS2296729-00-3
ARS-1620	MedChem Express	Cat#HY-U00418; CAS1698055-85-4
FTI-277 hydrochloride	VWR chemicals	Cat#BIOV2874-5; CAS180977-34-8
Deltazinone1	Piramal Pharma Solutions custom synthesis as in (Papke *et al.*, 2016)	N/A
Deltarasin	Selleck Chemicals	Cat#S7224; CAS1440898-61-2

Deltasonamide1	Piramal Pharma Solutions custom synthesis as in (Martin-Gago *et al.*, 2017a)	N/A
Mevastatin	Alfa Aesar by Thermo Fisher Scientific	Cat#J61357.MB; CAS73573-88-3
Trametinib	MedChem Express	Cat#SC-364639; CAS871700-17-3
Vemurafenib (PLX4032, RG7204)	Selleck Chemicals	Cat#S1267; CAS918504-65-1
Squarunkin A	Axon Medchem	Cat#2778; CAS2101958-02-3
IMP-1088	Cayman Chemicals	Cat#25366-1; CAS2059148-82-0
Atorvastatin (calcium salt hydrate)	Cayman Chemicals	Cat#10493; CAS357164-38-6
Sildenafil	MedChem Express	Cat#38756; CAS139755-83-2
Tadalafil	MedChem Express	Cat#HY-90009A; CAS171596-29-5
Deltaflexin-2	(Siddiqui *et al.*, 2020a)	N/A
1	This paper	N/A
2	This paper	N/A
3	This paper	N/A
4 (Deltaflexin3)	This paper	N/A
5	This paper	N/A
6	This paper	N/A
7	This paper	N/A
8	This paper	N/A
9	This paper	N/A
10	This paper	N/A
11	This paper	N/A
12	This paper	N/A
13	This paper	N/A
14	This paper	N/A
15	This paper	N/A
16	This paper	N/A
Critical commercial assays		
Gateway LR Clonase II enzyme mix	Thermo Fisher Scientific	Cat#11791020
jetPRIME transfection reagent	Polyplus	Cat#101000046
Lipofectamine 2000 transfection reagent	Thermo Fisher Scientific	Cat#11668019
Coelenterazine 400a; 2,8-Dibenzyl-6-phenyl-imidazo[1,2a]pyrazin-3-(7H)-one; DeepBlueC	Gold Biotechnology	Cat#C-320-1
alamarBlue cell viability reagent	Thermo Fisher Scientific	Cat#DAL1100
Experimental models: Cell lines		
Human cell line, HEK293-EBNA (HEK)	Prof. Florian M. Wurm, EPFL	RRID:CVCL_6974
Human cell line, SW620	ATCC	CCL-227, RRID:CVCL_0547
Human cell line, MIA PaCa-2	ATCC	CRM-CRL-1420, RRID:CVCL_0428
Human cell line, cell line, PANC-1	ATCC	CRL-1469, RRID:CVCL_0480

Human cell line, MDA-MB-231	ATCC	HTB-26, RRID:CVCL_0062
Human cell line, NCI-H358	ATCC	CRL-5807, RRID:CVCL_1559
Human cell line, SW480	DSMZ	ACC-313, RRID:CVCL_0546
Human cell line, Hs 578T	DSMZ	ACC 781, RRID:CVCL_0332
Human cell line, T24	DSMZ	ACC 376, RRID:CVCL_0554
Human cell line, IGR-39	DSMZ	ACC 239, RRID:CVCL_2076
Mouse cell line, WT MEF cells	ATCC	CRL-2991, RRID:CVCL_L690
Mouse cell line, *PDE6D* KO MEF cells	Prof. Richard A. Kahn, Emory University School of Medicine	N/A
Experimental models: Organisms/strains		
SPF eggs	VALO BioMedia GmbH	N/A
Oligonucleotides		
ON-TARGETplus SMARTpool siRNA Human PDE6D 5147 4 targets	DHARMACON	Cat#L-004310-00-0005
ON-TARGETplus SMARTpool siRNA mouse PDE6d 4 targets	DHARMACON	Cat#L-062279-01-0005
Hs_FNTA_6 CCGGGATGCTATTGAGTTAAA	QIAGEN	Cat#SI02661995
Negative Control siRNA AATTCTCCGAACGTGTCACGT	QIAGEN	Cat#1027310
Recombinant DNA		
C413-E36_CMV promoter	(Wall *et al*, 2014)	Addgene, #162927
C453-E04_CMV promoter	(Wall *et al.*, 2014)	Addgene, #162973
pDest-305	(Wall *et al.*, 2014)	Addgene, #161895
pDest-312	(Wall *et al.*, 2014)	Addgene, #161897
C231-E13_Rluc8-stop	(Wall *et al.*, 2014)	Addgene, FNL Combinatorial Cloning Platform, kit #1000000211
C511-E03_Rluc8-no stop	(Wall *et al.*, 2014)	Addgene, FNL Combinatorial Cloning Platform, kit #1000000211
pDONR235-GFP2_stop	(Okutachi *et al.*, 2021)	N/A
pDONR257-GFP2_no stop	(Okutachi *et al.*, 2021)	N/A
Hs. KRas4B G12V	RAS mutant collection V2.0, RAS-Initiative	Addgene, #83132
Hs. HRas G12V	RAS mutant collection V2.0, RAS-Initiative	Addgene, #83184
Hs. PDE6D	R3 RAS Pathway Clone Collection #1, RAS-Initiative	#R702-E30
Hs. UNC119A (NM_005417.4, without stop codon)	Genecust	N/A
Hs. Src (NM_005148.4, without stop codon)	Genecust	N/A
pDest305-CMV-GFP2- K-Ras4BG12V	(Okutachi *et al.*, 2021)	N/A
pDest305-CMV-Rluc8- K-Ras4BG12V	(Okutachi *et al.*, 2021)	N/A
pDest305-CMV-GFP2- H-RasG12V	(Okutachi *et al.*, 2021)	N/A

pDest305-CMV-Rluc8- H-RasG12V	(Okutachi *et al.*, 2021)	N/A
pDest312-CMV-Rluc8- PDE6D	This paper	N/A
pDest312-CMV-UNC119A-Rluc8	This paper	N/A
pDest312-CMV-SRC-GFP2	This paper	N/A
pcDNA3.1(+)	Invitrogen	#V79020
pDest-His6-MBP-PDE6D	Ras-Initiative	#R702-X31-566
Software and algorithms		
Maestro	Schrödinger Release 2019-2; Maestro, Schrödinger, LLC: New York, NY, USA, 2019.	https://www.schrodinger.com/products/maestro
Glide	(Friesner *et al.*, 2006)	https://www.schrodinger.com/products/glide
OPLS3	(Harder *et al*, 2016)	https://www.schrodinger.com/products/opls4
VSGB 2.0 solvation model	(Li *et al*, 2011)	https://doi.org/10.1002/prot.23106
SeeSAR v10.3	BioSolveIT GmbH	https://www.biosolveit.de/SeeSAR
OpenBabel v2.3.2	(O'Boyle *et al*, 2011)	http://openbabel.org/
BREEZE pipeline	(Potdar *et al*, 2020)	https://breeze.fimm.fi/
SynergyFinder v3.0	(Ianevski *et al*, 2020)	https://synergyfinder.fimm.fi/
Project DRIVE	(McDonald Iii *et al.*, 2017)	https://oncologynibr.shinyapps.io/drive/
MARS Data Analysis Software	BMG LABTECH	https://www.bmglabtech.com/en/microplate-reader-software/
R v4.2.1	(R, 2022)	https://www.r-project.org/
GraphPad Prism v9.5.1	GraphPad by Dotmatics,	https://www.graphpad.com/
Other		
CLARIOstar Plus Microplate Reader	BMG LABTECH	https://www.bmglabtech.com/en/clariostar-plus/
Odyssey CLx Infrared Imaging System	LI-COR Biosciences	https://www.licor.com/bio/odyssey-clx/
ÄKTA pure chromatography system	Cytiva	https://www.cytivalifesciences.com/en/us/shop/chromatography/chromatography-systems/akta-pure-p-05844
Elmasonic S 40 H	Elma	https://www.elma-ultrasonic.com/

Cell lines

HEK293-EBNA (HEK) cells were a gift of Prof. Florian M. Wurm, EPFL, Lausanne, Switzerland, and were cultured in Dulbecco's modified Eagle's medium (DMEM, #41965-039). WT MEF and MEF PDE6D KO cells (obtained from Prof. Richard A. Kahn, Emory

University School of Medicine, Atlanta, USA) were cultured in DMEM. NCI-H358, MDA-MB-231 and IGR-39 were maintained in Roswell Park Memorial Institute medium (RPMI, #52400-025). PANC-1, MIA PaCa-2, Hs 578T and T24 were maintained in DMEM. SW620 and SW480 were maintained in Leibovitz's L-15 medium (#11415-064). All media were supplemented with 10 % v/v fetal bovine serum (#10270-106), 2 mM L-glutamine (#25030-024) and penicillin 100 U/mL/ streptomycin 100 µg/mL (#15140-122) (complete medium). All cell culture media and reagents were from Gibco, Thermo Fisher Scientific. Cells were grown at 37 °C in a water-saturated, 5 % CO_2 atmosphere and sub-cultured twice a week. Cell lines SW620 and SW480 were cultured without CO_2.

Bacterial strains

Competent *E. coli* DH10B (New England Biolabs, #C3019I), *E. coli* BL21 Star (DE3)pLysS (New England Biolabs, #C2527H) were grown in Luria-Bertani (LB) medium at 37 °C, with appropriate antibiotics unless otherwise mentioned.

Expression constructs

All expression constructs were produced by multi-site Gateway cloning technology as described (Wall *et al.*, 2014). Briefly, entry clones with compatible LR recombination sites, encoding the CMV promoter, Rluc8 or GFP2 tag and a gene of interest. The location of the tag in the expression constructs is indicated by its position in the construct name, i.e., a tag at the N-terminus of the protein of interest is written before the name of the protein. Genes were obtained either from the Ras-Initiative (K-Ras4BG12V, H-RasG12V both from the RAS mutant clone collection, kit #1000000089 and PDE6D #R702-E30) or by custom synthesis from GeneCust (Src, UNC119A). The cDNAs encoding human c-Src kinase and human UNC119A inserted in the pDONR221 vector were obtained from GeneCust. The three entry clones of promotor, tag and gene of interest were then inserted into pDest-305 or pDest-312 as a destination vector using Gateway LR Clonase II enzyme mix (#11791020, Thermo Fisher Scientific). The reaction mix was transformed into ccdB sensitive *E. coli* strain DH10B (# C3019I, New England Biolabs) and positive clones were selected in the presence of ampicillin. The His6-MBP-Tev-PDEd construct for PDE6D protein production was obtained from the Ras-Initiative (#R702-X31-566).

In silico docking of compounds

The synthetic rationale for first round compounds was based on computational docking. Three-dimensional coordinates for the molecular structure and sequence of the open and closed conformations of the PDE6D protein (PDB ID: 4JV8 and 1KSH, respectively) were retrieved from the RCSB protein data bank (Zimmermann *et al.*, 2013). The 3D structures

of all docked compounds were constructed using Maestro software in the Schrödinger software (Schrödinger Release 2019-2; Maestro, Schrödinger, LLC: New York, NY, USA, 2019). The geometry optimization of docked compounds was performed using the OPLS3 force field (Harder *et al.*, 2016). Powell conjugated gradient algorithm method was applied with a convergence criterion of 0.01 kcal/ (mol Å) and maximum iterations of 1,000.

Molecular docking simulations were performed by using the program Glide (Friesner *et al.*, 2006). Flexible compound, extra precision mode and the Epik state penalties were included in the protocol. The MM-GBSA method with VSGB 2.0 solvation model was used to calculate compound binding affinities (Hou *et al*, 2011). For MM-GBSA calculations, residues within a distance of 8.0 Å from the compound were assigned as flexible.

Computational evaluations to derive second round compounds was slightly different. While using the same protein data as for first round compounds, the putative binding pocket of PDE6D was re-inferred using the software SeeSAR v10.3 ("SeeSAR" 2020) with default parameters and prior domain knowledge to select and refine the most relevant pocket. Compound chemical formulas, defined as SMILES strings, were converted to 3D structures using OpenBabel v2.3.2 with default parameters (O'Boyle *et al.*, 2011). Compounds were docked to PDE6D (PDB ID 4JV8) using SeeSAR v10.3 and the optimal docking pose was manually selected by ranking poses according to their predicted binding affinity and filtering compounds to ensure acceptable lipophilic compound efficiency, limited torsions of the compound backbone and minimal intra- and inter-molecular clashes of the resulting protein-ligand complex.

Expression and purification of PDE6D

Recombinant PDE6D protein was produced according to a published protocol that was adapted (Dharmaiah *et al.*, 2016). Briefly, *E. coli* BL21 Star™ (DE3)pLysS strain (#C602003, Thermo Fisher Scientific) was transformed with pDest-His6-MBP-PDE6D and grown at 37 °C in LB medium supplemented with ampicillin at 1:1,000 dilution from 100 mg/ mL stock. When OD reached 0.6, protein expression was induced by adding isopropyl β-D-1-thiogalactopyranoside (IPTG, #437145X, VWR) at 16 °C overnight. Next, the 4 L cultures were pelleted by centrifugation, the pellets were rinsed with PBS and stored at -20 °C until purification.

Purification was conducted using ÄKTA pure chromatography system (Cytiva). All buffers were degassed by placing for 5 min in ultrasonic bath. The cells were lysed by sonication on ice in a buffer composed of 50 mM Tris-HCl, pH 7.5, 150 mM NaCl, 1 mM β-mercaptoethanol, 0.5 mg/ ml lysozyme (#89833, Thermo Fisher Scientific) and protease inhibitor cocktail (#A32955, Pierce). For sonication, a Bioblock Scientific ultrasonic

processor instrument (Elmasonic S 40 H, Elma) was used. Lysates were cleared by centrifugation at 18,000 g for 20 min at 4 °C. Cleared supernatant was loaded onto a prepacked HisTrapHP column (#17-5248-02, Cytiva) equilibrated in a binding buffer, which had the same composition as lysis buffer, but without lysozyme and containing 35 mM imidazole. After washing with 20 column volumes, the bound material was eluted by isocratic elution using 100 % of eluting buffer (50 mM Tris-HCl, pH 7.5, 150 mM NaCl, 1 mM β-mercaptoethanol, 500 mM imidazole). The eluted fractions were analyzed by resolving on 4-20 % SDS-PAGE (#4561094 or #4651093 BioRAD) and stained with Roti-Blue quick (#4829-2, Carl ROTH). Fractions were concentrated on AmiconUltra centrifugal filters (molecular weight cut-off, MWCO of 30 kDa, Merck Millipore) by centrifuging at 7,500 g and pulled for dialysis into buffer containing 50 mM Tris-HCl, pH 7.5, 150 mM NaCl, 3 mM DTE, using D-Tube dialyzer with molecular weight cut-off (MWCO) 12-14 kDa, overnight at 4 °C. Next, samples were centrifuged for 15 min at 4,000 g and 4 °C and then loaded onto a size exclusion chromatography column (HiLoad 16/ 600 Superdex 75 pg, with 120 mL column volume, #28989333, Cytiva) at a flow rate of 1 mL/ min, with elution with two column volumes. Fractions were analyzed as above, then concentrated to a volume of about 500 µL. In the next step, protein tags were removed by tobaccoetchvirus (TEV) protease (#T4455, Sigma-Aldrich) (1:25 w/w, TEV/ fusion protein) during overnight dialysis. This step was repeated twice, with 50 % and 70 % approximate cleavage efficiencies. The cleaved mixture was loaded onto HisTrapHP column and the non-bound (tag-free) PDE6D was collected. The collected PDE6D fractions were concentrated using MICROSEP Advance (MWCO 10 kDa, # 88527, Pierce) by centrifugation at 7,500 g and 4 °C. The sample was finally dialyzed overnight in a buffer composed of 20 mM HEPES, pH 7.4, 150 mM NaCl, 5 mM $MgCl_2$ and 1 mM TCEP. The PDE6D final concentration of 245.3 µM was determined by Bradford assay. Final purification yield from 4 L starting bacterial culture was 890 µg of PDE6D.

Fluorescence polarization assay

The IC50 and Kd of compounds to purified PDE6D were determined in a displacement assay using fluorescein-labelled Atorvastatin (F-Ator) or fluorescein-labelled farnesylated Rheb (F-Rheb) peptide as probes (Ismail *et al.*, 2011; Zimmermann *et al.*, 2013). F-Ator was used at 5 nM concentration with 5 nM of PDE6D and F-Rheb peptide was used at 0.5 µM concentration with 2 µM PDED. Assays were carried out in black low volume round bottom 384-well plates (#4514, Corning) with a reaction volume of 20 µL for F-Ator- and 10 µL for F-Rheb-based experiments. Compounds were three-fold diluted in assay buffer (DPBS no Ca^{2+}/Mg^{2+}; #14190-094, Gibco) with 0.05 % CHAPS (#1479, Carl Roth) for F-Ator based experiments or in a freshly prepared buffer composed of 30 mM Tris, 150 mM

NaCl and 3 mM dithiothreitol for F-Rheb based experiments, as described previously (Blazevits *et al*, 2016; Siddiqui *et al.*, 2020a). The fluorescence polarization signals were read on the CLARIOstar plate reader (BMG Labtech GmbH) with λ_{ex} = 482 ± 8 nm and λ_{em} = 530 ± 20 nm at 25 °C. The blank corrected milli Polarization value (mP or P × 1,000) calculated from the MARS (BMG Labtech) program was plotted against the logarithmic concentration of inhibitors. The data were fitted into log inhibitor vs. response 4-parametric equation of Prism (GraphPad) to obtain the IC50 values. The IC50 values were converted into Kd using the modified Cheng-Prusoff equation, $K_d = \frac{IC_{50}}{1+\frac{[L]}{K_D}}$, where Kd is the dissociation constant between PDE6D and inhibitor, [L] is the ligand or probe concentration used in the assay and K_D is the dissociation constant between the PDE6D and the ligand or fluorescent probe (Siddiqui *et al.*, 2020a).The reported K_D values were 7.1 ± 4 nM for F-Ator to PDE6D (Zimmermann *et al.*, 2013) and from 0.15 µM (Ismail *et al.*, 2011) to 0.45 µM (Fansa *et al.*, 2016) for F-Rheb to PDE6D. The mean of the F-Rheb K_D value of 0.3 µM was used for the calculations. Note that the concentration of PDE6D is not part of the equation.

Bioluminescence Resonance Energy Transfer (BRET) assay

BRET assays were essentially performed as described by us previously (Manoharan *et al.*, 2023; Manoharan *et al*, 2022; Okutachi *et al.*, 2021). Briefly, 150,000 to 200,000 HEK293-EBNA cells were plated in 1 mL complete DMEM per well of 12-well cell culture plates (#665180, Greiner bio-one, Merck KGaA). After 24 h, donor and acceptor plasmids were transfected into cells using 3 µL of jetPRIME transfection reagent (#114–75, Polyplus) following the manufacturer's instructions.

For BRET donor saturation titration experiments, the concentration of donor plasmid (50 ng) was kept constant, and the concentration of acceptor plasmid was increased from 0 to 1,000 ng. The empty pcDNA3.1 plasmid was used to top-up the total DNA load per well to 1,050 ng.

After determination of the optimal acceptor to donor plasmid ratio from titration experiments (A/D plasmid ratio 20:1 for GFP2-K-RasG12V/ Rluc8-PDE6D, 5:1 for GFP2-K-RasG12V/ Rluc8-K-RasG12V, 3:1 for GFP2-HRasG12V/ Rluc8-HRasG12V and 20:1 for UNC119A-Rluc8/ Src-GFP2), compound dose-response experiments were performed. 24 h after transfection, cells were treated for another 24 h with DMSO 0.1 % v/v as vehicle control or with compounds at 5 to 8 different concentrations ranging from 20 µM to 0.15 µM, prepared as 2-fold dilution series in complete medium.

To study the effect of siRNA-mediated knockdown, cells were plated and after 24 h co-transfected with 50 nM siRNA and 500 ng plasmid DNA per well (same A/D plasmid ratio

as described above) using 4 µl Lipofectamine 2000 (#11668019, Thermo Fisher Scientific) in Opti-MEM medium (#31985062, Gibco).

BRET-measurements were performed on a CLARIOstar plate reader at 25 °C after 48 h as described (Manoharan *et al.*, 2023; Manoharan *et al.*, 2022; Okutachi *et al.*, 2021). Technical quadruplicates were measured using specific channels for the luminophores (GFP2-acceptor signal, RFU, at λ_{ex} = 405 ± 10 nm and at λ_{em} = 515 ± 10 nm; after 10 µM coelenterazine 400a (#C-320, Gold Biotechnology) addition, simultaneous recording of Rluc8-signals for donor signal, RLU, λ_{em} = 410 ± 40 nm and for the BRET-signal at λ = 515 ± 15 nm). The BRET ratio was calculated as before (Manoharan *et al.*, 2023; Manoharan *et al.*, 2022; Okutachi *et al.*, 2021).

For BRET donor saturation titration experiments, the BRET ratio was plotted against the relative expression. The relative expression of acceptor to donor ([Acceptor]/[Donor]) was determined as the ratio between RFU and RLU. All independent repeat experiments were plotted at once using these normalized data i.e., BRET ratio against relative expression. The data were fitted into one phase association equation of Prism 9 (GraphPad) and the top asymptote Ymax-value was taken as the BRETtop. It represents the maximal BRET ratio reached within the defined [Acceptor]/[Donor] ratio. Statistical analysis between the BRETtop values was performed using the student's t-test.

2D cell proliferation assay

Cancer cells were seeded at a density of 1,000 cells/ 100 µL complete medium into 96-well cell culture plates (#655180, Greiner bio-one, Merck KGaA). After 24 h, control and test compounds were added to the cells with DMSO (0.1 % v/v) as a vehicle control. Compound activities were analyzed from 9-point dose-response curves, with compounds prepared as 2-fold dilution series ranging from 40 µM to 0.15 µM (PDE6Di and FTI-277) or from 20 µM to 0.02 µM for MAPK-control compounds. Following incubation for 72 h with the compounds, the cell viability was assessed using the alamarBlue reagent (#DAL1100, Thermo Fisher Scientific) according to the manufacturer's instructions. After addition of alamarBlue reagent at a 10 % v/v final volume, cells were incubated for 2 to 4 h at 37 °C. Then, the fluorescence intensity was read at λ_{ex} = 530 ± 10 nm and λ_{em} = 590 ± 10 nm at 25 °C using a CLARIOstar plate reader. The obtained raw fluorescence intensity data were normalized to vehicle control (100 % viability) and plotted against the compound concentration.

Drug sensitivity score analysis (DSS3)

As described before (Okutachi *et al.*, 2021), a drug sensitivity score (DSS) analysis was performed in order to quantify the drug sensitivity with a more robust parameter than the IC50 or EC50 values. DSS values are normalized area under the curve (AUC) measures of

dose-response inhibition data, where the DSS3-score takes drug-responses better into account that are achieved across a broad concentration range (Yadav *et al.*, 2014). Drug response data from BRET assays or 2D cell proliferation assays were prepared according to the example file on the Breeze website (https://breeze.fimm.fi/), uploaded and analyzed (Potdar *et al.*, 2020). The output file included DSS3 scores as well as several other drug sensitivity measures such as IC50 and AUC.

Synergy analysis of drug combinations

The synergistic potential of compounds was analyzed essentially as described before (Manoharan *et al.*, 2022). For PDE6D/ K-RasG12V BRET-experiments, full dose-response analyses of Deltaflexin3 (between 7 µM to 0.014 µM) or Sildenafil (between 320 µM to 1.8 µM) alone or for Deltaflexin3 in combination with Sildenafil maintained at a fixed concentration of either 10, 20, 30 µM were performed. For 2D proliferation experiments, full dose-response analyses of Deltaflexin3 (between 80 µM to 0.156 µM) or Sildenafil (between 160 µM to 0.312 µM) alone or for Deltaflexin3 in combination with Sildenafil maintained at a fixed concentration of either 10, 20, 30 or for some 40 µM were performed. Comparison between the drug response profiles of the combinations and the profiles of each single agent was then carried out using the web-application SynergyFinder (Ianevski *et al.*, 2020)(https://synergyfinder.fimm.fi). We employed the HSA model, which considers that the expected drug combination effect corresponds to the maximum of the single agent responses at the corresponding concentrations. The resulting HSA synergy score S_{HSA} is defined as follows

$S_{HSA} = E_{A,B,\ldots,N} - \max(E_A, E_B, \ldots, E_N)$

with $E_{A,B,\ldots,N}$ being the combination effect between N drugs and E_A, E_B,…, E_N being the single agent responses at the corresponding concentrations.

ATARiS gene dependence score

Gene dependence scores of selected genes of interest for cancer cell lines used in this study were obtained from the drive data portal (https://oncologynibr.shinyapps.io/drive/). The DRIVE project has provided the dependence data of 7,837 genes for 398 cancer cell lines, as determined by large-scale RNAi screening in cell viability assays (McDonald Iii *et al.*, 2017). A double gradient heatmap for the extracted gene dependence scores was then generated using GraphPad Prism software.

Immunoblotting

Following a 16 h serum starvation, MIA PaCa-2 cells were treated with 0.1 % v/v DMSO vehicle control or with compounds at 37 °C for 4 h and then stimulated with 200 ng/mL

human epidermal growth factor (hEGF, #E9644, Sigma) at 37 °C for 10 min. *In situ* cell lysis was performed in ice-cold lysis buffer (50 mM Tris-HCl pH 7.5, 150 mM NaCl, 0.1 % v/v SDS, 5 mM EDTA, 1 % v/v Nonidet P-40, 1 % v/v Triton X-100, 1 % v/v sodium-deoxycholate, 1 mM Na_3VO_4, 10 mM NaF, 100 µM leupeptin and 100 µM E64D protease inhibitor) supplemented with a cocktail of protease inhibitors (#A32955, Pierce) and a cocktail of phosphatase inhibitors (PhosSTOP, #4906845001, Roche Diagnostics GmbH). After lysate clarification, the total protein concentration was determined by Bradford assay using the Quick Start Bradford 1x Dye reagent (#5000205, Bio-Rad) and BSA (#23209, Thermo Fisher Scientific) as a standard. Proteins (50 µg per lane) were resolved by SDS-PAGE in a 10 % v/v homemade polyacrylamide gel under reducing conditions and transferred to a nitrocellulose membrane by semi-dry transfer (kit #1704272, Bio-Rad). Membranes were saturated in phosphate-buffered saline (PBS) containing 2 % w/v bovine serum albumin (#A6588, AppliChem GmbH) and 0.2 % Tween for 1 h at room temperature, then incubated with primary antibodies overnight at 4 °C. For phospho-ERK and phospho-S6 detection, a combination of mouse anti-phospho-ERK and rabbit anti-ERK or a combination of rabbit anti-phospho-S6 and mouse anti-S6 antibodies were used, respectively (see Key Resources). Incubation with secondary antibodies was performed for 1 h at room temperature. Each antibody incubation was followed by at least three wash steps in PBS supplemented with 0.2 % v/v Tween 20. Signal intensities were quantified using the Odyssey Infrared Image System (LI-COR Biosciences). The ratio between the intensities obtained for phosphorylated protein versus total protein was calculated and then normalized to the sum of all the ratios calculated for one blot to make blots comparable by accounting for technical day-to-day variability. For representative purposes, data were scaled to the controls present on each blot and are represented as the mean ± SEM of at least three independent biological repeats. The slope of the dose-response data was determined from fitting a line using GraphPad Prism. For each blot, either β-actin or GAPDH levels were determined as a loading control.

Chorioallantoic membrane (CAM) assay

Fertilized chicken eggs were obtained from VALO BioMedia GmbH (Osterholz-Scharmbeck, Germany) and, on day 1, the development of the embryos was started by incubating the eggs at 37 °C in a > 60 % humidified egg hatcher incubator (MG200/300, Fiem). A small hole was made with the help of an 18 Gauge needle (#305196, Becton Dickinson) into the narrower end of each egg on day 3 and was kept covered with parafilm to avoid contamination. On day 8, 2×10^6 MDA-MB-231 cells, or 3.5×10^6 MIA PaCa-2 cells were resuspended in 10 µL cell culture medium without FBS and mixed 1:1 with Matrigel (#356234, Corning). This mix was then deposited in sterilized 5 mm diameter plastic rings

cut from PCR tubes (#683201, Greiner bio-one, Merck KGaA) on the surface of a chicken embryo chorioallantoic membrane. After 1 day, the growing tumors were treated with a volume identical to the deposited cell suspension of 0.2 % v/v vehicle control or test compounds 2× concentrated in medium without FBS (Siddiqui *et al.*, 2020b; Siddiqui *et al.*, 2021). Treatment was performed daily and after 5 days of treatment the microtumors were harvested at day 14. Then the tumor weight was determined using a balance (E12140, Ohaus).

Survival analysis

All data were retrieved from TCGA Pan-Cancer Atlas (https://dev.xenabrowser.net/datapages/?cohort=TCGA%20Pan-Cancer%20) (PANCAN). The 647 cancer samples with non-silent KRAS mutation were selected. We used the list of non-silent somatic mutations as defined in Xena (https://ucsc-xena.gitbook.io/project/overview-of-features/visual-spreadsheet/mutation-columns). Expression data was retrieved for *PDE6D* and *PRKG2* genes data in "batch effects normalized mRNA data" units, and samples were split in 4 groups according to high or low expression of each gene, setting the limit at median expression value for each gene. The difference between the two curves was tested using Kaplan Meyer estimation. Data analyses were performed in R version 4.2.1 (R, 2022). Survival analyses and plots were done using survival v.3.4 (Therneau & Grambsch, 2000) and survminer v 0.4 (Alboukadel *et al*, 2021) libraries.

Quantification and Statistical Analysis

For statistical analysis and plot preparation, GraphPad Prism (version 9.5.1 for Windows, GraphPad Software, USA, www.graphpad.com) was used. The sample size n represents the number of independent biological repeats and is indicated in the respective figure legends. All graphs show mean values ± SEM across all technical and biological repeats. We determined statistical differences to control samples by employing one-way ANOVA with Tukey's multiple comparison test, unless otherwise mentioned in the legends. A p value of < 0.05 is considered statistically significant. Statistical significance levels are annotated in the plots as * = $p < 0.05$; ** = $p < 0.01$; *** = $p < 0.001$; **** = $p < 0.0001$.

Data availability

This study did not report standardized datatypes. All unique/ stable reagents generated in this study are available from the corresponding author with a completed materials transfer agreement.

Ancillary Information

Supplemental Information

Supplementary Figure S1: Data supplementing information in the main figures.

Data S1: Compound Synthesis. Chemical synthesis routes and compound analytics.

Data S2: Activity Data Summary. Collects data from plots by figure and shows in the first tab a table collecting all activity data per compound.

Data S3: Survey of potential PDE6D cargo amongst all small GTPases. Based on the four residues upstream of the prenylated cysteine, we identified those small GTPases that are putative PDE6D cargo and contain serine or threonine residues in that stretch that could be targeted by Sildenafil-stimulated PKG2 phosphorylation.

Author Contributions

PK characterized compounds by BRET, in proliferation experiments, extracted ATARiS information, performed synergy experiments and analyzed these data.

ESR and MB performed immunoblot experiments and analyses and ESR carried out the CAM assay and analyzed WB and CAM assay results.

GM collected FP data and evaluated them.

AG did gene expression and survival analyses.

VV and AK generated the in silico library and performed computational docking experiments of first round compounds.

ML and EG performed computational docking experiments of second round compounds.

PK and ESR helped to prepare the manuscript.

DKA initiated the study, supervised the project, designed compounds, and wrote the manuscript.

Competing Interests

DKA is author of patents on PDE6D inhibitors developed in this study. DKA received a Grant4Targets grant (Ref. 2019-08-2426) from Bayer AG. The other authors declare no potential conflicts of interest.

Acknowledgements

We thank Professor Richard A. Kahn (Emory University School of Medicine, Atlanta, USA) for providing the PDE6D KO cell line. We are grateful to Dr. Eyad K. Fansa (Max Planck Institut, Dortmund, Germany) for giving us FITC-labelled farnesylated Rheb peptide.

DKA received a Grant4Targets grant (Ref. 2019-08-2426) from Bayer AG.

This work was supported by grants from the Luxembourg National Research Fund (FNR): AFR individual grant 13589879 to PK and PoC20/15269106-inhibitPDE-RASv2 to DKA.

References

1 Skoulidis, F. *et al.* Sotorasib for Lung Cancers with KRAS p.G12C Mutation. *N Engl J Med* **384**, 2371-2381, doi:10.1056/NEJMoa2103695 (2021).

2 Fell, J. B. *et al.* Identification of the Clinical Development Candidate MRTX849, a Covalent KRAS(G12C) Inhibitor for the Treatment of Cancer. *J Med Chem* **63**, 6679-6693, doi:10.1021/acs.jmedchem.9b02052 (2020).

3 Steffen, C. L., Kaya, P., Schaffner-Reckinger, E. & Abankwa, D. Eliminating oncogenic RAS: back to the future at the drawing board. *Biochem Soc Trans* **51**, 447-456, doi:10.1042/BST20221343 (2023).

4 Punekar, S. R., Velcheti, V., Neel, B. G. & Wong, K. K. The current state of the art and future trends in RAS-targeted cancer therapies. *Nat Rev Clin Oncol* **19**, 637-655, doi:10.1038/s41571-022-00671-9 (2022).

5 Pavic, K., Chippalkatti, R. & Abankwa, D. Drug targeting opportunities en route to Ras nanoclusters. *Adv Cancer Res* **153**, 63-99, doi:10.1016/bs.acr.2021.07.005 (2022).
6 Cox, A. D., Der, C. J. & Philips, M. R. Targeting RAS Membrane Association: Back to the Future for Anti-RAS Drug Discovery? *Clin Cancer Res* **21**, 1819-1827, doi:10.1158/1078-0432.CCR-14-3214 (2015).
7 Zimmermann, G. *et al.* Small molecule inhibition of the KRAS-PDEdelta interaction impairs oncogenic KRAS signalling. *Nature* **497**, 638-642, doi:10.1038/nature12205 (2013).
8 Dharmaiah, S. *et al.* Structural basis of recognition of farnesylated and methylated KRAS4b by PDEdelta. *Proc Natl Acad Sci U S A* **113**, E6766-E6775, doi:10.1073/pnas.1615316113 (2016).
9 Yelland, T. *et al.* Stabilization of the RAS:PDE6D Complex Is a Novel Strategy to Inhibit RAS Signaling. *J Med Chem* **65**, 1898-1914, doi:10.1021/acs.jmedchem.1c01265 (2022).
10 Chandra, A. *et al.* The GDI-like solubilizing factor PDEdelta sustains the spatial organization and signalling of Ras family proteins. *Nat Cell Biol* **14**, 148-158, doi:10.1038/ncb2394 (2011).
11 Cho, K. J. *et al.* AMPK and Endothelial Nitric Oxide Synthase Signaling Regulates K-Ras Plasma Membrane Interactions via Cyclic GMP-Dependent Protein Kinase 2. *Mol Cell Biol* **36**, 3086-3099, doi:10.1128/MCB.00365-16 (2016).
12 Fansa, E. K., Kosling, S. K., Zent, E., Wittinghofer, A. & Ismail, S. PDE6delta-mediated sorting of INPP5E into the cilium is determined by cargo-carrier affinity. *Nat Commun* **7**, 11366, doi:10.1038/ncomms11366 (2016).
13 Schmick, M. *et al.* KRas localizes to the plasma membrane by spatial cycles of solubilization, trapping and vesicular transport. *Cell* **157**, 459-471, doi:10.1016/j.cell.2014.02.051 (2014).
14 Ismail, S. A. *et al.* Arl2-GTP and Arl3-GTP regulate a GDI-like transport system for farnesylated cargo. *Nat Chem Biol* **7**, 942-949, doi:10.1038/nchembio.686 (2011).
15 Martin-Gago, P. *et al.* A PDE6delta-KRas Inhibitor Chemotype with up to Seven H-Bonds and Picomolar Affinity that Prevents Efficient Inhibitor Release by Arl2. *Angew Chem Int Ed Engl* **56**, 2423-2428, doi:10.1002/anie.201610957 (2017).
16 Papke, B. *et al.* Identification of pyrazolopyridazinones as PDEdelta inhibitors. *Nat Commun* **7**, 11360, doi:10.1038/ncomms11360 (2016).
17 Murarka, S. *et al.* Development of Pyridazinone Chemotypes Targeting the PDEdelta Prenyl Binding Site. *Chemistry* **23**, 6083-6093, doi:10.1002/chem.201603222 (2017).
18 Klein, C. H. *et al.* PDEdelta inhibition impedes the proliferation and survival of human colorectal cancer cell lines harboring oncogenic KRas. *Int J Cancer* **144**, 767-776, doi:10.1002/ijc.31859 (2019).
19 Paiva, S. L. & Crews, C. M. Targeted protein degradation: elements of PROTAC design. *Curr Opin Chem Biol* **50**, 111-119, doi:10.1016/j.cbpa.2019.02.022 (2019).
20 Winzker, M. *et al.* Development of a PDEdelta-Targeting PROTACs that Impair Lipid Metabolism. *Angew Chem Int Ed Engl* **59**, 5595-5601, doi:10.1002/anie.201913904 (2020).
21 Cheng, J., Li, Y., Wang, X., Dong, G. & Sheng, C. Discovery of Novel PDEdelta Degraders for the Treatment of KRAS Mutant Colorectal Cancer. *J Med Chem* **63**, 7892-7905, doi:10.1021/acs.jmedchem.0c00929 (2020).

22 Chen, L., Zhuang, C., Lu, J., Jiang, Y. & Sheng, C. Discovery of Novel KRAS-PDEdelta Inhibitors by Fragment-Based Drug Design. *J Med Chem* **61**, 2604-2610, doi:10.1021/acs.jmedchem.8b00057 (2018).
23 Jiang, Y. *et al.* Structural Biology-Inspired Discovery of Novel KRAS-PDEdelta Inhibitors. *J Med Chem* **60**, 9400-9406, doi:10.1021/acs.jmedchem.7b01243 (2017).
24 Chen, L. *et al.* Discovery of novel KRAS–PDEdelta inhibitors with potent activity in patient-derived human pancreatic tumor xenograft models. *Acta Pharm Sin B* **12**, 274-290, doi:10.1016/j.apsb.2021.07.009 (2022).
25 Chen, D. *et al.* Fragment-based drug discovery of triazole inhibitors to block PDEdelta-RAS protein-protein interaction. *Eur J Med Chem* **163**, 597-609, doi:10.1016/j.ejmech.2018.12.018 (2019).
26 Canovas Nunes, S. *et al.* Validation of a small molecule inhibitor of PDE6D-RAS interaction with favorable anti-leukemic effects. *Blood Cancer J* **12**, 64, doi:10.1038/s41408-022-00663-z (2022).
27 Siddiqui, F. A. *et al.* PDE6D Inhibitors with a New Design Principle Selectively Block K-Ras Activity. *ACS Omega* **5**, 832-842, doi:10.1021/acsomega.9b03639 (2020).
28 Friesner, R. A. *et al.* Extra precision glide: docking and scoring incorporating a model of hydrophobic enclosure for protein-ligand complexes. *J Med Chem* **49**, 6177-6196, doi:10.1021/jm051256o (2006).
29 Yadav, B. *et al.* Quantitative scoring of differential drug sensitivity for individually optimized anticancer therapies. *Sci Rep* **4**, 5193, doi:10.1038/srep05193 (2014).
30 Guzman, C., Oetken-Lindholm, C. & Abankwa, D. Automated High-Throughput Fluorescence Lifetime Imaging Microscopy to Detect Protein-Protein Interactions. *J Lab Autom* **21**, 238-245, doi:10.1177/2211068215606048 (2016).
31 Siddiqui, F. A., Parkkola, H., Manoharan, G. B. & Abankwa, D. Medium-Throughput Detection of Hsp90/Cdc37 Protein-Protein Interaction Inhibitors Using a Split Renilla Luciferase-Based Assay. *SLAS Discov* **25**, 195-206, doi:10.1177/2472555219884033 (2020).
32 Parkkola, H., Siddiqui, F. A., Oetken-Lindholm, C. & Abankwa, D. FLIM-FRET Analysis of Ras Nanoclustering and Membrane-Anchorage. *Methods Mol Biol* **2262**, 233-250, doi:10.1007/978-1-0716-1190-6_13 (2021).
33 Najumudeen, A. K., Kohnke, M., Solman, M., Alexandrov, K. & Abankwa, D. Cellular FRET-Biosensors to Detect Membrane Targeting Inhibitors of N-Myristoylated Proteins. *PLoS One* **8**, e66425, doi:10.1371/journal.pone.0066425 (2013).
34 Dewees, S. I. *et al.* Phylogenetic profiling and cellular analyses of ARL16 reveal roles in traffic of IFT140 and INPP5E. *Mol Biol Cell* **33**, ar33, doi:10.1091/mbc.E21-10-0509-T (2022).
35 Manoharan, G. B., Laurini, C., Bottone, S., Ben Fredj, N. & Abankwa, D. K. K-Ras Binds Calmodulin-Related Centrin1 with Potential Implications for K-Ras Driven Cancer Cell Stemness. *Cancers (Basel)* **15**, doi:10.3390/cancers15123087 (2023).
36 Garivet, G. *et al.* Small-Molecule Inhibition of the UNC-Src Interaction Impairs Dynamic Src Localization in Cells. *Cell Chem Biol* **26**, 842-851 e847, doi:10.1016/j.chembiol.2019.02.019 (2019).
37 Mousnier, A. *et al.* Fragment-derived inhibitors of human N-myristoyltransferase block capsid assembly and replication of the common cold virus. *Nat Chem* **10**, 599-606, doi:10.1038/s41557-018-0039-2 (2018).
38 McDonald Iii, E. R. *et al.* Project DRIVE: A Compendium of Cancer Dependencies and Synthetic Lethal Relationships Uncovered by Large-Scale, Deep RNAi

Screening. *Cell* **170**, 577-586.e510, doi:papers3://publication/doi/10.1016/j.cell.2017.07.005 (2017).
39 Siddiqui, F. A., Vukic, V., Salminen, T. A. & Abankwa, D. Elaiophylin Is a Potent Hsp90/ Cdc37 Protein Interface Inhibitor with K-Ras Nanocluster Selectivity. *Biomolecules* **11**, doi:10.3390/biom11060836 (2021).
40 Lokman, N. A., Elder, A. S. F., Ricciardelli, C. & Oehler, M. K. Chick chorioallantoic membrane (CAM) assay as an in vivo model to study the effect of newly identified molecules on ovarian cancer invasion and metastasis. *Int J Mol Sci* **13**, 9959-9970, doi:10.3390/ijms13089959 (2012).
41 Yelland, T., Garcia, E., Samarakoon, Y. & Ismail, S. The Structural and Biochemical Characterization of UNC119B Cargo Binding and Release Mechanisms. *Biochemistry* **60**, 1952-1963, doi:10.1021/acs.biochem.1c00251 (2021).
42 Ho, A. L. *et al.* Tipifarnib in Head and Neck Squamous Cell Carcinoma With HRAS Mutations. *J Clin Oncol* **39**, 1856-1864, doi:10.1200/JCO.20.02903 (2021).
43 Liu, H., Kiseleva, A. A. & Golemis, E. A. Ciliary signalling in cancer. *Nat Rev Cancer* **18**, 511-524, doi:10.1038/s41568-018-0023-6 (2018).
44 Thomas, S. *et al.* A homozygous PDE6D mutation in Joubert syndrome impairs targeting of farnesylated INPP5E protein to the primary cilium. *Hum Mutat* **35**, 137-146, doi:10.1002/humu.22470 (2014).
45 Zhang, H. *et al.* Deletion of PrBP/delta impedes transport of GRK1 and PDE6 catalytic subunits to photoreceptor outer segments. *Proc Natl Acad Sci U S A* **104**, 8857-8862, doi:10.1073/pnas.0701681104 (2007).
46 Wall, V. E., Garvey, L. A., Mehalko, J. L., Procter, L. V. & Esposito, D. Combinatorial assembly of clone libraries using site-specific recombination. *Methods Mol Biol* **1116**, 193-208, doi:10.1007/978-1-62703-764-8_14 (2014).
47 Harder, E. *et al.* OPLS3: A Force Field Providing Broad Coverage of Drug-like Small Molecules and Proteins. *J Chem Theory Comput* **12**, 281-296, doi:10.1021/acs.jctc.5b00864 (2016).
48 Hou, T., Wang, J., Li, Y. & Wang, W. Assessing the performance of the MM/PBSA and MM/GBSA methods. 1. The accuracy of binding free energy calculations based on molecular dynamics simulations. *J Chem Inf Model* **51**, 69-82, doi:10.1021/ci100275a (2011).
49 O'Boyle, N. M. *et al.* Open Babel: An open chemical toolbox. *J Cheminform* **3**, 33, doi:10.1186/1758-2946-3-33 (2011).
50 Blazevits, O. *et al.* Galectin-1 dimers can scaffold Raf-effectors to increase H-ras nanoclustering. *Sci Rep* **6**, 24165, doi:10.1038/srep24165 (2016).
51 Okutachi, S. *et al.* A Covalent Calmodulin Inhibitor as a Tool to Study Cellular Mechanisms of K-Ras-Driven Stemness. *Front Cell Dev Biol* **9**, 665673, doi:10.3389/fcell.2021.665673 (2021).
52 Manoharan, G. B., Okutachi, S. & Abankwa, D. Potential of phenothiazines to synergistically block calmodulin and reactivate PP2A in cancer cells. *PLoS One* **17**, e0268635, doi:10.1371/journal.pone.0268635 (2022).
53 Potdar, S. *et al.* Breeze: an integrated quality control and data analysis application for high-throughput drug screening. *Bioinformatics* **36**, 3602-3604, doi:10.1093/bioinformatics/btaa138 (2020).
54 Ianevski, A., Giri, A. K. & Aittokallio, T. SynergyFinder 2.0: visual analytics of multi-drug combination synergies. *Nucleic Acids Res* **48**, W488-W493, doi:10.1093/nar/gkaa216 (2020).
55 R, C. T. R: A Language and Environment for Statistical Computing. (2022).

56 Therneau, T. M. & Grambsch, P. M. *Modeling Survival Data: Extending the Cox Model*. (Springer New York, NY, 2000).
57 Alboukadel, K., Marcin, K. & Przemyslaw, B. survminer: Drawing Survival Curves using 'ggplot2'. (2021).
58 Li, J. *et al.* The VSGB 2.0 model: a next generation energy model for high resolution protein structure modeling. *Proteins* **79**, 2794-2812, doi:10.1002/prot.23106 (2011).

Table of Contents Graphic

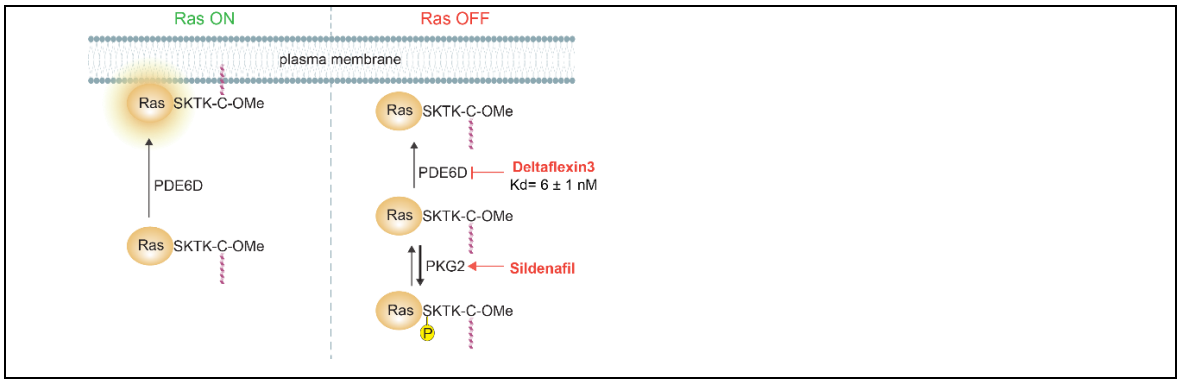

3.3. Ciliary K-Ras protects C2C12 progenitors from differentiation (III)

Rohan Chippalkatti, Bianca Parisi, **Pelin Kaya**, Elisabeth Schaffner-Reckinger, Sara Bottone, Lynn Mangen, Yashar Rouzbahani, Christian Eggeling, Daniel Kwaku Abankwa

Status: ready to submit manuscript

Personal contributions of Pelin Kaya

- Designed, performed, and analyzed the BRET assay data then generated and compiled listed figures for this manuscript:
    - **Figure 6**
    - **Figure 7(a-b)**
- Performed cell culture and protein lysis for the immunoblotting assays then generated and compiled listed figure for this manuscript:
    - **Figure 7(c)**
- Designed and generated chimeric expression constructs by multi-site gateway cloning system.

Manuscript III: Introduction

The primary cilium is microtubule-based highly specialized antenna-like organelle on the cell surface that is found on many eukaryotic cells. It serves as a polymodal sensory organelle because it contains diverse signaling components (Anderson & Stearns, 2009; Gerdes *et al*, 2009; Wilsch-Brauninger & Huttner, 2021). Overall, the regulation of cilia presence is closely tied to the progression of the cell cycle. Consequently, there exists an inverse relationship between the primary cilium's presence and cell proliferation when a cell undergoes division, the cilium is resorbed into cell while allowing for centrosomes to function as mitotic poles (Pugacheva *et al*, 2007). Depletion of cilia is seen in various types of cancer, such as pancreatic and renal cancers (Higgins *et al*, 2019). It was determined that primary cilia were present in 25% of cancer cells from patients with PDAC (Emoto *et al*, 2014). Several studies suggested that the activation of ERK signaling may be involved in regulating cilia and the regulation of cilia length (Kim *et al*, 2013; Wang *et al*, 2013).

The mechanisms by which KRAS impacts cancer stemness and the potential strategy for targeting this activity is still limited. Our investigation focused on examining the distribution patterns of different variants of KRAS within centriolar organelles, known to play a role in regulating stemness, as well as investigating their impact on the differentiation process in mouse muscle C2C12 cells. This particular cell line represents an ideal model system due to its characteristic population of ciliated stem/progenitor cells that exhibit differentiation when exposed to low serum conditions, coinciding with a decline in RAS-MAPK signaling. It is worth to note that, even under differentiating conditions, oncogenic KRAS expression preserve the stem-like state. The localization of KRAS at the primary cilium of C2C12 progenitor cells may be propagated via the mother centriole to the mother centrosome, which have been observed that asymmetrically partition into the stemness retaining cell. By performing cellular BRET-interaction experiments in HEK cells, we were able to observe that the phosphomimetic S181D-mutation reduces its affinity with PDE6D. This reduction in affinity between KRAS and PDE6D correlates with a decrease in the ciliary localization of KRAS within C2C12 cells. In order to accurately measure this effect, we developed a flow cytometry-based assay specifically designed for C2C12 cell differentiation. Through this assay, we were able to demonstrate that mutations or pharmacological interventions which lead to decreased ciliary localization of KRAS indeed promote cell differentiation.

Ciliary K-Ras protects C2C12 progenitors from differentiation

Rohan Chippalkatti [1], Bianca Parisi [1], Pelin Kaya [1], Elisabeth Schaffner-Reckinger [1], Sara Bottone [1], Lynn Mangen [1], Yashar Rouzbahani [2], Christian Eggeling [2,3], Daniel Kwaku Abankwa [1*]

[1] Cancer Cell Biology and Drug discovery group, Department of Life Sciences and Medicine, University of Luxembourg, Esch-sur-Alzette, Luxembourg
[2] Faculty of Physics and Astronomy, Institute of Applied Optics and Biophysics, Friedrich Schiller University Jena, Jena, Germany
[3] Leibniz Institute of Photonic Technology e.V., Jena, Germany

[*] Corresponding author: daniel.abankwa@uni.lu

Abstract
It is currently believed that all major Ras signaling emerges from the plasma membrane, where it transduces mitogenic signals to drive cell proliferation. However, it is also known that Ras impacts on cell differentiation, but exactly how is not understood.
Here we show that as compared to H-Ras and N-Ras, K-Ras most abundantly localizes to the primary cilium membrane of C2C12 cells. The presence of B-Raf and active MEK in the cilium suggests that K-Ras is active. Localization of K-Ras to the cilium depends on the trafficking chaperone PDE6D. Consequently, reduction of its PDE6D-association by phosphorylation of Ser181 at the C-terminus of K-Ras ablates its ciliary localization. Importantly, treatments that reduce ciliary K-Ras localization increase differentiation of C2C12 cells. Conversely, oncogenic K-Ras mutants with enhanced ciliary localization that are otherwise sequestered to the nucleo-cytoplasm, are sufficient to block differentiation as their parental counterparts with normal plasma membrane distribution.
Our data suggest a model, where during asymmetric divisions of C2C12 progenitor cells, ciliary K-Ras is asymmetrically enriched at the mother centrosome-associated ciliary remnant in the stemness-retaining progenitor. Based on these data, we propose a major role for K-Ras in maintaining proper asymmetric fate outcomes during stem/ progenitor cell divisions in the adult organism. We postulate that this mechanism is fundamentally conserved and represents the decisive perturbation caused by aberrant Ras-signaling in cancer and RASopathies.

Introduction
The oncogenic activity of Ras is classically associated with cell proliferation, given that Ras-signaling via Raf-Mek-Erk drives S-phase entry. In line with this, essentially all major cancer cell assays and screens rely on cell proliferation, confirming the importance of the MAPK-pathway for proliferation (Barretina *et al*, 2012; McDonald *et al*, 2017; Tsherniak *et al*, 2017). However, at the same time it is known that Ras signaling fundamentally impacts on cellular differentiation, a process that is intertwined with the cell cycle (Crespo & Leon, 2000).
During development, stem cells and progenitors can divide symmetrically to expand the progenitor pool or fully differentiate (Morrison & Kimble, 2006). Asymmetric divisions self-renew the progenitor, while also giving rise to a differentiated daughter cell. This latter mode of division may therefore be particularly relevant to maintain adult tissues. These natural homeostatic processes are perturbed in cancer, where cancer associated mutations stimulate symmetrical divisions at the expense of asymmetrical divisions in cancer stem cells (Cicalese *et al*, 2009).
In agreement with this observation, we recently showed that transformation with oncogenic K-Ras mutants blocks differentiation of C2C12 myoblasts into Pax7-/ MyHC+ myocytes/ tubes (**Chippalkatti et al. manuscript in submission**). We proposed a model, whereby oncogenic K-Ras blocks the maturation of Pax7-/ MyHC- transit amplifying cells, that constitute the bulk of cells in the C2C12 cell line, into differentiated cells. Importantly, knockdown of K-Ras during differentiation decreases the numbers of Pax7+/ MyHC- progenitors, which are the endogenous stem-like cells in the C2C12 cell line. This suggests that K-Ras has a protective role to maintain the small population of progenitors. Exactly how at the cellular level Ras proteins impact on stemness and differentiation is not known (Chippalkatti & Abankwa, 2021).
Polarity factors such as, Partitioning Defective (PAR)-family proteins or cell fate determinants,

such as Numb, asymmetrically partition to one daughter cell thus guiding asymmetric fate outcomes in stem cells and progenitors (Morrison & Kimble, 2006). Likewise, several cellular organelles asymmetrically distribute, such as the mother centrosome, which confers stemness to the inheriting cell in mammalian models (Chen & Yamashita, 2021; Wilsch-Brauninger & Huttner, 2021). However, the molecular factors of the mother centrosome that impart stemness traits have not been characterized so far.

The primary cilium functions as an antenna-like organelle on the apical surface not only of several epithelial cells, but in particular of stem cells and progenitors (Lai & Jiang, 2020). The axoneme at its core contains a several micrometer-long 9 + 0 tubulin duplet bundle, which emerges from the mother centriole of the basal body at the base of the cilium. During cell division, the mother centrosome remains associated with the membrane remnant of the primary cilium, which facilitates ciliogenesis in the inheriting daughter cell (Anderson & Stearns, 2009; Paridaen *et al*, 2013). Given that the cilium is replete with receptors and other signaling components of stemness and developmental pathways, such as Sonic hedgehog, Wnt and Notch, asymmetric onset of signaling in these pathways in the daughter cell with facilitated ciliogenesis, is thought to preserve stemness properties (Anderson & Stearns, 2009; Chen & Yamashita, 2021).
Several transport mechanisms realize the specific trafficking of ciliary proteins into the primary cilium along the axoneme (Lai & Jiang, 2020). A diffusion barrier formed by the Y-links and transition fibers of the ciliary gate keeps the ciliary compartment, including its distinct membrane, separated from the rest of the cell (Garcia-Gonzalo & Reiter, 2017). However, proteins below approximately 40 kDa can enter the cilium freely via diffusion. For membrane anchored, lipid modified proteins this is enabled by trafficking chaperones, such as UNC119A/B and PDE6D (Fansa & Wittinghofer, 2016; Garcia-Gonzalo & Reiter, 2017). These chaperones solubilize their membrane bound cargo by binding their myristoyl- or prenyl-moieties, respectively. An allosteric release mechanism mediated by the small GTPases Arl2 and Arl3 then offloads cargo proteins (Fansa & Wittinghofer, 2016; Ismail *et al.*, 2011). GTP-Arl2 can only eject cargo with lower, micromolar or submicromolar affinities, such as Src- and Ras-proteins (Fansa & Wittinghofer, 2016; Ismail *et al.*, 2011). Its activity in the perinuclear area releases PDE6D-bound K-Ras, which is subsequently trapped on the recycling endosomes for vesicular forward trafficking to the plasma membrane (Schmick *et al.*, 2014). However, plasma membrane delivery of K-Ras appears to occur via redundant pathways as only an estimated 50 % seems to be facilitated by PDE6D (Pavic *et al.*, 2022)(**Kaya P. et al. submitted; bioRxiv https://doi.org/10.1101/2023.08.23.554263, manuscript II**). The guanine nucleotide exchange factor (GEF) of related Arl3 is the ciliary marker protein Arl13B, a G domain containing protein that is likewise active only if GTP-bound (Gotthardt *et al*, 2015). Hence for both UNC119A/B and PDE6D, nanomolar affinity cargo such as NPHP3 and INPP5E, respectively, are offloaded only by GTP-Arl3 inside the cilium (Fansa *et al.*, 2016). Consequently, also low affinity cargo should be released into the cilium. Indeed, a recent report described ciliary localization of K-Ras, albeit its functional role there remained unexplored (Yelland *et al.*, 2022).
While the major affinity contribution of PDE6D cargo is provided by the prenyl-moiety, affinity is significantly modulated by the four residues upstream of the prenylated cysteine (Dharmaiah *et al.*, 2016; Yelland *et al.*, 2022). These residues can engage with the entrance of the hydrophobic pocket of PDE6D. Thus high-affinity cargo INPP5E-inspired mutations K182S/K184I in K-Ras (K-Ras-SI) increased its affinity to PDE6D to the subnanomolar regime. Consequently, K-Ras-SI showed enhanced ciliary localization (Yelland *et al.*, 2022).

Affinity to PDE6D can be downmodulated by two charged and bulky residues, such as Lys, Arg, Glu, in both the -1 and -2 position relative to the prenylated cysteine. Similarly, it appears that palmitoylation on nearby cysteines can obstruct binding to PDE6D (Dharmaiah *et al.*, 2016). This explains why in cells mono-palmitoylated N-Ras and dually-palmitoylated H-Ras are worse cargos than K-Ras, which is not palmitoylated (Chandra *et al.*, 2011; Siddiqui *et al.*, 2020a) (**Kaya P. et al. manuscript II**).

The current model for Ras signaling suggests that it encounters all its major regulators and effectors at the plasma membrane. Hence, PDE6D, which is also significant in the cycle for the forward trafficking of K-Ras to the plasma membrane, was proposed as a surrogate drug target for K-Ras. Several types of PDE6D inhibitors have been developed, however, with limited effect on both cell proliferation and Ras-signaling (Martin-Gago *et al.*, 2017a; Murarka *et al.*, 2017; Papke *et al.*, 2016; Siddiqui *et al.*, 2020a; Zimmermann *et al.*, 2013). Even though inhibitor optimization against the hydrophobic pocket generates increasingly more hydrophobic and thus insoluble compounds, we recently managed to raise a highly soluble PDE6D inhibitor, Deltaflexin3 (**Kaya P. et al. manuscript II**). We demonstrated that it can synergize with approved sildenafil, which increases PKG2-mediated phosphorylation of Ser181 on K-Ras and thus reduces PDE6D-affinity (Cho *et al.*, 2016; Dharmaiah *et al.*, 2016).

Here we show that amongst the cancer associated Ras isoforms, K-Ras shows the strongest localization to the primary cilium of C2C12 progenitors. This localization is PDE6D dependent and significantly inhibited by phosphorylation of Ser181. We demonstrate that inhibition of ciliary K-Ras promotes C2C12 cell differentiation. Moreover, an oncogenic K-Ras mutant that localizes only to the primary cilium, while being sequestered from other membranes, is sufficient to suppress differentiation as its parental counterpart. This supports a model, where active ciliary K-Ras protects stemness via its localization to the cilium.

Results

K-Ras localization to the primary cilium depends on PDE6D

GTP-Arl3 is abundant in the primary cilium where it functions as an allosteric release factor of high and low affinity clients of the trafficking chaperone PDE6D (Fansa *et al.*, 2016). We therefore expected that cancer associated Ras proteins that bind with low affinity to PDE6D are also released into the cilium.

In order to understand the ciliary functions of Ras, we employed the heterogenous murine C2C12 myoblast cell line, which contains ~1 % fast dividing Pax7+ progenitors, while the remainder of the cell line constitutes slowly dividing Pax7- transit amplifying cells under high serum conditions (Chippalkatti et al. submitted; bioRxiv DOI: https://doi.org/ 10.1101/2023.10.05.561021). Confocal image analysis revealed that the large majority of progenitors are ciliated (~80 %), while only ~10 % of the transit amplifying cells carry primary cilia (**Fig. S1a**).

We transiently expressed GFP2-tagged wild type (wt) K-Ras (**Fig. 1a**), N-Ras (**Fig. 1b**) and H-Ras (**Fig. 1c**) in C2C12 cells and examined their co-localization with Arl13B, a marker of the primary cilium membrane. While K-Ras was significantly enriched in the cilium, N-Ras and H-Ras were almost excluded (**Fig. 1d**). This was in line with the cellular PDE6D engagement of these Ras proteins, which is blocked if Ras is palmitoylated near the

prenylated C-terminal cysteine (Chandra *et al.*, 2011; Dharmaiah *et al.*, 2016). Consistent with a PDE6D-dependent delivery of K-Ras to the cilium, depletion of PDE6D, essentially abrogated ciliary K-Ras localization (**Fig. 1e,f**).

STED-superresolution imaging suggested that a minor fraction of K-Ras is associated with the centrioles of the ciliary basal body (**Fig. 1g**). However, the majority of K-Ras distributes along the Arl13B-positive ciliary membrane (**Fig. 1h**). In addition, we observed GFP2-B-Raf on the basal body (**Fig. 1i**), and active, phosphorylated MEK inside the cilium (**Fig. 1j**). Thus, K-Ras and essential MAPK-pathway components localize to the primary cilium and are likely to be active.

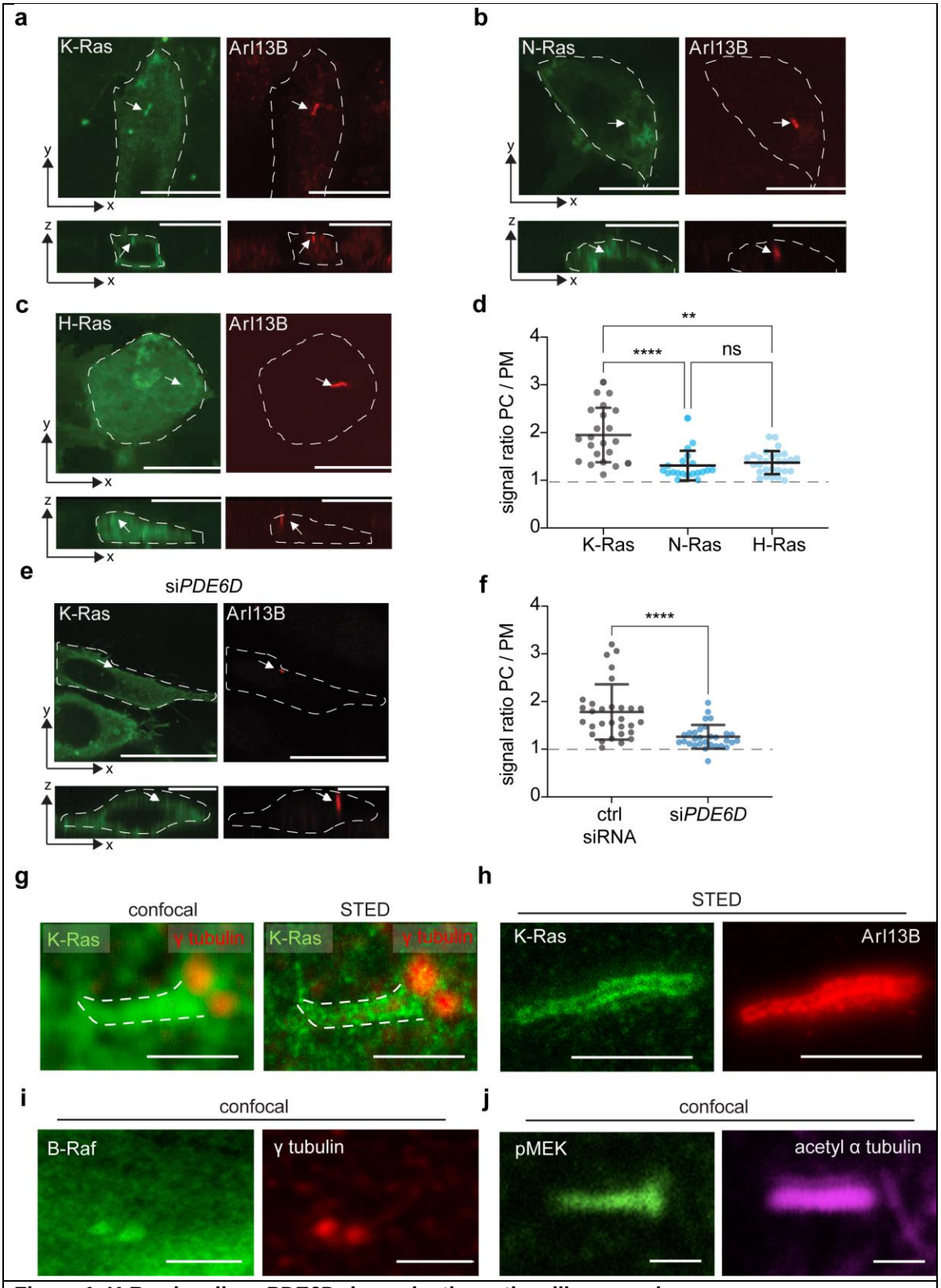

Figure 1. K-Ras localizes PDE6D-dependently on the ciliary membrane.
(**a-c**) Representative confocal images of C2C12 cells grown in high serum transfected with GFP2-K-Ras (a), GFP2-N-Ras (b) or GFP2-H-Ras (c) and immunolabeled for Arl13B marking the cilium (arrow). *Bottom*, images show orthogonal views. Scale bar = 10 µm.
(**d**) Data as in (a-c) were quantified for relative enrichment of Ras proteins on the primary cilium (PC) as compared to the plasma membrane (PM). Individual data points (n = 30 per condition) from

N = 3 independent biological repeats. Means ± SD are plotted. Statistical analysis was done with the Kruskal-Wallis test. Multiple columns were compared using Dunn's post hoc test.
(**e**) C2C12 cells grown in high serum and expressing GFP2-K-Ras treated with control (ctrl) or PDE6D-targeting siRNA pool (100 nM) for 48 h. Scale bar = 10 µm.
(**f**) Data as in (e) were quantified for relative enrichment of Ras proteins on the primary cilium (PC) as compared to the plasma membrane (PM). Individual data points (n = 30 per condition) from N = 3 independent biological repeats. Statistical analysis was done using the Mann-Whitney test.
(**g**) Representative confocal (left) and STED (right) images of GFP2-K-Ras relative to the basal body which is immunolabelled with antibodies against γ tubulin. GFP2-K-Ras was visualized by immunolabelling with GFP-nanobodies conjugated to ATTO 647N. Dashed lines indicate approximate location of the cilium. Scale bar = 2 µm.
(**h**) Representative STED images of GFP2-K-Ras visualized relative to the ciliary membrane marked with antibodies against Arl13B. GFP2-K-Ras was visualized by immunolabelling with GFP nanobodies conjugated to ATTO 647N. Scale bar = 2 µm.
(**i**) Representative confocal images reveal colocalization of GFP2-B-Raf with basal body marker γ tubulin, visualized by immunolabelling. Scale bar = 2 µm.
(**j**) Immunolabelling of phospho-MEK1/2 (Ser217/221) and ciliary marker acetyl α tubulin. Scale bar = 2 µm. (g-j) Imaging data of C2C12 cells grown in high serum are shown.

Ser181-phosphorylation of K-Ras decreases its ciliary localization

The micromolar affinity between K-Ras and PDE6D in vitro is significantly reduced by alanine- and to a greater extent by the phosphomimetic glutamate-mutation of Ser181, which is found in close proximity to the farnesylated C-terminus of K-Ras (Dharmaiah *et al.*, 2016). Accordingly, intracellular BRET-binding experiments with PDE6D revealed significantly reduced $BRET_{top}$ interaction values for S181A and S181D mutants of K-Ras in HEK293 EBNA cells (hereafter HEK293) (**Fig. 2a**). Given the dependence of K-Ras on PDE6D for its ciliary localization (**Fig. 1f**), we expected that ciliary localization of the K-Ras S181-mutants would be compromised in C2C12 cells. While K-Ras S181A accumulated almost as the parent (**Fig. 2b,d**), ciliary localization of the phosphomimetic K-Ras S181D mutant was indeed significantly reduced to background levels (**Fig. 2c,d**).

Phosphorylation of Ser181 of K-Ras is mediated by the kinase PKG2, downstream of the ciliary AMPK-pathway (Cho *et al.*, 2016; Lai & Jiang, 2020). PKG2 is a cGMP-activated kinase, which can be stimulated by the analogue 8Br-cGMP or clinically approved inhibitors of cGMP-degrading phosphodiesterase-5 (PDE5), such as sildenafil (Cho *et al.*, 2016). Activation of PKG2 with these drugs is therefore expected to block binding of K-Ras to PDE6D and thus its trafficking to the cilium. Indeed, both 8Br-cGMP (IC50 = 226 ± 11 µM) (**Fig. 2e**) and sildenafil (IC50 = 25 ± 4 µM) (**Fig. 2f**) dose-dependently decreased the BRET between K-Ras and PDE6D, while having no effect on non-phosphorylatable K-Ras S181A (**Fig. 2e,f**). Accordingly, localization of K-Ras to the cilium was abrogated by treatment with 8Br-cGMP (**Fig. 2g,h**), while ciliary localization of K-Ras S181A remained unaffected (**Fig. S1b**). The same was observed with sildenafil (**Fig. 2i,j**), albeit the dynamic range was compressed due to effects of the solvent (0.2 % DMSO).

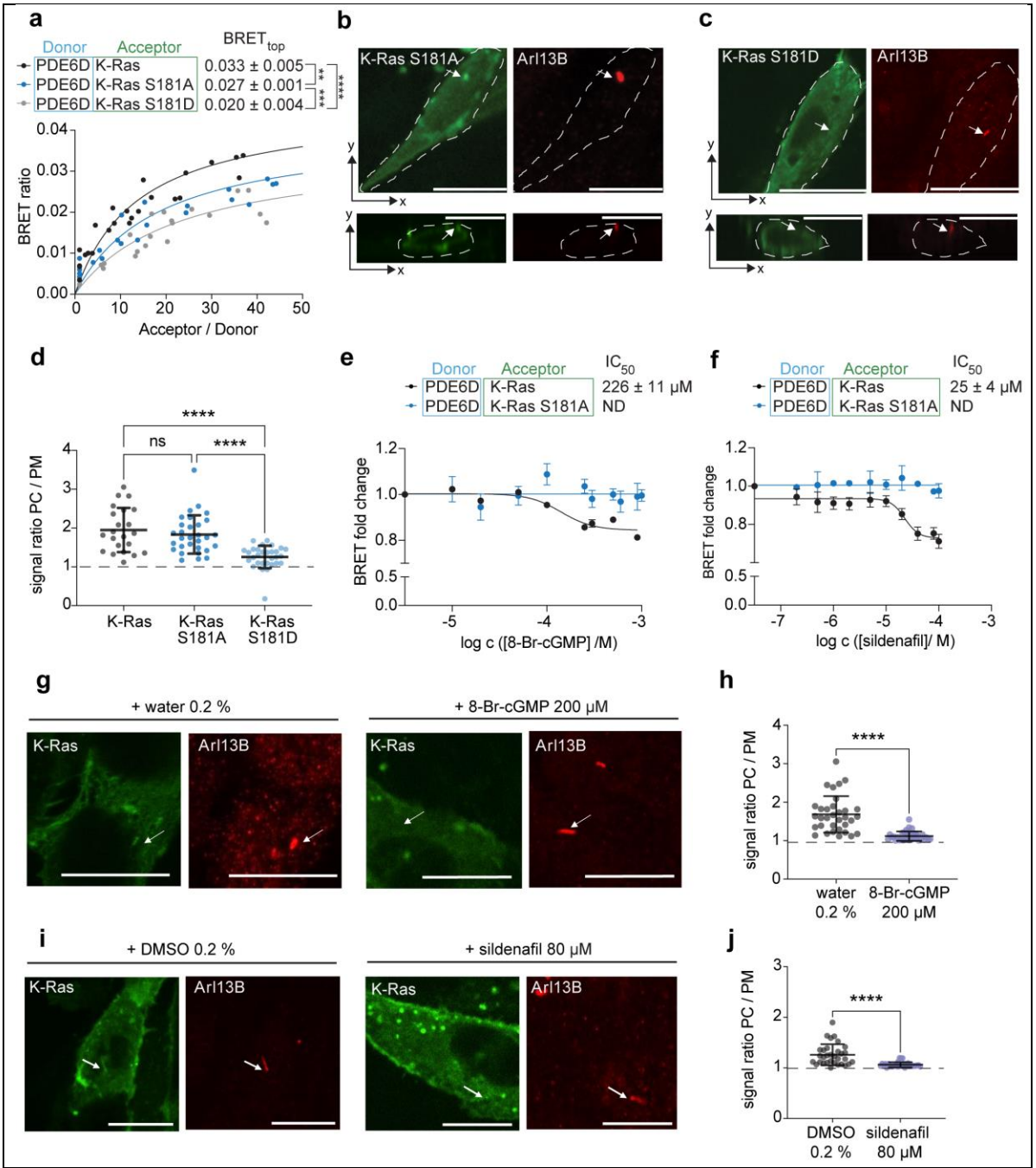

Figure 2. Phosphorylation of Ser181 on K-Ras reduces PDE6D engagement and ciliary localization.

(**a**) BRET-titration curves of RLuc8-PDE6D and GFP2-K-Ras Ser181-mutants expressed in HEK293 cells; N = 3. Statistical analysis was performed with the extra sum-of-squares F-test.

(**b,c**) Representative confocal images of C2C12 cells grown under high serum expressing GFP2-K-Ras S181A (b) or GFP2-K-Ras S181D (c) and immunolabelled for ciliary marker Arl13B (arrows). Scale = 10 µm.

(**d**) Data as in (b,c) were quantified for relative ciliary (PC) localization of K-Ras mutants as compared to the plasma membrane (PM). Individual data points (n = 30 per condition) from N = 3 independent biological repeats. Statistical analysis was done with the Kruskal-Wallis test. Multiple columns were compared using Dunn's post hoc test.

(**e,f**) Dose-dependent effect of 8Br-cGMP tested at concentrations from 10 µM to 1000 µM (e) or sildenafil tested at concentrations from 200 nM to 1000 µM (f) for 24 h on BRET-interaction between RLuc8-PDE6D and GFP2-K-Ras or GFP2-K-Ras Ser181A in HEK293 cells; N = 3. Donor to

acceptor ratio was fixed at 1:8.
(**g-j**) Confocal images of C2C12 cells expressing GFP2-K-Ras and treated as indicated in high serum for 2 days and immunolabelled for ciliary marker Arl13B (g,i; arrows). Scale = 10 µm. Quantification of data as in (g,i) for **relative ciliary localization** of GFP2-K-Ras (h,j). Individual data points (n = 30 per condition) from N = 3 independent biological repeats. Statistical analysis was done with the Mann-Whitney test.

Treatments that inhibit ciliary K-Ras localization increase differentiation of C2C12 cells

We previously provided evidence that the ciliated Pax7+ progenitors that make up only ~1 % of the C2C12 cell line is maintained by asymmetric divisions under high serum conditions. While one cell retains the progenitor state, the other becomes a transit amplifying Pax7-/ MyHC- cell, which make up the bulk of the C2C12 cell line (Chippalkatti et al. submitted; bioRxiv DOI: https://doi.org/ 10.1101/2023.10.05.561021) (**Fig. 3a**).
We hypothesized that active ciliary K-Ras remains associated with the ciliary remnant as progenitors enter mitosis, allowing its activity to co-segregate with the mother centrosome and protect the progenitor state in the inheriting cell. Hence, blocking ciliary K-Ras would prevent the protection of the progenitor state, increase the number of transit amplifying cells in a pseudo-symmetrical division, leading to a net increase of differentiated cells.

We quantified differentiation as the fraction of MyHC+ cells using our recently established, automated flow cytometry-based C2C12 cell differentiation assay (Parisi *et al*, 2023). In agreement with our hypothesis, sildenafil, which blocks PDE6D binding (**Fig. 2f**) and thus ciliary localization of K-Ras (**Fig. 2i,j**), dose-dependently increased the fraction of differentiated cells (**Fig. 3b**). Conversely, knockdown of the PKG2 gene (*PRKG2*) increased BRET between K-Ras and PDE6D (**Fig. S1c,d**), which would facilitate ciliary accumulation of K-Ras. Consequently, PKG2 knockdown dose-dependently reduced differentiation (**Fig. 3c**).

Our differentiation assay furthermore allows to assess transient genetic perturbations of EGFP-tagged K-Ras mutants, by gating for cells with low levels (up to 10 × above autofluorescence background) of GFP-signal that corresponds to near native expression levels as we previously established (Chippalkatti et al. submitted; bioRxiv DOI: https://doi.org/ 10.1101/2023.10.05.561021). Transient perturbations are expected to last for approximately 2 days, i.e. exactly during the differentiation switch. This transient manipulation is necessary, as stable clones of genes that impact on stemness and differentiation, would inevitably destroy the self-maintenance of the C2C12 cell pool.

As observed before for oncogenic K-Ras mutant (Chippalkatti et al. submitted; bioRxiv DOI: https://doi.org/ 10.1101/2023.10.05.561021) expression of K-Ras G12C SI significantly reduced the fraction of differentiated cells (**Fig. 3d**), due to the block of further differentiation of transit amplifying cells. Treatment with the covalent G12C-specific inhibitor AMG 510/ sotorasib fully rescued the differentiation of K-Ras G12C-transformed C2C12 cells, confirming that oncogenic or active K-Ras is cell-autonomously required to inhibit differentiation (**Fig. 3d**).

Next, we tested whether the inhibition of differentiation by oncogenic K-Ras G12C can be pharmacologically rescued by sildenafil treatment. Indeed, sildenafil could counteract and

overall restore the native differentiation level in K-Ras G12C transformed cells (**Fig. 3e**).

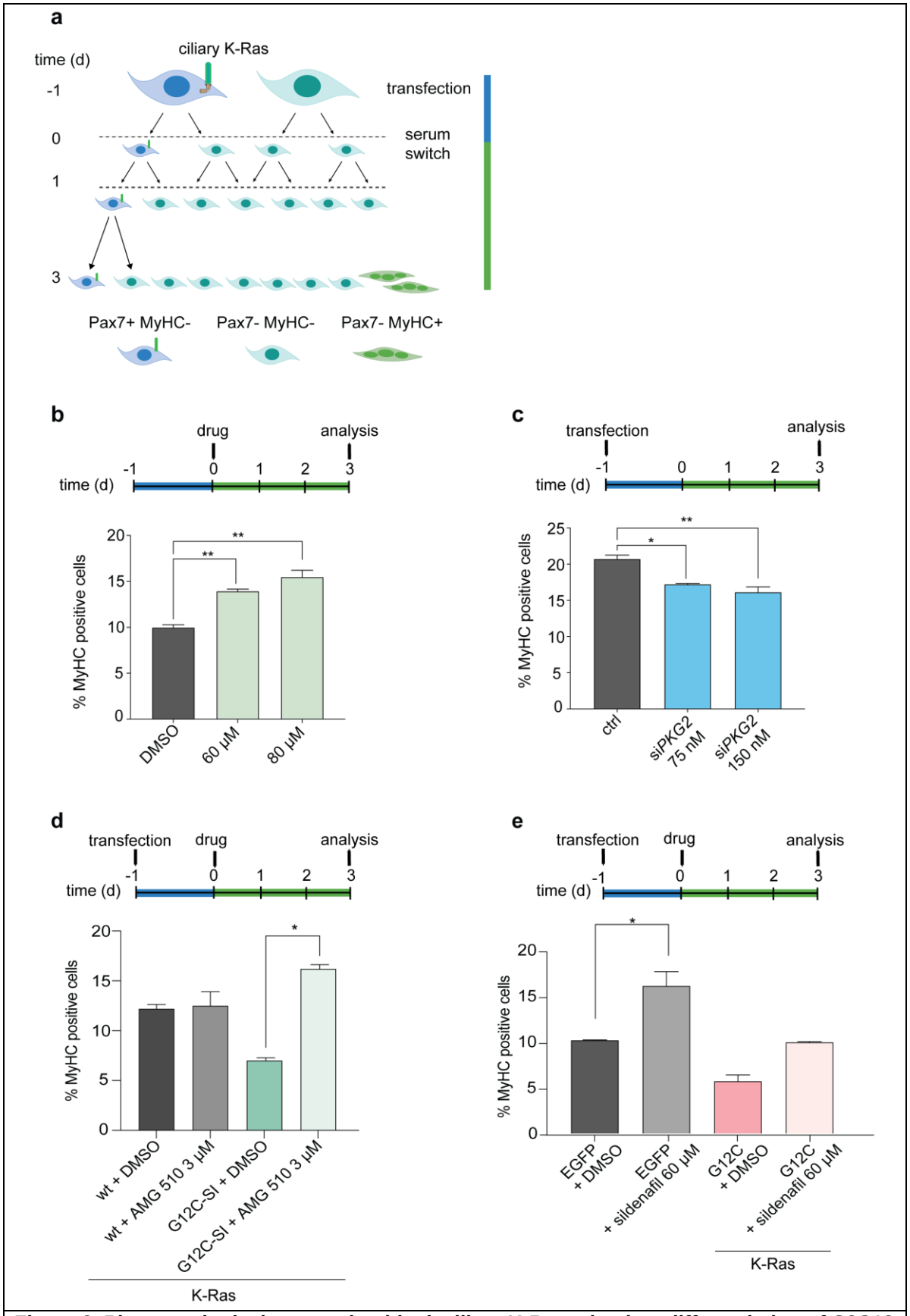

Figure 3. Pharmacological agents that block ciliary K-Ras stimulate differentiation of C2C12

cells.
(**a**) Schematic illustrates fates of ciliated progenitors with ciliary K-Ras (left) and non-ciliated transit amplifying myoblasts without cilium (right) upon differentiation in low serum.
(**b-e**) Timelines on top indicate transfections of siRNA or EGFP-tagged Ras constructs, drug treatments and analysis time point for C2C12 cell differentiation quantified by MyHC expression. High serum culture period is in blue and low serum culture period in green. DMSO controls are 0.2 % (v/v) DMSO in vehicle. N = 3 for all experiments; Statistical analysis was done with the Fisher's exact test.

Restricting oncogenic K-Ras to the cilium still blocks C2C12 cell differentiation

To better understand the functions of K-Ras that emerge from the primary cilium in the context of cell differentiation, we employed the artificial K-Ras SI mutant (Yelland *et al.*, 2022). In this mutant two lysine residues upstream of the farnesylated cysteine of K-Ras were converted into serine and isoleucine as in the high-affinity PDE6D cargo INPP5E (**Fig. 4a**). Thus, the affinity of K-Ras to PDE6D increased from micromolar to subnanomolar levels (Yelland *et al.*, 2022).

Consistently, the BRET-signal of K-Ras SI with PDE6D was dramatically increased as compared to the wild-type (**Fig. 4b**). It by far exceeded the effect of the PKG2 knockdown that would decrease S181-phosphorylation and thus restore a higher PDE6D affinity (**Fig. S1c**). Due to its high PDE6D affinity, increased PDE6D levels can furthermore efficiently sequester K-Ras SI to the nucleo-cytoplasm, thus inactivating bulk membrane associated K-Ras signaling by keeping it away from the plasma membrane (Yelland *et al.*, 2022).
However, in our ciliated C2C12 progenitors K-Ras SI localization was almost normal (**Fig. 4c**), unless PDE6D was co-expressed (**Fig. 4d**). Importantly, under these latter conditions K-Ras SI was sequestered by PDE6D into the nucleo-cytoplasm, while showing also significantly increased localization to the cilium (**Fig. 4e**). This is consistent with the fact that inside the cilium, high affinity cargo, such as K-Ras SI can still be displaced from PDE6D by Arl3 (Fansa *et al.*, 2016).

We therefore focused on the condition with 1:1 PDE6D co-expression to establish the unique situation, where K-Ras SI is localized to the cilium, but otherwise sequestered to the nucleo-cytoplasm. In line with this sequestration, relative pERK-levels of K-Ras G12C SI were significantly reduced to background levels (**Fig. 4f**). Interestingly, overexpression of PDE6D with the parental oncogenic K-Ras G12C significantly increased MAPK-output (**Fig. 4f**), consistent with the notion that forward trafficking of K-Ras G12C to the plasma membrane as the major origin of bulk MAPK-signaling is enhanced.

We next analyzed the consequences on C2C12 cell differentiation. Both K-Ras G12D and K-Ras G12D SI suppressed differentiation, as observed previously for other oncogenic K-Ras-mutants (**Chippalkatti et al.**). Intriguingly, the K-Ras G12D SI did so also with co-expression of PDE6D, which abrogates bulk MAPK-output (**Fig. 4g**).

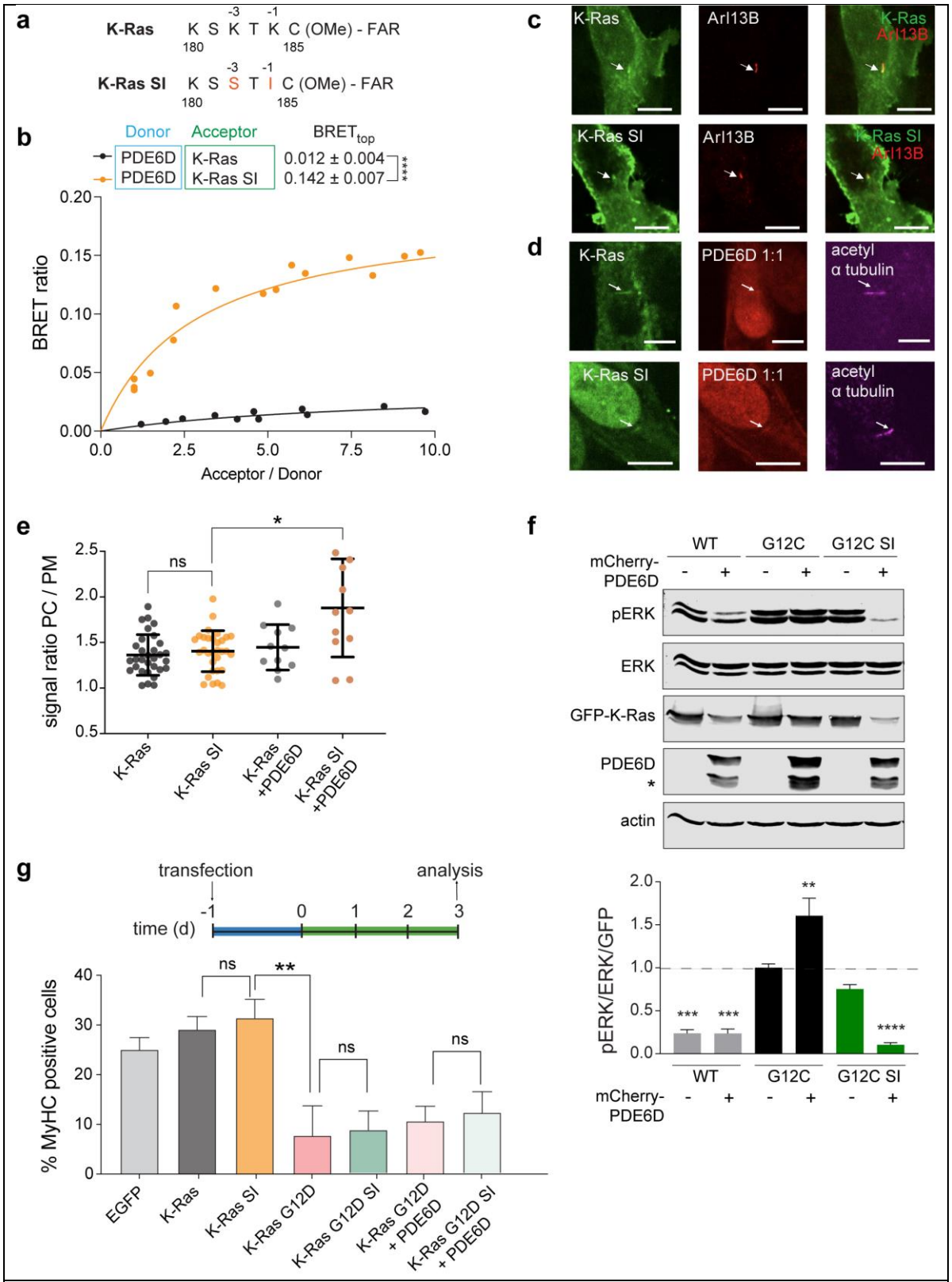

Figure 4. Ciliary confined K-Ras-SI is sufficient to block differentiation.

(**a**) Schematic showing mutations K182S/ K184I in the K-Ras SI mutant as compared to wt. OMe- carboxymethyl; FAR- farnesyl.

(**b**) BRET-titration curve of RLuc8-PDE6D and GFP2-K-Ras SI as compared to GFP2-K-Ras in HEK293 cells; N = 3. Statistical analysis was performed using extra sum-of-squares F-test.

(**c,d**) Representative confocal images of C2C12 cells grown under high serum expressing GFP2-K-Ras (top) or GFP2-K-Ras SI (bottom) and immunolabelled for ciliary marker Arl13B (arrows). When

mCherry-PDE6D was co-expressed at 1:1 DNA ratio with the K-Ras constructs, K-Ras SI was mostly sequestered to the nucleo-cytoplasm but remained on the cilium, visualized by acetyl α tubulin immunolabelling (d). Scale = 10 µm.
(**e**) Quantification of data as in (c,d) for relative ciliary localization of indicated conditions. Individual data points (n ≥ 11 per condition) from N = 2-3. Statistical analysis was done with the Kruskal-Wallis test. Multiple columns were compared using Dunn's post hoc test.
(**f**) Quantified immunoblot data of normalized phosphorylated ERK (pERK) expression from indicated GFP2-tagged K-Ras constructs expressed in HEK293 cells with or without co-expression of mCherry-PDE6D at 1:1 DNA ratio for 24 h. Means ± SEM are plotted from N = 3 experiments. Statistical analysis was done using One-way-ANOVA with multiple comparisons. Asterisk marks truncated/ cleaved protein consistently observed following transfection of mCherry-PDE6D.
(**g**) Timeline on top indicates transfection of EGFP-only control (EGFP) or EGFP-tagged Ras constructs and analysis time point for C2C12 cell differentiation quantified by MyHC expression. High serum culture period is in blue and low serum culture period in green. N=3 for all samples; statistical analysis was done with the Fisher's exact test.

Discussion

Here we show that assisted by PDE6D K-Ras traffics to the primary cilium, where it localizes to the ciliary membrane, while N-Ras and H-Ras show only a minor localization there. Other MAPK-components are also found in the cilium, notably active phosphorylated MEK, suggesting that K-Ras is active in the cilium. We find that blocking access of K-Ras to the cilium promotes differentiation of C2C12 cells, indicating that ciliary K-Ras somehow protects the progenitor state. Conversely, manipulations that increase the interaction of K-Ras with PDE6D also augment ciliary K-Ras and have a net inhibitory effect on differentiation.
Our data suggest a novel fundamental role of Ras proteins to guide cell differentiation from the primary cilium and centrosomes. Intriguingly, the tendency of the three Ras isoforms to bind to PDE6D and traffic to the cilium, as we describe here, correlates with their exploitation in cancer (Hobbs *et al.*, 2016). Others already provided evidence that oncogenic K-Ras most potently blocks differentiation of F9 mouse embryonal carcinoma stem cells, followed by N-Ras and least H-Ras (Quinlan *et al.*, 2008). Given this match, it may be plausible to assume that our findings apply also in other differentiation models.

Based on our data, we propose that active, ciliary K-Ras remains associated with the membrane remnant of the primary cilium during asymmetric divisions of progenitor cells. Its pathway activity up to MEK-activation may thus become asymmetrically apportioned with the mother centrosome into the daughter cell that retains stemness, while the other becomes a Pax7-/ MyHC- transit amplifying cell committed to differentiation (**Fig. 3a**). Differentiation of C2C12 cells is concurrent with upregulation of SPRED1 and thus potential engagement of the GAP NF1 (Wakioka *et al*, 2001). We predict that this step then erases active K-Ras only in the transit amplifying cells in the peri-centrosomal region and that this inactivation is necessary for differentiation to occur. Our model thus places the aberrant activity of NF1-GAP resistant oncogenic Ras into a specific developmental context.
If progenitors are transformed by oncogenic Ras, cilia formation is typically suppressed. Thus, we speculate that oncogenic Ras would randomly and therefore approximately equally distribute to the centrosomes in 50 % of divisions. Progenitors would effectively shift from their asymmetrical to a pseudo-symmetrical division, eventually expanding the progenitor pool and/ or the number of transit amplifying cells. As explained above, the latter cells can then not further differentiate, leading to their aberrant accumulation at the expense of

differentiated cells (Chippalkatti et al. submitted; bioRxiv DOI: https://doi.org/10.1101/2023.10.05.561021).

MAPK-activity drives cell proliferation hence cilia formation is blocked, which is reserved for the differentiated postmitotic or silent state (Higgins *et al.*, 2019). Interestingly though, the K-Ras G12C SI mutant with a significantly decreased MAPK-activity when PDE6D is co-expressed, can in a few cells permits the formation of cilia and can hence localize there. Reduced MAPK-activity suggests a lower mitotic activity of K-Ras G12C SI transformed cells. Nevertheless, we observe a suppression of differentiation almost as much as with parental oncogenic K-Ras, further confirming that not MAPK-driven over-proliferation of progenitors or transit amplifying cells is the root defect caused by this mutant, but the inhibition of differentiation. This places the Ras hotspot mutations that mediate NF1 resistance into the context of cell differentiation.

Given that other MAPK components B-Raf and active MEK1/2 can be found on the basal body and in the cilium, this begs the question as to their specific phosphorylation targets on these locations that would eventually protect stemness. The particular importance of MEK1 activity is supported by data suggesting that it is uncoupled from ERK during mitosis (Harding *et al*, 2003). This is plausible, as the typically nuclear activities of ERK relate to it promoting S-phase entry by activating a transcriptional program in an intact nucleus (Torii *et al*, 2006).
Consistent with the significance of MEK not just for cell proliferation, but also differentiation, MEK inhibitor trametinib was able to restore differentiation in C2C12 cells transformed with a variety of mutant Ras (Chippalkatti et al. submitted; bioRxiv DOI: https://doi.org/10.1101/2023.10.05.561021). This is mirrored by the efficacy of MEK inhibitors in the clinic both in cancer and RASopathy treatments (Castel *et al*, 2020). It may be interesting to note in this context that there are RASopathies with mutant Ras, Raf and MEK, but not ERK (Castel *et al.*, 2020).
Conversely, the importance of the Ras-signaling cascade down to MEK may also explain the significant toxicities that are associated with MEK inhibition, as it may be crucial to maintain progenitors and thus normal tissue regeneration. Future work will show, which spatio-temporal signaling events of the Ras-pathway on centriolar organelles are required to maintain stemness properties. Such knowledge would immediately offer novel opportunities to interfere with the disruption of differentiation by oncogenic Ras.

Our data point to an important physiological regulation of asymmetric cell divisions by the Ser181-phosphorylation of K-Ras. The endogenous pathway stimulating K-Ras Ser181-phosphorylation by PKG2 is the LKB1-AMPK pathway (Cho *et al.*, 2016). It becomes active on the basal body upon mechanical stimulation of the cilium and if the AMP/ ATP ratio increases upon energy depletion, leading to quiescence (Lai & Jiang, 2020). Hence quiescence promoting conditions would phosphorylate K-Ras and keep it out of the cilium, which makes sense as ciliary K-Ras is only required if cells start to asymmetrically divide again. Consistent with the non-synchronized, mitotically mixed population of cells, we were able to up- and down-modulate the BRET of K-Ras/ PDE6D with sildenafil, which stimulates PKG2 and thus Ser181-phosphorylation.

While we employ sildenafil here as a tool compound to increase Ser181-phosphorylation and skew differentiation, a treatment approach that builds on our mechanism is conceivable. We reported previously that the combination of our PDE6D inhibitor Deltaflexin3 with the PKG2

activator sildenafil was synergistically more potent to block MAPK-signaling and tumor growth. However, this combination would more efficiently target the high *PDE6D*/ low *PRKG2* (gene of PKG2) patient population, which we found has a better survival than those with the inverse signature (**Kaya P. manuscript II**).
This may point to this gene signature being protective, which is explained by the model elaborated here, where the normal progenitor self-renewal during asymmetric divisions is supported by K-Ras being efficiently trafficked to the cilium in the high *PDE6D*/ low *PRKG2* signature context. We therefore speculate that suboptimal functioning of this system (such as within low *PDE6D*/ high *PRKG2* patients), may lead to a loss of the normal, non-transformed progenitors in the cell competition with Ras-transformed progenitors inside the original stem/ progenitor cell niche. Incidentally, such a cell competition mechanism may explain the protective, tumor suppressive activity of wt Ras that is suggested by some data (Matallanas *et al*, 2011). Administering sildenafil once a transformed progenitor starts to dominate a niche may therefore be detrimental.
However, in cases where this is not happening, an alternative treatment could present itself. It is assumed that stem cell depletion is responsible for a drop in cancer cases in the population older than 70-75 years (White *et al*, 2014). Applying sildenafil over a longer period of time and before the transformation of any progenitors, may deplete the progenitor pool, thus lowering the number of cells that can be transformed. This may come at the cost of a reduced regenerative capacity at least in some tissues. It remains to be seen what patient statistics of sildenafil users will show in the future. One problem in the analysis of such data may be the irregular and possibly too low dose of sildenafil applications.

Our Ser181-data overall agree with previous results showing that oncogenic K-Ras with the phosphomimetic S181D-mutation is less able to drive a stemness pathway (Wang *et al*, 2015b). A different model was proposed, where Ser181-phosphorylation blocks the interaction with calmodulin (CaM), which is otherwise sequestered by active K-Ras. Sequestration of CaM by K-Ras G12V leads to a reduction in non-canonical Wnt-pathway activity as characterized by a drop in Fzd8 expression. Although CaM was suggested as a trafficking chaperone of K-Ras alike to PDE6D (Grant *et al*, 2020), our recent data suggest that K-Ras membrane association is relatively independent of CaM and both proteins may be in a complex together with Ras effectors (Babu Manoharan *et al*, 2023). However, given that CaM has a distinct distribution to the centrosomes during cell division (Li *et al*, 1999; Yu *et al*, 2004), it could be employed to fix K-Ras there together with effectors or facilitate restricted K-Ras trafficking in particular during that period. Similarly, the CaM-related centrin proteins that may asymmetrically distribute to the centrosomes could accumulate K-Ras in this manner (Babu Manoharan *et al.*, 2023). If association of oncogenic K-Ras with the centrosomes is mediated by CaM or related proteins this would shift CaM-inhibition and potentially also the stimulation of Ser181-phosphorylation back into focus. Indeed, CaM inhibitors can potently block K-Ras associated stemness traits of cancer cells, however, given the plethora of functions, targeting CaM in this context is not trivial (Okutachi *et al.*, 2021). Understanding such centrosomal complexes and the targets of the active Ras-pathway there may be highly significant for drug targeting, as oncogene transformed cells typically do not have a cilium (Higgins *et al.*, 2019; Nobutani *et al*, 2014).
In analogy to the Ser181-modulated ciliary localization, a similar palmitoylation-based regulation mechanism may apply to N-Ras and to some extent also H-Ras in certain developmental contexts. If palmitoylation was spatio-temporally restricted near the cilium during asymmetric progenitor division, mono-palmitoylated N-Ras more likely than dual-

palmitoylated H-Ras, would bind to PDE6D and traffic into the cilium. Such a mechanism could explain, why a non-palmitoylatable N-Ras G12D C181S abrogates myeloid transformation and alters hematopoetic stem and progenitor populations (Zambetti *et al*, 2020).

Given that K-Ras is the Ras isoform that localizes most to the cilium, it is exquisitely amenable to asymmetric distribution via the ciliary remnant. With this critical function in stem/ progenitor cell maintenance, we predict that the mutation of K-Ras in cancer is primarily deleterious, because it withdraws it from the regulation of normal asymmetric divisions.
We foresee that our model can readily explain the diverse disease phenotypes of Ras in cancer and RASopathies, where all mutants perturb the balance between stem/ progenitor cells and differentiated cells (Chippalkatti et al. submitted; bioRxiv DOI: https://doi.org/10.1101/2023.10.05.561021). While all (NF1-GAP insensitive) oncogenic, hot-spot K-Ras mutants expand the pool of transit amplifying cells at the expense of differentiated cells, RASopathy derived mutants show intermediate phenotypes, between those of wild type K-Ras overexpression and of the oncogenic mutants.
Moreover, our model suggests that certain phenotypes of RASopathies and multisystemic ciliopathies, such as intellectual disabilities, cardiovascular and skeletal abnormalities do not just overlap broadly by chance, but because of defects within a bigger ciliary-Ras-pathway that is critical for differentiation and stemness protection (Lee & Gleeson, 2011; Rauen, 2013; Tobin & Beales, 2009).

While our data were collected in C2C12 cells in vitro, there is no reason to believe that this molecular cell biological mechanism would not apply to other cell types, where the same molecular machinery operates over and over. Our data therefore tentatively suggest a mechanism of how oncogenic Ras reprograms progenitor cells into primordial ‘cancer stem cells’ that drive aberrant differentiation. This may explain, why the natural frequency of stem cell divisions underlies the susceptibility of tissues to develop cancer (Tomasetti & Vogelstein, 2015). It does not originate in increased proliferation by oncogenic Ras, but by the fate-switch that is introduced and then expands in the background of the normal tissue stem cell division frequency.

We here describe a novel fundamental role for K-Ras, which guides stemness retention during asymmetric divisions of progenitors via its localization in the primary cilium. This finding may critically shift our attention to the specific Ras biology on centriolar organelles and during differentiating cell divisions. Our mechanism further implies that oncogenic Ras has to be specifically drug targeted in differentiating cell cycles probably at locations associated with centriolar organelles i.e., at sites that are distinct from the plasma membrane. In addition to cancer and developmental diseases, we foresee a broad impact of our mechanism in all areas of stem cell and regenerative research, including many aging associated diseases.

Methods

Cell lines

C2C12 (CRL-1772), HEK293-EBNA (CRL-1573) and HEK293-EBNA c18 (CRL-10852) cells were obtained from the American Type Culture Collection. Cells were maintained in Dulbecco's Modified Eagle's Medium (DMEM; cat. no. 11965092, Thermo Fisher Scientific) supplemented with ~9 % (v/v) fetal bovine serum (FBS; cat. no. 10270106, Thermo Fisher Scientific), 2 mM L-glutamine (cat. no. A2916801, Thermo Fisher Scientific) and 1 % penicillin/ streptomycin (cat. no. 10378016, Thermo Fisher Scientific). In the context of C2C12 cell cultivation this medium is referred to as 'high serum medium'. Cells were incubated in a humidified incubator at 37 °C, with 5 % CO_2 and passaged twice per week at a confluency of 50 - 60 %. For differentiation experiments, C2C12 cells were first allowed to proliferate and attain ~ 90 % confluency. The cell culture medium was then exchanged with 'low serum medium', which is DMEM supplemented with 2 % horse serum (HS; cat. no. 16050130), 2 mM L-glutamine and 1 % penicillin/ streptomycin. Fresh low serum medium was added every day for three days. Specific treatment conditions are indicated in the figures.

Drugs and reagents

Sildenafil (cat no. HY-15025) and AMG 510 (HY-114277) were purchased from MedChemExpress. 8-Br-cGMP (cat. no. 51116-01-9) was obtained from Merck.

Antibodies and reagents for immunofluorescence

The following primary antibodies were utilized for confocal/STED microscopy; mouse monoclonal anti-Pax7 (cat. no MAB1675, Bio-Techne; dilution 1:50), rabbit polyclonal anti-Arl13B (177-11-1AP, Proteintech; dilution 1:500), mouse monoclonal anti-acetyl tubulin (cat no. ab24610, Abcam; dilution 1:500), rabbit polyclonal anti-γ tubulin (cat. no. ab113171, abcam; dilution 1:500) and rabbit polyclonal anti-phospho MEK1/2 (Ser217/221) (cat. no. 9121, Cell Signaling; dilution 1:200). Secondary antibodies used were as follows; goat anti-rabbit Alexa Fluor 594 (cat. no. A-11012, ThermoFisher scientific; dilution 1:200), goat anti-mouse Alexa Fluor 647 (cat. no. A-21235, ThermoFisher scientific; dilution 1:200) and goat anti-Mouse Alexa Fluor 488 (cat. no. A-11029, ThermoFisher scientific; dilution 1:200). Other reagents used were Alexa Fluor 647-Phalloidin (cat. no A-12381, ThermoFisher scientific; dilution 1:40) and ChromoTek GFP-booster ATTO647N (cat. no. gba647n, Proteintech; dilution 1:200). Hoechst 33342 (cat. no. 62249) was purchased from ThermoFisher scientific.

Antibodies for immunoblotting

Mouse monoclonal anti-phospho-p44/42ERK (Thr202/Tyr204) (cat. no. 9106) and rabbit polyclonal anti-ERK (cat. no. 9102) were obtained from Cell Signaling Technology. Mouse monoclonal anti-PDE6D (cat. no. sc-166854) was purchased from Santa Cruz Biotechnology. Rabbit polyclonal anti-GFP (cat. no. SAB4301138) antibody and mouse monoclonal anti-actin antibody (cat. no. A5441) were sourced from Merck. Rabbit polyclonal anti-cGKII (PKG2) (cat. no. PA5-101156) was obtained from ThermoFisher scientific.

Plasmid transfection in C2C12 cells

C2C12 cells were transfected with plasmid constructs (**Table S1**) as indicated in the figures using jetPRIME transfection kit (cat. no. 55-134, Polyplus-transfection). Cells cultured in high serum were transfected at a confluency of 50 - 60 %. Plasmid DNA amounts were as per manufacturers' guidelines e.g., 2 µg plasmid DNA was diluted in 200 µL jetPRIME buffer with 4 µl jetPRIME reagent. This mixture was incubated for 10 min at room temperature and added

dropwise to one well of a 6 well plate containing cells with 2 mL high serum medium. After 4 h the medium was replaced with fresh high serum medium.

siRNA transfection in C2C12 cells

For siRNA transfections in 6 well plates, typically 75-150 nM siRNA was diluted in 250 µL Opti-MEM transfection medium (cat. no. 31985062, ThermoFisher scientific) containing 7.5 µL Lipofectamine RNAiMAX reagent (cat. no. 13778015, ThermoFisher scientific). Transfection was performed when cells grown in high serum culture medium reached 50 – 60 % confluency. The transfection mix in Opti-MEM was then added to 2 mL high serum medium per well of a 6 well plate. This medium was subsequently replaced with fresh high serum medium 24 h after transfection, and then replaced with low serum medium 3-4 h later to trigger differentiation. Silencer select negative control siRNA (cat. no. 4390843, ThermoFisher scientific) was used as a non-targeting negative control siRNA at a final concentration corresponding to that of the highest target siRNA concentration employed. All siRNAs and sources are provided in **Table S2**.

Immunofluorescence

C2C12 cells were seeded on coverslips with a thickness of 0.17 mm in 6-well plates (cat. no. 10062-892, Avantor) at 200,000 cells/ well. They were transfected subsequently with the indicated GFP2-tagged constructs and cultured for 48 h in high serum medium. Where PKG2-modulator treatments were required, these compounds/ reagents were diluted in high serum (final concentrations provided in the respective figure legends), added to cells 24 h after transfection and incubated for a period of 48 h. Cells were then fixed with 4 % (w/v) paraformaldehyde in PBS and permeabilized with 0.5 % Triton X-100 for 10 min. Then, cells were washed with 0.05 % Tween 20 in PBS (PBST) and incubated 30 min with 2 % BSA in PBST. Specific antigen labelling was done for 1 h using primary antibodies. Cells were subsequently washed 3 × 5 min with PBST, followed by 1 h incubation with secondary antibodies or with Phalloidin-Alexa Fluor 647. After washing 5 min with PBST, nuclei were counterstained with 0.2 µg/ mL Hoechst 33342 in PBST and washed again with PBST. A drop of Vectashield mounting medium (cat. no. H-1000-10, Vector Laboratories) was added on glass slides and the coverslips were mounted on them.

Confocal imaging

Fixed cells on coverslips were imaged using a 60 × NA 1.3 oil immersion objective on a Nikon Ti-E microscope equipped with a Yokogawa CSU-W1 spinning disk confocal unit and an Andor iXon Ultra EMCCD camera. GFP2 was visualized by excitation with a 488 nm laser line and detected using EGFP emission settings (535/20 band pass filter). Excitation of Alexa Fluor 594 and Alexa Fluor 647 was with 561 nm and 640 nm laser lines, respectively. Alexa Fluor 594 was visualized with the 560/40 band pass filter and Alexa Fluor 647 was visualized with the 700/35 band pass filter. Z stacks were acquired with 0.3 µm spacing between each optical section. Images were acquired with Nikon NIS-elements software and analyzed in Fiji/ ImageJ (Schindelin *et al*, 2012). To quantify relative abundance of Ras on the cilium, 3D orthogonal views were obtained for each image using Fiji. The intensity of GFP2-Ras-constructs was measured on the primary cilium (PC) in the orthogonal stacks, as the mean fluorescence intensity of a region of interest around the cilium identified by Arl13B labelling. The intensity of Ras at the plasma membrane (PM) was the average signal of a region of interest around the entire PM. Subsequently the relative ciliary localization PC/PM-ratio was calculated by dividing the two averaged signals.

STED imaging

To visualize K-Ras with STED microscopy, C2C12 cells expressing GFP2-K-Ras were fixed with 4 % (w/v) paraformaldehyde and immunolabelled with ChromoTek GFP-booster ATTO647N (GFP-booster) (cat. no. gba647n, Proteintech; dilution 1:200). To visualize primary cilia, cells were immunolabelled with primary antibody against Arl13B (177-11-1AP, Proteintech; dilution 1:500) and goat anti-Rb Alexa Fluor 594 secondary antibody (cat. no. A-11012, ThermoFisher Scientific; dilution 1:200). Samples were mounted on glass slides with Vectashield mounting medium.

The STED imaging was performed using the Abberior Infinity Line microscope (Abberior GmbH, Göttingen, Germany) equipped with Imspector software version 16.3.16118-w2224 and an Olympus 60 × oil objective (1.42 NA). To obtain two-color STED images, the fixed cell samples labelled with ATTO647N, and Alexa Fluor 594 dyes were excited with 640 nm and 561 nm picosecond pulsed laser diodes at 40 MHz (Abberior GmbH, Göttingen, Germany), respectively. STED imaging was conducted using the 775 nm pulsed STED laser (NKT Photonics Switzerland GmbH, Regensdorf, Switzerland) at 40 MHz to capture the desired STED images for both fluorophores. Emitted light was detected by using an avalanche photodiode detector (Excelitas Technologies Corp., USA) with 5 µs dwell time and line averaging of 10. To avoid crosstalk between the two channels, the samples were initially excited exclusively with the 640 nm laser at 16.7 µW power, while the 775 nm STED laser at 177.6 mW power was used to acquire STED images of ATTO 647N-labelled samples. After a brief interval of 1-2 min, the second channel was activated, employing the 561 nm laser at 3.42 µW power and the 775 nm STED laser at 365.9 mW power, to obtain STED images of Alexa Fluor 594-labelled samples. In this study, the detection range for ATTO 647N was set from 650 nm to 754 nm, while for Alexa Fluor 594, the detection range was set from 584 nm to 713 nm. These ranges were chosen to ensure optimal detection of fluorescence signals emitted by the respective dyes. Images were exported at 16-bit in the Abberior .MSR format. Following data acquisition, Huygens professional software version 23.4 was employed for STED image deconvolution. The imaging parameters for each image were predefined. Subsequently, the Huygens Deconvolution Wizard was utilized, offering the option to use either the measured or theoretical point spread function (PSF). The theoretical PSF, based on predefined imaging parameters, was generated within the Huygens software. Additionally, the software automatically estimated the background and signal-to-noise ratio for each image, facilitating their utilization in the Classic Maximum Likelihood Estimation algorithm for generating deconvolved images.

Flow cytometry-based C2C12 cell differentiation assay

The differentiation assay was performed on a flow cytometer Guava easyCyte HT-2L flow cytometer (Cytek Biosciences) as described by us recently (Parisi *et al.*, 2023). In brief, C2C12 cells were seeded at a density of 200,000 cells/ well in 6 well plates and treated as indicated in the figure legends. Low serum medium with drugs was replaced every day for three days. Cells were then harvested by trypsinization for 5 min and pelleted by centrifugation at 500 × g for 5 min. The cell pellet was fixed with 4 % (w/v) formaldehyde in PBS for 10 min. After washing with PBS, cells were permeabilized with 0.5 % Triton X-100 in PBS for 10 min. Subsequently cells were washed with PBST and immunolabelled with eFluor

660-conjugated anti-myosin 4 (myosin heavy chain/MyHC) antibody (cat no. 50-6503-82, ThermoFisher scientific), diluted 1:100 in PBST for 1 h at 4 °C. Cells were pelleted by centrifugation at 500 × g for 5 min and resuspended in PBST for flow cytometric analysis. Gates and detection channel settings were set up using non-labelled, EGFP-only expressing and MyHC-positive cells. Intact cells were analyzed for the expression of EGFP in the GFP-low bin (up to 10x above background fluorescence) and MyHC. EGFP-variants were detected by 488 nm excitation and the Grn-B (525/30) band pass filter. MyHC was immunolabelled using an eFluor 600-conjugated antibody and detected using 640 nm excitation and the Red-R (664/20) band pass emission filter. Differentiation was quantified as the percentage of MyHC-positive cells in the GFP-low bin. Quantification was here performed manually, using the GuavaSoft 4.0 software (Cytek Biosciences).

BRET assay

BRET assays were performed following our previously described protocol (Babu Manoharan *et al.*, 2023; Okutachi *et al.*, 2021) Briefly, 200,000 HEK293 EBNA cells were plated and maintained for at least 72 h in high serum medium in 12 well cell culture plates (cat. no. 665180, Greiner bio-one, Merck KGaA). 24 h after seeding, a donor construct tagged with RLuc8, and an acceptor construct tagged with GFP2 (listed in **Table S1**) were transfected into cells using 3 µL of jetPRIME transfection reagent (cat. no. 55-134, Polyplus).

BRET-titration experiments for donor saturation were performed by transfecting a constant concentration of donor plasmid (50 ng) and an increasing concentration of acceptor plasmid (from 0 to 1,000 ng). An identical total DNA load of 1,050 ng per well was achieved by adding empty pcDNA3.1 plasmid. Cells were cultured for 48 h in high serum culture medium and prepared for BRET assay.

After determination of the optimal acceptor to donor plasmid ratio from the titration experiments which is indicated in the respective figure legends, dose-response experiments were performed. 24 h after transfection, medium was exchanged with fresh medium containing increasing compound concentrations. Concentration ranges were for sildenafil 200 nM to 100 µM; for 8-Br-cGMP 10 µM to 1000 µM. DMSO at 0.1 % (v/v) was the vehicle control. After another 24 h incubation the cells were harvested and prepared for the BRET assay.

To study the effect of siRNA-mediated knockdown, HEK cells were transfected after 24 h with 75 nM PKG2 siRNA using 3.5 µLof Lipofectamine RNAiMAX (cat. no. 13778, Thermo Fisher Scientific) and Opti-MEM (cat. no. 31986062, Gibco, Thermo Fisher Scientific). After another 24 h, medium was exchanged with fresh medium and cells were transfected with RLuc8- and GFP2-tagged plasmids as described for the BRET-titration experiments. After incubation for 48 h, the cells were harvested and prepared for the BRET assay.

A CLARIOstar plate reader was used to perform BRET-measurements at 25 °C as described before (Babu Manoharan *et al.*, 2023; Okutachi *et al.*, 2021). Four technical replicates were measured for each experimental condition using channels that are specific for the luminophores (GFP2-acceptor signal RFU at λex = 405 ± 10 nm and at λem = 515 ± 10 nm; after addition of 10 µM coelenterazine 400a (cat. no. C-320, Gold Biotechnology) simultaneous recording of RLuc8-signals for donor signal RLU λem = 410 ± 40 nm and for the BRET-signal at λ = 515 ± 15 nm was performed). The calculation of the BRET ratio was done as previously described (Babu Manoharan *et al.*, 2023; Okutachi *et al.*, 2021).

For BRET donor saturation titration experiments the acceptor to donor ratio was calculated, which corresponds to the ratio between RFU and RLU and represents relative expression. This ratio was then normalized to a control value where 50 ng each of the acceptor and donor

plasmids were transfected. Acceptor/donor ratios obtained in this manner were plotted against the BRET ratio.
All data typically obtained from three biological repeats were plotted at once using nonlinear regression models and were fitted into one phase association equation of Prism 9 (GraphPad). The Y_{MAX} value, which represents the top asymptote on the Y-axis, was taken as characteristic $BRET_{top}$ value, which represents the maximal BRET ratio reached within the defined [Acceptor]/[Donor] ratio range. For dose-response experiments, the logarithm of the inhibitor concentration was plotted against the BRET ratio and the data were fitted by a log (inhibitor) vs. response variable slope (four parameters) equation of Prism which also provided the IC_{50} values.

Immunoblotting
For transient transfection, 500,000 HEK293 EBNA cells were plated in 2 mL complete DMEM per well of 6 well plates. After 24 h, cells were transfected with 2 µg of each plasmid DNA using a volume of 7.5 µL for single transfections and of 12 µL lipofectamine 2000 (cat. no. 11668019, Thermo Fisher Scientific) for double transfections in Opti-MEM medium (cat. no. 31985062, Gibco).
24 h after transfection, in situ cell lysis was performed in ice-cold lysis buffer (50 mM Tris-HCl pH 7.5, 150 mM NaCl, 0.1 % v/v SDS, 5 mM EDTA, 1 % v/v Nonidet P-40, 1 % v/v Triton X-100, 1 % v/v sodium-deoxycholate, 1 mM Na_3VO_4, 10 mM NaF, 100 µM leupeptin and 100 µM E64D protease inhibitor) containing cocktails of protease inhibitors (cat. no. A32955, Pierce) and of phosphatase inhibitors (PhosSTOP, cat. no. 4906845001, Roche Diagnostics GmbH). The lysates were clarified by centrifugation and a Bradford assay using the Quick Start Bradford 1x Dye reagent (cat. no. 5000205, Bio-Rad) was performed to determine the total protein concentration. Bovine serum albumin (cat. no. 23209, Thermo Fisher Scientific) was used to establish a standard curve.
Proteins (40 µg per lane) were resolved by SDS-PAGE in 10 % v/v polyacrylamide gels under reducing conditions and transferred by semi-dry transfer onto nitrocellulose membranes (cat. no. 1704272, Bio-Rad). Following saturation in PBS with 2 % w/v BSA (cat. no. A6588, AppliChem GmbH) and 0.2 % Tween for 1 h at room temperature, membranes were incubated with primary antibodies overnight at 4 °C. For phospho-ERK quantification, a combination of mouse anti-phospho-ERK and rabbit anti-ERK was used. mCherry-tagged PDE6D was revealed with a mouse anti-PDE6D and GFP2-tagged K-Ras with a rabbit anti-GFP antibody. Actin staining using a mouse anti-actin antibody was performed as a loading control. Incubation with corresponding secondary antibodies was carried out for 1 h at room temperature. At least three wash steps in PBS supplemented with 0.2 % v/v Tween 20 were performed after each antibody incubation. An Odyssey Infrared Image System (LI-COR Biosciences) was used to quantify signal intensities. First, the ratio between the intensities obtained for phospho-ERK versus total ERK was calculated for each experimental condition. Then, normalization to the sum of all the ratios obtained for one blot was done to make blots comparable by taking into account technical day-to-day variability. Finally, data were expressed relative to the control condition present on each blot and represented as the mean ± SEM of at least N = 3 independent biological repeats.

Cell cycle analysis with propidium iodide
Reagents from the propidium iodide flow cytometry kit (cat. no. ab139418, Abcam) were used to perform this assay, according to the manufacturer's instructions. Briefly, C2C12 cells were seeded at a density of 200,000 cells/mL in 6 well plates and transfected with the desired

EGFP-tagged constructs. Upon further 48 h culture in high serum medium, cells were collected by trypsinization in 1.5 mL Eppendorf tubes. After centrifugation at 500 *g* for 5 min, the pellet was washed with PBS, and subsequently fixed with ice-cold 70 % ethanol for 1 h at 4 °C. After another washing step with PBS, 200 μL PI solution (prepared according to the manufacturer's instructions) was added to each tube containing cells and incubated in the dark at 37 °C. Excitation for both EGFP and propidium iodide was achieved with the 488 nm laser line. EGFP and PI fluorescence was detected using the Grn-B (525/30) band pass filter and the Red-B (661/15) band pass filter respectively. Cells expressing EGFP-tagged constructs in the GFP-low bin (see differentiation analysis) only were considered for analysis. PI fluorescence was visualized as a histogram using the Red-B channel in linear scale and the fraction representing proliferating cells was determined as described previously and plotted as % proliferating cells (Shen *et al*, 2017).

Statistical analysis

If not stated otherwise means and standard deviations (SD) are plotted. Data were analyzed using Graph Pad prism 9.0 software. The number of independent biological repeats (N) and datapoints (n) for each data set is provided in the figure legends.

Imaging data are representative of phenotypes observed in N ≥ 3 independent biological repeats.

Statistical tests are specified in the figure legends. A p-value of < 0.05 was considered statistically significant and the statistical significance levels were annotated as: * = $P < 0.05$; ** = $P < 0.01$; *** = $P < 0.001$; **** = $P < 0.0001$, or ns = not significant.

References

Anderson CT, Stearns T (2009) Centriole age underlies asynchronous primary cilium growth in mammalian cells. *Curr Biol* 19: 1498-1502

Babu Manoharan G, Guzman C, Najumudeen AK, Abankwa D (2023) Detection of Ras nanoclustering-dependent homo-FRET using fluorescence anisotropy measurements. *Eur J Cell Biol* 102: 151314

Barretina J, Caponigro G, Stransky N, Venkatesan K, Margolin AA, Kim S, Wilson CJ, Lehar J, Kryukov GV, Sonkin D *et al* (2012) The Cancer Cell Line Encyclopedia enables predictive modelling of anticancer drug sensitivity. *Nature* 483: 603-607

Castel P, Rauen KA, McCormick F (2020) The duality of human oncoproteins: drivers of cancer and congenital disorders. *Nat Rev Cancer* 20: 383-397

Chandra A, Grecco HE, Pisupati V, Perera D, Cassidy L, Skoulidis F, Ismail SA, Hedberg C, Hanzal-Bayer M, Venkitaraman AR *et al* (2011) The GDI-like solubilizing factor PDEdelta sustains the spatial organization and signalling of Ras family proteins. *Nat Cell Biol* 14: 148-158

Chen C, Yamashita YM (2021) Centrosome-centric view of asymmetric stem cell division. *Open Biol* 11: 200314

Chippalkatti R, Abankwa D (2021) Promotion of cancer cell stemness by Ras. *Biochem Soc Trans* 49: 467-476

Cho KJ, Casteel DE, Prakash P, Tan L, van der Hoeven D, Salim AA, Kim C, Capon RJ, Lacey E, Cunha SR *et al* (2016) AMPK and Endothelial Nitric Oxide Synthase Signaling Regulates K-Ras Plasma Membrane Interactions via Cyclic GMP-Dependent Protein Kinase 2. *Mol Cell Biol* 36: 3086-3099

Cicalese A, Bonizzi G, Pasi CE, Faretta M, Ronzoni S, Giulini B, Brisken C, Minucci S, Di Fiore PP, Pelicci PG (2009) The tumor suppressor p53 regulates polarity of self-renewing divisions in mammary stem cells. *Cell* 138: 1083-1095

Crespo P, Leon J (2000) Ras proteins in the control of the cell cycle and cell differentiation. *Cell Mol Life Sci* 57: 1613-1636

Dharmaiah S, Bindu L, Tran TH, Gillette WK, Frank PH, Ghirlando R, Nissley DV, Esposito D, McCormick F, Stephen AG *et al* (2016) Structural basis of recognition of farnesylated and methylated KRAS4b by PDEdelta. *Proc Natl Acad Sci U S A* 113: E6766-E6775

Fansa EK, Kosling SK, Zent E, Wittinghofer A, Ismail S (2016) PDE6delta-mediated sorting of INPP5E into the cilium is determined by cargo-carrier affinity. *Nat Commun* 7: 11366

Fansa EK, Wittinghofer A (2016) Sorting of lipidated cargo by the Arl2/Arl3 system. *Small GTPases* 7: 222-230

Garcia-Gonzalo FR, Reiter JF (2017) Open Sesame: How Transition Fibers and the Transition Zone Control Ciliary Composition. *Cold Spring Harb Perspect Biol* 9

Gotthardt K, Lokaj M, Koerner C, Falk N, Giessl A, Wittinghofer A (2015) A G-protein activation cascade from Arl13B to Arl3 and implications for ciliary targeting of lipidated proteins. *Elife* 4

Grant BMM, Enomoto M, Ikura M, Marshall CB (2020) A Non-Canonical Calmodulin Target Motif Comprising a Polybasic Region and Lipidated Terminal Residue Regulates Localization. *Int J Mol Sci* 21

Harding A, Giles N, Burgess A, Hancock JF, Gabrielli BG (2003) Mechanism of mitosis-specific activation of MEK1. *J Biol Chem* 278: 16747-16754

Higgins M, Obaidi I, McMorrow T (2019) Primary cilia and their role in cancer. *Oncol Lett* 17: 3041-3047

Hobbs GA, Der CJ, Rossman KL (2016) RAS isoforms and mutations in cancer at a glance. *J Cell Sci* 129: 1287-1292

Ismail SA, Chen YX, Rusinova A, Chandra A, Bierbaum M, Gremer L, Triola G, Waldmann H, Bastiaens PI, Wittinghofer A (2011) Arl2-GTP and Arl3-GTP regulate a GDI-like transport system for farnesylated cargo. *Nat Chem Biol* 7: 942-949

Lai Y, Jiang Y (2020) Reciprocal Regulation between Primary Cilia and mTORC1. *Genes (Basel)* 11

Lee JE, Gleeson JG (2011) A systems-biology approach to understanding the ciliopathy disorders. *Genome Med* 3: 59

Li CJ, Heim R, Lu P, Pu Y, Tsien RY, Chang DC (1999) Dynamic redistribution of calmodulin in HeLa cells during cell division as revealed by a GFP-calmodulin fusion protein technique. *J Cell Sci* 112 (Pt 10): 1567-1577

Martin-Gago P, Fansa EK, Klein CH, Murarka S, Janning P, Schurmann M, Metz M, Ismail S, Schultz-Fademrecht C, Baumann M *et al* (2017) A PDE6delta-KRas Inhibitor Chemotype with up to Seven H-Bonds and Picomolar Affinity that Prevents Efficient Inhibitor Release by Arl2. *Angew Chem Int Ed Engl* 56: 2423-2428

Matallanas D, Romano D, Al-Mulla F, O'Neill E, Al-Ali W, Crespo P, Doyle B, Nixon C, Sansom O, Drosten M *et al* (2011) Mutant K-Ras activation of the proapoptotic MST2 pathway is antagonized by wild-type K-Ras. *Mol Cell* 44: 893-906

McDonald ER, 3rd, de Weck A, Schlabach MR, Billy E, Mavrakis KJ, Hoffman GR, Belur D, Castelletti D, Frias E, Gampa K *et al* (2017) Project DRIVE: A Compendium of Cancer Dependencies and Synthetic Lethal Relationships Uncovered by Large-Scale, Deep RNAi Screening. *Cell* 170: 577-592 e510

Morrison SJ, Kimble J (2006) Asymmetric and symmetric stem-cell divisions in development and cancer. *Nature* 441: 1068-1074

Murarka S, Martin-Gago P, Schultz-Fademrecht C, Al Saabi A, Baumann M, Fansa EK, Ismail S, Nussbaumer P, Wittinghofer A, Waldmann H (2017) Development of Pyridazinone Chemotypes Targeting the PDEdelta Prenyl Binding Site. *Chemistry* 23: 6083-6093

Nobutani K, Shimono Y, Yoshida M, Mizutani K, Minami A, Kono S, Mukohara T, Yamasaki T, Itoh T, Takao S *et al* (2014) Absence of primary cilia in cell cycle-arrested human breast cancer cells. *Genes Cells* 19: 141-152

Okutachi S, Manoharan GB, Kiriazis A, Laurini C, Catillon M, McCormick F, Yli-Kauhaluoma J, Abankwa D (2021) A Covalent Calmodulin Inhibitor as a Tool to Study Cellular Mechanisms of K-Ras-Driven Stemness. *Front Cell Dev Biol* 9: 665673

Papke B, Murarka S, Vogel HA, Martin-Gago P, Kovacevic M, Truxius DC, Fansa EK, Ismail S, Zimmermann G, Heinelt K *et al* (2016) Identification of pyrazolopyridazinones as PDEdelta inhibitors. *Nat Commun* 7: 11360

Paridaen JTML, Wilsch-Bräuninger M, Huttner WB (2013) Asymmetric Inheritance of Centrosome- Associated Primary Cilium Membrane Directs Ciliogenesis after Cell Division. *Cell* 155: 333-344

Pavic K, Chippalkatti R, Abankwa D (2022) Drug targeting opportunities en route to Ras nanoclusters. *Adv Cancer Res* 153: 63-99

Quinlan MP, Quatela SE, Philips MR, Settleman J (2008) Activated Kras, but not Hras or Nras, may initiate tumors of endodermal origin via stem cell expansion. *Mol Cell Biol* 28: 2659-2674

Rauen KA (2013) The RASopathies. *Annu Rev Genomics Hum Genet* 14: 355-369

Schindelin J, Arganda-Carreras I, Frise E, Kaynig V, Longair M, Pietzsch T, Preibisch S, Rueden C, Saalfeld S, Schmid B *et al* (2012) Fiji: an open-source platform for biological-image analysis. *Nat Methods* 9: 676-682

Schmick M, Vartak N, Papke B, Kovacevic M, Truxius DC, Rossmannek L, Bastiaens PIH (2014) KRas localizes to the plasma membrane by spatial cycles of solubilization, trapping and vesicular transport. *Cell* 157: 459-471

Shen Y, Vignali P, Wang R (2017) Rapid Profiling Cell Cycle by Flow Cytometry Using Concurrent Staining of DNA and Mitotic Markers. *Bio Protoc* 7

Siddiqui FA, Alam C, Rosenqvist P, Ora M, Sabt A, Manoharan GB, Bindu L, Okutachi S, Catillon M, Taylor T *et al* (2020) PDE6D Inhibitors with a New Design Principle Selectively Block K-Ras Activity. *ACS Omega* 5: 832-842

Tobin JL, Beales PL (2009) The nonmotile ciliopathies. *Genet Med* 11: 386-402

Tomasetti C, Vogelstein B (2015) Cancer etiology. Variation in cancer risk among tissues can be explained by the number of stem cell divisions. *Science* 347: 78-81

Torii S, Yamamoto T, Tsuchiya Y, Nishida E (2006) ERK MAP kinase in G cell cycle progression and cancer. *Cancer Sci* 97: 697-702

Tsherniak A, Vazquez F, Montgomery PG, Weir BA, Kryukov G, Cowley GS, Gill S, Harrington WF, Pantel S, Krill-Burger JM *et al* (2017) Defining a Cancer Dependency Map. *Cell* 170: 564-576 e516

Wakioka T, Sasaki A, Kato R, Shouda T, Matsumoto A, Miyoshi K, Tsuneoka M, Komiya S, Baron R, Yoshimura A (2001) Spred is a Sprouty-related suppressor of Ras signalling. *Nature* 412: 647-651

Wang MT, Holderfield M, Galeas J, Delrosario R, To MD, Balmain A, McCormick F (2015) K-Ras Promotes Tumorigenicity through Suppression of Non-canonical Wnt Signaling. *Cell* 163: 1237-1251

White MC, Holman DM, Boehm JE, Peipins LA, Grossman M, Henley SJ (2014) Age and cancer risk: a potentially modifiable relationship. *Am J Prev Med* 46: S7-15

Wilsch-Brauninger M, Huttner WB (2021) Primary Cilia and Centrosomes in Neocortex Development. *Front Neurosci* 15: 755867

Yelland T, Garcia E, Parry C, Kowalczyk D, Wojnowska M, Gohlke A, Zalar M, Cameron K, Goodwin G, Yu Q *et al* (2022) Stabilization of the RAS:PDE6D Complex Is a Novel Strategy to Inhibit RAS Signaling. *J Med Chem* 65: 1898-1914

Yu YY, Chen Y, Dai G, Chen J, Sun XM, Wen CJ, Zhao DH, Chang DC, Li CJ (2004) The association of calmodulin with central spindle regulates the initiation of cytokinesis in HeLa cells. *Int J Biochem Cell Biol* 36: 1562-1572

Zambetti NA, Firestone AJ, Remsberg JR, Huang BJ, Wong JC, Long AM, Predovic M, Suciu RM, Inguva A, Kogan SC *et al* (2020) Genetic disruption of N-RasG12D palmitoylation perturbs hematopoiesis and prevents myeloid transformation in mice. *Blood* 135: 1772-1782

Zimmermann G, Papke B, Ismail S, Vartak N, Chandra A, Hoffmann M, Hahn SA, Triola G, Wittinghofer A, Bastiaens PI *et al* (2013) Small molecule inhibition of the KRAS-PDEdelta interaction impairs oncogenic KRAS signalling. *Nature* 497: 638-642

Supplementary Information

Supplementary Tables

Table S1. List of plasmids used in this study

pDest305-CMV-GFP2-Kras4B-WT
pDest305-CMV-mEGFP-Kras4B-WT
pDest305-CMV-GFP2-Hras-WT
pDest305-CMV-mEGFP-Hras-WT
pDest305-CMV-GFP2-Nras-WT
mGFP-C3-HA-Nras-WT
pDest305-CMV-GFP2-Kras4B-S181A
pDest305-CMV-GFP2-Kras4B-S181D
pDest305-CMV-GFP2-B-Raf
pDest305-CMV-GFP2-Kras4B-SI
pDest305-CMV-GFP2-Kras4B G12C
pDest305-CMV-EGFP-Kras4B G12C
pDest305-CMV-GFP2-Kras4B G12C-SI
pDest305-CMV-EGFP-Kras4B G12C-SI
pDest305-CMV-EGFP-Kras4B G12D
pDest305-CMV-EGFP-Kras4B G12D-SI
pEGFP-N1
pDest305-CMV-GFP2-Kras4B G12C-Rit1
pDest305-CMV-EGFP-Kras4B G12C-Rit1
pDest305-CMV-GFP2-Myr(Src)-K-Ras4B G12C
pDest305-CMV-GFP2-Myr(NPHP)-K-Ras4B G12C
pmCherry-PDE6D (Siddiqui *et al.*, 2020a)
pDest312-CMV-UNC119B-RLuc8

Table S2. List of siRNAs used in this study

Target	**sequence**	**source**	**Cat. no.**
PDE6D (mouse) smart pool of 4 siRNAs	5’UCUCAUACCUUUAACUUGU3’, 5’CGCCUGAGUCCCAGAUGAU3’, 5’CAAAGGACAAUGCCUAGAA3’, 5’GCGCAAACAUGGGAACAAA 3’	Horizon Discovery	L-062279-01-0005
PRKG2 (mouse) custom siRNA	5’CUGCUUGGAAGUGGAAUACUA 3’	Horizon Discovery	CTM-739126

Supplementary Figures

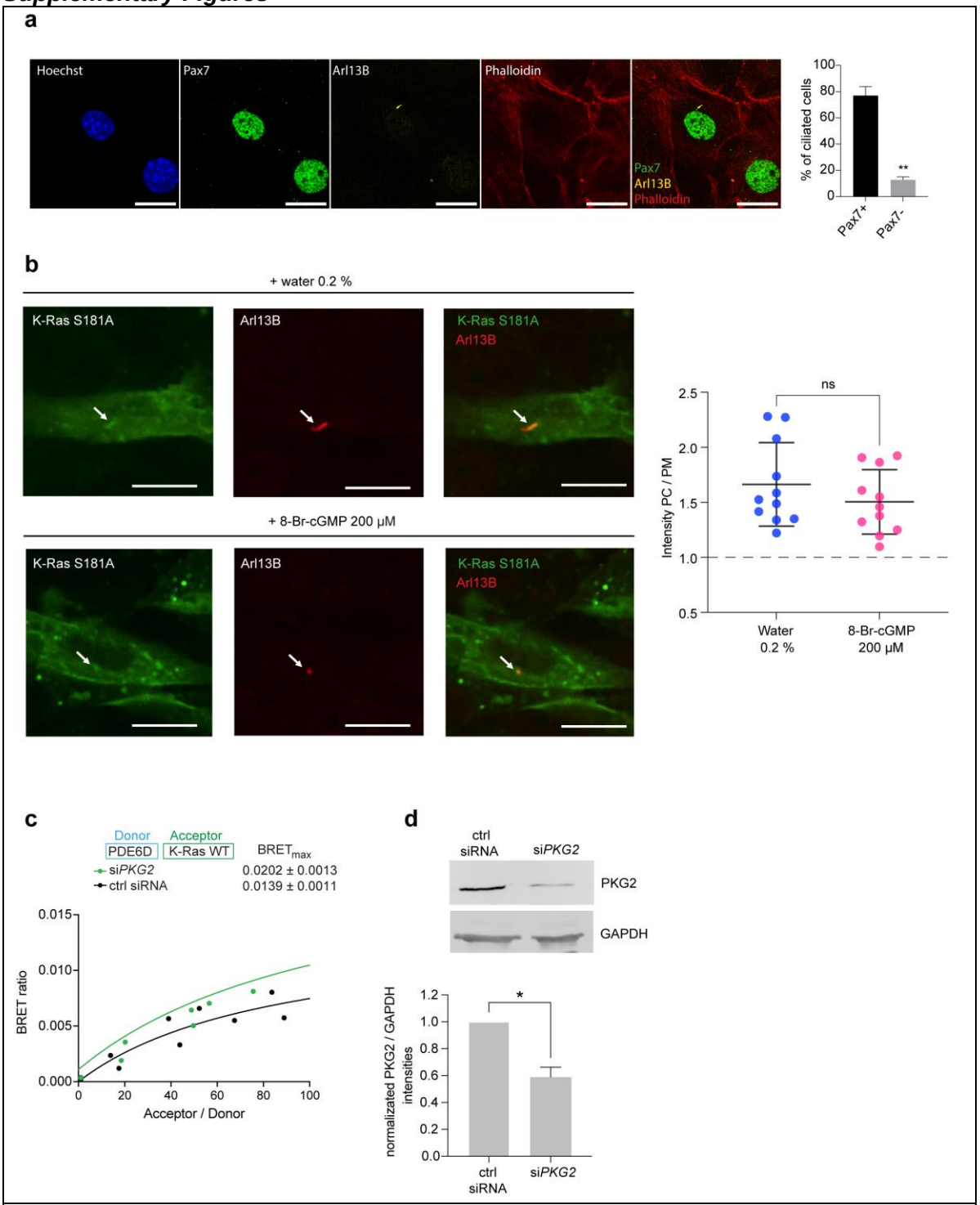

Figure S1

(**a**) C2C12 cells immunolabelled with antibodies against Pax7 (green) and Arl13B (yellow). Actin is visualized with Phalloidin-Alexa Fluor 647 (red) and nuclei are counterstained with Hoechst 33342 (blue). Scale bar = 10 µm. Quantification for the occurrence of cilia in Pax7+ (n = 220) and Pax7- cells (n = 310) is presented on the right. N = 3 independent biological repeats. Statistical analysis was done with Student's t-test.

(**b**) Representative confocal images of C2C12 cells grown under high serum and expressing GFP2-K-Ras S181A. Cells were treated with 8-Br-cGMP for 2 days in high serum. Data on the right were quantified for relative ciliary (PC) localization of K-Ras mutants as compared to the plasma

membrane (PM). Individual data points (n = 11 per condition) from N = 1 biological repeat. Statistical analysis was done with the Mann-Whitney test. Scale bar = 10 µm.
(**c**) BRET-titration curves of RLuc8-PDE6D and GFP2-K-Ras expressed in HEK293 cells, treated with the indicated siRNAs at 75 nM, 24 h after transfection with GFP2/ RLuc8-tagged constructs. Analyzed 48 h after siRNA transfection; N = 3.
(**d**) Knockdown of PKG2 protein upon treatment with PKG2 siRNA (75 nM) in HEK293 cells was evaluated by immunoblotting.

4. Conclusions And Perspectives

One of the most highly sought-after targets for cancer drug therapy is K-Ras. In our concise review, we aim to assess the strategies employed to directly target different druggable regions of Ras. We analyzed the insights and challenges gained from the development of allele-specific covalent and non-covalent inhibitors for Ras, the potential role of macromolecular binders and small molecule binders as potential drug candidates.

To overcome challenges associated with directly targeting K-Ras, researchers have proposed the use of PDE6D, a trafficking chaperone protein, as a surrogate target. This approach has led to the development of inhibitors that specifically block the prenyl-binding pocket of PDE6D. Nevertheless, the efficacy of these inhibitors has been hindered by challenges relating to their solubility and effectiveness in inhibiting intracellular pathways. Consequently, it has not been possible to evaluate them in vivo.

In this thesis, we are describing a new and potent PDE6D inhibitor called Deltaflexin3, which demonstrates the highest selectivity for K-Ras and the least off-target effects of any previously known inhibitors. Furthermore, we have utilized the mutual reliance of K-Ras on its farnesyl-tail and an unphosphorylated Ser181 for binding to PDE6D. By doing so, we have established a synergistic combination strategy involving Deltaflexin3 and the approved PKG2-activating drug sildenafil. This combination demonstrates potent inhibition of downstream Ras-signaling pathways as well as suppression of cancer cell growth in both 2D cell-based assays and ex vivo microtumor models. However, patients belonging to the KRAS-mutated target group, which are expected to show greater sensitivity towards this combined treatment approach, exhibit higher survival rates compared to individuals from the opposite group characterized by low levels of PDE6D expression but high PRKG2-expression.

The possibility of alternative transport to both the plasma membrane and PC/centrosomes was explored by analyzing myristoylated constructs to examine how the localization patterns of these different variants influence MAPK signaling and cell differentiation. Specifically, we expect higher levels of pERK when the variants are localized on the plasma membrane. As expected, in contrast Src constructs, with the NPHP3 constructs, there was a decrease in overall pERK signal. This is because the K-Ras chimeric proteins expressed from these constructs are primarily transported to primary cilium and centrosomes rather than the plasma membrane.

- The utilization of PROTAC degraders for targeting RAS provides a promising opportunity to inhibit RAS may provide a more controlled drug action and reducing on-target toxicity. Nevertheless, further evaluation is necessary in clinical settings to determine its viability and effectiveness.

- One challenge associated with targeting PDE6D as a potential therapeutic agent is its wide range of cargo molecules. Only a portion of the K-Ras protein, which is transported to the plasma membrane, relies on PDE6D for this process. Consequently, inhibiting PDE6D would not solely impact K-Ras and its association with KRAS-mutant cancer cells but also influence numerous other cargos regulated by PDE6D.

  In light of these findings, it may be worthwhile to consider exploring the developmental role played by PDE6D to gain further insights into its functional significance.

- Our examination of the survival rates for patients exhibiting this specific gene expression pattern, as observed in KRAS-mutant cancers within the PanCanAtlas dataset, reveals that those with this low PDE6D/high PRKG2 pattern have a considerably improved overall survival. Therefore, caution should be exercised when considering drug-targeting strategies such as utilizing a combination therapy involving PDE6Di/Sildenafil for the treatment of patients expressing these genetic markers.

- The role of K-Ras in cancer cell differentiation is a significant discovery, especially considering the involvement of cancer stem cells in disease relapse. Unraveling the underlying mechanism can lead to the identification of new drug targets. Investigating the complex pathways involved in K-Ras trafficking towards centriolar organelles may provide valuable insights for this purpose.

5. REFERENCES

Abankwa D, Gorfe AA (2020) Mechanisms of Ras Membrane Organization and Signaling: Ras Rocks Again. *Biomolecules* 10

Abankwa D, Gorfe AA, Hancock JF (2008a) Mechanisms of Ras membrane organization and signalling: Ras on a rocker. *Cell Cycle* 7: 2667-2673

Abankwa D, Hanzal-Bayer M, Ariotti N, Plowman SJ, Gorfe AA, Parton RG, McCammon JA, Hancock JF (2008b) A novel switch region regulates H-ras membrane orientation and signal output. *EMBO J* 27: 727-735

Abdelkarim H, Banerjee A, Grudzien P, Leschinsky N, Abushaer M, Gaponenko V (2019) The Hypervariable Region of K-Ras4B Governs Molecular Recognition and Function. *Int J Mol Sci* 20

Abraham SJ, Nolet RP, Calvert RJ, Anderson LM, Gaponenko V (2009) The Hypervariable Region of K-Ras4B Is Responsible for Its Specific Interactions with Calmodulin. *Biochemistry* 48: 7575-7583

Agamasu C, Ghirlando R, Taylor T, Messing S, Tran TH, Bindu L, Tonelli M, Nissley DV, McCormick F, Stephen AG (2019) KRAS Prenylation Is Required for Bivalent Binding with Calmodulin in a Nucleotide-Independent Manner. *Biophys J* 116: 1049-1063

Ahearn I, Zhou M, Philips MR (2018) Posttranslational Modifications of RAS Proteins. *Cold Spring Harb Perspect Med* 8

Ahearn IM, Court HR, Siddiqui F, Abankwa D, Philips MR (2021) NRAS is unique among RAS proteins in requiring ICMT for trafficking to the plasma membrane. *Life Sci Alliance* 4

Ahearn IM, Haigis K, Bar-Sagi D, Philips MR (2011) Regulating the regulator: post-translational modification of RAS. *Nat Rev Mol Cell Biol* 13: 39-51

Ahearn IM, Haigis K, Bar-Sagi D, Philips MR (2012) Regulating the regulator: post-translational modification of RAS. *Nature Reviews Molecular Cell Biology* 13: 39-51

Alboukadel K, Marcin K, Przemyslaw B (2021) survminer: Drawing Survival Curves using 'ggplot2'.

Anderson CT, Stearns T (2009) Centriole age underlies asynchronous primary cilium growth in mammalian cells. *Curr Biol* 19: 1498-1502

Ashery U, Yizhar O, Rotblat B, Kloog Y (2006) Nonconventional trafficking of Ras associated with Ras signal organization. 7: 1119-1126

Awad MM, Liu S, Rybkin, II, Arbour KC, Dilly J, Zhu VW, Johnson ML, Heist RS, Patil T, Riely GJ *et al* (2021) Acquired Resistance to KRAS(G12C) Inhibition in Cancer. *N Engl J Med* 384: 2382-2393

Babu Manoharan G, Guzman C, Najumudeen AK, Abankwa D (2023) Detection of Ras nanoclustering-dependent homo-FRET using fluorescence anisotropy measurements. *Eur J Cell Biol* 102: 151314

Bandaru P, Kondo Y, Kuriyan J (2019) The Interdependent Activation of Son-of-Sevenless and Ras. *Cold Spring Harb Perspect Med* 9

Banworth MJ, Liang Z, Li G (2022) A novel membrane targeting domain mediates the endosomal or Golgi localization specificity of small GTPases Rab22 and Rab31. *J Biol Chem* 298: 102281

Bardia A, Gounder M, Rodon J, Janku F, Lolkema MP, Stephenson JJ, Bedard PL, Schuler M, Sessa C, LoRusso P *et al* (2020) Phase Ib Study of Combination Therapy with MEK Inhibitor Binimetinib and Phosphatidylinositol 3-Kinase Inhibitor Buparlisib in Patients with Advanced Solid Tumors with RAS/RAF Alterations. *Oncologist* 25: e160-e169

Barretina J, Caponigro G, Stransky N, Venkatesan K, Margolin AA, Kim S, Wilson CJ, Lehar J, Kryukov GV, Sonkin D *et al* (2012) The Cancer Cell Line Encyclopedia enables predictive modelling of anticancer drug sensitivity. *Nature* 483: 603-607

Bender AT, Beavo JA (2006) Cyclic nucleotide phosphodiesterases: molecular regulation to clinical use. *Pharmacol Rev* 58: 488-520

Bender RHF, Haigis KM, Gutmann DH (2015) Activated K-Ras, but Not H-Ras or N-Ras, Regulates Brain Neural Stem Cell Proliferation in a Raf/Rb-Dependent Manner. *STEM CELLS* 33: 1998-2010
Berg TJ, Gastonguay AJ, Lorimer EL, Kuhnmuench JR, Li R, Fields AP, Williams CL (2010) Splice variants of SmgGDS control small GTPase prenylation and membrane localization. *J Biol Chem* 285: 35255-35266
Bernal Astrain G, Nikolova M, Smith MJ (2022) Functional diversity in the RAS subfamily of small GTPases. *Biochem Soc Trans* 50: 921-933
Blazevits O, Mideksa YG, Solman M, Ligabue A, Ariotti N, Nakhaeizadeh H, Fansa EK, Papageorgiou AC, Wittinghofer A, Ahmadian MR *et al* (2016) Galectin-1 dimers can scaffold Raf-effectors to increase H-ras nanoclustering. *Sci Rep* 6: 24165
Blaževitš O, Mideksa YG, Šolman M, Ligabue A, Ariotti N, Nakhaeizadeh H, Fansa EK, Papageorgiou AC, Wittinghofer A, Ahmadian MR *et al* (2016) Galectin-1 dimers can scaffold Raf-effectors to increase H-ras nanoclustering. *Scientific Reports* 6: 24165
Bond MJ, Chu L, Nalawansha DA, Li K, Crews CM (2020) Targeted Degradation of Oncogenic KRASG12C by VHL-Recruiting PROTACs. *ACS Central Science* 6: 1367-1375
Broutin S, Stewart A, Thavasu P, Paci A, Bidart JM, Banerji U (2016) Insights into significance of combined inhibition of MEK and m-TOR signalling output in KRAS mutant non-small-cell lung cancer. *Br J Cancer* 115: 549-552
Burdon T, Stracey C, Chambers I, Nichols J, Smith A (1999) Suppression of SHP-2 and ERK Signalling Promotes Self-Renewal of Mouse Embryonic Stem Cells. *Developmental Biology* 210: 30-43
Canon J, Rex K, Saiki AY, Mohr C, Cooke K, Bagal D, Gaida K, Holt T, Knutson CG, Koppada N *et al* (2019) The clinical KRAS(G12C) inhibitor AMG 510 drives anti-tumour immunity. *Nature* 575: 217-223
Canovas Nunes S, De Vita S, Anighoro A, Autelitano F, Beaumont E, Klingbeil P, McGuinness M, Duvert B, Harris C, Yang L *et al* (2022) Validation of a small molecule inhibitor of PDE6D-RAS interaction with favorable anti-leukemic effects. *Blood Cancer J* 12: 64
Castel P, Rauen KA, McCormick F (2020) The duality of human oncoproteins: drivers of cancer and congenital disorders. *Nat Rev Cancer* 20: 383-397
Chandra A, Grecco HE, Pisupati V, Perera D, Cassidy L, Skoulidis F, Ismail SA, Hedberg C, Hanzal-Bayer M, Venkitaraman AR *et al* (2011) The GDI-like solubilizing factor PDEdelta sustains the spatial organization and signalling of Ras family proteins. *Nat Cell Biol* 14: 148-158
Chen C, Yamashita YM (2021) Centrosome-centric view of asymmetric stem cell division. *Open Biol* 11: 200314
Chen D, Chen Y, Lian F, Chen L, Li Y, Cao D, Wang X, Chen L, Li J, Meng T *et al* (2019) Fragment-based drug discovery of triazole inhibitors to block PDEdelta-RAS protein-protein interaction. *Eur J Med Chem* 163: 597-609
Chen K, Zhang Y, Qian L, Wang P (2021a) Emerging strategies to target RAS signaling in human cancer therapy. *J Hematol Oncol* 14: 116
Chen K, Zhang Y, Qian L, Wang P (2021b) Emerging strategies to target RAS signaling in human cancer therapy. *J Hematol Oncol* 14: 116
Chen L, Zhang J, Wang X, Li Y, Zhou L, Lu X, Dong G, Sheng C (2022) Discovery of novel KRAS–PDEdelta inhibitors with potent activity in patient-derived human pancreatic tumor xenograft models. *Acta Pharm Sin B* 12: 274-290
Chen L, Zhuang C, Lu J, Jiang Y, Sheng C (2018) Discovery of Novel KRAS-PDEdelta Inhibitors by Fragment-Based Drug Design. *J Med Chem* 61: 2604-2610
Chen YN, LaMarche MJ, Chan HM, Fekkes P, Garcia-Fortanet J, Acker MG, Antonakos B, Chen CH, Chen Z, Cooke VG *et al* (2016) Allosteric inhibition of SHP2 phosphatase inhibits cancers driven by receptor tyrosine kinases. *Nature* 535: 148-152
Cheng J, Li Y, Wang X, Dong G, Sheng C (2020) Discovery of Novel PDEdelta Degraders for the Treatment of KRAS Mutant Colorectal Cancer. *J Med Chem* 63: 7892-7905

Cherfils J, Zeghouf M (2013) Regulation of small GTPases by GEFs, GAPs, and GDIs. *Physiol Rev* 93: 269-309
Chippalkatti R, Abankwa D (2021) Promotion of cancer cell stemness by Ras. *Biochem Soc Trans* 49: 467-476
Chiu CF, Ho MY, Peng JM, Hung SW, Lee WH, Liang CM, Liang SM (2013) Raf activation by Ras and promotion of cellular metastasis require phosphorylation of prohibitin in the raft domain of the plasma membrane. *Oncogene* 32: 777-787
Cho KJ, Casteel DE, Prakash P, Tan L, van der Hoeven D, Salim AA, Kim C, Capon RJ, Lacey E, Cunha SR *et al* (2016) AMPK and Endothelial Nitric Oxide Synthase Signaling Regulates K-Ras Plasma Membrane Interactions via Cyclic GMP-Dependent Protein Kinase 2. *Mol Cell Biol* 36: 3086-3099
Cicalese A, Bonizzi G, Pasi CE, Faretta M, Ronzoni S, Giulini B, Brisken C, Minucci S, Di Fiore PP, Pelicci PG (2009) The tumor suppressor p53 regulates polarity of self-renewing divisions in mammary stem cells. *Cell* 138: 1083-1095
Citalan-Madrid AF, Garcia-Ponce A, Vargas-Robles H, Betanzos A, Schnoor M (2013) Small GTPases of the Ras superfamily regulate intestinal epithelial homeostasis and barrier function via common and unique mechanisms. *Tissue Barriers* 1: e26938
Colicelli J (2004) Human RAS superfamily proteins and related GTPases. *Sci STKE* 2004: RE13
Courtois-Cox S, Genther Williams SM, Reczek EE, Johnson BW, McGillicuddy LT, Johannessen CM, Hollstein PE, MacCollin M, Cichowski K (2006) A negative feedback signaling network underlies oncogene-induced senescence. *Cancer Cell* 10: 459-472
Cox AD, Der CJ, Philips MR (2015) Targeting RAS Membrane Association: Back to the Future for Anti-RAS Drug Discovery? *Clin Cancer Res* 21: 1819-1827
Cox AD, Fesik SW, Kimmelman AC, Luo J, Der CJ (2014) Drugging the undruggable RAS: Mission possible? *Nat Rev Drug Discov* 13: 828-851
Crespo P, Leon J (2000) Ras proteins in the control of the cell cycle and cell differentiation. *Cell Mol Life Sci* 57: 1613-1636
Crespo P, León J (2000) Ras proteins in the control of the cell cycle and cell differentiation. *Cellular and Molecular Life Sciences CMLS* 57: 1613-1636
Dance M, Montagner A, Salles JP, Yart A, Raynal P (2008) The molecular functions of Shp2 in the Ras/Mitogen-activated protein kinase (ERK1/2) pathway. *Cell Signal* 20: 453-459
David M, Petit D, Bertoglio J (2012) Cell cycle regulation of Rho signaling pathways. *Cell Cycle* 11: 3003-3010
Dewees SI, Vargova R, Hardin KR, Turn RE, Devi S, Linnert J, Wolfrum U, Caspary T, Elias M, Kahn RA (2022) Phylogenetic profiling and cellular analyses of ARL16 reveal roles in traffic of IFT140 and INPP5E. *Mol Biol Cell* 33: ar33
Dharmaiah S, Bindu L, Tran TH, Gillette WK, Frank PH, Ghirlando R, Nissley DV, Esposito D, McCormick F, Stephen AG *et al* (2016) Structural basis of recognition of farnesylated and methylated KRAS4b by PDEdelta. *Proc Natl Acad Sci U S A* 113: E6766-E6775
Dunnett-Kane V, Nicola P, Blackhall F, Lindsay C (2021) Mechanisms of Resistance to KRAS(G12C) Inhibitors. *Cancers (Basel)* 13
Ebnet K, Gerke V (2022) Rho and Rab Family Small GTPases in the Regulation of Membrane Polarity in Epithelial Cells. *Front Cell Dev Biol* 10: 948013
Emoto K, Masugi Y, Yamazaki K, Effendi K, Tsujikawa H, Tanabe M, Kitagawa Y, Sakamoto M (2014) Presence of primary cilia in cancer cells correlates with prognosis of pancreatic ductal adenocarcinoma. *Hum Pathol* 45: 817-825
Engelman JA, Chen L, Tan X, Crosby K, Guimaraes AR, Upadhyay R, Maira M, McNamara K, Perera SA, Song Y *et al* (2008) Effective use of PI3K and MEK inhibitors to treat mutant Kras G12D and PIK3CA H1047R murine lung cancers. *Nat Med* 14: 1351-1356
Fansa EK, Kosling SK, Zent E, Wittinghofer A, Ismail S (2016) PDE6delta-mediated sorting of INPP5E into the cilium is determined by cargo-carrier affinity. *Nat Commun* 7: 11366
Fansa EK, Wittinghofer A (2016) Sorting of lipidated cargo by the Arl2/Arl3 system. *Small GTPases* 7: 222-230

Fedele C, Ran H, Diskin B, Wei W, Jen J, Geer MJ, Araki K, Ozerdem U, Simeone DM, Miller G *et al* (2018) SHP2 Inhibition Prevents Adaptive Resistance to MEK Inhibitors in Multiple Cancer Models. *Cancer Discov* 8: 1237-1249
Fell JB, Fischer JP, Baer BR, Blake JF, Bouhana K, Briere DM, Brown KD, Burgess LE, Burns AC, Burkard MR *et al* (2020) Identification of the Clinical Development Candidate MRTX849, a Covalent KRAS(G12C) Inhibitor for the Treatment of Cancer. *J Med Chem* 63: 6679-6693
Feng H, Zhang Y, Bos PH, Chambers JM, Dupont MM, Stockwell BR (2019) K-RasG12D Has a Potential Allosteric Small Molecule Binding Site. *Biochemistry* 58: 2542-2554
Ferlay J, Colombet M, Soerjomataram I, Parkin DM, Pineros M, Znaor A, Bray F (2021) Cancer statistics for the year 2020: An overview. *Int J Cancer*
Flemington V, Davies EJ, Robinson D, Sandin LC, Delpuech O, Zhang P, Hanson L, Farrington P, Bell S, Falenta K *et al* (2021) AZD0364 Is a Potent and Selective ERK1/2 Inhibitor That Enhances Antitumor Activity in KRAS-Mutant Tumor Models when Combined with the MEK Inhibitor, Selumetinib. *Mol Cancer Ther* 20: 238-249
Friesner RA, Murphy RB, Repasky MP, Frye LL, Greenwood JR, Halgren TA, Sanschagrin PC, Mainz DT (2006) Extra precision glide: docking and scoring incorporating a model of hydrophobic enclosure for protein-ligand complexes. *J Med Chem* 49: 6177-6196
Garcia-Gonzalo FR, Reiter JF (2017) Open Sesame: How Transition Fibers and the Transition Zone Control Ciliary Composition. *Cold Spring Harb Perspect Biol* 9
Garivet G, Hofer W, Konitsiotis A, Klein C, Kaiser N, Mejuch T, Fansa E, Alsaabi R, Wittinghofer A, Bastiaens PIH *et al* (2019) Small-Molecule Inhibition of the UNC-Src Interaction Impairs Dynamic Src Localization in Cells. *Cell Chem Biol* 26: 842-851 e847
Gerdes JM, Davis EE, Katsanis N (2009) The vertebrate primary cilium in development, homeostasis, and disease. *Cell* 137: 32-45
Germann UA, Furey BF, Markland W, Hoover RR, Aronov AM, Roix JJ, Hale M, Boucher DM, Sorrell DA, Martinez-Botella G *et al* (2017) Targeting the MAPK Signaling Pathway in Cancer: Promising Preclinical Activity with the Novel Selective ERK1/2 Inhibitor BVD-523 (Ulixertinib). *Mol Cancer Ther* 16: 2351-2363
Gotthardt K, Lokaj M, Koerner C, Falk N, Giessl A, Wittinghofer A (2015) A G-protein activation cascade from Arl13B to Arl3 and implications for ciliary targeting of lipidated proteins. *Elife* 4
Grant BMM, Enomoto M, Ikura M, Marshall CB (2020) A Non-Canonical Calmodulin Target Motif Comprising a Polybasic Region and Lipidated Terminal Residue Regulates Localization. *Int J Mol Sci* 21
Grilley-Olson JE, Bedard PL, Fasolo A, Cornfeld M, Cartee L, Razak AR, Stayner LA, Wu Y, Greenwood R, Singh R *et al* (2016) A phase Ib dose-escalation study of the MEK inhibitor trametinib in combination with the PI3K/mTOR inhibitor GSK2126458 in patients with advanced solid tumors. *Invest New Drugs* 34: 740-749
Guzman C, Oetken-Lindholm C, Abankwa D (2016) Automated High-Throughput Fluorescence Lifetime Imaging Microscopy to Detect Protein-Protein Interactions. *J Lab Autom* 21: 238-245
Hait WN, Lazo JS (1986) Calmodulin: a potential target for cancer chemotherapeutic agents. *J Clin Oncol* 4: 994-1012
Hallin J, Engstrom LD, Hargis L, Calinisan A, Aranda R, Briere DM, Sudhakar N, Bowcut V, Baer BR, Ballard JA *et al* (2020) The KRAS(G12C) Inhibitor MRTX849 Provides Insight toward Therapeutic Susceptibility of KRAS-Mutant Cancers in Mouse Models and Patients. *Cancer Discov* 10: 54-71
Han CW, Jeong MS, Jang SB (2017) Structure, signaling and the drug discovery of the Ras oncogene protein. *BMB Rep* 50: 355-360
Harder E, Damm W, Maple J, Wu C, Reboul M, Xiang JY, Wang L, Lupyan D, Dahlgren MK, Knight JL *et al* (2016) OPLS3: A Force Field Providing Broad Coverage of Drug-like Small Molecules and Proteins. *J Chem Theory Comput* 12: 281-296
Harding A, Giles N, Burgess A, Hancock JF, Gabrielli BG (2003) Mechanism of mitosis-specific activation of MEK1. *J Biol Chem* 278: 16747-16754

Hatzivassiliou G, Haling JR, Chen H, Song K, Price S, Heald R, Hewitt JF, Zak M, Peck A, Orr C *et al* (2013) Mechanism of MEK inhibition determines efficacy in mutant KRAS- versus BRAF-driven cancers. *Nature* 501: 232-236
Hatzivassiliou G, Song K, Yen I, Brandhuber BJ, Anderson DJ, Alvarado R, Ludlam MJ, Stokoe D, Gloor SL, Vigers G *et al* (2010) RAF inhibitors prime wild-type RAF to activate the MAPK pathway and enhance growth. *Nature* 464: 431-435
Henis YI, Hancock JF, Prior IA (2009) Ras acylation, compartmentalization and signaling nanoclusters (Review). *Mol Membr Biol* 26: 80-92
Higgins M, Obaidi I, McMorrow T (2019) Primary cilia and their role in cancer. *Oncol Lett* 17: 3041-3047
Ho AL, Brana I, Haddad R, Bauman J, Bible K, Oosting S, Wong DJ, Ahn MJ, Boni V, Even C *et al* (2021) Tipifarnib in Head and Neck Squamous Cell Carcinoma With HRAS Mutations. *J Clin Oncol* 39: 1856-1864
Hobbs GA, Der CJ, Rossman KL (2016) RAS isoforms and mutations in cancer at a glance. *J Cell Sci* 129: 1287-1292
Hocker HJ, Cho KJ, Chen CY, Rambahal N, Sagineedu SR, Shaari K, Stanslas J, Hancock JF, Gorfe AA (2013) Andrographolide derivatives inhibit guanine nucleotide exchange and abrogate oncogenic Ras function. *Proc Natl Acad Sci U S A* 110: 10201-10206
Hong DS, Fakih MG, Strickler JH, Desai J, Durm GA, Shapiro GI, Falchook GS, Price TJ, Sacher A, Denlinger CS *et al* (2020) KRAS(G12C) Inhibition with Sotorasib in Advanced Solid Tumors. *N Engl J Med* 383: 1207-1217
Hou T, Wang J, Li Y, Wang W (2011) Assessing the performance of the MM/PBSA and MM/GBSA methods. 1. The accuracy of binding free energy calculations based on molecular dynamics simulations. *J Chem Inf Model* 51: 69-82
Huang L, Hofer F, Martin GS, Kim SH (1998) Structural basis for the interaction of Ras with RalGDS. *Nat Struct Biol* 5: 422-426
Hurd TW, Fan S, Margolis BL (2011) Localization of retinitis pigmentosa 2 to cilia is regulated by Importin beta2. *J Cell Sci* 124: 718-726
Ianevski A, Giri AK, Aittokallio T (2020) SynergyFinder 2.0: visual analytics of multi-drug combination synergies. *Nucleic Acids Res* 48: W488-W493
Ismail SA, Chen YX, Miertzschke M, Vetter IR, Koerner C, Wittinghofer A (2012) Structural basis for Arl3-specific release of myristoylated ciliary cargo from UNC119. *EMBO J* 31: 4085-4094
Ismail SA, Chen YX, Rusinova A, Chandra A, Bierbaum M, Gremer L, Triola G, Waldmann H, Bastiaens PI, Wittinghofer A (2011) Arl2-GTP and Arl3-GTP regulate a GDI-like transport system for farnesylated cargo. *Nat Chem Biol* 7: 942-949
Jaiswal M, Fansa EK, Kosling SK, Mejuch T, Waldmann H, Wittinghofer A (2016) Novel Biochemical and Structural Insights into the Interaction of Myristoylated Cargo with Unc119 Protein and Their Release by Arl2/3. *J Biol Chem* 291: 20766-20778
Janes MR, Zhang J, Li LS, Hansen R, Peters U, Guo X, Chen Y, Babbar A, Firdaus SJ, Darjania L *et al* (2018) Targeting KRAS Mutant Cancers with a Covalent G12C-Specific Inhibitor. *Cell* 172: 578-589 e517
Jiang Y, Zhuang C, Chen L, Lu J, Dong G, Miao Z, Zhang W, Li J, Sheng C (2017) Structural Biology-Inspired Discovery of Novel KRAS-PDEdelta Inhibitors. *J Med Chem* 60: 9400-9406
Kannt A, Dikic I (2021) Expanding the arsenal of E3 ubiquitin ligases for proximity-induced protein degradation. *Cell Chem Biol* 28: 1014-1031
Karoulia Z, Gavathiotis E, Poulikakos PI (2017) New perspectives for targeting RAF kinase in human cancer. *Nat Rev Cancer* 17: 676-691
Kauko O, O'Connor CM, Kulesskiy E, Sangodkar J, Aakula A, Izadmehr S, Yetukuri L, Yadav B, Padzik A, Laajala TD *et al* (2018) PP2A inhibition is a druggable MEK inhibitor resistance mechanism in KRAS-mutant lung cancer cells. *Sci Transl Med* 10
Kazi A, Xiang S, Yang H, Chen L, Kennedy P, Ayaz M, Fletcher S, Cummings C, Lawrence HR, Beato F *et al* (2019) Dual Farnesyl and Geranylgeranyl Transferase Inhibitor Thwarts Mutant KRAS-Driven Patient-Derived Pancreatic Tumors. *Clin Cancer Res* 25: 5984-5996

Kim JI, Kim J, Jang HS, Noh MR, Lipschutz JH, Park KM (2013) Reduction of oxidative stress during recovery accelerates normalization of primary cilia length that is altered after ischemic injury in murine kidneys. *Am J Physiol Renal Physiol* 304: F1283-1294
Klein CH, Truxius DC, Vogel HA, Harizanova J, Murarka S, Martin-Gago P, Bastiaens PIH (2019) PDEdelta inhibition impedes the proliferation and survival of human colorectal cancer cell lines harboring oncogenic KRas. *Int J Cancer* 144: 767-776
Knyphausen P, Kuhlmann N, de Boor S, Lammers M (2015) Lysine-acetylation as a fundamental regulator of Ran function: Implications for signaling of proteins of the Ras-superfamily. *Small GTPases* 6: 189-195
Kong Au T, Chow Leung P (1998) Identification of the binding and inhibition sites in the calmodulin molecule for ophiobolin A by site-directed mutagenesis. *Plant Physiol* 118: 965-973
Konitsiotis AD, Rossmannek L, Stanoev A, Schmick M, Bastiaens PIH (2017) Spatial cycles mediated by UNC119 solubilisation maintain Src family kinases plasma membrane localisation. *Nat Commun* 8: 114
Kubara K, Yamazaki K, Ishihara Y, Naruto T, Lin HT, Nishimura K, Ohtaka M, Nakanishi M, Ito M, Tsukahara K *et al* (2018) Status of KRAS in iPSCs Impacts upon Self-Renewal and Differentiation Propensity. *Stem Cell Reports* 11: 380-394
Kunath T, Saba-El-Leil MK, Almousailleakh M, Wray J, Meloche S, Smith A (2007) FGF stimulation of the Erk1/2 signalling cascade triggers transition of pluripotent embryonic stem cells from self-renewal to lineage commitment. *Development* 134: 2895-2902
Kwan AK, Piazza GA, Keeton AB, Leite CA (2022) The path to the clinic: a comprehensive review on direct KRAS(G12C) inhibitors. *J Exp Clin Cancer Res* 41: 27
Lai Y, Jiang Y (2020) Reciprocal Regulation between Primary Cilia and mTORC1. *Genes (Basel)* 11
Lane KT, Beese LS (2006) Thematic review series: lipid posttranslational modifications. Structural biology of protein farnesyltransferase and geranylgeranyltransferase type I. *J Lipid Res* 47: 681-699
Lee JE, Gleeson JG (2011) A systems-biology approach to understanding the ciliopathy disorders. *Genome Med* 3: 59
Lerner EC, Zhang TT, Knowles DB, Qian Y, Hamilton AD, Sebti SM (1997) Inhibition of the prenylation of K-Ras, but not H- or N-Ras, is highly resistant to CAAX peptidomimetics and requires both a farnesyltransferase and a geranylgeranyltransferase I inhibitor in human tumor cell lines. *Oncogene* 15: 1283-1288
Li CJ, Heim R, Lu P, Pu Y, Tsien RY, Chang DC (1999) Dynamic redistribution of calmodulin in HeLa cells during cell division as revealed by a GFP-calmodulin fusion protein technique. *J Cell Sci* 112 (Pt 10): 1567-1577
Li J, Abel R, Zhu K, Cao Y, Zhao S, Friesner RA (2011) The VSGB 2.0 model: a next generation energy model for high resolution protein structure modeling. *Proteins* 79: 2794-2812
Li L, Wu Y, Yang Z, Xu C, Zhao H, Liu J, Chen J, Chen J (2021) Discovery of KRas G12C-IN-3 and Pomalidomide-based PROTACs as degraders of endogenous KRAS G12C with potent anticancer activity. *Bioorganic Chemistry* 117: 105447
Li ZL, Buck M (2017) Computational Modeling Reveals that Signaling Lipids Modulate the Orientation of K-Ras4A at the Membrane Reflecting Protein Topology. *Structure* 25: 679-689 e672
Liu H, Kiseleva AA, Golemis EA (2018) Ciliary signalling in cancer. *Nat Rev Cancer* 18: 511-524
Liu M, Sjogren AK, Karlsson C, Ibrahim MX, Andersson KM, Olofsson FJ, Wahlstrom AM, Dalin M, Yu H, Chen Z *et al* (2010) Targeting the protein prenyltransferases efficiently reduces tumor development in mice with K-RAS-induced lung cancer. *Proc Natl Acad Sci U S A* 107: 6471-6476
Llavero F, Arrazola Sastre A, Luque Montoro M, Martin MA, Arenas J, Lucia A, Zugaza JL (2021) Small GTPases of the Ras superfamily and glycogen phosphorylase regulation in T cells. *Small GTPases* 12: 106-113

Lokman NA, Elder ASF, Ricciardelli C, Oehler MK (2012) Chick chorioallantoic membrane (CAM) assay as an in vivo model to study the effect of newly identified molecules on ovarian cancer invasion and metastasis. *Int J Mol Sci* 13: 9959-9970

Lopez-Alcalá C, Alvarez-Moya B, Villalonga P, Calvo M, Bachs O, Agell N (2008) Identification of Essential Interacting Elements in K-Ras/Calmodulin Binding and Its Role in K-Ras Localization*. *Journal of Biological Chemistry* 283: 10621-10631

Lu H, Liu C, Velazquez R, Wang H, Dunkl LM, Kazic-Legueux M, Haberkorn A, Billy E, Manchado E, Brachmann SM *et al* (2019) SHP2 Inhibition Overcomes RTK-Mediated Pathway Reactivation in KRAS-Mutant Tumors Treated with MEK Inhibitors. *Mol Cancer Ther* 18: 1323-1334

Manoharan GB, Laurini C, Bottone S, Ben Fredj N, Abankwa DK (2023) K-Ras Binds Calmodulin-Related Centrin1 with Potential Implications for K-Ras Driven Cancer Cell Stemness. *Cancers (Basel)* 15

Manoharan GB, Okutachi S, Abankwa D (2022) Potential of phenothiazines to synergistically block calmodulin and reactivate PP2A in cancer cells. *PLoS One* 17: e0268635

Martin-Gago P, Fansa EK, Klein CH, Murarka S, Janning P, Schurmann M, Metz M, Ismail S, Schultz-Fademrecht C, Baumann M *et al* (2017a) A PDE6delta-KRas Inhibitor Chemotype with up to Seven H-Bonds and Picomolar Affinity that Prevents Efficient Inhibitor Release by Arl2. *Angew Chem Int Ed Engl* 56: 2423-2428

Martin-Gago P, Fansa EK, Wittinghofer A, Waldmann H (2017b) Structure-based development of PDEdelta inhibitors. *Biol Chem* 398: 535-545

Matallanas D, Romano D, Al-Mulla F, O'Neill E, Al-Ali W, Crespo P, Doyle B, Nixon C, Sansom O, Drosten M *et al* (2011) Mutant K-Ras activation of the proapoptotic MST2 pathway is antagonized by wild-type K-Ras. *Mol Cell* 44: 893-906

Matsubara K, Kishida S, Matsuura Y, Kitayama H, Noda M, Kikuchi A (1999) Plasma membrane recruitment of RalGDS is critical for Ras-dependent Ral activation. *Oncogene* 18: 1303-1312

McDonald ER, 3rd, de Weck A, Schlabach MR, Billy E, Mavrakis KJ, Hoffman GR, Belur D, Castelletti D, Frias E, Gampa K *et al* (2017) Project DRIVE: A Compendium of Cancer Dependencies and Synthetic Lethal Relationships Uncovered by Large-Scale, Deep RNAi Screening. *Cell* 170: 577-592 e510

McDonald Iii ER, de Weck A, Schlabach MR, Billy E, Mavrakis KJ, Hoffman GR, Belur D, Castelletti D, Frias E, Gampa K *et al* (2017) Project DRIVE: A Compendium of Cancer Dependencies and Synthetic Lethal Relationships Uncovered by Large-Scale, Deep RNAi Screening. *Cell* 170: 577-586.e510

Molina-Arcas M, Samani A, Downward J (2021) Drugging the Undruggable: Advances on RAS Targeting in Cancer. *Genes (Basel)* 12

Moon BS, Jeong WJ, Park J, Kim TI, Min do S, Choi KY (2014) Role of oncogenic K-Ras in cancer stem cell activation by aberrant Wnt/β-catenin signaling. *J Natl Cancer Inst* 106: djt373

Morris EJ, Jha S, Restaino CR, Dayananth P, Zhu H, Cooper A, Carr D, Deng Y, Jin W, Black S *et al* (2013) Discovery of a novel ERK inhibitor with activity in models of acquired resistance to BRAF and MEK inhibitors. *Cancer Discov* 3: 742-750

Morrison SJ, Kimble J (2006) Asymmetric and symmetric stem-cell divisions in development and cancer. *Nature* 441: 1068-1074

Mousnier A, Bell AS, Swieboda DP, Morales-Sanfrutos J, Perez-Dorado I, Brannigan JA, Newman J, Ritzefeld M, Hutton JA, Guedan A *et al* (2018) Fragment-derived inhibitors of human N-myristoyltransferase block capsid assembly and replication of the common cold virus. *Nat Chem* 10: 599-606

Murarka S, Martin-Gago P, Schultz-Fademrecht C, Al Saabi A, Baumann M, Fansa EK, Ismail S, Nussbaumer P, Wittinghofer A, Waldmann H (2017) Development of Pyridazinone Chemotypes Targeting the PDEdelta Prenyl Binding Site. *Chemistry* 23: 6083-6093

Najumudeen AK, Jaiswal A, Lectez B, Oetken-Lindholm C, Guzman C, Siljamaki E, Posada IM, Lacey E, Aittokallio T, Abankwa D (2016) Cancer stem cell drugs target K-ras signaling in a stemness context. *Oncogene* 35: 5248-5262
Najumudeen AK, Kohnke M, Solman M, Alexandrov K, Abankwa D (2013) Cellular FRET-Biosensors to Detect Membrane Targeting Inhibitors of N-Myristoylated Proteins. *PLoS One* 8: e66425
Nakajima EC, Drezner N, Li X, Mishra-Kalyani PS, Liu Y, Zhao H, Bi Y, Liu J, Rahman A, Wearne E *et al* (2022) FDA Approval Summary: Sotorasib for KRAS G12C-Mutated Metastatic NSCLC. *Clin Cancer Res* 28: 1482-1486
Nancy V, Callebaut I, El Marjou A, de Gunzburg J (2002) The delta subunit of retinal rod cGMP phosphodiesterase regulates the membrane association of Ras and Rap GTPases. *J Biol Chem* 277: 15076-15084
Ng K, Tabernero J, Hwang J, Bajetta E, Sharma S, Del Prete SA, Arrowsmith ER, Ryan DP, Sedova M, Jin J *et al* (2013) Phase II study of everolimus in patients with metastatic colorectal adenocarcinoma previously treated with bevacizumab-, fluoropyrimidine-, oxaliplatin-, and irinotecan-based regimens. *Clin Cancer Res* 19: 3987-3995
Nikolova S, Guenther A, Savai R, Weissmann N, Ghofrani HA, Konigshoff M, Eickelberg O, Klepetko W, Voswinckel R, Seeger W *et al* (2010) Phosphodiesterase 6 subunits are expressed and altered in idiopathic pulmonary fibrosis. *Respir Res* 11: 146
Nobutani K, Shimono Y, Yoshida M, Mizutani K, Minami A, Kono S, Mukohara T, Yamasaki T, Itoh T, Takao S *et al* (2014) Absence of primary cilia in cell cycle-arrested human breast cancer cells. *Genes Cells* 19: 141-152
O'Boyle NM, Banck M, James CA, Morley C, Vandermeersch T, Hutchison GR (2011) Open Babel: An open chemical toolbox. *J Cheminform* 3: 33
Okutachi S, Manoharan GB, Kiriazis A, Laurini C, Catillon M, McCormick F, Yli-Kauhaluoma J, Abankwa D (2021) A Covalent Calmodulin Inhibitor as a Tool to Study Cellular Mechanisms of K-Ras-Driven Stemness. *Front Cell Dev Biol* 9: 665673
Oliveira AF, Yasuda R (2014) Imaging the activity of Ras superfamily GTPase proteins in small subcellular compartments in neurons. *Methods Mol Biol* 1071: 109-128
Ou SI, Koczywas M, Ulahannan S, Janne P, Pacheco J, Burris H, McCoach C, Wang JS, Gordon M, Haura E *et al* (2020) A12 The SHP2 Inhibitor RMC-4630 in Patients with KRAS-Mutant Non-Small Cell Lung Cancer: Preliminary Evaluation of a First-in-Man Phase 1 Clinical Trial. *Journal of Thoracic Oncology* 15: S15-S16
Paiva SL, Crews CM (2019) Targeted protein degradation: elements of PROTAC design. *Curr Opin Chem Biol* 50: 111-119
Papke B, Der CJ (2017) Drugging RAS: Know the enemy. *Science* 355: 1158-1163
Papke B, Murarka S, Vogel HA, Martin-Gago P, Kovacevic M, Truxius DC, Fansa EK, Ismail S, Zimmermann G, Heinelt K *et al* (2016) Identification of pyrazolopyridazinones as PDEdelta inhibitors. *Nat Commun* 7: 11360
Paridaen JTML, Wilsch-Bräuninger M, Huttner WB (2013) Asymmetric Inheritance of Centrosome- Associated Primary Cilium Membrane Directs Ciliogenesis after Cell Division. *Cell* 155: 333-344
Parisi B, Sünnen M, Chippalkatti R, Abankwa DK (2023) A flow-cytometry-based pipeline for the rapid quantification of C2C12 cell differentiation. *STAR Protocols* 4: 102637
Parker JA, Mattos C (2018) The K-Ras, N-Ras, and H-Ras Isoforms: Unique Conformational Preferences and Implications for Targeting Oncogenic Mutants. *Cold Spring Harb Perspect Med* 8
Parkkola H, Siddiqui FA, Oetken-Lindholm C, Abankwa D (2021) FLIM-FRET Analysis of Ras Nanoclustering and Membrane-Anchorage. *Methods Mol Biol* 2262: 233-250
Pavic K, Chippalkatti R, Abankwa D (2022) Drug targeting opportunities en route to Ras nanoclusters. *Adv Cancer Res* 153: 63-99
Pechlivanis M, Ringel R, Popkirova B, Kuhlmann J (2007) Prenylation of Ras facilitates hSOS1-promoted nucleotide exchange, upon Ras binding to the regulatory site. *Biochemistry* 46: 5341-5348

Posch C, Moslehi H, Feeney L, Green GA, Ebaee A, Feichtenschlager V, Chong K, Peng L, Dimon MT, Phillips T *et al* (2013) Combined targeting of MEK and PI3K/mTOR effector pathways is necessary to effectively inhibit NRAS mutant melanoma in vitro and in vivo. *Proc Natl Acad Sci U S A* 110: 4015-4020
Potdar S, Ianevski A, Mpindi JP, Bychkov D, Fiere C, Ianevski P, Yadav B, Wennerberg K, Aittokallio T, Kallioniemi O *et al* (2020) Breeze: an integrated quality control and data analysis application for high-throughput drug screening. *Bioinformatics* 36: 3602-3604
Poulikakos PI, Zhang C, Bollag G, Shokat KM, Rosen N (2010) RAF inhibitors transactivate RAF dimers and ERK signalling in cells with wild-type BRAF. *Nature* 464: 427-430
Prior IA, Hood FE, Hartley JL (2020) The Frequency of Ras Mutations in Cancer. *Cancer Res* 80: 2969-2974
Prior IA, Muncke C, Parton RG, Hancock JF (2003) Direct visualization of Ras proteins in spatially distinct cell surface microdomains. *J Cell Biol* 160: 165-170
Pugacheva EN, Jablonski SA, Hartman TR, Henske EP, Golemis EA (2007) HEF1-dependent Aurora A activation induces disassembly of the primary cilium. *Cell* 129: 1351-1363
Punekar SR, Velcheti V, Neel BG, Wong KK (2022) The current state of the art and future trends in RAS-targeted cancer therapies. *Nat Rev Clin Oncol* 19: 637-655
Qian L, Chen K, Wang C, Chen Z, Meng Z, Wang P (2020) Targeting NRAS-Mutant Cancers with the Selective STK19 Kinase Inhibitor Chelidonine. *Clin Cancer Res* 26: 3408-3419
Qu L, Pan C, He SM, Lang B, Gao GD, Wang XL, Wang Y (2019) The Ras Superfamily of Small GTPases in Non-neoplastic Cerebral Diseases. *Front Mol Neurosci* 12: 121
Quinlan MP, Quatela SE, Philips MR, Settleman J (2008) Activated Kras, but not Hras or Nras, may initiate tumors of endodermal origin via stem cell expansion. *Mol Cell Biol* 28: 2659-2674
R CT (2022) R: A Language and Environment for Statistical Computing.
Rauen KA (2013) The RASopathies. *Annu Rev Genomics Hum Genet* 14: 355-369
Resh MD (2016) Chapter 13 - Lipid Modification of Proteins. In: *Biochemistry of Lipids, Lipoproteins and Membranes (Sixth Edition)*, Ridgway N.D., McLeod R.S. (eds.) pp. 391-414. Elsevier: Boston
Rocks O, Peyker A, Kahms M, Verveer PJ, Koerner C, Lumbierres M, Kuhlmann J, Waldmann H, Wittinghofer A, Bastiaens PI (2005) An acylation cycle regulates localization and activity of palmitoylated Ras isoforms. *Science* 307: 1746-1752
Schindelin J, Arganda-Carreras I, Frise E, Kaynig V, Longair M, Pietzsch T, Preibisch S, Rueden C, Saalfeld S, Schmid B *et al* (2012) Fiji: an open-source platform for biological-image analysis. *Nat Methods* 9: 676-682
Schmick M, Vartak N, Papke B, Kovacevic M, Truxius DC, Rossmannek L, Bastiaens PIH (2014) KRas localizes to the plasma membrane by spatial cycles of solubilization, trapping and vesicular transport. *Cell* 157: 459-471
Seabra MC (1998) Membrane association and targeting of prenylated Ras-like GTPases. *Cell Signal* 10: 167-172
Shen Y, Vignali P, Wang R (2017) Rapid Profiling Cell Cycle by Flow Cytometry Using Concurrent Staining of DNA and Mitotic Markers. *Bio Protoc* 7
Shima F, Ijiri Y, Muraoka S, Liao J, Ye M, Araki M, Matsumoto K, Yamamoto N, Sugimoto T, Yoshikawa Y *et al* (2010) Structural Basis for Conformational Dynamics of GTP-bound Ras Protein*. *Journal of Biological Chemistry* 285: 22696-22705
Siddiqui FA, Alam C, Rosenqvist P, Ora M, Sabt A, Manoharan GB, Bindu L, Okutachi S, Catillon M, Taylor T *et al* (2020a) PDE6D Inhibitors with a New Design Principle Selectively Block K-Ras Activity. *ACS Omega* 5: 832-842
Siddiqui FA, Parkkola H, Manoharan GB, Abankwa D (2020b) Medium-Throughput Detection of Hsp90/Cdc37 Protein-Protein Interaction Inhibitors Using a Split Renilla Luciferase-Based Assay. *SLAS Discov* 25: 195-206
Siddiqui FA, Vukic V, Salminen TA, Abankwa D (2021) Elaiophylin Is a Potent Hsp90/Cdc37 Protein Interface Inhibitor with K-Ras Nanocluster Selectivity. *Biomolecules* 11

Simanshu DK, Nissley DV, McCormick F (2017) RAS Proteins and Their Regulators in Human Disease. *Cell* 170: 17-33
Singh V, Davidson AC, Hume PJ, Humphreys D, Koronakis V (2019) Arf GTPase interplay with Rho GTPases in regulation of the actin cytoskeleton. *Small GTPases* 10: 411-418
Skoulidis F, Li BT, Dy GK, Price TJ, Falchook GS, Wolf J, Italiano A, Schuler M, Borghaei H, Barlesi F *et al* (2021) Sotorasib for Lung Cancers with KRAS p.G12C Mutation. *N Engl J Med* 384: 2371-2381
Smalley I, Smalley KSM (2018) ERK Inhibition: A New Front in the War against MAPK Pathway-Driven Cancers? *Cancer Discov* 8: 140-142
Stavridis MP, Lunn JS, Collins BJ, Storey KG (2007) A discrete period of FGF-induced Erk1/2 signalling is required for vertebrate neural specification. *Development* 134: 2889-2894
Steffen CL, Kaya P, Schaffner-Reckinger E, Abankwa D (2023) Eliminating oncogenic RAS: back to the future at the drawing board. *Biochem Soc Trans* 51: 447-456
Stephen LA, Ismail S (2016) Shuttling and sorting lipid-modified cargo into the cilia. *Biochemical Society transactions* 44: 1273-1280
Sung H, Ferlay J, Siegel RL, Laversanne M, Soerjomataram I, Jemal A, Bray F (2021) Global Cancer Statistics 2020: GLOBOCAN Estimates of Incidence and Mortality Worldwide for 36 Cancers in 185 Countries. *CA Cancer J Clin* 71: 209-249
Tanaka T, Thomas J, Van Montfort R, Miller A, Rabbitts T (2021) Pan RAS-binding compounds selected from a chemical library by inhibiting interaction between RAS and a reduced affinity intracellular antibody. *Sci Rep* 11: 1712
Therneau TM, Grambsch PM (2000) *Modeling Survival Data: Extending the Cox Model*. Springer New York, NY
Thomas S, Wright KJ, Le Corre S, Micalizzi A, Romani M, Abhyankar A, Saada J, Perrault I, Amiel J, Litzler J *et al* (2014) A homozygous PDE6D mutation in Joubert syndrome impairs targeting of farnesylated INPP5E protein to the primary cilium. *Hum Mutat* 35: 137-146
Tidow H, Nissen P (2013) Structural diversity of calmodulin binding to its target sites. *FEBS J* 280: 5551-5565
Tobin JL, Beales PL (2009) The nonmotile ciliopathies. *Genet Med* 11: 386-402
Tomasetti C, Vogelstein B (2015) Cancer etiology. Variation in cancer risk among tissues can be explained by the number of stem cell divisions. *Science* 347: 78-81
Torii S, Yamamoto T, Tsuchiya Y, Nishida E (2006) ERK MAP kinase in G cell cycle progression and cancer. *Cancer Sci* 97: 697-702
Tsherniak A, Vazquez F, Montgomery PG, Weir BA, Kryukov G, Cowley GS, Gill S, Harrington WF, Pantel S, Krill-Burger JM *et al* (2017) Defining a Cancer Dependency Map. *Cell* 170: 564-576 e516
Tulpule A, Guan J, Neel DS, Allegakoen HR, Lin YP, Brown D, Chou YT, Heslin A, Chatterjee N, Perati S *et al* (2021) Kinase-mediated RAS signaling via membraneless cytoplasmic protein granules. *Cell* 184: 2649-2664.e2618
Van QN, Prakash P, Shrestha R, Balius TE, Turbyville TJ, Stephen AG (2021) RAS Nanoclusters: Dynamic Signaling Platforms Amenable to Therapeutic Intervention. *Biomolecules* 11
Vivanco I, Sawyers CL (2002) The phosphatidylinositol 3-Kinase AKT pathway in human cancer. *Nat Rev Cancer* 2: 489-501
Wakioka T, Sasaki A, Kato R, Shouda T, Matsumoto A, Miyoshi K, Tsuneoka M, Komiya S, Baron R, Yoshimura A (2001) Spred is a Sprouty-related suppressor of Ras signalling. *Nature* 412: 647-651
Wall VE, Garvey LA, Mehalko JL, Procter LV, Esposito D (2014) Combinatorial assembly of clone libraries using site-specific recombination. *Methods Mol Biol* 1116: 193-208
Wang M-T, Holderfield M, Galeas J, Delrosario R, To MD, Balmain A, McCormick F (2015a) K-Ras Promotes Tumorigenicity through Suppression of Non-canonical Wnt Signaling. *Cell* 163: 1237-1251

Wang MT, Holderfield M, Galeas J, Delrosario R, To MD, Balmain A, McCormick F (2015b) K-Ras Promotes Tumorigenicity through Suppression of Non-canonical Wnt Signaling. *Cell* 163: 1237-1251
Wang S, Wei Q, Dong G, Dong Z (2013) ERK-mediated suppression of cilia in cisplatin-induced tubular cell apoptosis and acute kidney injury. *Biochimica et Biophysica Acta (BBA) - Molecular Basis of Disease* 1832: 1582-1590
Wang W, Zhang Q, Acland GM, Mellersh C, Ostrander EA, Ray K, Aguirre GD (1999) Molecular characterization and mapping of canine cGMP-phosphodiesterase delta subunit (PDE6D). *Gene* 236: 325-332
Ward RA, Anderton MJ, Bethel P, Breed J, Cook C, Davies EJ, Dobson A, Dong Z, Fairley G, Farrington P *et al* (2019) Discovery of a Potent and Selective Oral Inhibitor of ERK1/2 (AZD0364) That Is Efficacious in Both Monotherapy and Combination Therapy in Models of Nonsmall Cell Lung Cancer (NSCLC). *J Med Chem* 62: 11004-11018
White MC, Holman DM, Boehm JE, Peipins LA, Grossman M, Henley SJ (2014) Age and cancer risk: a potentially modifiable relationship. *Am J Prev Med* 46: S7-15
Wilsch-Brauninger M, Huttner WB (2021) Primary Cilia and Centrosomes in Neocortex Development. *Front Neurosci* 15: 755867
Winzker M, Friese A, Koch U, Janning P, Ziegler S, Waldmann H (2020) Development of a PDEdelta-Targeting PROTACs that Impair Lipid Metabolism. *Angew Chem Int Ed Engl* 59: 5595-5601
Wright KJ, Baye LM, Olivier-Mason A, Mukhopadhyay S, Sang L, Kwong M, Wang W, Pretorius PR, Sheffield VC, Sengupta P *et al* (2011) An ARL3-UNC119-RP2 GTPase cycle targets myristoylated NPHP3 to the primary cilium. *Genes Dev* 25: 2347-2360
Wright LP, Philips MR (2006) Thematic review series: lipid posttranslational modifications. CAAX modification and membrane targeting of Ras. *J Lipid Res* 47: 883-891
Yadav B, Pemovska T, Szwajda A, Kulesskiy E, Kontro M, Karjalainen R, Majumder MM, Malani D, Murumagi A, Knowles J *et al* (2014) Quantitative scoring of differential drug sensitivity for individually optimized anticancer therapies. *Sci Rep* 4: 5193
Yelland T, Garcia E, Parry C, Kowalczyk D, Wojnowska M, Gohlke A, Zalar M, Cameron K, Goodwin G, Yu Q *et al* (2022) Stabilization of the RAS:PDE6D Complex Is a Novel Strategy to Inhibit RAS Signaling. *J Med Chem* 65: 1898-1914
Yelland T, Garcia E, Samarakoon Y, Ismail S (2021) The Structural and Biochemical Characterization of UNC119B Cargo Binding and Release Mechanisms. *Biochemistry* 60: 1952-1963
Yin C, Zhu B, Zhang T, Liu T, Chen S, Liu Y, Li X, Miao X, Li S, Mi X *et al* (2019) Pharmacological Targeting of STK19 Inhibits Oncogenic NRAS-Driven Melanomagenesis. *Cell* 176: 1113-1127.e1116
Yu YY, Chen Y, Dai G, Chen J, Sun XM, Wen CJ, Zhao DH, Chang DC, Li CJ (2004) The association of calmodulin with central spindle regulates the initiation of cytokinesis in HeLa cells. *Int J Biochem Cell Biol* 36: 1562-1572
Zambetti NA, Firestone AJ, Remsberg JR, Huang BJ, Wong JC, Long AM, Predovic M, Suciu RM, Inguva A, Kogan SC *et al* (2020) Genetic disruption of N-RasG12D palmitoylation perturbs hematopoiesis and prevents myeloid transformation in mice. *Blood* 135: 1772-1782
Zeng M, Xiong Y, Safaee N, Nowak RP, Donovan KA, Yuan CJ, Nabet B, Gero TW, Feru F, Li L *et al* (2020) Exploring Targeted Degradation Strategy for Oncogenic KRASG12C. *Cell Chemical Biology* 27: 19-31.e16
Zhang H, Li S, Doan T, Rieke F, Detwiler PB, Frederick JM, Baehr W (2007) Deletion of PrBP/delta impedes transport of GRK1 and PDE6 catalytic subunits to photoreceptor outer segments. *Proc Natl Acad Sci U S A* 104: 8857-8862
Zhang Z, Guiley KZ, Shokat KM (2022a) Chemical acylation of an acquired serine suppresses oncogenic signaling of K-Ras(G12S). *Nat Chem Biol* 18: 1177-1183
Zhang Z, Morstein J, Ecker AK, Guiley KZ, Shokat KM (2022b) Chemoselective Covalent Modification of K-Ras(G12R) with a Small Molecule Electrophile. *J Am Chem Soc* 144: 15916-15921

Zhou Y, Hancock JF (2021) Lipid Profiles of RAS Nanoclusters Regulate RAS Function. *Biomolecules* 11
Zhou Y, Prakash P, Liang H, Cho KJ, Gorfe AA, Hancock JF (2017) Lipid-Sorting Specificity Encoded in K-Ras Membrane Anchor Regulates Signal Output. *Cell* 168: 239-251 e216
Zhou Y, Prakash PS, Liang H, Gorfe AA, Hancock JF (2021) The KRAS and other prenylated polybasic domain membrane anchors recognize phosphatidylserine acyl chain structure. *Proc Natl Acad Sci U S A* 118
Zimmermann G, Papke B, Ismail S, Vartak N, Chandra A, Hoffmann M, Hahn SA, Triola G, Wittinghofer A, Bastiaens PI *et al* (2013) Small molecule inhibition of the KRAS-PDEdelta interaction impairs oncogenic KRAS signalling. *Nature* 497: 638-642

APPENDICES

Kaya et al. **An improved PDE6D inhibitor combines with Sildenafil to synergistically inhibit KRAS mutant cancer cell growth**

Supplementary Information Figure S1

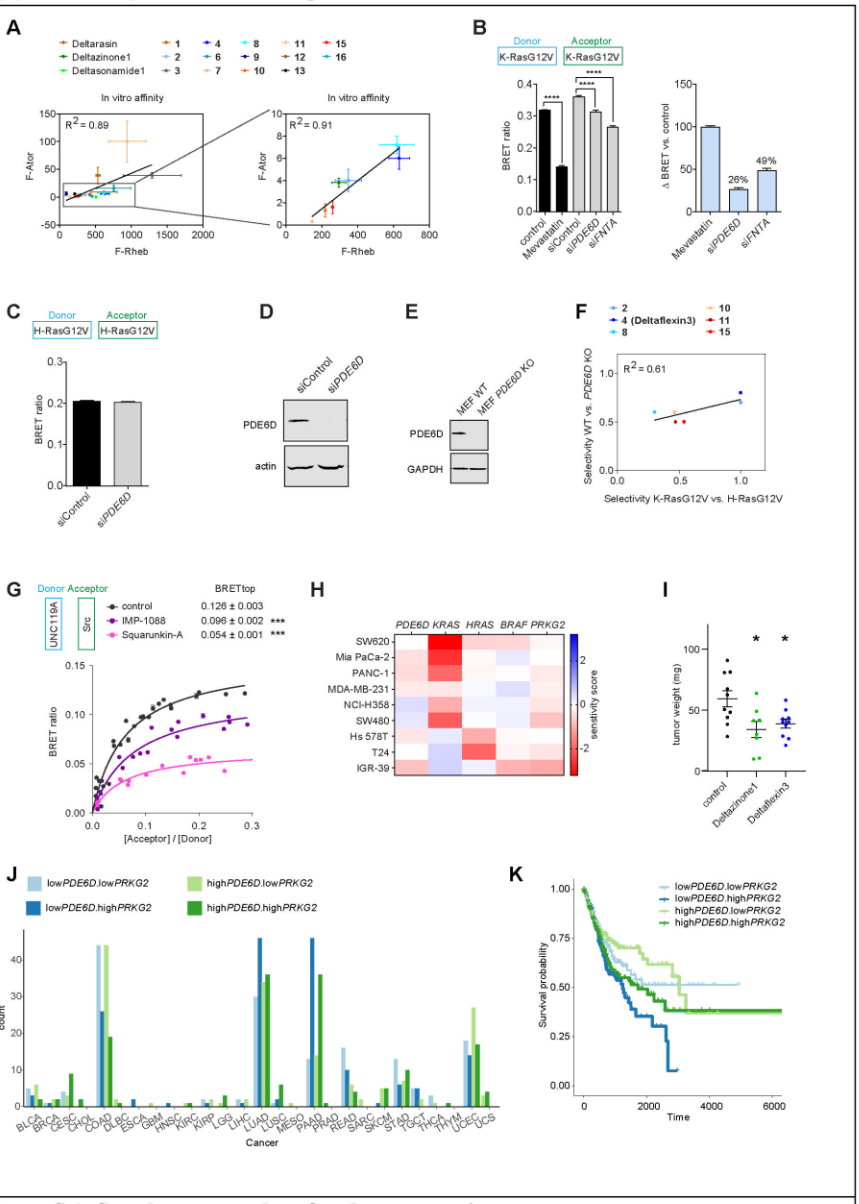

Figure S 1. Supplementary data for the manuscript.

(**A**) Correlation plots of inhibitor/ PDE6D-Kd values acquired using either F-Rheb or F-Ator as probes (**Data S2**). Data of compound **14** were excluded, due to its much lower affinity.

(**B**) K-RasG12V-membrane anchorage BRET is reduced by 5 µM Mevastatin treatment and knockdown of *PDE6D* or *FNTA* to different extents; n ≥ 3 (left). Derived from these data we prepared a plot of the loss of BRET ratio as compared to respective controls, by setting the loss of the Mevastatin treatment to 100% (right).

(**C**) H-RasG12V-membrane anchorage BRET is not affected by knockdown of *PDE6D*; n ≥ 3.

(**D**) Representative immunoblot data showing *PDE6D* knockdown efficiency in HEK293 EBNA cells; n ≥ 3. Immunoblot data showing *FNTA* knockdown efficiency in HEK293 EBNA cells were previously reported by us (Manoharan et al., 2023).

(**E**) Representative immunoblot data verifying *PDE6D* knockout in *PDE6D*-KO MEF cells.

(**F**) Correlation plot of K-RasG12V-BRET selectivity on the x-axis (**Fig. 2B**) vs. WT/KO-viability data derived PDE6D-selectivity (**Fig. 3A**).

(**G**) BRET-titration curves of the UNC119A/ Src complex after treatment with 5 µM of the N-myristoyl-transferase inhibitor IMP-1088 or 5 µM the UNC119-inhibitor Squarunkin A; n ≥ 3. Statistical comparisons of BRETtop values to controls were done using two-tailed Student's t-test.

(**H**) Heatmap of the ATARiS-sensitivity scores of selected genes for all cancer cell lines used in this study. Negative values indicate a decrease of proliferation upon gene knockdown and therefore a higher dependency of the cell line on that gene.

(**I**) Weights of MDA-MB-231 derived microtumors (≥ 8 per condition from n = 3) from CAM assays after treatment with 10 µM of indicated compounds.

(**J**) Number of *KRAS*-mutant patient tumor samples with indicated high or low gene expression level combinations of *PDE6D* and *PRKG2* (gene for PKG2) by cancer type (TCGA study abbreviations).

(**K**) Overall survival of *KRAS*-mutant patient tumor samples from TCGA with indicated high or low gene expression level combinations of *PDE6D* and *PRKG2* (gene for PKG2). Number of patients per group: 157 (low*PDE6D*.low*PRKG2*), 165 (low*PDE6D*.high*PRKG2*), 166 (high*PDE6D*.low*PRKG2*), 159 (high*PDE6D*.high*PRKG2*). Kaplan-Meyer test for the difference between low*PDE6D*.high*PRKG2* and high*PDE6D*.low*PRKG2* groups: p = 0.0006.